

PDF hosted at the Radboud Repository of the Radboud University Nijmegen

The following full text is a publisher's version.

For additional information about this publication click this link.

<http://hdl.handle.net/2066/157073>

Please be advised that this information was generated on 2017-12-05 and may be subject to change.

The role of glucose in oxidative phosphorylation dysfunctional myoblasts

Dania Carmen Liemburg-Apers

The role of glucose in mitochondrial oxidative phosphorylation dysfunctional myoblasts

© 2016 Dania Carmen Liemburg-Apers

ISBN: 978-94-6233-236-2

The research described in this thesis was performed at the department of Biochemistry, Radboud University Medical Centre Nijmegen, the Netherlands, and was supported by the CSBR (Centres for Systems Biology Research) initiative from ZonMW (Grant: #CSBR09/013V).



Cover image: A C2C12 myoblasts expressing a FRET-based glucose sensor. Upon the addition of extracellular glucose, the fluorescence intensity of Citrine (Red) increases in time (left to right), while the fluorescence intensity of CFP (blue) decreases, causing an increase in the Citrine/CFP ratio (purple).

Cover design: Alexander Apers

Printing: Gildeprint Drukkerijen – www.gildeprint.nl

The role of glucose in oxidative phosphorylation dysfunctional myoblasts

Proefschrift

ter verkrijging van de graad van doctor
aan de Radboud Universiteit Nijmegen
op gezag van de rector magnificus,
volgens besluit van het college van decanen
in het openbaar te verdedigen op donderdag 26 mei 2016
om 10.30 uur precies

door

Dania Carmen Liemburg-Apers

geboren op 14 juli 1985

te Hoofddorp

Promotoren

Prof. dr. J.A.M. Smeitink
Prof. dr. R.E. Brock

Copromotoren

Dr. W.J.H. Koopman
Dr. P.H.G.M. Willems

Manuscriptcommissie

Prof. dr. J.G.J. Hoenderop (voorzitter)
Prof. dr. M. Gotthardt
Prof. dr. H.J.M. Smeets (MUMC)

Table of Contents

List of abbreviations	7
CHAPTER 1. General introduction	9
CHAPTER 2. Quantitative glucose sensing in mammalian cells	29
CHAPTER 3. Mitochondrial dysfunction triggers a rapid compensatory increase in steady-state glucose flux	43
CHAPTER 4. Increased cellular glucose uptake in differentiating <i>Ndufs4</i> KO myoblasts	79
CHAPTER 5. Stimulation of glucose influx by acute mitochondrial dysfunction requires LKB1, AMPK and Sirt2	101
CHAPTER 6. General discussion	129
References	145
Summary	169
Samenvatting	173
Dankwoord	177
Curriculum Vitae	181
List of publications	183

List of abbreviations

[GLC]	glucose concentration
$\Delta\Psi$	mitochondrial membrane potential
AA	antimycin A
AMP	adenosine monophosphate
AMPK	AMP-activated protein kinase
ATM	ataxia telangiectasia mutated
ATP	adenosine triphosphate
CI-CV	mitochondrial complex I – complex V
CFP	cyan fluorescent protein
CytoB	cytochalasin B
ER	endoplasmic reticulum
ETC	electron transport chain
FLII	FLII ¹² Pglu-700 μ δ 6
FRET	fluorescence resonance energy transfer
G6P	glucose-6-phosphate
GGBP	glucose galactose-binding protein
GLUT	glucose transporter
HEt	hydroethidium
HK	hexokinase
HT	HEPES-Tris
IAA	iodoacetate
KO	knockout
LDH	lactate dehydrogenase
MFS	major facilitator superfamily
NAD(H)	nicotinamide adenine nucleotide (reduced)
NADPH	nicotinamide adenine nucleotide phosphate
NDUFS	NADH dehydrogenase ubiquinone flavoprotein subunit
NMN	nicotinamide mononucleotide
OLI	oligomycin A
OXPPOS	oxidative phosphorylation
PA	piericidin A

PBP	periplasmic binding protein
PM	plasma membrane
PMF	proton motive force
PPP	pentose phosphate pathway
ROI	region of interest
ROS	reactive oxygen species
RU	ratio unit
SLC	solute carrier
TCA	tricarboxylic acid
WT	wild type

CHAPTER 1

General introduction



Partially published in:

**Dania C. Liemburg-Apers, Peter H. G. M. Willems, Werner J. H. Koopman,
Sander Grefte.**

Arch Toxicol. (2015) 89(8):1209-2

Cellular glucose uptake and metabolism

In order to survive and perform vital cellular processes such as migration, transport, and cell division, cells require energy. Monosaccharides, amino acids, and fatty acids derived from food are taken up by cells and the energy stored in these biomolecules is used to produce adenosine triphosphate (ATP), the energy currency of cells. The monosaccharide glucose is one of the main energy sources for our body. In the majority of cells, glucose crosses the plasma membrane by facilitated diffusion along the glucose-gradient. This equilibrative glucose transport is mediated by glucose transporters (GLUTs). On the contrary, in cells of the intestine and renal proximal tubule, glucose is actively transported against a concentration gradient. This accumulative glucose transport is mediated by sodium-glucose linked transporters (SGLTs), which use the potential energy stored in the sodium-gradient to co-transport glucose. In this thesis we will focus on GLUT-mediated glucose uptake.

GLUT isoforms

GLUTs are integral membrane glycoproteins which belong to the Solute Carrier Family 2 (SLC2), which is part of the Major Facilitator Superfamily (MFS). The SLC2 family comprises 14 members, which all contain 12 transmembrane (TM) α -helices, with intracellular facing N- and C-termini, and a large intracellular loop between TM domain 6 and 7 (Mueckler et al., 1985). GLUTs can be divided in 3 classes based on sequence similarities (Augustin, 2010). Class I comprises the 'classic' and well-characterized transporters GLUT1-4 and GLUT14. Class II comprises GLUT5, 7, 9, 11, which transport fructose. Class III comprises GLUT6, 8, 10, 12, 13, which contain an internalization signal and are mostly localized intracellular (Augustin, 2010). Class I and II GLUTs contain a relatively large extracellular loop between TM domain 1 and 2, which has an N-glycosylation site (Fig. 1A). In Class III GLUTs the N-glycosylation site is localized in a relatively large extracellular loop between TM domain 9 and 10 (Fig. 1B). The GLUT isoforms differ in their substrate specificity, kinetic parameters, tissue distribution, and mode of regulation (Table 1).

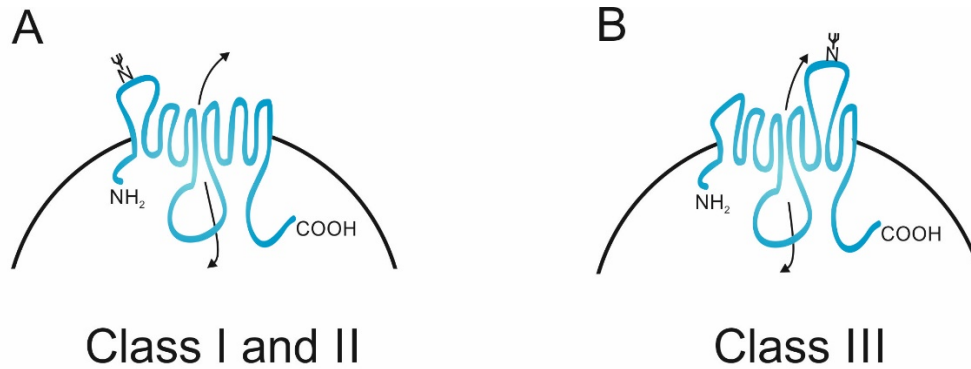


Figure 1. Predicted topology of class I and II (panel A) and class III (panel B) GLUTs. The N-glycosylation site is positioned in the relatively larger extracellular loop between TM domain 1 and 2 (class I and II) or between TM domain 9 and 10 (class III).

Table 1. Characteristics of class I GLUTs. Data compiled from (Augustin, 2010) and the UniProtKB database.

	$K_{m(app)}$ for 2-DG	Expression	Substrates	Peptide length
GLUT1	3 - 5 mM	Endothelial cells Epithelial cells Erythrocytes Astrocytes	Glucose Mannose Galactose Glucosamine Hydroascorbic acid	492 aa
GLUT2	17 mM	Kidney Intestine Pancreas Liver	Glucose Mannose Galactose Glucosamine Fructose	524 aa
GLUT3	1.4 mM	Neurons Spermatozoa	Glucose Mannose Galactose Maltose Xylose Hydroascorbic acid	496 aa
GLUT4	5 mM	Muscle Adipocytes Heart	Glucose Glucosamine Hydroascorbic acid	509 aa

2-DG, 2-deoxy-D-glucose; aa, amino acids; $K_{m(app)}$, apparent K_m .

The tissue-specific expression of GLUTs, allows for a tissue-specific regulation of glucose uptake (Bell et al., 1990, Gould and Holman, 1993). For example, upon differentiation of the murine skeletal muscle-derived C2C12 myoblast cell line into multinucleated myotubes, Glut1 is down-regulated and Glut4 is upregulated (Fig.

2). This change in Glut expression during myogenesis was also observed in primary fetal rat myoblasts and the rat skeletal muscle-derived myoblasts cell line L6 (Mitsumoto and Klip, 1992, Guillet-Deniau et al., 1994). Under basal conditions, the majority of GLUT4 in muscle cells is retained in intracellular vesicles that are derived from the *trans*-Golgi network. Retention of these vesicles requires the activity of the Rab GTPase activating proteins TBC1D1 and TBC1D4 (Eguez et al., 2005, Larance et al., 2005, Sano et al., 2003). Stimulation by insulin or exercise induces translocation of these vesicles to the plasma membrane. Although the full signaling cascade regulating vesicle translocation is still incompletely understood, Akt-mediated inhibition of TBC1D1/TBC1D4 plays an essential role (Eguez et al., 2005, Funaki et al., 2004, Kohn et al., 1998, Larance et al., 2005, Sano et al., 2003, Ng et al., 2008).

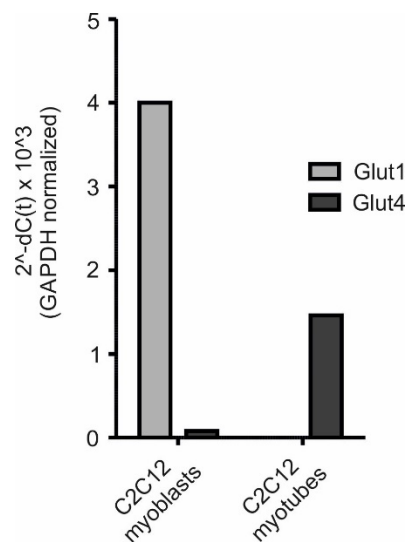


Figure 2. mRNA levels of Glut1 and 4 were analyzed by qPCR. C2C12 myoblasts express Glut1. Culturing for 5 days in low serum differentiation medium induces myotube formation and Glut4 expression. Primer sequences are listed in the ‘material and methods’ section of chapter 3.

GLUT1 is expressed during all stages of embryonic development (Hogan et al., 1991). After birth, GLUT1 expression decreases, but most cell types still express low levels of GLUT1 to mediate basal glucose uptake. However, GLUT1 expression remains high in cells that primarily depend on glycolysis for ATP generation such as erythrocytes and certain tumor cells. In the latter, GLUT1 is frequently up-regulated (Baer et al., 1997, Brown and Wahl, 1993, Nishioka et al., 1992), which is associated with poor survival in various malignant tumors (Szablewski, 2013).

Under basal conditions, a substantial amount of GLUT1 is stored in the endoplasmic reticulum (ER), the Golgi, and endosomes (Luiken et al., 2004, Holman et al., 1990, Farrell and Pardridge, 1991, Cornford et al., 1994). Stimulation by growth factors increases GLUT1 plasma membrane abundance by decreasing the rate of internalization and by promoting recycling of intracellular GLUT1 in a serum/glucocorticosteroid regulated kinase 1 (SGK1)- and Akt-dependent manner (Wieman et al., 2007, Palmada et al., 2006). In addition, protein kinase C (PKC) stimulates translocation of GLUT1 to the plasma membrane by phosphorylating Ser226, which is localized in the largest intracellular loop (Lee et al., 2015, Cooper et al., 1999). The affinity of GLUT1 depends on the glycosylation status at Asn45. Mutation of this residue leads to a 2-fold increase in the K_m for 2-deoxy-D-glucose (2-DG) (Asano et al., 1991). Glucose depletion for more than 12 hours renders GLUT1 hypoglycosylated, which decreases its affinity for glucose but greatly increases the protein half-life of GLUT1. Re-addition of glucose restores glycosylation and reduces the protein half-life to normal (McMahon and Frost, 1995). The above regulatory mechanisms can help cells to cope with differences in energy demand and available energy sources, respectively.

GLUT transport mechanism

Based on homology-modeling and the structure of GLUT1, the transport mechanism of GLUTs was proposed to be an alternating access model in which the carrier cycles between four different conformations (Jardetzky, 1966, Deng et al., 2014, Krupka and Deves, 1981, Lieb and Stein, 1974). Crystalized human GLUT1 revealed that the N- and C-terminal domains are connected by an intracellular helical bundle, which comprises 4 short α -helices (Deng et al., 2014). Interactions between this intracellular helical bundle and the TM domains was proposed to maintain the carrier in an outward-open conformation in the absence of substrate. Binding of substrate to the exofacial binding site, drives a conformational change from an occluded-occupied to an inward-open conformation, in which the endofacial sugar binding site is exposed (Fig. 3; 1→2→3). This part of the cycle is termed translocation. The lower substrate concentration inside the cell shifts equilibrium towards dissociation and the substrate is released. Next, the carrier is able to return to the outward-open conformation, which in the absence of substrate is termed relaxation (Fig. 3; 3→4→1).

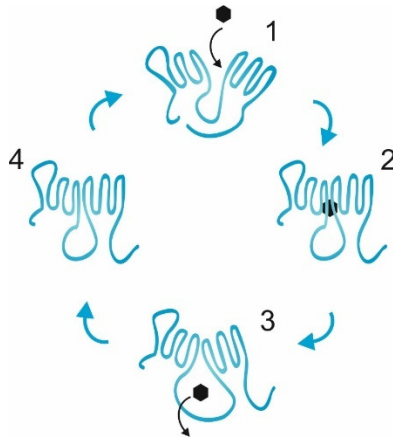


Figure 3. GLUT transport mechanism. GLUT cycles between 4 conformations: 1) outward-open, 2) occluded-occupied, 3) inward-open, and 4) occluded-empty.

GLUT1 kinetics are asymmetric, meaning that the V_{\max} and K_m for glucose uptake are lower than the V_{\max} and K_m for glucose efflux (Baker and Widdas, 1988, Batt and Schachter, 1973). At physiological temperature this asymmetry is observed as a 2.5-fold higher affinity for glucose uptake compared to glucose efflux (Lowe and Walmsley, 1986). This asymmetry is at least in part mediated by binding of ATP to GLUT1, which induces a 4-fold reduction in K_m and 2.4-fold reduction in V_{\max} for glucose uptake (Carruthers, 1986). Another important feature of GLUT1 is *trans*-acceleration, which means that glucose transport is faster when glucose is present on the opposite (*trans*)-side of the membrane. Based on the above described model this means that glucose translocation is faster than relaxation. This slower relaxation is mediated by TM domain 6, which was proposed to inhibit relaxation (Vollers and Carruthers, 2012). Although each GLUT1 molecule represents a fully functional catalytic unit, reduced GLUT1 is a dimer and non-reduced GLUT1 is a tetramer (Graybill et al., 2006, Sogin and Hinkle, 1978, Hebert and Carruthers, 1992, Zottola et al., 1995). Dimeric GLUT1 comprises two structurally associated but functionally independent GLUT1 subunits (Gorga and Lienhard, 1981). Tetrameric GLUT1 comprises a dimer of GLUT1 dimers in which subunits functionally interact in an anti-parallel manner so that, at any time two carriers are in the outward-open conformation and two carriers are in the inward-open conformation (Cloherty et al., 2001, Hamill et al., 1999, Hebert and Carruthers, 1992, Zottola et al., 1995). Reorientation of two carriers in one direction induces reorientation of the coupled carriers in the opposite direction. When translocation is faster than relaxation, translocation of two carriers could accelerate the relaxation of the coupled two carriers, thereby inducing *trans*-acceleration.

Glucose metabolism

Once inside the cell, glucose is phosphorylated by hexokinase (HK) to form glucose-6-phosphate (G6P). Phosphorylated glucose can be used anabolic to form NADPH and nucleotide precursors via the pentose phosphate pathway (PPP) or to be stored as glycogen. Alternatively, glucose can be used catabolic via the glycolytic pathway, which comprises 10 enzymes that oxidize glucose in a step-wise manner (Fig. 4). The net yield of glycolysis is 2 molecules of pyruvate, 2 molecules of ATP, and 2 molecules of reduced nicotinamide adenine dinucleotide (NADH). In the absence of oxygen, pyruvate is converted to lactate by lactate dehydrogenase (LDH) and secreted out of the cell (Fig. 4). Alternatively, when sufficient oxygen is available, pyruvate enters the mitochondria where it is converted by pyruvate dehydrogenase (PDH) into acetyl-coenzyme-A (AcCoA), which is further oxidized by the tricarboxylic acid (TCA) cycle (Fig 4). Oxidation of 1 molecule of AcCoA by the TCA cycle yields 1 molecule of ATP, 4 molecules of NADH, and 1 molecule of reduced flavin adenine dinucleotide (FADH₂). The latter two serve as electron donors for mitochondrial complex I (CI or NADH:ubiquinone oxidoreductase) and complex II (CII or succinate:ubiquinone oxidoreductase) of the electron transport chain (ETC). The electrons are subsequently transported by ubiquinone to complex III (CIII or ubiquinol:cytochrome-c oxidoreductase) and by cytochrome-c to complex IV (CIV or cytochrome-c oxidase) where they react with oxygen to form water. At CI, CIII and CIV protons are expelled from the mitochondrial matrix across the mitochondrial inner membrane (MIM). This proton pumping establishes an inward-directed proton motive force (PMF) that consists of a chemical (ΔpH) and electrical ($\Delta\psi$) component. Via complex V (CV or F₁F₀-ATP synthase), protons are allowed to flow back into the matrix to fuel generation of ATP from ADP and inorganic phosphate (P_i) (Fig. 4). Together with the ETC, CV constitutes the mitochondrial oxidative phosphorylation (OXPHOS) system. Under optimal conditions, OXPHOS yields 30 molecules of ATP per glucose. However, due to the presence of uncoupling-proteins and other $\Delta\psi$ -consuming processes, the actual ATP yield is lower.

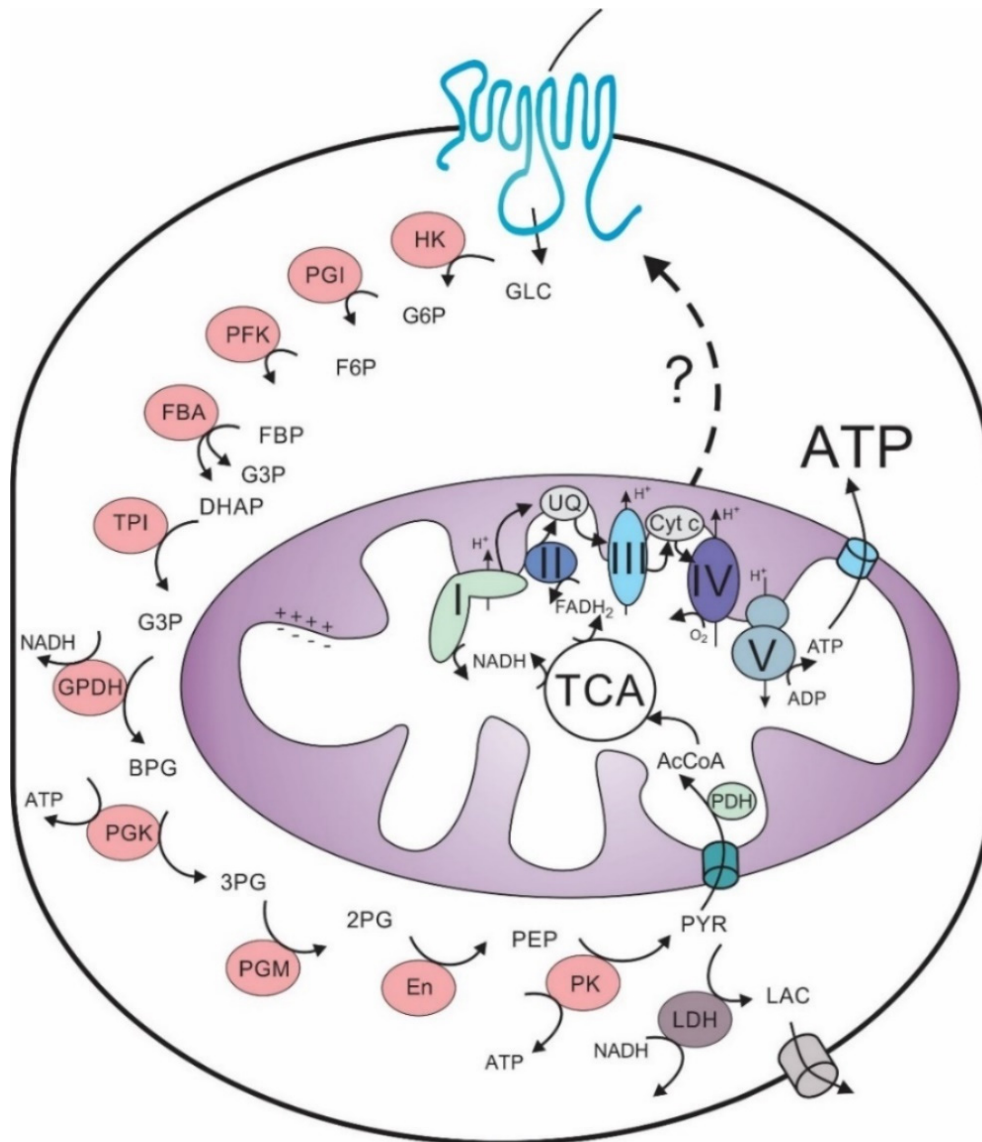


Figure 4. Schematic representation of glucose catabolic metabolism. Glucose (GLC) is taken up by GLUT and phosphorylated by hexokinase (HK) to glucose-6-phosphate (G6P). Next, G6P is converted by phosphoglucose isomerase (PGI) to fructose-6-phosphate (F6P). F6P is phosphorylated by phosphofruktokinase (PFK) to fructose 1,6-bisphosphate (FBP). FBP is broken down by fructose 1,6-bisphosphate aldolase (FBA) to dihydroxyacetone phosphate (DHAP) and glyceraldehyde 3-phosphate (G3P). DHAP is converted by triose phosphate isomerase (TPI) to G3P. G3P is converted by glyceraldehyde-3-phosphate dehydrogenase (GPDH) to 1,3-bisphosphoglycerate (BPG), yielding NADH. BPG is phosphorylated by phosphoglycerate kinase (PGK) to 3-phosphate glycerate (3PG), yielding ATP. 3PG is converted by phosphoglycerate mutase (PGM) to 2-phosphate glycerate (2PG). 2PG is converted by endolase (En) to phosphoenolpyruvate (PEP). Finally, PEP is converted by pyruvate kinase (PK) to pyruvate (PYR), yielding ATP. PYR can be converted by lactate dehydrogenase (LDH) to lactate (LAC), consuming NADH, or imported into the mitochondria by the mitochondrial pyruvate carrier (MPC), where it is converted by pyruvate dehydrogenase (PDH) to acetyl coenzyme A (AcCoA). AcCoA is oxidized within the tricarboxylic acid (TCA) cycle, yielding NADH and FADH₂, which serve as electron donors for complex I (CI) and complex II (CII). The electrons are transported by ubiquinone (UQ) to complex III (CIII) and by cytochrome-*c* (Cyt *c*) to complex IV (CIV) where they react with O₂. At CI, CIII and CIV protons are pumped across the mitochondrial inner membrane, which results in an inward-directed proton motive force. Via complex V (CV), protons flow back into the matrix to fuel generation of ATP. ATP is exported from the mitochondrial matrix by the adenine nucleotide translocator (ANT).

Mitochondrial oxidative phosphorylation dysfunction

To date, mutations in more than 240 genes encoding mitochondrial proteins have been linked to a wide variety of both multi-systemic and tissue-specific mitochondrial disorders (Thorburn, 2004, Koopman et al., 2012). The incidence of mitochondrial disease is about 1-5 in 10.000 live births (Thorburn, 2004) and the majority of mutations affect the complexes of OXPHOS system (Wallace, 1999). Isolated CI deficiency is the most common OXPHOS disorder and often presents as Leigh or Leigh-like syndrome, which is a progressive, subcortical encephalopathy (Leigh, 1951, Rahman et al., 1996). CI consist of 37 nuclear encoded and 7 mitochondrial encoded proteins, which are assembled into a ~1 MDa holo-complex. Pathogenic mutations causing isolated CI deficiency can reside in the structural components or assembly factors. Fully assembled CI comprises a peripheral NADH dehydrogenase module, an electron conducting hydrogenase module, and an integral proton pumping module (Balsa et al., 2012, Hunte et al., 2010). In the peripheral arm, electrons derived from NADH are accepted by flavin mononucleotide (FMN), transported through 8 iron-sulfur (FeS) clusters, and donated to ubiquinone. In primary skin fibroblasts from patients bearing mutations in different CI subunits, the activity of this complex ranges from 5-82% of the lowest control value (Koene et al., 2012, Verkaart et al., 2007b, Voets et al., 2012). Interestingly, this residual CI activity does not correlate with clinical features in patients. This can at least in part be attributed to differences in genetic background, the presence of compensatory mechanisms, and differences in energy demand (Koopman et al., 2012). Besides inherited disorders, OXPHOS dysfunction has been linked to a number of age-related diseases such as Parkinson's disease, Alzheimer's disease, amyotrophic lateral sclerosis (ALS), diabetes type II, and cancer (Breuer et al., 2013a, Chandra and Singh, 2011, Martin, 2011, Ritov et al., 2010, Swerdlow, 2012).

Cellular biochemical consequences of OXPHOS dysfunction are among others reduced mitochondrial membrane potential ($\Delta\Psi$), aberrant calcium and ATP homeostasis, aberrations in mitochondrial structure, and increased mitochondrial reactive oxygen species (ROS) levels (Blanchet et al., 2011). Correlation of these and other biochemical parameters obtained from primary CI patient skin fibroblasts revealed that fibroblasts from patients with a lower age of disease

onset and death, displayed a larger reduction in CI activity, a larger increase in mitochondrial fragmentation, lower cellular levels of OXPHOS proteins, and a larger increase in ROS levels (Blanchet et al., 2011). In the following sections, mitochondrial ROS production and its role in the regulation of glucose uptake will be discussed.

Mitochondrial ROS production

To prevent generation of excessive mitochondrial ROS and induction of oxidative stress, mitochondria possess powerful antioxidant systems. One of these consists of manganese-dependent superoxide dismutase (MnSOD or SOD2), an enzyme that is localized in the mitochondrial matrix and rapidly converts superoxide to hydrogen peroxide. This conversion is also catalyzed by the copper/zinc-dependent superoxide dismutase (Cu/ZnSOD or SOD1), which is localized in the cytosol, nucleus and mitochondrial intermembrane space (Murphy, 2009, Tyler, 1975, Weisiger and Fridovich, 1973). In turn, hydrogen peroxide can be converted into water by the action of catalases that are mainly located in the peroxisomes and also in mitochondria (Salvi et al., 2007). However, within mitochondria, hydrogen peroxide is mainly removed by the action of glutathione peroxidase-1 (Gpx1) (Cox et al., 2010, Esposito et al., 2000, Esworthy et al., 1997), peroxiredoxins 3 and 5 (Prx3 and Prx5) and the thioredoxin-2 (Trx2) system (Chae et al., 1999, Chang et al., 2004, Cox et al., 2010), which require glutathione (GSH). Oxidized GSH (GSSG) is recycled to GSH by the action of glutathione reductase. Similarly, oxidized Trx2 is recycled by Trx reductase. Both of these systems require NADPH (Arner, 2009, Carlberg and Mannervik, 1985), which is regenerated in the cytosol by glucose-6-phosphate-dehydrogenase (G6PDH) via the PPP (Le Goffe et al., 2002). Alternatively, NADPH can be regenerated in the mitochondrial matrix by nicotinamide nucleotide transhydrogenase (NNT), which uses NADH and the PMF (Hatefi and Yamaguchi, 1996, Rydstrom, 2006, Yin et al., 2012). When mitochondrial ROS production exceeds the capacity of the cell's antioxidant systems or when the latter systems are less active, increased ROS levels can induce cell damage (oxidative stress). In principle, superoxide can react with protein FeS clusters (Liochev and Fridovich, 1994), which, in the presence of hydrogen peroxide, induce generation of hydroxyl radicals (Fenton reaction). The latter are highly reactive and can damage lipids, proteins, and DNA (Martinez-Reyes and Cuezva, 2014, Valko et al., 2006). Given the fact that iron is effectively sequestered

(Kakhlon and Cabantchik, 2002), the relevance of the Fenton reaction is not fully established *in vivo*. Superoxide can react with NO to form peroxynitrite (ONOO⁻) (Pacher et al., 2005). When rising too high, hydrogen peroxide can induce over-oxidization of cysteine residues from sulfenic acid (-SO⁻) to sulfinic acid (-SO₂H) and sulfonic acid (-SO₃H). In case of CI, such over-oxidation is associated with irreversible deactivation of CI (Hurd et al., 2008, Mailloux et al., 2014). In general, if ROS levels exceed a certain threshold, they will impair OXPHOS complexes and further stimulate ROS production (Galloway and Yoon, 2012). In the light of the above, it is not surprising that increased ROS levels, although not always oxidative stress, are observed during various pathological conditions. For example, primary fibroblasts derived either from CI deficient mice or patients show increased ROS levels, but no obvious signs of oxidative stress (Koopman et al., 2007, Valsecchi et al., 2013, Verkaart et al., 2007a, Verkaart et al., 2007b). Increased ROS levels also have been observed in multiple types of cancer (e.g., prostate, colorectal, ovarian, pancreatic, breast, liver, bladder, melanoma, glioma), neurodegenerative diseases (e.g., Alzheimer's disease and Parkinson's disease), and during insulin-resistance and diabetes (Afanas'ev, 2011, Freeman et al., 2006, Kumar et al., 2008, Pi and Collins, 2010, Sabens Liedhegner et al., 2012, Sanchez-Gomez et al., 2013).

Regulation of glucose uptake by mitochondrial ROS

Mitochondrial OXPHOS dysfunction triggers several adaptive responses. One of these is an increase in the rate of glucose uptake and glycolysis (Wu and Wei, 2012). Stimulation of cellular glucose uptake is frequently observed during conditions of oxidative stress. Exogenous addition of hydrogen peroxide stimulates glucose uptake in skeletal muscle (Higaki et al., 2008, Jensen et al., 2008, Kim et al., 2006), C2C12 myoblasts, clone 9 liver cells, and 3T3 fibroblasts (Prasad and Ismail-Beigi, 1999). Upon electrical stimulation, endogenous ROS also induced an increase in glucose uptake in muscle cells (Merry et al., 2010, Pinheiro et al., 2010). Below we will discuss the role of ROS in the regulation of glucose uptake at the level of GLUT transcription, GLUT translocation, and GLUT activation.

Transcriptional regulation of GLUT expression by ROS

Protein expression levels of human GLUT1 are controlled by a promoter region and several putative enhancer regions that contain binding sites for various transcription factors including specificity proteins (Sp1) (Vinals et al., 1997) and hypoxia-inducible factor-1 (HIF-1) (Ebert et al., 1995). Mild oxidative stress induced by either glucose/glucose oxidase (Glc/GO) or xanthine/xanthine oxidase (Xan/XO) has been shown to up-regulate GLUT1 expression by increasing the transcription rate and mRNA stability leading to increased GLUT1 protein and glucose transport activity (Kozlovsky et al., 1997). As far as we know, there is no experimental evidence demonstrating the involvement of Sp1 in ROS-induced stimulation of GLUT1 expression, and therefore, we here focus on the role of HIF-1.

HIF-1 consists of two subunits, HIF-1 α and HIF-1 β . Under normoxic conditions, prolines within the oxygen-dependent degradation domains (ODDs) of HIF-1 α are hydroxylated by prolyl-4-hydroxylases (PHDs) (Ivan et al., 2001). This hydroxylation acts as an ubiquitination signal leading to proteasomal degradation of HIF-1 α . In the absence of oxygen, HIF-1 α ubiquitinylation is inhibited allowing its interaction with HIF-1 β to drive transcription of various target genes, including GLUT1 (Hayashi et al., 2004, Iyer et al., 1998, Oquidid et al., 1999, Wood et al., 1998). During hypoxia, ROS levels increase and play an important role in HIF-1 α stabilization (Brunelle et al., 2005, Chandel et al., 2000, Guzy et al., 2005, Mansfield et al., 2005, Sanjuan-Pla et al., 2005, Schroedl et al., 2002). Preventing ROS-mediated HIF-1 α stabilization represses GLUT1 expression and glucose uptake in Lewis lung carcinoma, HT-29 colon, and T47D breast cancer cells (Jung et al., 2013). Upon mitochondrial DNA depletion (Chandel et al., 2000, Mansfield et al., 2005) and in mouse embryonic fibroblasts (MEFs) lacking cytochrome-c (Mansfield et al., 2005), hypoxia-induced HIF-1 α stabilization is abrogated. This suggests that hypoxia-induced ROS are of mitochondrial origin. Knockout of the Rieske iron-sulfur protein (RISP) in mitochondrial CIII decreases ROS production during hypoxia and attenuates hypoxic stabilization of HIF-1 α (Guzy et al., 2005). Therefore, RISP-mediated mitochondrial ROS production appears to be involved in HIF-1 α stabilization during hypoxia. At the RISP site, electrons are transferred one-by-one from ubiquinol to cytochrome-c1. This one-electron donation generates a highly reactive ubisemiquinone, which can act as a source for superoxide generation. Over-expression of catalase (Chandel et al., 2000, Guzy et al., 2005) or GPx1

(Brunelle et al., 2005, Emerling et al., 2005) abolishes HIF-1 α stabilization during hypoxia, whereas over-expression of SOD1 or SOD2 does not (Brunelle et al., 2005, Guzy et al., 2005). In addition, exogenous hydrogen peroxide is sufficient to stabilize HIF-1 α under normoxic conditions (Chandel et al., 2000, Jung et al., 2008, Mansfield et al., 2005). This suggests that the stabilization of HIF-1 α primarily involves hydrogen peroxide via inactivation of PHDs (Fig. 5) and subsequent reduction of HIF-1 α ubiquitinylation (Chandel et al., 1998, Guzy and Schumacker, 2006). However, HIF-1 α ubiquitinylation is incompletely blocked by exogenous or hypoxia-derived hydrogen peroxide (Guzy et al., 2005), suggesting the involvement of additional mechanisms.

Alternatively, ROS-induced HIF-1 α stabilization was proposed to be mediated by specific signaling routes. Phosphoinositide 3-kinase (PI3K) appears to be involved in HIF-1 α stabilization by mitochondrial ROS in Hep3B cells (Fig. 5; arrow 1) (Chandel et al., 2000). Compatible with this mechanism, PI3K inhibition lowered GLUT1 transcription under hypoxic and normoxic conditions (Chen et al., 2001). In addition, both p38 mitogen-activated protein kinase (MAPK p38) and its upstream kinases MKK3/6 are activated by hypoxia-derived ROS and are essential in HIF-1 α stabilization and the ensuing increase in GLUT1 mRNA levels (Emerling et al., 2005). Activation of MAPK p38 by ROS is mediated by apoptosis signal-regulating kinase 1 (ASK1), which is normally bound to Trx. Oxidation of Trx releases ASK1 leading to activation of its downstream targets MKK3, MKK4, MKK6 and MMK7 and subsequently JNK and MAPK p38 (Nagai et al., 2007). Also, AMP-activated protein kinase (AMPK) can be activated by ROS during hypoxia (Emerling et al., 2009). This protein plays a key role in energy metabolism and cellular adaptation to ROS (Wu et al., 2014). Various metabolic stress conditions can activate AMPK through phosphorylation of Thr172 by upstream kinases such as LKB1 (Hardie, 2011). In addition, AMP-interaction stimulates AMPK activation by promoting AMPK phosphorylation, preventing AMPK dephosphorylation, and inducing allosteric activation of AMPK (Davies et al., 1995, Hardie and Ashford, 2014). Oxidative stress can inhibit the ETC, potentially leading to an increased AMP:ATP ratio (Hawley et al., 2010). However, under hypoxic conditions, AMPK is also activated by mitochondrial ROS in an LKB1-dependent and AMP:ATP-independent manner (Emerling et al., 2009, Mungai et al., 2011). In muscle cells, AMPK activation stimulated GLUT1 expression and twofold increased cellular glucose uptake (Fryer

et al., 2002). Besides activation of HIF-1 α , AMPK can up-regulate GLUT1 via degradation of thioredoxin-interacting protein (TXNIP) (Fig. 5; arrow 1). TXNIP reduces the level of GLUT1 mRNA in the nucleus. TXNIP is degraded upon Ser308 phosphorylation by AMPK, leading to increased GLUT1 mRNA and protein levels (Wu et al., 2013).

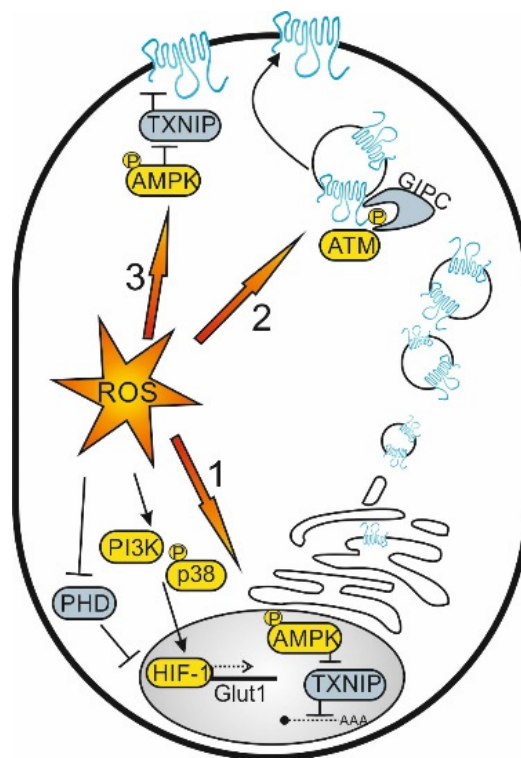


Figure 5. Glucose uptake can be regulated by: (1) altering the expression level of GLUTs, (2) stimulating translocation of GLUTs from internal vesicles to the plasma membrane and (3) changing the intrinsic activity of GLUTs at the plasma membrane. Proteins that are activated by ROS are depicted in yellow. ATM, ataxia telangiectasia mutated; GIPC, G α -interacting protein-interacting protein C-terminus; HIF-1, hypoxia-inducible factor 1; P-AMPK, phosphorylated (activated) AMP-activated protein kinase; PHD, prolyl hydroxylase domain; P-p38, phosphorylated (activated) p38 mitogen-activated protein kinase; PI3K, phosphoinositide 3-kinase, ROS, reactive oxygen species, TXNIP, thioredoxin-interacting protein.

Regulation of GLUT-vesicle translocation to the plasma membrane by ROS

The cellular capacity for glucose uptake is co-determined by the abundance of functional GLUTs at the plasma membrane. This means that glucose uptake can be regulated by GLUT trafficking between the cytosol and the plasma membrane. During exercise, muscle contraction is associated with increased ROS levels, believed to represent a fast adaptive response to an increase in energy demand (Chambers et al., 2009, Murrant et al., 1999, Wretman et al., 2001). In these cells,

endogenous (*i.e.*, those induced by contraction) and exogenous ROS stimulate glucose uptake via a mechanism involving activation of Akt and/or AMPK (Higaki et al., 2008, Sandstrom et al., 2006, Toyoda et al., 2004). ROS can activate Akt (Fernandes et al., 2011, Niwa et al., 2003), which probably involves inactivation of cysteine-based phosphatases (Okoh et al., 2011). ROS can activate AMPK by modification of cysteine residues on its α -catalytical subunit (Zmijewski et al., 2010). Once activated, Akt and AMPK phosphorylate TBC1D4 and TBC1D1, leading to GLUT4 translocation (Geraghty et al., 2007, Kramer et al., 2006, Taylor et al., 2008, Thong et al., 2007).

Translocation of GLUT1 to the plasma membrane (Fig. 5; arrow 2) is regulated by ataxia telangiectasia mutated (ATM) (Andrisse et al., 2013). This protein is a member of the family of phosphatidylinositol-3-kinase-related protein kinases (PIKKs) and plays an important role in the response to DNA damage after which it becomes phosphorylated. However, ATM can also localize to the cytosol where it is activated by ROS and involved in cytosolic signaling (Alexander and Walker, 2010). ATM is thiol-oxidized by ROS to form an active dimer of two covalently linked monomers (Guo et al., 2010). Activated ATM localizes near mitochondria and mitochondria are necessary for ROS-induced ATM activation (Morita et al., 2014). This suggests that ATM dimerization and activation are stimulated by mitochondrial ROS. Evidence was provided that ATM is activated by ROS during treatment with the chemotherapeutic agent doxorubicin (Kurz et al., 2004). In muscle, ATM activation by doxorubicin mediates targeting of GLUT1 to the cell surface by phosphorylation of GLUT1 at S490. This serine residue is part of a C-terminal PDZ motif, and phosphorylation of this residue induces interaction of GLUT1 with the PDZ-interacting protein, G α -interacting protein and C-terminus (GIPC1) (Andrisse et al., 2013). GIPC1 interaction promotes GLUT1 trafficking to the cell surface and stimulates glucose uptake (Fig. 5; arrow 2) (Wieman et al., 2009).

Regulation of GLUT1 activity at the plasma membrane by ROS

Regulation of glucose uptake can also occur directly at the plasma membrane. This type of regulation occurs on a relatively short-term time scale (*i.e.*, within 1 hour) and represents a relatively fast mechanism that allows the cells to cope with metabolic stress (Fig. 5; arrow 3). The intrinsic activity of GLUTs can be modulated by conformational changes or posttranslational modifications that increase

glucose affinity (Asano et al., 1991, Levine et al., 2002). In addition, V_{max} can be modulated by activation or deactivation of GLUTs at the plasma membrane. A number of metabolic inhibitors and AMPK activators acutely stimulate glucose uptake without increasing the amount of GLUT molecules at the plasma membrane (Abbud et al., 2000, Barnes et al., 2002, Hamrahian et al., 1999, Shetty et al., 1993, Shi et al., 1995). It was proposed that this increase is due to the release of 'masking proteins', which display an inhibitory interaction with the GLUT cytoplasmic domain under basal conditions (Shi et al., 1995). Stomatin was proposed being a masking protein as it interacts with the C-terminus of GLUT1, and its over-expression reduces GLUT1 intrinsic activity (Rungaldier et al., 2013, Zhang et al., 2001). Another potential masking protein is TXNIP, which displays an inhibitory interaction with GLUT1 (Wu et al., 2013). AMPK-induced degradation of TXNIP (see previous section) would unmask GLUT1 leading to enhancement of GLUT1-mediated glucose influx (Fig. 5; arrow 3). Although stimulation of GLUT intrinsic activity is often observed during metabolic stress, the role of ROS in this pathway is still incompletely understood. In a leukemic cell line, ROS generated by NAD(P)H oxidase (Nox) stimulated glucose uptake via Src-mediated phosphorylation of GLUT1 (Prata et al., 2008). On the other hand, antioxidants were ineffective in preventing GLUT1 activation during azide-induced CIV inhibition (Hamrahian et al., 1999). Taken together, various signaling pathways have been implied in the stimulation of glucose uptake as an adaptive response during oxidative stress (Fig. 5). At a relatively slow timescale, ROS-induced signals stimulate glucose uptake via up-regulation of GLUT protein expression. Rapid stimulation of glucose uptake can occur at the level of GLUT translocation and regulation of GLUT intrinsic activity. Interestingly, several of the signaling proteins are ROS-sensitive (*i.e.*, AMPK and TXNIP) and involved in both slow and fast responses. This suggests that ROS-induced stimulation of glucose uptake is part of a (adaptive) mechanism triggered by oxidative and/or metabolic stress.

The role of glucose in ROS scavenging

The above evidence supports the conclusion that increased ROS levels stimulate cellular glucose uptake both at slow and fast time scales. However, inhibition of GLUT1 activity in myoblasts was paralleled by increased ROS levels (Andrisse et al., 2014). This might indicate that glucose uptake also plays a role in regulating the balance between ROS production and scavenging, suggesting that glucose uptake must be tightly controlled to maintain cellular energy homeostasis and redox status. Glucose entry into the PPP is protective against hydrogen peroxide-induced cytotoxicity (Le Goffe et al., 2002). Mechanistically, this protection is probably due to an increased PPP flux, leading to a higher NADPH/NADP⁺ ratio and GSH level. Compatible with this hypothesis, skin fibroblasts derived from patients with myoclonic epilepsy with ragged red fibers (MERRF; a syndrome that has been associated with a mutation in the tRNA^{Lys} gene of mtDNA) displayed GLUT1 up-regulation and increased NADPH and GSH levels (Wu and Wei, 2012). Preventing this NADPH increase induced ROS over-production and cell death (Wu and Wei, 2012). Glucose entry into the PPP and subsequently increased levels of NADPH is stimulated by ATM-induced activation of G6PD, which is the first and rate determining enzyme of the PPP (Cosentino et al., 2011). In a *Drosophila* model for Huntington's disease, which is particularly vulnerable to oxidative stress, overexpression of G6PD in neurons increased the tolerance to hydrogen peroxide (Besson et al., 2015). This increased tolerance was proposed to be mediated by increased activity of NADPH-dependent antioxidant systems because overexpression of *Drosophila* homologues of Prx2 and Trx significantly extended the flies lifespan. Moreover, GLUT1 contributes to ROS scavenging by mediating the transport of dehydroascorbic acid (DHA), the oxidized form of vitamin C, which is recycled back to vitamin C inside the cell (Rumsey et al., 1997, Guaiquil et al., 2001). Vitamin C is a potent antioxidant, which can prevent oxidative cell death (Guaiquil et al., 2001). Experimental evidence suggests that GLUT1 also co-localizes with mitochondria to facilitate mitochondrial uptake of DHA and quench ROS induced by mitochondrial uncoupling (Kc et al., 2005). In summary, enhanced PPP glucose entry and GLUT-mediated antioxidant uptake appear to be relevant for cellular ROS removal.

Aim and outline of this thesis

The aim of this thesis is to assess the role of cellular glucose uptake in mitochondrial OXPHOS dysfunction. This aim was addressed by studying: (i) the effect of pharmacologically or genetically induced CI dysfunction on the rate of glucose uptake and consumption, (ii) how glucose uptake stimulation affects the glycolytic ATP production, and (iii) the mode of regulation of glucose uptake in CI/CIII-inhibited myoblasts. **Chapter 2** provides an overview of available fluorescent glucose sensors and their applications. In **Chapter 3** the development of a microscopy protocol for live-cell quantitative glucose uptake measurements is presented. Using this protocol, the kinetic parameters of glucose uptake and consumption in CI- and CIII-inhibited C2C12 myoblasts are determined and used to construct a mathematical model, which allows prediction of the glycolytic flux and ATP production. **Chapter 4** focusses on glucose uptake in primary skeletal muscle myoblasts from *Ndufs4* knockout mice and how this parameter is affected by different culturing conditions. **Chapter 5** explains the mechanism by which CI- and CIII-inhibition regulates glucose uptake in C2C12 myoblasts. In **Chapter 6**, the obtained results are integrated and discussed in a broader perspective.

CHAPTER 2

Quantitative glucose sensing in mammalian cells



Adapted from:

Dania C. Liemburg-Apers, Hiromi Imamura, Marleen Forkink, Marco Nootboom, Herman G. Swarts, Roland Brock, Jan A. M. Smeitink, Peter H. G. M. Willems and Werner J. H. Koopman

Pharm Res. (2011) 28(11):2745-5

Abstract

The functioning and survival of mammalian cells requires an active energy metabolism. The monosaccharide glucose constitutes a key source of cellular energy. Following its import across the plasma membrane glucose is converted into pyruvate by the glycolysis pathway. Pyruvate oxidation supplies substrates for the ATP-generating mitochondrial oxidative phosphorylation (OXPHOS) system. To gain cell-biochemical knowledge about the operation and regulation of the cellular energy metabolism in the healthy and diseased state, quantitative knowledge is required about (changes in) metabolite concentrations under (non) steady-state conditions. This information can for instance be used to construct more realistic *in silico* models of cell metabolism, which facilitates understanding the consequences of metabolic dysfunction as well as on- and off-target effects of mitochondrial drugs. Here we review the current state-of-the-art concerning the live-cell quantification of the key cellular metabolite glucose, using protein-based sensors that apply the principle of FRET (fluorescence resonance energy transfer). We further summarize the properties and applications of the FRET-based sensors, their calibration, pitfalls and future perspectives.

Introduction

Energy availability in a living cell depends on the balance between energy production by breakdown of biomolecules (catabolism) and energy demand. This balance constitutes part of a cell's metabolism, which involves a large collection of molecular intermediates (metabolites). The concentration of metabolites continually changes in time and/or space in response to alterations in the cellular environment and metabolic activity. Within cells, adenosine triphosphate (ATP) is the most important energy currency. ATP hydrolysis yields adenosine diphosphate (ADP) and inorganic phosphate (P_i), providing the energy that fuels numerous cellular processes. In most cells, ATP is generated by the metabolic conversion of the monosaccharide glucose, which is taken up from the extracellular environment. In this sense, glucose is a key player in cellular metabolism. We present how protein-based sensors can be used to quantify the (sub)cellular concentration of glucose and discuss sensor calibration, possible pitfalls and future perspectives.

Quantification of glucose levels in living cells

Principles of FRET

For the purpose of quantifying glucose in different cellular compartments, a variety of protein-based metabolite sensors are available (Deuschle et al., 2006, Deuschle et al., 2005a, Deuschle et al., 2005b, Fehr et al., 2003, Fehr et al., 2005). Sensors that are based on the same principle are available for lactate, pyruvate, maltose, ribose, citrate, glutamate, and ATP (Berg et al., 2009, Ewald et al., 2011, Imamura et al., 2009, Okumoto et al., 2008, San Martin et al., 2014, San Martin et al., 2013, Tsuboi et al., 2004, Deuschle et al., 2005b). The detection principle of most of these reporter molecules is based on the principle of Fluorescence Resonance Energy Transfer (FRET). FRET is the distance- and orientation-dependent (non-radiative) transfer of energy, which can occur between a fluorescent donor molecule and a fluorescent acceptor molecule. FRET (donor→acceptor) only takes place if donor and acceptor are very close to each other (*i.e.* within 1-10 nm). For FRET to happen, the emission spectrum of donor needs to partially overlap with the absorption spectrum of the acceptor. FRET

efficiency (E) is given by $E = R_0^6 / (R_0^6 + r^6)$, with r being the distance between donor and the acceptor, and R_0 (the Förster distance) being the distance of half-maximal FRET efficiency. If the wavelength is expressed in nm and $J(\lambda)$ is in units of $M^{-1} \cdot cm^3$, the Förster distance (in Å) for a FRET pair is given by: $R_0 = 9.78 \cdot 10^3 \cdot [\kappa^2 \cdot n^{-4} \cdot Q_D \cdot J(\lambda)]^{1/6}$ (Lakowicz, 2006). In this equation κ^2 is a factor describing the relative orientation in space of the transition dipoles of the FRET pair (typically assumed to be 2/3), n is the refractive index, Q_D is the quantum-yield of the donor (*i.e.* the ratio of the number of photons emitted to the number absorbed), and $J(\lambda)$ represents the overlap-integral, which accounts for the degree of overlap between the emission and absorption spectra of the donor and acceptor, respectively.

A 'good' FRET pair contains a donor with a high quantum-yield, contains an acceptor with a large molecular extinction coefficient, displays maximal overlap between the donor emission and acceptor absorption spectrum, and displays minimal excitation of the acceptor at the maximal excitation wavelength of the donor. In many biosensors, (variants of) enhanced cyan fluorescent protein (ECFP) and yellow fluorescent protein (EYFP) are used as (donor→acceptor) FRET pairs. The ECFP-EYFP pair has an R_0 of ~5.5 nm. By fusing ECFP and EYFP to the N- and C-termini (or *vice versa*) of a suited metabolite-sensing protein, metabolite-induced conformational changes in the sensing protein will induce changes in the ECFP→EYFP FRET signal. In this sense, metabolite binding and unbinding are associated with opposite changes in FRET efficiency that can be visualized as changes in ECFP and EYFP emission intensity by fluorescence microscopy. For instance, in case of a sensor in which metabolite binding increases FRET efficiency, increased FRET is associated with a lower ECFP and higher EYFP fluorescence intensity, and decreased FRET is associated with higher ECFP and lower EYFP fluorescence intensity. By taking the ratio between the EYFP and ECFP emission signals, a quantitative measure of FRET is obtained.

When using FRET-based biosensors for single cell imaging, it is critical to obtain a signal with a high signal-to-noise ratio. This means that the donor and acceptor fluorescence signals need to be well above aspecific (background) fluorescence levels, which can arise from cellular autofluorescence, to prevent that small FRET changes are obscured by background noise. Additionally, the biosensor will display large FRET changes upon concentration changes of the to-be-detected biomolecule. This means that maximizing the dynamic range of the FRET sensor is

of crucial importance. To achieve the latter, one strategy is the use of 'improved' versions of CFP (*e.g.*, Cerulean, super-enhanced CFP) and YFP (*e.g.*, Venus, Citrine) because the FRET efficiency generally depends on the photo-physical properties of the donor and acceptor fluorophores.

FRET-based biosensors for glucose sensing

Bacterial periplasmic binding proteins (PBPs) have been applied as sensing proteins in FRET-based biosensors. PBPs display a high affinity for specific metabolites and possess considerable similarity at the level of their tertiary structure. PBPs consist of two globular domains that are connected by a hinge region. Substrate binding occurs in the cleft between the two domains and the substrate is engulfed via a hinge-twist motion, leading to a major conformational change in the protein. By flanking the PBP with a donor and acceptor fluorescent protein, the conformational change occurring in the PBP is translated into a change in FRET. The PBP family can be divided into two classes. In type I PBPs, the N- and C-terminus are located at the proximal ends of the globular domains. Upon substrate binding, the termini and fluorophores in the sensor, move further apart from each other and FRET is decreased (Fehr et al., 2003). In type II PBPs, the termini are located at the distal ends of the globular domains and move closer to each other upon substrate binding, leading to an increase in FRET. The majority of the FRET-based glucose biosensors use the periplasmic glucose/galactose-binding protein (GGBP) from the bacterium *E. coli* for glucose sensing. GGBP is a type I PBP and is involved in chemotaxis towards glucose and galactose in many bacteria. So GGBP is able to detect both glucose and galactose, but its affinity for glucose is approximately two times higher compared to galactose (Fehr et al., 2003). Although the precise galactose concentration in cells is not firmly established, the plasma galactose concentration in healthy humans (0.17 mM) is far below that of blood glucose (5 mM). GGBP-based glucose sensors do not respond to the glycolysis-inhibitor 2-deoxy-D-glucose (2-DG) (Fehr et al., 2003).

Table 1. Properties of FRET-based glucose biosensors.

Sensor name	K _d (μM) [%]	Range (μM) [§]	Ratio change ^{&}	FRET pair ^{&&}	Reference
FLIPglu-170n	0.17	0.02 - 1.5	-0.23	EYFP → EYFP	(Fehr et al., 2003)
FLIPglu-600 μ	590	65 - 5301	-0.29	EYFP → EYFP	(Fehr et al., 2003)
FLIPglu-600 $\mu\Delta$ 13	590	n.r.	-0.7	EYFP → EYFP	(Deuschle et al., 2005b)
FLI ¹² Pglu600 μ	583	n.r.	2.66	EYFP → Citrine	(Deuschle et al., 2005b)
FLIPglu-3.2m Δ 13	3200	n.r.	-0.6	EYFP → EYFP	(Deuschle et al., 2005a)
FLIPglu-2 $\mu\Delta$ 13	2	n.r.	-0.8	EYFP → EYFP	(Deuschle et al., 2005a)
FLI ¹² Pglu-700 $\mu\delta$ 6	660	50 - 9600	2.3	EYFP → Citrine	(Takanaga et al., 2008)
FLIPglu-30 $\mu\Delta$ 13	28.5	n.r.	n.r.	EYFP → Venus	(Takanaga and Frommer, 2010)
FLIPglu-control (CT)	>100.000	n.a.	n.a.	EYFP → EYFP	(Fehr et al., 2003)

[%]Determined *in vitro*.

[§]Dynamic detection range.

[&]Maximal ratio change determined *in vitro*. This value might vary with experimental conditions. Positive values indicate that FRET efficiency is increased upon glucose binding. Negative values indicate that FRET efficiency is decreased upon glucose binding.

^{&&}Donor→Acceptor FRET pair.

n.a., not appropriate, n.r., not reported in the cited reference.

One of the first FRET-based glucose sensors consisted of a GGBP flanked by ECFP and EYFP and was designated "fluorescence indicator protein for glucose with an *in vitro* K_d of 170 nM" ("FLIPglu-170n"; Table 1). This sensor contains the wild-type GGBP, displaying a relatively high affinity for glucose. However, the blood glucose concentration is much higher (see previous section) and, therefore, intracellular glucose levels might be far above the K_d of FLIPglu-170n.

To allow quantification of higher glucose levels, Phe16 in GGBP was mutated into an alanine. This reduced the substrate affinity of GGBP, resulting in a sensor with a K_d of 590 μ M, (FLIPglu-600 μ ; Table 1). Relative to FLIPglu-170n, FLIPglu-600 μ also displayed a somewhat higher maximum EYFP/ECFP ratio change and increased glucose specificity. A "control" sensor was generated by mutating aspartic acid at position 236 in GGBP to an alanine, leading to greatly decreased glucose sensitivity ("FLIPglu-control (CT)"; $K_d \geq 100$ mM; Table 1).

To further increase the maximum ratio change of FLIPglu-600 μ , two strategies were applied to reduce the rotational freedom of its two fluorophores (Deuschle et al., 2005b). In a first approach, the sensor-structure was made more rigid by deleting various amino acids of the 'composite linkers', being the less well-structured sequences connecting the fluorophores to the GGBP. The mutant with a deletion of 15 amino acids in the N-terminal linker and 16 amino acids in the C-terminal linker, named FLIPglu-600 $\mu\Delta$ 13, showed the highest increase in maximum ratio change relative to FLIPglu-600 μ (Table 1). The second approach involved the insertion of ECFP into the backbone of GGBP to decrease its rotational freedom. Additionally, EYFP was replaced by Citrine, a YFP mutant which is less pH- and chloride-sensitive than EYFP and displays an increased *in vivo* folding efficiency (Griesbeck et al., 2001). The resulting sensor, 'fluorescent indicator - ECFP insertion at position 12 - protein for glucose with an *in vitro* K_d of 590 μ M' (FLII¹²Pglu-600 μ), displayed the highest increase in maximum ratio change compared to FLIPglu-600 μ (Table 1).

In an attempt to increase the maximum ratio change even further, various amino acid deletions were created in the composite linker between GGBP and Citrine of FLII¹²Pglu-600 μ (Takanaga et al., 2008). The mutant in which only the six amino acids of the synthetic linker between GGBP and Citrine were removed (FLII¹²Pglu-700 $\mu\delta$ 6), displayed the highest *in vivo* ratio change relative to FLII¹²Pglu-600 μ (Table 1). Furthermore, by mutating the GGBP a range of affinity mutants was

engineered (*i.e.* FLIPglu-170n Δ 13, FLIPglu-2 μ Δ 13, FLIPglu-3.2m Δ 13, FLIPglu-30 μ Δ 13) to cover a wide range of glucose affinities (Table. 1). In case of FLIPglu-30 μ Δ 13, EYFP was replaced by a mutant variant (Venus), which displays improved *in vivo* maturation (Nagai et al., 2001).

Application of FRET-based glucose sensors

The glucose sensors introduced above have been applied in a collection of mammalian cell lines to assess steady-state glucose levels and flux rates under a variety of experimental conditions. For instance, FLIPglu-600 μ was used to analyze glucose dynamics in the cytosol of COS-7 cells (Fehr et al., 2003). It was found that this sensor responded rapidly to changes in extracellular glucose concentration in a reversible manner. Using the *in vitro* K_d of FLIPglu-600 μ , the cytosolic glucose concentration in COS-7 was estimated to be generally 50% lower than the extracellular glucose concentration. This suggests that glucose is metabolized at a high rate in these cells. In C2C12 muscle cells, the FLIPglu-600 μ sensor revealed a higher glucose concentration near the plasma membrane and a lower perinuclear concentration (John et al., 2008). The latter might be due to the presence of hexokinase (HK) bound to perinuclear mitochondria. When C2C12 cells were cultured in a medium with a high-glucose concentration (25 mM), cytosolic glucose levels were lower than when cells were cultured in a low-glucose medium (<5 mM). High external glucose levels reduced the rate of glucose uptake in Chinese hamster ovary (CHO) cells, suggesting downregulation of GLUT1. In these cells, the cytosolic glucose concentration was maintained at ~1 mM when extracellular glucose concentration equaled 10 mM (John et al., 2008). In CHO cells displaying a low glucose uptake rate, cytosolic glucose accumulation was observed upon glycolysis inhibition by iodoacetate (IAA). Glucose uptake was not affected by glycolysis inhibition. Upon removal of extracellular glucose there was little glucose clearance, suggesting that glucose efflux is absent. In contrast, in cells displaying a high glucose uptake rate, less glucose accumulation was observed upon inhibition of glycolysis (John et al., 2008). When human embryonic kidney (HEK) cells were cultured in a high-glucose medium, the rate of decrease in cytosolic glucose concentration was increased in response to acute changes in extracellular glucose concentration, suggesting that glycolytic enzymes are more active in these

cells (John et al., 2008). When cells were pre-cultured in a high-glucose medium, acute lowering of the extracellular glucose concentration increased cytosolic glucose levels, possibly by stimulating the generation of glucose from non-carbohydrate carbon substrates (*i.e.* gluconeogenesis) (John et al., 2008). Conversely, cells pre-cultured in a low-glucose medium displayed a decrease in intracellular glucose level upon acutely increasing the extracellular glucose level, suggesting that glycolysis is stimulated by low external glucose. Taken together, the above findings suggest a mechanism in which glucose homeostasis is dynamically controlled by alterations in glucose transport and metabolism. This mechanism might serve to prevent toxic effects of too high cytosolic glucose as well as to prevent the glucose level from dropping below the K_m of HK.

FLIPglu-600 μ was also applied to measure glucose fluxes between the endoplasmic reticulum (ER) and cytosol (Fehr et al., 2005). To this end, FLIPglu-600 μ was modified to contain ER targeting and retention signals. No differences between the cytosolic and ER glucose concentration were observed. Similarly, the glucose flux rate across the ER membrane and plasma membrane did not differ. However, when a high-affinity glucose sensor was used (FLIPglu-30 $\mu\Delta$ 13) and measurements were carried out in low-glucose medium, the steady state glucose concentration, as well as the glucose flux rate across the ER membrane and plasma membrane were different (Takanaga and Frommer, 2010). The latter study also revealed that, following their biosynthesis in the ER, GLUTs were active during their transport to the plasma membrane and mediated glucose transport over the ER membrane. In 3T3-L1 fibroblasts, FLIPglu-600 μ was used to monitor cytosolic glucose dynamics under conditions of inhibited glycogen synthesis (Chowdhury et al., 2014). The increase in cytosolic free glucose induced by insulin was approximately 10-fold higher in cells with inhibited glycogen synthase activity, which was proposed to be mediated by an imbalance between the glucose uptake and the use of glucose for glycogen synthesis.

Using FLI¹²Pglu-700 $\mu\delta$ 6, the glycolytic rate was investigated in fibroblasts, adipocytes, myoblasts, astrocytes, neurons, and HeLa cells (Bittner et al., 2010). To this end, glucose transport across the plasma membrane was reduced either by lowering the extracellular glucose concentration or by specifically inhibiting GLUTs. Average glycolytic rates were demonstrated to be higher in undifferentiated cells (C2C12 myoblasts and 3T3-L1 fibroblasts) and tumor cell

lines (HeLa cells) than in astrocytes, neurons, and differentiated 3T3-L1 adipocytes. Moreover, the variability in glycolytic rate between individual cells was higher for astrocytes, 3T3-L1 fibroblasts, C2C12 myoblasts, and HeLa cells, when compared to neurons and 3T3-L1 adipocytes. Finally, Hou and colleagues provided a detailed protocol for monitoring glucose levels in the cytosol of mammalian cell cultures through the use of FRET-based glucose sensors (Hou et al., 2011).

Calibration and pitfalls of FRET-based glucose sensors

Calibration

Using FRET-based sensors, alterations in glucose concentration are reflected by changes in emission ratio between the respective fluorophores. In general, this approach allows comparison of glucose levels within the same cell (type) between individual experiments if the fluorescence recordings have been carried out under standardized conditions (e.g. temperature, excitation source, fluorescence filters). However, a proper cell-biochemical understanding of glucose metabolism requires knowledge about absolute concentrations. This means that the measured ratio (changes) need(s) to be translated into exact concentrations by means of calibration.

A method has been described that makes use of the *in vitro* K_d of the sensor (Fehr et al., 2003, Fehr et al., 2005, Takanaga et al., 2008, Takanaga and Frommer, 2010). A point of concern with this approach is that the *in vitro* K_d does not necessarily equal the *in vivo* 'apparent' K_d due to effects of the cellular environment. Nevertheless, an estimate of the *in vivo* 'apparent' K_d of the sensor can be obtained by varying the external glucose concentration and plotting the ratio signal of the cytosolic sensor as a function of external glucose concentration. However, this strategy does not provide information about the absolute intracellular glucose concentration.

In addition, a more general protocol can be used for calibration of glucose. This strategy relies on controlled plasma membrane permeabilization, followed by clamping the cytosolic glucose concentration with different levels of external glucose. Typically, cells are permeabilized using a detergent like digitonin, which interacts with plasma membrane cholesterol, or the pore-forming bacterial toxin *Streptolysin O*. To prevent morphological cell changes, damage to intracellular

compartments, and cell detachment, the optimal permeabilization conditions need to be experimentally established for each cell type. Key parameters to consider are cell density, detergent concentration, detergent incubation time, and temperature. During permeabilization, the ionic composition and pH of the extracellular medium should closely mimic the intracellular situation. Another point of concern is the possible loss of intracellular proteins including the sensor itself from the cell. To prevent this from happening, permeabilization should be as mild as possible and holes in the plasma membrane should prevent passage of molecules >5 kDa. The calibration of organelle-targeted FRET sensors is still problematic. In case of the ER, one possible strategy might involve isolation of the ER from the cell, followed by calibration using appropriate media and a spectrofluorometer.

Pitfalls

To facilitate signal detection, the discussed FRET sensors are often expressed using a strong promoter. If expression levels are too high, the sensor might act as a buffer and thereby influence glucose homeostasis. Buffering effects become particularly important if a sensor with a low K_d is expressed at a high level to detect a substrate that is present at a low concentration. To check for buffering effects, the ratio of the sensor can be plotted as a function of its expression level for individual cells. If buffering is absent, there should be no correlation between these parameters.

Another potential problem associated with high expression levels and/or the exogenous nature of the sensor protein is its breakdown by proteolysis. This can be investigated by Western blotting of (native) gels using an FP-specific antibody or in-gel fluorescence analysis (Dieteren et al., 2008). We have applied an insect (baculoviral) transfection system, as well as stable cell lines, to allow (controlled) expression of the sensor at relatively low levels.

Obviously, it is crucial to use a sensor with a detection range matching the expected range of metabolite concentrations in the cellular compartment. To validate the obtained results, parallel experiments with low- and high-affinity sensors might be relevant, as well as determining the detection range of the sensor by *in situ* calibration.

To rule out a-specific effects on the signal of the FRET sensor, the best option is to carry out parallel experiments in which a 'control' sensor (unable to bind the substrate) is used (Table 1; CT). For the presented glucose sensors, genuine alterations in metabolite concentration will induce opposite changes in the CFP and YFP emission intensity. In contrast, a pH change will increase or decrease the CFP and YFP signals in the same direction.

Summary and future perspectives

Glucose constitutes a main source for ATP production in most mammalian cells, either directly by glycolysis (*e.g.* in cancer cells) or through the combined action of glycolysis and oxidative phosphorylation. In addition to its role as a substrate, glucose also acts as regulator of metabolic pathways, placing this metabolite at the centre of cell metabolism. Metabolic dysfunction occurs during normal human aging and a large variety of pathological conditions including type II diabetes, muscular dystrophies, inherited metabolic disorders, Parkinson's disease, Alzheimer's disease, metabolic syndrome, certain forms of cancer, and ischemia-reperfusion injury. Development of rational treatment strategies for these metabolic diseases requires a comprehensive understanding of how metabolic homeostasis is maintained and how cells respond to alterations in metabolic homeostasis. This information is also crucial to understand the consequences of metabolic dysfunction induced by off-target drug effects (Wallace, 2008). Because cell metabolism is dynamic and highly compartmentalized, experimental strategies are required that allow visualization of glucose concentration in time and space. Here we presented how quantitative live cell microscopy of FRET-based protein sensors can be used for this purpose. We expect that this technology will be of great value to understand the cell biological mechanism and consequences of metabolic dysfunction in patient-derived cells. Moreover, obtaining quantitative and spatiotemporal data is essential for construction of realistic mathematical models of metabolism (Chapter 3). The latter will allow a systems level understanding of metabolism in healthy and diseased cells and can be used to guide development of specific intervention strategies.

Acknowledgements

This work was supported by an equipment grant of NWO (Netherlands Organization for Scientific Research, No: 911-02-008), the Dutch Ministry of Economic Affairs (Innovative Onderzoeks Projecten (IOP) Grant: #IGE05003), and by the CSBR (Centres for Systems Biology Research) initiative from NWO (No: CSBR09/013V).

CHAPTER 3

Mitoenergetic dysfunction triggers a rapid compensatory increase in steady-state glucose flux



Dania C. Liemburg-Apers, Tom J. J. Schirris, Frans G. M. Russel, Peter H. G. M. Willems and Werner J. H. Koopman

Biophys J (2015), 109(7):1372-86

Abstract

ATP can be produced in the cytosol by glycolytic conversion of glucose into pyruvate. The latter can be metabolized into lactate, which is released by the cell, or taken up by mitochondria to fuel ATP production by the tricarboxylic acid (TCA) cycle and oxidative phosphorylation (OXPHOS) system. Altering the balance between glycolytic and mitochondrial ATP generation is crucial for cell survival during mitoenergetic dysfunction, which is observed in a large variety of human disorders including cancer. To gain insight into the kinetic properties of this adaptive mechanism we here determined how acute (30 min) inhibition of OXPHOS affected cytosolic glucose homeostasis. Glucose dynamics were analyzed in single living C2C12 myoblasts expressing the fluorescent biosensor FLII¹²Pglu-700 μ 86 (FLII). Following *in situ* FLII calibration, the kinetic properties of glucose uptake (V_1) and glucose consumption (V_2) were determined independently and used to construct a minimal mathematical model of cytosolic glucose dynamics. After validating the model, it was applied to quantitatively predict V_1 and V_2 at steady-state (*i.e.* when $V_1=V_2=V_{\text{steady-state}}$) in the absence and presence of OXPHOS inhibitors. Integrating model predictions with experimental data on lactate production, cell volume and O_2 consumption revealed that glycolysis and mitochondria equally contribute to cellular ATP production in control myoblasts. Inhibition of OXPHOS induced a 2-fold increase in $V_{\text{steady-state}}$ and glycolytic ATP production flux. Both in the absence and presence of OXPHOS inhibitors, glucose was consumed at near maximal rates, meaning that glucose consumption is rate-limiting under steady-state conditions. Taken together, we here demonstrate that OXPHOS inhibition increases steady-state glucose uptake and consumption in C2C12 myoblasts. This activation fully compensates for the reduction in mitochondrial ATP production, thereby maintaining the balance between cellular ATP supply and demand.

Introduction

Glucose is among the prime substrates for cellular energy production and serves as a precursor for various biomolecules such as glycoproteins and glycolipids. Hence, the capacity of a cell for glucose uptake and conversion greatly impacts on its energetic and functional state. Glucose uptake is mediated by specific facilitative glucose transporters (Gluts). These integral plasma membrane proteins belong to the Solute Carrier (SLC) 2A subfamily, which consists of 14 different members that differ in their substrate specificity, transport kinetics, tissue distribution, and mode of regulation. The rate of Glut-mediated cellular glucose uptake depends on the amount of active Gluts on the plasma membrane, their kinetic properties, and the magnitude of the trans-plasma membrane glucose gradient, which co-dependes on the extracellular free glucose concentration ($[GLC]_{ext}$) and the cytosolic free glucose concentration ($[GLC]_c$). Once taken up, glucose is phosphorylated by the glycolysis enzyme hexokinase (HK) to form glucose-6-phosphate (G6P). Subsequently, G6P is converted into pyruvate and imported into mitochondria to fuel the tricarboxylic acid (TCA) cycle. The latter produces NADH (reduced nicotinamide adenine dinucleotide) and $FADH_2$ (reduced flavin adenine nucleotide), which serve as substrates for the mitochondrial oxidative phosphorylation (OXPHOS) system. Alternatively, pyruvate can be reversibly converted into lactate by lactate dehydrogenase (LDH) that is released by the cell into the extracellular medium. The OXPHOS system consists of five multiprotein complexes (CI-CV) that generate ATP by chemiosmotic coupling (Mitchell, 1961). CI-CIV constitute the electron transport chain (ETC) that extracts electrons from NADH (at CI) and $FADH_2$ (at CII). Subsequently, the electrons are transported to CIII and from thereon to CIV where they react with molecular oxygen (O_2). At CI, CIII and CIV protons (H^+) are transported from the mitochondrial matrix across the mitochondrial inner membrane to generate an inward-directed proton-motive force (PMF). Driven by the PMF, controlled H^+ back-flux via CV (*i.e.* the F_0F_1 -ATP synthase) is used to synthesize ATP from ADP and inorganic phosphate (P_i). ATP is generated by glucose breakdown during glycolysis (2 ATP per glucose molecule), by the TCA cycle (2 ATP per glucose molecule) and by the OXPHOS system (32 ATP per glucose molecule). The relative contribution of these systems to cellular ATP production depends on many parameters including the cell

type and the nature/availability of energy substrates. In practice, the actual number of ATP molecules generated probably lies within the range of 29-30 ATP molecules per oxidized glucose molecule (Rich, 2003).

In case of mitochondrial dysfunction, increased extracellular lactate levels were observed in fibroblasts from patients with mitochondrial disease (Pitkanen and Robinson, 1996), mouse embryonic fibroblasts (MEFs) from *Nduf4* knockout (KO) mice with isolated CI deficiency (Valsecchi et al., 2012), skin fibroblasts from patients with Myoclonic Epilepsy with Ragged Red Fibers (MERRF) syndrome (Wu and Wei, 2012), myotubes overexpressing the mitochondrial uncoupling protein 3 (Huppertz et al., 2001), polymerase gamma mutator mice (Saleem et al., 2015), and human embryonic kidney 293 cells (HEK293) with a knock-down of the CI subunit NDUF53 (Suhane et al., 2013). In addition, drug-induced mitochondrial dysfunction stimulated glucose uptake in Clone 9 cells (Barnes et al., 2002, Shetty et al., 1993, Shi et al., 1995, Jing et al., 2008, Hamrahian et al., 1999) and Glut1 upregulation and enhanced glucose uptake was demonstrated in cancer cells (Gambhir, 2002, Young et al., 2011). These results suggest that glycolysis-mediated ATP generation is activated by mitochondrial dysfunction (Wu and Wei, 2012). Currently, the balance and interactions between glucose uptake, glycolysis- and OXPHOS-mediated ATP production, as well as their regulation, is a subject of intense study (Patergnani et al., 2014, Haran and Gross, 2014, Drozdowicz-Tomsia et al., 2014, Dott et al., 2014, Jose et al., 2011). However, the various components of this dynamic system cannot be simultaneously accessed by experimental studies in single living cells. This necessitates the use of mathematical models (Lowe and Walmsley, 1986, Fehr et al., 2005, Barros et al., 2007, Wu et al., 2007, van Eunen et al., 2011, Marin-Hernandez et al., 2011, Alam et al., 2015).

In this study we aimed to demonstrate how acute OXPHOS dysfunction affects steady-state glucose uptake and consumption, lactate production, O₂ consumption and ATP production in C2C12 myoblasts. To this end we integrated experimental results with *in silico* predictions of a minimal model of glucose dynamics. This model correctly predicted the glycolytic flux in control and OXPHOS-inhibited cells and revealed that glycolysis and mitochondria equally contribute to ATP production when OXPHOS is active. We demonstrate that acute OXPHOS inhibition 2-fold increases glucose uptake and consumption, thereby fully

compensating for the loss in OXPHOS-mediated ATP generation and maintaining steady-state ATP homeostasis.

Materials and methods

Chemicals

Sodium iodoacetic acid (IAA), Cytochalasin B (CytoB), Cytochalasin D (CytoD), Antimycin A (AA), and p-trifluoromethoxy carbonyl cyanide phenyl hydrazone (FCCP) were obtained from Sigma-Aldrich (Zwijndrecht, The Netherlands). Piericidin A (PA) was obtained from Enzo Life Sciences (Raamsdonksveer, The Netherlands).

Cell culture

C2C12 myoblasts were cultured at 37° C (95% air, 5% CO₂) in Dulbecco's modified eagle's medium (DMEM-32430; Life Technologies – Invitrogen, Bleiswijk, The Netherlands), supplemented with 10% (v/v) fetal bovine serum (FBS). C2C12 myoblasts were seeded in fluorodishes® (#FD35-100, World Precision Instruments, Sarasota, USA) at a density of 40,000 cells/dish.

Transfection

One day after seeding, C2C12 cells were at 40% confluence. 1 µg DNA was mixed with 6 µl lipofectamine (Invitrogen) in 0.5 ml FBS-free DMEM. Following 20 min incubation at room temperature the transfection mix was added to the cells in FBS-free DMEM. After 6 hours this medium was replaced by DMEM containing 10% FBS. The glucose sensor FLII¹²Pglu-700µδ6 (Addgene Plasmid #17866; (Takanaga et al., 2008)) and its high affinity variant FLIPglu-170nΔ13V (Addgene Plasmid #18018; (Takanaga and Frommer, 2010)) were a gift from Dr. Wolf Frommer (Department of Plant Biology, Carnegie Institution for Science, CA, USA).

Single cell microscopy of cytosolic glucose dynamics

At 24 hours post-transfection the C2C12 myoblasts were at 80% confluence. Cells were washed and incubated for 3 min in HEPES-Tris (HT) buffer (adjusted to pH 7.4 with Tris) containing 4.2 mM KCl, 132 mM NaCl, 10 mM HEPES, 1.2 mM MgCl₂ and 1 mM CaCl₂. Next, the HT buffer was replaced with HT buffer containing 500 µM

iodoacetic acid (IAA) and incubated for another 15 min. Subsequently the fluorodish® was mounted on an inverted microscope (Nooteboom et al., 2012) (Axiovert 200 M, Carl Zeiss BV, Sliedrecht, The Netherlands), equipped with a x40/1.3 NA Plan NeoFluar objective (Carl Zeiss) and a CoolSNAP HQ monochrome CCD-camera (Roper Scientific, Vianen, The Netherlands). Microscopy hardware was controlled using Metafluor 6.0 software (Universal Imaging Corporation, Downingtown, PA, USA). FLII¹²Pglu-700 μ δ 6 and FLIPglu-170n Δ 13V were excited at 430 nm (CFP) for 300 ms using a Polychrome IV monochromator system (TILL Photonics, Gräfelfing, Germany). CFP fluorescence was detected using a 455DRLP dichroic mirror (XF2034, Omega Optical Inc, Brattleboro, VT, USA) and a 480AF30 (XF3075; Omega) emission filter. Citrine emission (Citrine_{FRET}) was measured using 430 nm excitation light (during 200 ms) and emission was detected using the 455DRLP dichroic mirror and a 535AF26 emission filter (XF3079; Omega). Time-lapse recordings were performed using an acquisition interval of 2.5 s.

Lactate measurements

C2C12 myoblasts were seeded in a T25 culture flask and cultured for one day, as described above. Next, cells were incubated in 1 ml HT buffer containing 2 mM glucose and either vehicle or mitochondrial inhibitors for 60-90 min. The buffer was collected and centrifuged for 5 min at 600g. Lactate levels were quantified using an Architect chemical analyzer (Abbott B.V., Hoofddorp, The Netherlands). For each sample, the cell number was determined using a Burker Turk hemocytometer.

O₂ consumption measurements

For respirometry analysis (Hutter et al., 2004) C2C12 myoblasts were counted using a Scepter® cell counter (Millipore, Billerica, USA) and $1.5 \cdot 10^6$ cells were transferred to the temperature-controlled (37°C) chamber of an Oxygraph-2k controlled by Datlab 5 recording (2 s time interval) and analysis software (Gnaiger, 2001) (Oroboros Instruments, Innsbruck, Austria). To measure O₂ consumption, cells were either resuspended in HT buffer containing 2 mM glucose or culture medium. After adding the cells to the respiration chamber, the O₂ consumption trace was allowed to stabilize for 10 minutes until routine respiration (routine-value) could be measured in the coupled state of respiratory control. Next, the

complex V (CV) inhibitor oligomycin A (2.5 μ M) was added to determine the leak respiration (leak-value). The maximal capacity of the ETC (ETS-value) was determined by subsequent titration with the mitochondrial uncoupler p-trifluoromethoxy carbonyl cyanide phenyl hydrazone (FCCP). Finally, minimal respiration (ROX-value) was assessed after adding a maximal concentration of the complex I (CI) inhibitor rotenone (ROT; 0.5 μ M) and of the complex III inhibitor antimycin A (AA; 0.5 μ M). This ROX-value was subtracted from the other respiratory rates to correct them for non-mitochondrial respiration.

Cellular ATP level measurements

The total amount of cellular ATP was measured after 24 hours using an ATP bioluminescence assay kit according to the manufacturer's protocol (CLS II; Roche Applied Science, Mannheim, Germany). Briefly, cells were harvested and counted using a Scepter® cell counter (Millipore, Billerica, USA) after which cellular ATP was released by adding the cell suspension to a boiling Tris-EDTA buffer (100 mM Tris, 4 mM EDTA, pH 7.75) for 2 min. Part of this solution was diluted 1:1 (v/v) with luciferase reagent, followed by measurement of the bioluminescence signal. ATP concentrations were calculated using a standard curve, and divided by cell count to obtain ATP values.

Q-PCR analysis

RNA was extracted from C2C12 cells according to the manufacturer's protocol (PureLink™ RNA Mini Kit, Invitrogen). cDNA was generated from 1 μ g RNA using the IScript cDNA synthesis kit (Biorad, Hercules, CA, USA) according to the manufacturer's protocol. Quantitative real-time PCR was performed in a final volume of 25 μ l containing 12.5 μ l SYBR®Green Supermix (Bio-Rad), 5 μ l (10x diluted) cDNA, 4.5 μ l RNase-free water, 1.5 μ l forward primer (2.5 μ M) and 1.5 μ l reverse primer (2.5 μ M). Primers for actin and Glut1-4 were obtained from Biogelio, Nijmegen, The Netherlands (see below). Amplification of cDNA was performed using a C1000 Thermal Cycler (Bio-Rad) and fluorescence was analyzed using the CFX96™ Real-Time System (Bio-Rad). The PCR conditions were 95 °C for 3 minutes (1 cycle), 95 °C for 15 s and 60 °C for 30 seconds (39 cycles), and finally a temperature increase starting at 65 °C to 95 °C with 0.5 °C intervals. RNA

expression was normalized against the mRNA level of actin (DCt) and represented as $2^{-DC(t)}$.

Glut1 TGCAGTTCGGCTATAACACTG and GGTGGTTCATGTTTGATTG

Glut2 TGTGATCAATGCACCTCAAG and TCATAGTTAATGGCAGCTTTCC

Glut3 ACTCTTTGTCAACCGCTTTG and ATCTTGGCGAATCCCATAAG

Glut4 CTTGGCTCCCTTCAGTTTG and CACGTTGCATTGTAGCTCTG

Actin CTAAGGCCAACCGTGAAAAG and TACGACCAGAGGCATACAGG

Single cell pH measurements

For cytosolic pH analysis, C2C12 myoblasts were loaded with the pH-sensitive reporter molecule BCECF (2',7'-Bis-(2-carboxyethyl)-5-(and-6)-carboxyfluorescein) (Life Technologies - Molecular Probes, Bleiswijk, The Netherlands) by incubating them with 5 μ M of the BCECF acetoxy-methyl (AM) ester form (BCECF-AM) in HT buffer for 15 min at 37 °C in the dark. Subsequently, cells were washed 3 times with HT buffer and imaged using an inverted microscope (see above). The H⁺-bound form of BCECF was excited at 440 nm (100 ms) using a 505DRLPXR dichroic mirror (XF2031; Omega). The H⁺-unbound form of BCECF was excited at 490 nm (100 ms) using the same dichroic mirror. Fluorescence images were recorded at 530 nm using a 535AF45 emission filter (XF3084; Omega). The ratio between the emission signal obtained at 490 nm and at 440 nm excitation was used as a measure of cellular pH (Ozkan and Mutharasan, 2002). Time-lapse recordings were performed using an acquisition interval of 6 s.

P/O ratio analysis

To determine the P/O ratio we slightly modified a previously described approach (De Rasmio et al., 2011). Briefly, cells were resuspended in mitochondrial respiration medium MiR05 (Krumschnabel et al., 2015) containing: 110 mM sucrose, 60 mM K⁺-lactobionate, 0.5 mM EGTA, 3 mM MgCl₂, 20 mM taurine, 10 mM KH₂PO₄, 20 mM HEPES adjusted to pH 7.1 with KOH at 30 °C, and 1 g/l BSA essentially fatty acid-free. Routine O₂ consumption was recorded as described in the Materials and Methods section. Next, the plasma membrane was permeabilized using digitonin (10 μ g / $1 \cdot 10^6$ cells) and malate (2 mM) and pyruvate (5 mM) were added. Upon addition of ADP (220 nM), the O₂ consumption rate was allowed to decrease to a stable level, indicating a complete conversion of ADP into

ATP. As a quality control (Kuznetsov et al., 2008), mitochondrial integrity was assessed by adding 10 μ M cytochrome-c (cyt-c). The P/O ratio was calculated by dividing the amount of ADP used by the amount of oxygen used by the mitochondria to consume all the ADP.

Image processing, statistical analysis and mathematical modeling

Microscopy images were stored in native Metafluor format (Universal Imaging Corporation) and analyzed off-line using Image Pro Plus 6.1 software (Media Cybernetics, Rockville, USA). Individual images were background corrected for the individual wavelengths by subtracting the average intensity in an extracellular region of interest (ROI). Next, cell-derived fluorescence signals were quantified using cytosolic circular regions of interest (ROIs). Average values are presented as mean \pm standard error of the mean (SEM). Curve fitting and statistical analysis was performed using Origin Pro 6.1 (OriginLab Corp., Northampton, USA) and GraphPad Prism 5 (Graphpad Software Inc., La Jolla, USA). Unless stated otherwise, statistical significance was assessed using an unpaired Student's t-test and expressed as: ***($p < 0.001$), **($p < 0.01$), and *($p < 0.05$) relative to the indicated condition. Mathematical modeling was performed using MATLAB/Simulink 6.1 (The Mathworks Inc., Natick, USA).

Results

***In situ* calibration of the FLII¹²Pglu-700 μ δ 6 glucose sensor in C2C12 myoblasts**

In this study we used the glucose biosensor FLII¹²Pglu-700 μ δ 6 (FLII) (Takanaga et al., 2008), which is based on the fluorescence resonance energy transfer (FRET) principle, to monitor dynamic changes in free cytosolic glucose concentration ([GLC]_c). As described in Chapter 2, FLII consists of a glucose binding domain sandwiched between cyan fluorescent protein (CFP) and the yellow fluorescent protein mutant Citrine). The glucose binding domain is derived from a periplasmic protein expressed in *E.coli* (Fehr et al., 2003). When glucose binds, the emission of Citrine upon CFP excitation ("Citrine_{FRET}") increases. Simultaneously, the CFP emission upon CFP excitation ("CFP") will decrease (Fig. 1A). Glucose unbinding will induce the reverse effect and the emission ratio (Citrine_{FRET}/CFP) can be used as a

readout of $[GLC]_c$. Manipulation of $[GLC]_c$ by changing the extracellular glucose concentration ($[GLC]_{ext}$; see next section for details) induced antiparallel changes in Citrine_{FRET} and CFP in FLII-expressing C2C12 myoblasts (Fig. 1B; upper panel). No alterations in cellular volume upon $[GLC]_{ext}$ manipulation were observed, as indicated by the lack of parallel changes in the individual CFP and Citrine_{FRET} emission signals (Fig. 1B; upper panel). Inspection of the Citrine_{FRET}/CFP signal revealed identical dynamic emission ratio in different subcellular regions of interest (ROIs; Fig. 1A; inset) and the whole cell (Fig. 1B; lower panel). For quantitative analysis and mathematical modeling of $[GLC]_c$ dynamics, calibration of the FLII emission ratio is required. Using a cell permeabilization strategy with β -Escin (a triterpenoid saponin) was not useful since it induced a shift in FLII signals (data not shown), as reported previously for C2C12 cells (John et al., 2008). Therefore, the *in situ* calibration curve was generated by incubating FLII-expressing C2C12 myoblasts with different $[GLC]_{ext}$ concentrations in the presence of the glucose consumption inhibitor iodoacetic acid (IAA; 500 μ M). IAA inhibits the glycolysis enzyme glyceraldehyde 3-phosphate dehydrogenase (GAPDH) leading to G6P accumulation and allosteric HK inhibition (Bittner et al., 2010). Following a 30 min incubation with various $[GLC]_{ext}$ and IAA, the FLII emission ratio was stable (Fig. 1C). This demonstrates that $[GLC]_{ext}$ and $[GLC]_c$ are fully equilibrated, allowing calibration of the FLII emission ratio (Bittner et al., 2010). For each $[GLC]_{ext}$ the measured (Citrine_{FRET}/CFP) emission ratio was corrected for the emission ratio obtained in the absence of extracellular glucose (“Citrine_{FRET}/CFP_{0mMGLC}”). This corrected emission ratio was termed R_{corr} .

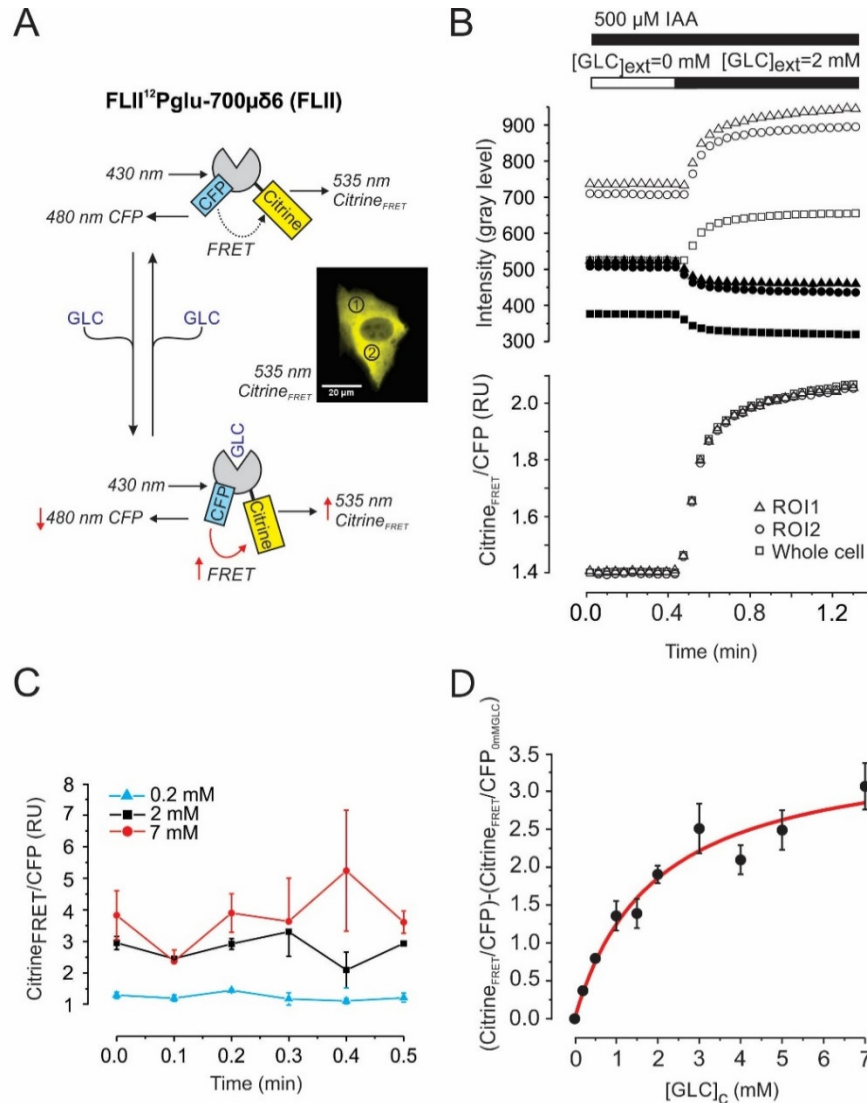


Figure 1. In situ calibration of the glucose sensor. (A) The glucose sensor FLII¹²Pglu-700μδ6 (FLII) consists of a glucose binding domain that is sandwiched between CFP and Citrine. Fluorescence resonance energy transfer (FRET) increases and decreases upon glucose (GLC) binding and unbinding to the sensor, respectively. The inset depicts a typical FLII-expressing C2C12 myoblast revealing the cytosolic localization of the sensor (Citrine image shown). Regions of interest (ROIs) used for temporal analysis of FLII fluorescence are marked by numerals. (B) Response of FLII to a stepwise increase in extracellular glucose ($[GLC]_{ext}$) in the presence of the glucose consumption inhibitor iodoacetic acid (IAA). The top panel shows the individual Citrine (open symbols) and CFP (filled symbols) average fluorescence intensity per pixel (background corrected) for the two ROIs indicated in panel A. In addition, the average fluorescence intensity per pixel (background corrected) for the total cell was determined by creating a cellular mask (binary image) of the cell and superimposing this mask onto the background corrected image. Calculation of the FLII emission ratio (Citrine_{FRET}/CFP) revealed identical ratio-unit (RU) changes in all signals (lower panel). (C) Stability of the FLII ratio signal following 30 min incubation at various $[GLC]_{ext}$ in the presence of 500 μM IAA. FLII images of different cells were acquired. The mean Citrine_{FRET}/CFP signal (\pm SD) of all cells within individual images were plotted as a function of time for 0.2 mM, 2 mM, and 7 mM $[GLC]_{ext}$. For each concentration, no significant differences were detected between time points (one-way ANOVA). (D) Average Citrine_{FRET}/CFP signal (\pm SEM) as a function of $[GLC]_{ext}$ (20 cells analyzed for each $[GLC]_{ext}$). Data was corrected by subtracting the FLII emission ratio obtained at $[GLC]_{ext}=0$. A Michaelis-Menten equation was used to fit the calibration curve ($R^2=0.96$).

The experimental *in situ* calibration curve was fitted using a Michaelis Menten equation:

$$R_{\text{corr}} = \frac{R_{\text{max}} \cdot [\text{GLC}]_c}{K_m + [\text{GLC}]_c} \quad (1)$$

with $[\text{GLC}]_c$ in mM, R_{corr} equaling the corrected FLII emission ratio (as defined above) and K_m representing the *in situ* FLII glucose affinity (in mM).

Fitting yielded a maximal FLII emission ratio (R_{max}) of 3.6 ± 0.4 and a K_m of 1.9 ± 0.5 mM (Fig. 1D). To allow calculation of $[\text{GLC}]_c(t)$ from the measured $R_{\text{corr}}(t)$ Eq.1 was rearranged into:

$$[\text{GLC}]_c(t) = \frac{K_m \cdot R_{\text{corr}}(t)}{R_{\text{max}} - R_{\text{corr}}(t)} \quad (2)$$

Analysis of glucose uptake and consumption in C2C12 myoblasts

In the most simple case, (Fig. 2A) dynamic changes in $[\text{GLC}]_c$ (*i.e.* $[\text{GLC}]_c(t)$) depend on the rate of glucose entry (V_1) across the plasma membrane and the rate of glucose consumption in the cell (V_2):

$$\frac{d[\text{GLC}]_c}{dt} = V_1 - V_2 \quad (3)$$

Cellular glucose entry is mediated by glucose transporters (Augustin, 2010). Q-PCR analysis revealed that Glut isoform 1 (Carruthers et al., 2009) is highly expressed in C2C12 myoblasts whereas Glut2, Glut3 and Glut4 were not detected (Fig. S1). This suggests that V_1 is dominated by Glut1-mediated glucose entry in our cell model. To dissect the contribution of V_1 and V_2 in determining $[\text{GLC}]_c$, we adapted a strategy previously described for cultured mouse astrocytes (Bittner et al., 2010). Quantification of V_1 requires inhibition of glucose consumption, which was achieved using IAA (Fig. 2A). Conversely, glucose entry was inhibited using Cytochalasin B (CytoB) (Fig. 2A), a noncompetitive and membrane-permeable inhibitor of Glut uniporters (Deves and Krupka, 1978, Fehr et al., 2003, Bittner et

al., 2010, Haran and Gross, 2014, Ulanovskaya et al., 2011). CytoB inhibits glucose transport by binding close to the glucose efflux site on the cytoplasmic domain of Gluts. Removal of extracellular glucose induced a drop in $[GLC]_c$ to zero within 3 min (Fig. 2B), indicating that cytosolic glucose is actively consumed. When CytoB treatment was carried out on IAA-pretreated cells, the decrease in $[GLC]_c$ was blocked in a dose- and time-dependent manner. It was found that 15 min pre-treatment with 500 μ M IAA fully blocked glucose consumption (Fig. 2C). The experimental strategy to measure V_1 in C2C12 myoblasts is schematically summarized in Figure 2D and allows analysis of glucose entry under zero-*trans* conditions (*i.e.* when $[GLC]_c$ is virtually zero prior to external glucose re-addition). It consists of cell seeding and transfection (Fig. 2D-a and 2D-b), optional treatment with a mitochondrial inhibitor (Fig. 2D-c; see below), removal of extracellular glucose (Fig. 2D-d), IAA treatment (Fig. 2D-e) and re-addition of external glucose (Fig. 2D-g). In the absence of IAA, increasing $[GLC]_{ext}$ from 0 to 2 mM induced a bi-phasic increase in $[GLC]_c$ in glucose-depleted myoblasts (Fig. 2E and F; open symbols/bars) consisting of a fast ($V_{1,No-IAA}$) and slow component ($V_{1slow,No-IAA}$). In myoblasts pre-incubated with IAA (500 μ M, 15 min) the rate of fast $[GLC]_c$ increase ($V_{1,IAA}$) was significantly higher than $V_{1,No-IAA}$, whereas the rate of increase of the slow phase ($V_{1slow,IAA}$ vs. $V_{1slow,No-IAA}$) was not affected (Fig. 2E and F). This demonstrates that in the absence of IAA, V_1 is underestimated due to glucose consumption, primarily during the fast phase. In the absence of IAA, CytoB induced an acute drop in $[GLC]_c$ at a rate $V_{2,No-IAA}$ (Fig. 2E and F). In contrast, no significant decrease in $[GLC]_c$ was observed (*i.e.* $V_{2,IAA}$ equaled zero) when CytoB was added to IAA-treated cells (Fig. 2E and F). Supported by the results presented in Fig. 2C, these findings demonstrate that glucose is not consumed in IAA-treated C2C12 cells. Applying Eq. 3 to the data presented in Fig. 2F suggests that: (i) in the presence of IAA: $V_2 \approx 0$ so $d[GLC]_c/dt = V_1 = V_{1,IAA} = 0.26 \pm 0.07(SD)$ mM/min, (ii) in the absence of IAA, V_1 is underestimated by an amount of $V_{2,No-IAA}$, so $d[GLC]_c/dt = V_{1,No-IAA} + V_{2,No-IAA} = 0.12 \pm 0.03(SD) + 0.08 \pm 0.06(SD) = 0.20 \pm 0.07(SD)$ mM/min. The fact that $V_{1,IAA}$ is $\approx V_{1,No-IAA} + V_{2,No-IAA}$ strongly suggests that the effect of IAA on V_1 is due to inhibition of V_2 rather than an aspecific effect of this inhibitor on Glut1.

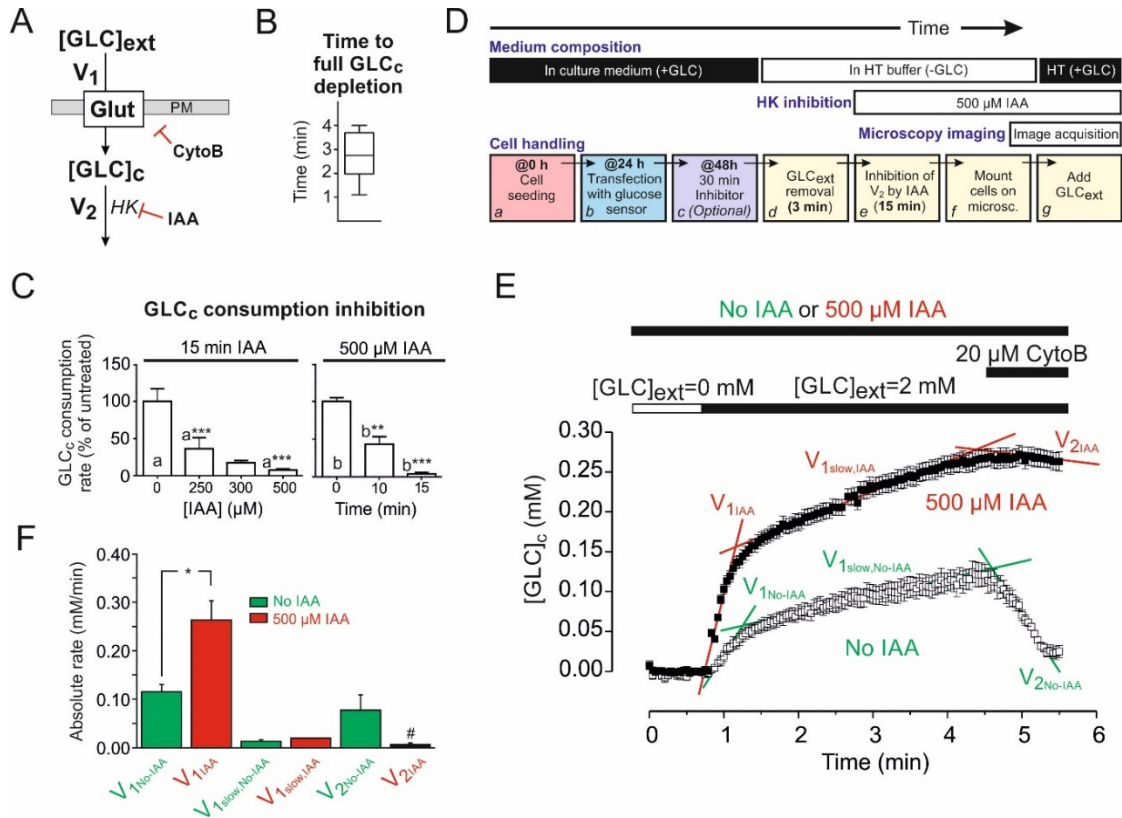


Figure 2. Experimental strategy for analysis of glucose uptake and consumption. (A) Principle of the approach. Glucose (GLC) enters from the extracellular space ($[GLC]_{ext}$) into the cytosol ($[GLC]_c$) via facilitative glucose transport (Glut) across the plasma membrane (PM) and is subsequently consumed. Glucose enters at a rate V_1 and is consumed at a rate V_2 . Cytochalasin B (cytoB) and iodoacetic acid (IAA; acting on hexokinase; HK) are used to inhibit V_1 and V_2 , respectively. (B) Boxplot of the average time required (\pm SD) for lowering $[GLC]_c$ to zero upon removal of $[GLC]_{ext}$ ($n=10$ cells; $N=2$ independent experiments). (C) Analysis of the concentration and duration of IAA treatment required for full inhibition of glucose consumption. Graph presents the mean (\pm SEM) of 15 cells per condition ($N=3$ independent experiments). Statistical significance was determined using the Kruskal-Wallis test. (D) Flowchart of the experimental approach. After cell seeding and FLII transfection, cells are optionally treated with mitochondrial inhibitors for 30 min. Subsequently, $[GLC]_{ext}$ was removed and V_2 inhibited by IAA, followed by microscopy imaging. (E) Representative example of a glucose uptake experiment in the absence (filled symbols) and presence (open symbols) of IAA. After a 3 min incubation in the absence of extracellular glucose, $[GLC]_{ext}$ was increased to 2 mM followed by addition of CytoB. Both in the absence and presence of IAA, $[GLC]_c$ displayed a biphasic increase at rates $V_{1,No-IAA}$ and $V_{1,IAA}$ and $V_{1,slow,No-IAA}$ and $V_{1,slow,IAA}$ upon external glucose addition. The effect of CytoB was reflected by the rates $V_{2,No-IAA}$ and $V_{2,IAA}$. (F) Average values (\pm SD) for the various rates depicted in panel E (determined from linear regression analysis; $n=12$ cells; $N=3$ independent experiments). #Not significantly different from zero determined by a one-way Student's t-test.

Control experiments demonstrated that glucose influx was inhibited by CytoB but not by CytoD, suggesting Glut-mediated glucose uptake in our cell system (Fig. S2A). Because proteinaceous FRET sensors can exhibit sensitivity to their local environment including pH (Borst et al., 2005, Willemsse et al., 2007, Moussa et al., 2014), the high-affinity glucose sensor described in Chapter 2 (FLIPglu-170n Δ 13V; $K_m= 0.17 \mu M$) (Takanaga and Frommer, 2010) was used as a control. In C2C12

myoblasts expressing this control sensor, no changes in fluorescence ratio signal upon manipulation of the extracellular glucose level were observed (Fig. S2B). This suggests that this cytosolic sensor is fully in its glucose-bound state (“saturated”) and that the observed changes in FLII ratio are unlikely caused by glucose-independent alterations in FRET efficiency. Moreover, in agreement with the data presented in Figure 1B (upper panel), the lack of effect on the high-affinity glucose sensor fluorescence signals, directly after glucose addition, demonstrates that $[GLC]_{ext}$ changes do not induce cell-volume changes.

Effect of mitochondrial inhibition on cellular glucose uptake and consumption in C2C12 myoblasts

Using the strategy in Fig. 2D, we next investigated the effect of short-term mitochondrial dysfunction on cellular glucose uptake and consumption. To this end, cells were incubated with mitochondrial inhibitors for 30 min prior to microscopy analysis. In these experiments piericidin A (PA) was used to inhibit complex I (CI) of the OXPHOS system. In parallel experiments, cells were treated with antimycin A (AA) to inhibit OXPHOS complex III (CIII). Respirometry analysis revealed that both inhibitors dose-dependently inhibited CI and CIII (Fig. S3). Full inhibition of mitochondrial O_2 consumption in intact C2C12 cells required a minimal concentration of 100 nM PA ($IC_{50}=8.4\pm 0.2$ nM) and 20 nM AA ($IC_{50}=8.5\pm 0.2$ nM). These concentrations were used during the remainder of the study. First, we quantified the effect of 30 min mitochondrial inhibition on the maximal rate of glucose entry for various $[GLC]_{ext}$ in IAA-treated cells (Fig. 3A). This was performed by calculating the maximal linear rate of $[GLC]_c$ increase from single-cell recordings (Fig. 3B), which increased as a function of $[GLC]_{ext}$ in vehicle-, PA- and AA-treated cells (Fig. 3C). Curve fitting using a Hill-equation revealed that the V_1 -associated K_m -value (Fig. 3D; Table 1-A1) and cooperativity factor n (Fig. 3E) were not affected in PA- and AA-treated cells. In contrast, inhibitor-treated cells displayed a large increase in maximal value of V_1 ($V_{1,max}$) (Fig. 3F; Table 1-A1).

Although IAA did not alter cytosolic pH, PA- and AA-treatment acidified the cytosol to a similar extent (Fig. S2C). Therefore, we determined whether pH changes affected the fluorescence ratio signal of FLII by transient addition of extracellular ammonium chloride (Ozkan and Mutharasan, 2002). Using the pH-sensor BCECF we observed that NH_4Cl addition and removal induced cytosolic alkalinization and acidification, respectively (Fig. S2D; upper panel). However, no changes in the FLII ratio signal were observed upon acidification (Fig. S2D; lower panel). These results, combined with the observation that CFP and Citrine_{FRET} emission changed antiparallel (Fig. 1B), make it unlikely that FLII signals were affected by cytosolic acidification in our experiments.

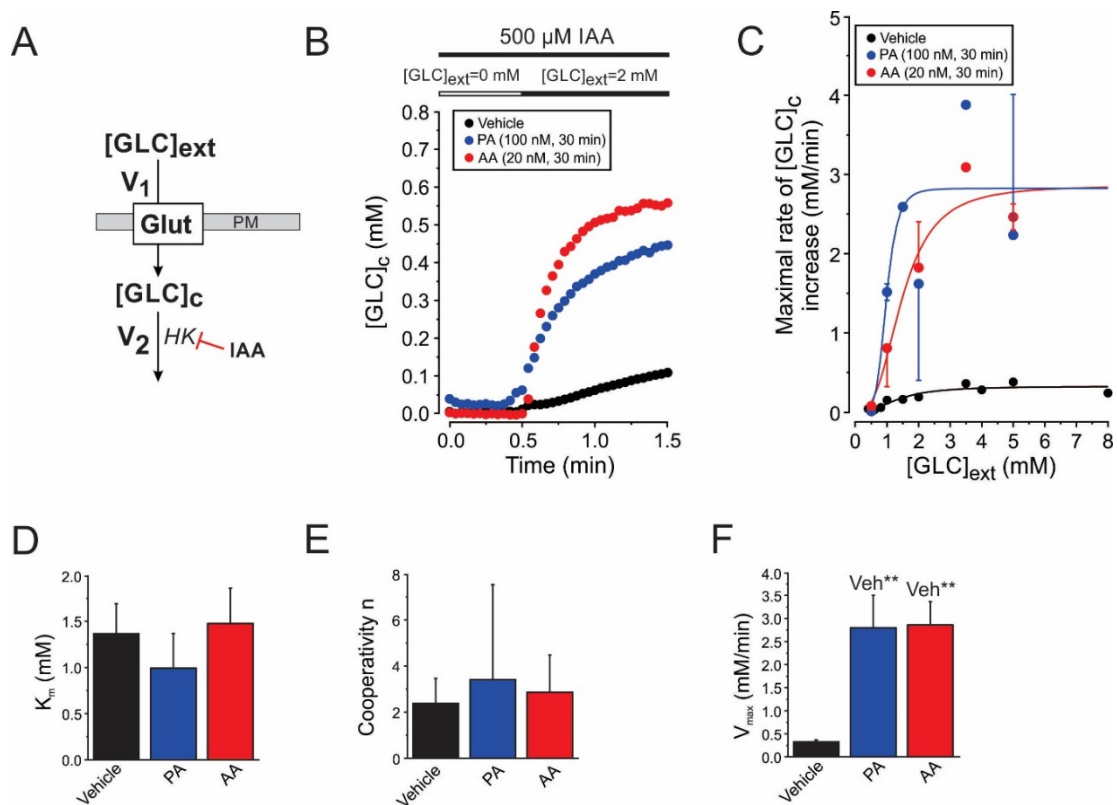


Figure 3. Effect of mitochondrial inhibition on cellular glucose uptake kinetics. (A) Inhibition of the glucose (GLC) consumption flux (V_2) allows analysis of glucose uptake (V_1). (B) Typical glucose uptake in cells pretreated with vehicle, PA or AA for 30 min. The maximal rate of linear increase of these curves was used as a measure of V_1 . (C) Mean (\pm SEM) of the maximal rate of $[\text{GLC}]_c$ increase as a function of $[\text{GLC}]_{\text{ext}}$ in vehicle-treated cells and cells treated with PA or AA ($n=20$ cells per condition; $N=4$ independent experiments). A Hill equation was used for curve fitting (Vehicle: $R^2=0.85$; PA: $R^2=0.68$; AA: $R^2=0.94$). (D) Average value (\pm SD) of K_m for vehicle-, PA- or AA-treated cells. (E) Similar to panel D, but now for the cooperativity parameter n . (F) Similar to panel D, but now for V_{max} .

Table 1. Experimental results, model parameters and model predictions.

PARAMETER	VEHICLE	PA	AA
A. MODEL DIRECTLY BASED UPON EXPERIMENTAL PARAMETERS (DEFAULT MODEL)			
1. GLUCOSE UPTAKE RATE (V_1) PARAMETERS [§]			
Experimental $K_{m,V1}$ (mM)	1.4±0.3	1.0±0.4	1.5±0.4
Experimental $V_{1,max}$ (mM/min)	0.32±0.05	2.8±0.7	2.9±0.5
2. GLUCOSE CONSUMPTION RATE (V_2) PARAMETERS [@]			
Experimental $V_{2,max}$ (mM/min)	0.67±0.07	1.23±0.12	1.7±0.3
$K_{m,V2}$ (mM)	0.06	0.06	0.06
3. [GLC] _c AT STEADY-STATE			
Experimental (mM)	0.49±0.11	0.66±0.09	0.51±0.07
Predicted (mM)	0.02	0.40	0.20
B. MODEL WITH ADJUSTED $V_{1,MAX}$ (OPTIMAL MODEL)			
1. GLUCOSE UPTAKE RATE (V_1) PARAMETERS			
Adjusted $V_{1,max}$ (mM/min)	1.86	4.20	4.80
2. [GLC] _c AT STEADY-STATE			
Predicted (mM)	0.49	0.66	0.51
3. GLUCOSE, PYRUVATE, LACTATE AND ATP RATES AT STEADY-STATE ^{&}			
Predicted $V_1=V_2=V_{steady-state}$ (mM/min)	0.60	1.14	1.50
Predicted pyruvate production rate $V_3=2 \cdot V_{steady-state}$ (mM/min)	1.20	2.28	3.00
Predicted rate of lactate release $V_7=V_4=V_3$ (mM/min) [#]	1.20	2.28	3.00
Experimental rate of lactate release V_7 (mM/min/cell)	1.8±0.6 (SD)	4.1±1.1 (SD)	3.5±1.6 (SD)
Predicted glycolytic ATP production rate $2 \cdot V_{steady-state}$ (mM/min)	1.20	2.28	3.00
Experimental ATP-linked O ₂ consumption rate (mM/min)	0.43±0.08 (SD)	0	0
Experimental P/O ratio	2.7±0.4 (SD)	n.d.	n.d.
Predicted mitochondrial ATP production rate (mM/min)	1.2±0.2 (SD)	0	0
Predicted total ATP production (mM/min)	2.39 (100%)	2.28 (95%)	3.00 (126%)
Experimental total ATP (pmol/cell)	30±13 (SD)	19±5 (SD)	30±18 (SD)

All experiments and model predictions were performed at an extracellular free glucose concentration ([GLC]_{ext}) of 2 mM.

[§]Measured under conditions of IAA-blocked glucose consumption.

[@]Measured under conditions of CytoB-blocked glucose uptake.

[&]Average C2C12 cell volume equaled $2.1 \cdot 10^{-12} \pm 0.4 \cdot 10^{-12}$ (SD) liter (n=14 cells).

Lactate production was measured during 60-90 min in three independent experiments. Routine O₂ consumption and P/O ratio were determined in at least four independent experiments. Total ATP after 24h incubation with vehicle, PA, or AA was measured in three independent experiments, performed *in duplo*.

[#]Assuming a negligible value for V_5

$K_{m,V1}$, affinity (K_m) of glucose uptake; $K_{m,V2}$, affinity (K_m) of glucose consumption; $V_{1,max}$, maximal rate (V_{max}) of glucose uptake; $V_{2,max}$, maximal rate (V_{max}) of glucose consumption; $V_{2,n}$, cooperativity (n) of glucose consumption.

Next, we analyzed the resting $[GLC]_c$ and the maximal linear rate of $[GLC]_c$ decrease upon acute CytoB treatment (Fig. 4A-B). In the literature a K_m value of 60 μM was reported for HK (Bertram and Pernarowski, 1998, Lowe and Walmsley, 1986). Since the steady-value of $[GLC]_c$ was 7- to 10-fold higher than this value, we considered the maximal linear rate of $[GLC]_c$ decrease upon acute CytoB treatment to reflect the maximal value of V_2 ($V_{2,max}$). Inhibitor treatment did not significantly alter the resting $[GLC]_c$ at 2 mM $[GLC]_{ext}$ (Fig. 4C; Table 1-A3) whereas $V_{2,max}$ was 1.8- and 2.5-fold higher in PA- and AA-treated cells respectively (Fig. 4D; Table 1-A2). Taken together, our results demonstrate that inhibition of CI and CIII increase the maximal rates of cellular glucose uptake ($V_{1,max}$) and consumption ($V_{2,max}$) within 30 min.

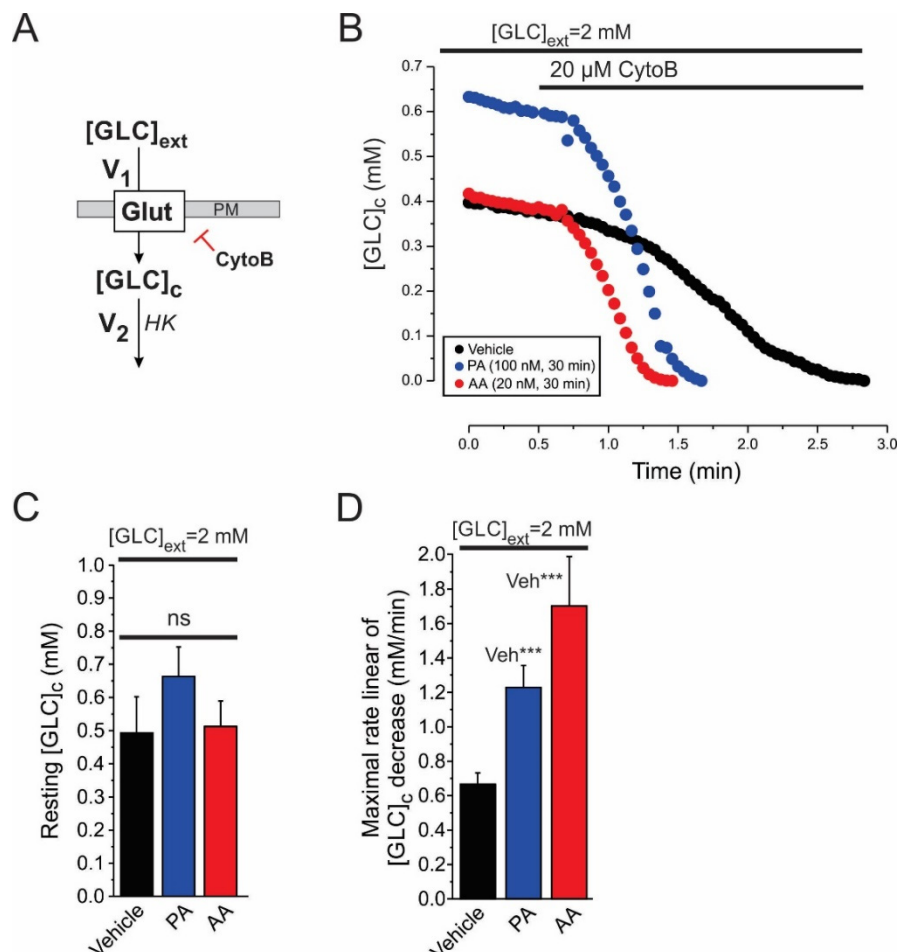


Figure 4. Effect of mitochondrial inhibition on cellular glucose consumption kinetics. (A) Inhibition of the glucose (GLC) uptake flux (V_1) allows analysis of glucose consumption (V_2). (B) Typical glucose consumption experiment in cells treated with vehicle, PA or AA for 30 min. (C) Average value (\pm SD) of resting $[GLC]_c$ for 2 mM $[GLC]_{ext}$ in the absence of CytoB for vehicle-, PA-, or AA- treated cells (D) The average value (\pm SD) of the maximal rate of linear decrease upon cytoB addition in panel B. V_2 (n=20 cells; N=4 independent experiments). N.s. not significant.

A minimal mathematical model for glucose uptake and consumption in C2C12 myoblasts

To gain insight into how V_1 and V_2 quantitatively contribute to the kinetics of the $[GLC]_c$ signal, we developed a mathematical model using Eq. 3. Since cellular volume changes were not observed (see above), cell volume in the model was assumed to be constant. Glut-mediated glucose influx (V_1) was modeled using an equation (Bertram and Pernarowski, 1998) that was previously used for quantitative prediction of Glut1-mediated glucose influx in HepG2 cells (Fehr et al., 2005):

$$V_1 = \text{Flux}_{\text{out} \rightarrow \text{in}} = \frac{V_{1,\text{max}} \cdot ([GLC]_{\text{ext}} - [GLC]_c) \cdot K_{m,V1}}{(K_{m,V1} + [GLC]_{\text{ext}}) \cdot (K_{m,V1} + [GLC]_c)} \quad (4)$$

With $V_{1,\text{max}}$ being the measured maximal value of V_1 (Table 1-A1; in mM/min), $K_{m,V1}$ the measured affinity (Table 1-A1; in mM), $[GLC]_{\text{ext}}$ the extracellular free glucose concentration (in mM) and $[GLC]_c$ the cytosolic free glucose concentration (in mM). We modeled cytosolic glucose consumption (V_2) using a Michaelis-Menten equation (Deichmann et al., 2014) that quantitatively predicted HK-mediated glucose consumption in HepG2 cells (Fehr et al., 2003):

$$V_2 = \frac{V_{2,\text{max}} \cdot [GLC]_c}{(K_{m,V2} + [GLC]_c)} \quad (5)$$

With $V_{2,\text{max}}$ being the measured maximal value of V_2 (Table 1-A2; in mM/min), $K_{m,V2}$ the affinity (in mM), and $[GLC]_c$ the cytosolic free glucose concentration (in mM). Under conditions that glucose influx is blocked, the rate at which $[GLC]_c$ drops will reflect maximal HK action (see above) so we used a $K_{m,V2}$ value of 60 μM (Table 1A-2) as described in the literature (Lowe and Walmsley, 1986, Wilson, 2003).

Parameter optimization and validation of the mathematical model

Using the experimental parameter values for V_1 and V_2 (Table 1) we performed a set of explorative simulations for the vehicle condition at 2 mM $[GLC]_{\text{ext}}$. This 'default model' quantitatively matched (not shown) the experimental data obtained in vehicle-, PA- and AA-treated cells, with respect to maximal rate of

[GLC]_c decrease (Fig. 4D). This suggests that the kinetic parameters measured for V₂ were correct for all three conditions. However, the default model predicted a much lower steady-state [GLC]_c (*i.e.* 0.02 mM) than the experimental value (0.49 mM) (Table 1A-3). In order to gain insight into why the predicted steady-state [GLC]_c was much lower, various parameters (*i.e.* K_{m,v1}, K_{m,v2}, V_{1,max}, V_{2,max}) were manually varied in the default model to fit the experimental steady-state [GLC]_c. This revealed that only when V_{1,max} was increased (*i.e.* from 0.32 to 1.86 mM/min), the predicted steady-state [GLC]_c matched its experimental value. Also for the PA- and AA-treated condition, the steady-state [GLC]_c predicted by the default model was too low (Table 1A-3). Similarly, this discrepancy disappeared when V_{1,max} was increased from 2.8 to 4.2 mM/min (PA-treated cells) and from 2.9 to 4.8 mM/min (AA-treated cells). In this way, 'optimal' models were obtained (Table 1-B). The too low V_{1,max} values reported in our experiments could be due to the fact that the rate of cellular glucose uptake was determined under the condition that [GLC]_c is virtually zero ('zero-trans' condition; (Cloherty et al., 1996). This would lead to an underestimation of V_{1,max} since [GLC]_c stimulates Glut-mediated glucose influx by a mechanism called 'trans-acceleration' (Carruthers, 1990, Liu et al., 2001). Indeed (Fig. S4A), the maximal rate of [GLC]_c increase was much higher when [GLC]_c equaled 0.4 mM (*i.e.* when glucose uptake was *trans*-accelerated) than when [GLC]_c was virtually zero (*zero-trans* condition). In this sense, the model-predicted underestimation of V_{1,max} in our experiments is very likely due to the use of *zero-trans* conditions.

Simulating the calibration procedure with the optimal model (vehicle-condition) predicted that [GLC]_c fully equilibrated with [GLC]_{ext} within 30 min for [GLC]_{ext} ≤ 4 mM (Fig. S5A). For [GLC]_{ext} > 4 mM this model predicted that [GLC]_c did not fully equilibrate with [GLC]_{ext} within this time period (Fig. S5A). However, correcting [GLC]_c for this effect did not significantly affect the FLII calibration curve and its K_m and R_{max} value (Fig. S5B).

Model prediction of steady-state glucose uptake and consumption

In a first set of simulations we used the optimal model to simulate the experiment in Figure 4B. Model predictions (Fig. 5A) quantitatively matched the experimental data obtained in vehicle, PA- and AA-treated cells, with respect to resting [GLC]_c (Fig. 4C) and maximal rate of [GLC]_c decrease (Fig. 4D). Next, we simulated the

experiment in Figure 2E, to predict the steady-state values of V_1 and V_2 (Fig. 5B). In the presence of 2 mM $[GLC]_{ext}$, V_1 and V_2 steady-state values (*i.e.* when $V_1=V_2=V_{steady-state}$) increased from 0.60 mM/min (vehicle) to 1.14 mM/min (PA) to 1.50 mM/min (AA), without significantly affecting steady-state $[GLC]_c$ (Fig. 4C). To quantify the effect of V_1 and V_2 upon the overall steady-state glucose flux we calculated flux control coefficients in the vehicle, PA- and AA- model (Fig. 5C-D). This was performed by determining the steady-state glucose flux values at various magnitudes of $V_{1,max}$ or $V_{2,max}$ (Rossignol et al., 2000, Alam et al., 2015). The arrows in Figure 5C indicate the values of $V_{1,max}$ (left panel) and $V_{2,max}$ (right panel) in the three optimal models. At each arrow we calculated the derivative to obtain the flux control coefficient (*i.e.* $(dFlux/Flux)/(dV_{max}/V_{max}) = (dFlux/dV_{max}) \cdot (V_{max}/Flux)$). For all three steady-state conditions, the flux control coefficient was much larger for V_2 than for V_1 (Fig. 5D), demonstrating that the steady-state glucose flux is primarily determined by the steady-state value of V_2 .

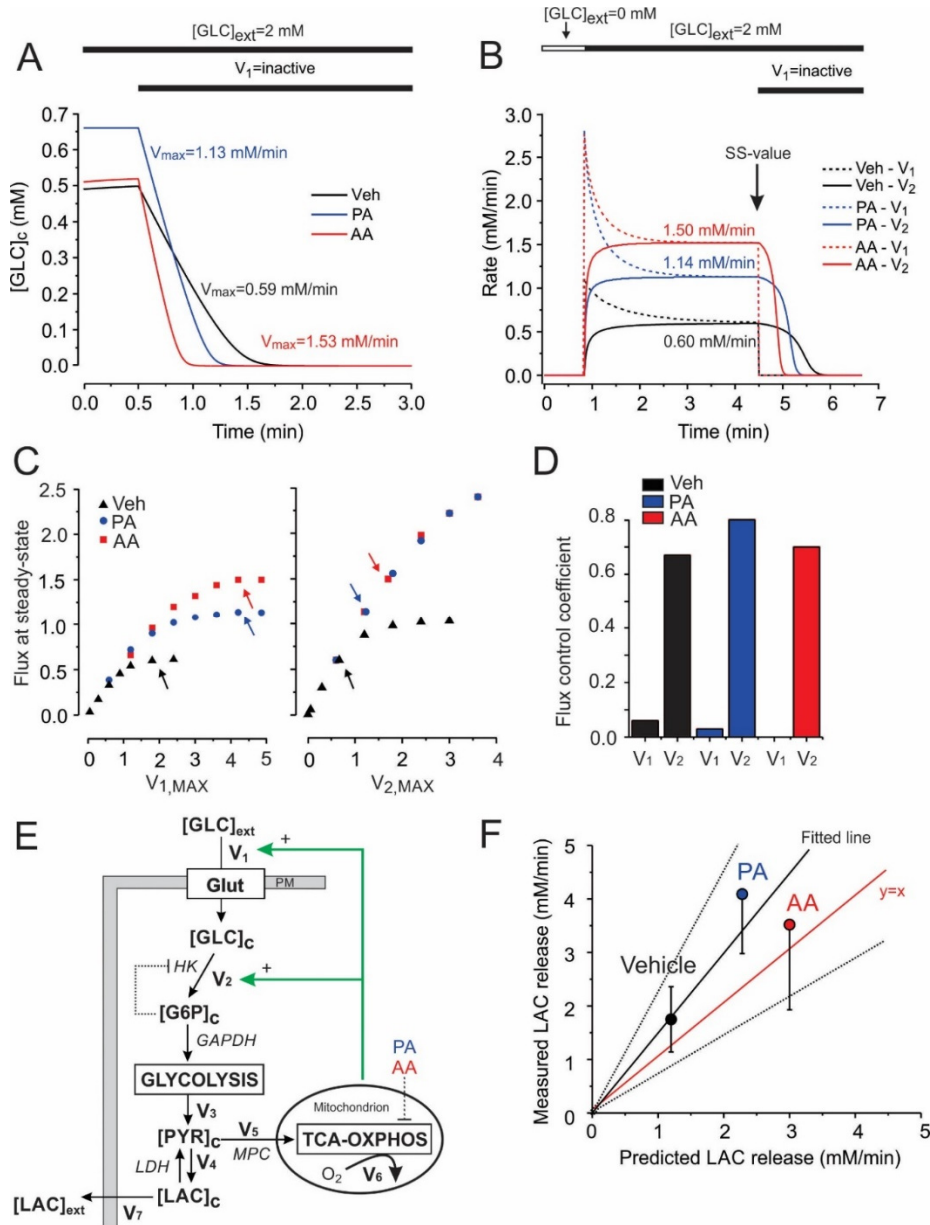


Figure 5. A minimal model of glucose uptake and consumption in C2C12 myoblasts. (A) $[GLC]_c$ dynamics predicted by the optimal model mimicking the experiments in Figure 4B for vehicle-, PA- and AA-treated cells. Glucose influx (V_1) was set to zero to simulate Glut inhibition by CytoB. Both resting $[GLC]_c$ (y-axis) and maximal linear rate of $[GLC]_c$ decrease (numerals) were predicted correctly. (B) Simulated experiment of Figure 2E to predict the steady-state values (numerals) of glucose influx (V_1 ; dotted lines) and consumption (V_2 ; continuous lines) in vehicle-, PA- and AA-treated cells. Glucose influx (V_1) was set to zero to simulate Glut inhibition by CytoB. SS indicates the steady-state situation. (C) Flux variation as a function of $V_{1,max}$ and $V_{2,max}$. The steady-state flux at 2 mM $[GLC]_{ext}$ was predicted for different values of $V_{1,max}$ (left panel) and $V_{2,max}$ (right panel). Arrows mark the V_{max} value in the respective models. (D) Flux control coefficients for V_1 and V_2 determined by calculating the derivatives of the traces in panel C (see Results for details). (E) Schematic representation of the various fluxes (V_1 , V_2 , V_3 , V_4 , V_5 , V_6 , V_7 ; see Results and Discussion for details). (F) Comparison between the predicted single-cell lactate (LAC) production flux (x-axis) and measured average (\pm SD) of LAC production flux (y-axis) in cells treated with vehicle, PA or AA in HT buffer containing 2 mM glucose ($N=3$ independent experiments). A linear equation was used for fitting ($R^2=0.90$; slope= 1.49 ± 0.29 ; dotted lines indicate 95% confidence limits).

Model prediction of steady-state lactate production

Mitochondrial O₂ consumption was fully blocked in inhibitor-treated cells (Fig. S3). This suggests (Fig. 5E) that the rate of mitochondrial pyruvate entry (V₅) is close to zero and that pyruvate (generated by glycolysis at a rate V₃) is converted into lactate at a rate V₄ and subsequently released by the cells at a rate V₇. Assuming that all consumed glucose is converted into lactate that is transported out of the cell, we used the predicted V_{steady-state} to calculate V₇. At 2 mM [GLC]_{ext} the optimal model predicts (Table 1-B3) that V_{steady-state} equals 1.14 mM/min (PA) and 1.50 mM/min (AA). Because glycolytic conversion yields two pyruvate molecules for each glucose molecule that is consumed, the predicted rates of pyruvate generation (V₃) and lactate release (V₇) equal $V_3=V_7=2 \cdot V_{\text{steady-state}}$, yielding 2.3 mM/min (PA) and 3.0 mM/min (AA). Experimental analysis (using the same medium used for FLII imaging) yielded lactate fluxes of 3.7 ± 1.1 (SD) fmol/min/cell (vehicle), 8.7 ± 1.5 (SD) fmol/min/cell (PA) and 7.5 ± 3.0 (SD) fmol/min/cell (AA). In order to compare these experimental values with the predictions of the mathematical model (which simulates a single cell) information about C2C12 myoblast volume is required. To this end, we first determined the area of FLII-expressing cells (using the Citrine_{FRET} image), yielding an average value of $1.2 \cdot 10^3 \pm 0.4 \cdot 10^3$ (SD) μm^2 (n=14 cells). Using data from the literature (Slomka and Gefen, 2011) it was found that C2C12 area and volume display a highly linear correlation (Fig. S6). From this correlation we estimated that the average C2C12 volume in our experiments equaled $2.1 \cdot 10^{-12} \pm 0.4 \cdot 10^{-12}$ (SD) liter, compatible with a previous estimate obtained by 3D microscopy analysis (Peeters et al., 2004). In case of PA-treated cells the measured value of V₇ equaled $(8.7 \pm 1.5 \text{ fmol/min/cell}) / (2.1 \cdot 10^{-12} \pm 0.4 \cdot 10^{-12} \text{ liter}) = 4.1 \pm 1.1 \text{ mM/min/cell}$. A similar calculation yields $1.8 \pm 0.6 \text{ mM/min/cell}$ and $3.5 \pm 1.6 \text{ mM/min/cell}$ for vehicle- and AA-treated cells, respectively. Quantitative comparison of these measured lactate fluxes with model predictions revealed a linear correlation (Fig. 5F). The fitted line did not significantly differ from $y=x$ (*i.e.* the latter fell within the 95% confidence limits of the fitted line), suggesting that the model correctly predicted lactate fluxes (V₇) for vehicle- and inhibitor-treated cells.

Model predictions of steady-state ATP production

Finally, we integrated model predictions and experimental results to analyze the balance between glycolytic and mitochondrial ATP production in C2C12 cells. For vehicle-treated cells the amount of ATP derived from glycolysis equaled $2 \cdot V_{\text{steady-state}}$ (*i.e.* 1.20 mM/min). To compare this flux with mitochondrial ATP production, we measured routine O_2 consumption (Fig. 6A). Following correction for leak respiration, the ATP-linked O_2 consumption rate equaled 15.4 ± 2.7 pmol/s/ 10^6 cells. Considering C2C12 cell volume, this yields an ATP-linked O_2 flux of 0.43 ± 0.08 (SD) mM/min (Table 1-B3). Next, the ATP production rate was calculated from this O_2 flux using the phosphorus/oxygen ratio (P/O ratio). The latter was determined by measuring the amount of O_2 required to convert 220 nmol ADP to ATP in permeabilized cells supplemented with pyruvate and malate (De Rasmio et al., 2011). This strategy revealed a P/O ratio of 2.7 ± 0.4 (SD) (Table 1-B3 and Fig. S7), meaning that ATP is produced by mitochondria at a rate of $(2.7 \pm 0.4) \cdot (0.43 \pm 0.08$ mM/min) = 1.2 ± 0.2 (SD) mM/min. Therefore, vehicle-treated C2C12 cells derive 50% of their cellular ATP from glycolysis and 50% from OXPHOS (Fig. 6B, Table 1-B3). For inhibitor-treated cells we assumed that ATP is exclusively generated by glycolysis, yielding fluxes of 2.28 mM/min (PA) and 3.00 mM/min (AA). Therefore, the total steady-state ATP production flux is virtually identical for vehicle- and inhibitor-treated cells (Fig. 6B): 2.39 mM/min (vehicle, set at 100%), 2.28 mM/min (PA; 95%) and 3.00 mM/min (AA; 126%). In line with these predictions, 24 hours treatment with vehicle-, PA and AA did not significantly affect total cellular ATP level (Fig. 6C, Table 1-B3) or the total number of cells (data not shown). This suggests that increased steady-state glucose uptake and consumption fully compensates for the loss of mitochondrial ATP production in PA- and AA-treated cells.

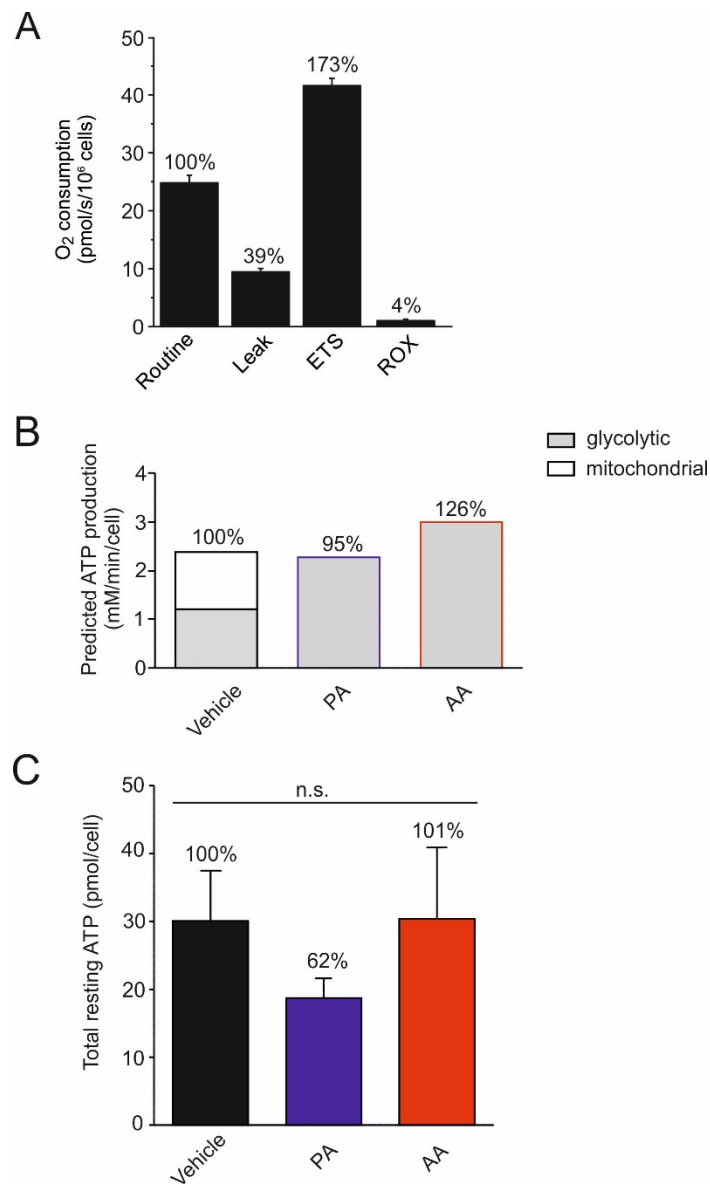


Figure 6. Analysis of O₂ consumption and total ATP concentration in C2C12 myoblasts. (A) Average values (\pm SEM) for routine, leak, maximal (ETS) and residual respiration (ROX) in C2C12 cells (N=6 independent experiments). (B) Prediction of the balance between glycolytic and mitochondrial ATP production in vehicle- and inhibitor-treated cells. See Results for details. (C) Average values (\pm SEM) of total ATP levels in cells treated for 24 hours with vehicle, PA or AA (N=3 independent experiments). Statistical significance was assessed using the Kruskal-Wallis test.

Discussion

This study focuses on gaining a quantitative understanding of the balance between steady-state glucose uptake/consumption, glycolytic and mitochondrial ATP production, and the effect of mitoenergetic dysfunction on this system. We provide integrated experimental and *in silico* evidence that the glycolytic pathway and mitochondria equally contribute to total ATP production in C2C12 myoblasts. Acute (30 min) OXPHOS inhibition induced a 2-fold increase in steady-state glucose uptake and consumption, which fully compensated for the drop in mitochondrial ATP production. Our results suggest a mechanism in which mitoenergetic dysfunction triggers compensatory activation of the glycolysis pathway, allowing metabolic flexibility.

***In situ* calibration and validation of the FLII glucose sensor**

Predictive mathematical modeling requires a quantitative measure of $[GLC]_c$. Therefore, we calibrated the emission ratio of the FLII sensor by incubating the cells with different $[GLC]_{ext}$ concentrations in the presence of the V_2 inhibitor IAA. The *in situ* FLII calibration curve displayed Michaelis-Menten kinetics and a K_m of 1.9 mM, which was 2.7-fold higher than its *in vitro* K_m -value (Bermejo et al., 2010). This illustrates the importance of *in situ* calibration (Moussa et al., 2014) and demonstrates that FLII most sensitively reports $[GLC]_c$ when $[GLC]_c$ is near 1.9 mM. Of note, discrepancies between *in situ* and *in vitro* K_m -values are not uncommon, as illustrated by the 8-fold increase in K_m for the proteinaceous Ca^{2+} sensor “PericamR” when expressed in the mitochondrial matrix (Filippin et al., 2003). We demonstrated that the FLII ratio is not affected by cytosolic acidification in our experiments, compatible with previous findings in yeast cultures (Bermejo et al., 2010). Taken together, we provided evidence that the employed calibration procedure and experimental conditions are suited for quantitative measurement of $[GLC]_c(t)$ using the FLII sensor.

Quantification of cellular glucose uptake and consumption

In previous studies cellular glucose uptake (V_1) was measured using a radio-labeled variant of glucose (*i.e.* 2-deoxy-D-glucose or 2-DG), which inhibits HK and is phosphorylated by this enzyme (Kletzien and Perdue, 1973, Purich and Fromm, 1971). However, this approach cannot be used to study the relatively rapid

temporal glucose dynamics at the (sub)cellular level. In addition, fluorescently labeled glucose analogues such as 2-(N-(7-nitrobenz-2-oxa-1,3-diazol-4-yl)amino)-2-deoxyglucose (2-NBDG) and 6-(N-(7-nitrobenz-2-oxa-1,3-diazol-4-yl)amino)-6-deoxyglucose (6-NBDG) have been used to quantify V_1 (Zou et al., 2005, Jung et al., 2011). However, these glucose analogues display a different affinity for Glut transporters than glucose (Barros et al., 2009). Here we experimentally dissected the contribution of V_1 to $[GLC]_c$ dynamics, by removing $[GLC]_{ext}$ and preventing cytosolic glucose consumption (V_2) using IAA. Measurements of zero-*trans* glucose uptake were performed by extracellular addition of glucose to cells with zero glucose on the *trans* (*i.e.* intracellular) site. Upon glucose addition, the rate of change in $[GLC]_c$ (*i.e.* $d[GLC]_c/dt$) was determined by quantifying the maximal slope of the calibrated FLII signal. This slope was then used as a measure of the initial rate of glucose uptake. Because the sum of V_1 and V_2 in the absence of IAA is similar to the experimental value of V_1 in the presence of IAA, it appears that IAA does not affect glucose uptake. Q-PCR analysis revealed that Glut1 is expressed, whereas Glut2, Glut3 and Glut4 transcripts were not detected. This suggests that V_1 primarily reflects Glut1-mediated glucose uptake. In vehicle-treated cells the maximal rate of V_1 ($V_{1,max}$) was 0.32 ± 0.05 mM/min and its K_m -value ($K_{m,V1}$) equaled 1.4 ± 0.3 mM. Similar $K_{m,V1}$ values (*i.e.* 0.38-2.00 mM) were reported in previous studies (Cloherty et al., 1996, Fehr et al., 2005, Takanaga et al., 2008, Naftalin, 2008), suggesting that our experimental strategy to determine $K_{m,V1}$ is valid. The maximal value of V_2 ($V_{2,max}$) was determined in the presence of the V_1 -blocker CytoB (Bittner et al., 2010). Because HK displays a glucose-affinity of ~ 60 μ M (Saleem et al., 2015, Wilson, 2003) it operates (near) it's V_{max} at the measured $[GLC]_c$ concentrations.

OXPHOS inhibition stimulates cellular glucose uptake

Thirty min treatment with PA or AA did not significantly affect the affinity of glucose uptake ($K_{m,V1}$) but induced an 8-fold increase in $V_{1,max}$, compatible with previous results in OXPHOS-inhibited cells (Barros et al., 2007, Cloherty et al., 2001, Bonder and Mooseker, 1986, Barnes et al., 2002, Jing and Ismail-Beigi, 2007). Similar to another study (Behrooz and Ismail-Beigi, 1997), qPCR analysis revealed that inhibitor treatment did not alter Glut mRNA levels (data not shown). Although PA and AA are chemically dissimilar and target different OXPHOS complexes, they

equipotentially stimulated glucose uptake. This suggests that the latter is due to OXPHOS inhibition rather than off-target effects of PA and AA, supporting a mechanism in which acute mitochondrial dysfunction stimulates Glut1-mediated glucose uptake in C2C12 myoblasts. A similar phenomenon was induced by extracellular alkalization, possibly by modification of Glut cysteine residues (Gunnink et al., 2014). However, here we measured that OXPHOS inhibition lowered cytosolic pH and increased extracellular lactate levels, which argues against involvement of alkalization-induced Glut1 activation. Alternatively, OXPHOS inhibition might induce a drop in ATP level leading to reduced ATP-induced inhibition of Glut1 activity (Blodgett et al., 2007, Levine et al., 2002). Our results argue against such a mechanism since: (i) they suggest that the drop in OXPHOS-mediated ATP production is fully compensated for by increased glycolytic activity, and (ii) they demonstrate that total cellular ATP amount is not significantly reduced in cells treated with OXPHOS inhibitors for 24 h. Glut1 activity might also be increased by a mechanism involving AMP-activated protein kinase (AMPK), activation (phosphorylation) of which was linked to stimulation of glucose transport during OXPHOS inhibition (Barnes et al., 2002, Ozkan and Mutharasan, 2002, Wu et al., 2013). Alternatively, Glut1 redox modification and oligomerization were demonstrated to regulate Glut1 activity (Hebert and Carruthers, 1992, Zottola et al., 1995, De Zutter et al., 2013, Kuipers et al., 2013) and the amount of active Glut1 at the plasma membrane might be increased by stimulation of Glut1 translocation from internal storage vesicles to the plasma membrane or by activation of plasma membrane-localized Glut1 by OXPHOS inhibition (Barnes et al., 2002, Shi et al., 1995, Shetty et al., 1993, Hamrahian et al., 1999). In Chapter 5 the mechanism by which OXPHOS inhibition stimulates glucose uptake will be discussed in more detail.

OXPHOS inhibition stimulates cellular glucose consumption

OXPHOS inhibition induced a 2-fold increase in the maximal rate of glucose consumption ($V_{1,max}$). Genomic expression profiling (<http://www.ncbi.nlm.nih.gov/geo/>; GEO accession: GDS2420) suggests that C2C12 myoblasts express HK isoforms I and II. HK-mediated phosphorylation of glucose leads to formation of G6P, which allosterically inhibits HKI and HKII. In case of HKI this inhibition is antagonized by P_i , whereas the latter activates HKII (Wilson, 1995).

This suggests that increased glucose consumption might be explained by P_i -induced activation of HKII during OXPHOS inhibition. However, as discussed above, our results argue against such a mechanism since glycolytic activity fully compensated for the loss in OXPHOS-mediated ATP production in PA- or AA-treated cells and total cellular ATP was not affected after 24 hours inhibitor treatment. Glucose consumption might also be increased in OXPHOS-inhibited cells by activation of glucokinase, a low-affinity ($K_m=8$ mM) HK isozyme (Meglasson and Matschinsky, 1983). However: (i) the above expression profile suggests that glucokinase is not expressed in C2C12 myoblasts (confirmed in (Otaegui et al., 2002)), and (ii) the steady-state resting $[GLC]_c$ was 10-fold lower than the K_m of glucokinase in vehicle-treated and OXPHOS-inhibited cells. In addition to HK activation, increased glucose consumption likely involves stimulation of other (glycolytic) enzymes including phosphofructokinase and pyruvate kinase.

A minimal model of cytosolic glucose dynamics

To predict steady-state glucose uptake and consumption fluxes, we constructed a minimal mathematical model that consisted of two equations: (i) a reversible Michaelis-Menten equation for glucose uptake (V_1) and (ii) an irreversible Michaelis-Menten equation for glucose consumption (V_2). The glucose uptake equation does not account for asymmetry (*i.e.* different kinetic parameters for glucose influx and efflux) or *trans*-accelerated transport. The kinetic parameters for V_1 ($K_{m,V1}$ and $V_{1,max}$) and V_2 ($V_{2,max}$) were experimentally determined and included in the model. In case of V_2 , we used a glucose-affinity ($K_{m,V2}$) of 60 μ M compatible with values previously reported for HK and HK-mediated glucose consumption in C2C12 cells (Wilson, 2003, Fehr et al., 2005, Bittner et al., 2010). Initially, the model predicted a too low steady-state $[GLC]_c$ in vehicle- and inhibitor-treated cells (default model). Manual parameter optimization revealed that our experimental strategy systematically underestimated $V_{1,max}$, which had to be increased from 0.32 to 1.86 mM/min (vehicle), from 2.8 to 4.20 mM/min (PA) and from 2.9 to 4.80 mM/min (AA) to generate quantitatively correct predictions (optimal model). Triggered by these model predictions, we provided experimental evidence suggesting that our experimental method underestimates the rate of glucose uptake due to a lower $[GLC]_c$. Importantly, the adjusted $V_{1,max}$ values in the

optimal model fell within a similar range as those reported for Glut1-mediated glucose entry in HepG2 cells (*i.e.* 7.2 mM/min; (Fehr et al., 2005)).

Predicting the glycolytic flux at steady-state

Model predictions yielded a steady-state value of $V_1=V_2=V_{\text{steady-state}}$ of 0.60 mM/min in vehicle-treated cells. $V_{\text{steady-state}}$ was 2-fold higher in PA- and AA-treated cells. Under all three conditions V_2 displayed the largest flux control coefficient (*i.e.* ~ 0.6), indicating that the glucose flux was primarily determined by the steady-state value of V_2 . The flux control coefficient of V_1 was below 0.1 for all three conditions. In comparison, the flux control coefficient of glucose uptake upon oxygen consumption ranged between 0.3-0.5 and increased upon lowering external glucose in *T. brucei* (Bakker et al., 1999). In PA- and AA-treated cells mitochondrial O_2 consumption was fully blocked, meaning that mitochondrial pyruvate entry (V_5) is negligible. Under these conditions, we assumed that all the glucose (consumed at rate $V_{\text{steady-state}}$) is converted into lactate and released from the cell at a predicted rate V_7 . The latter prediction agreed with lactate release measurements, supporting the validity of our minimal model and suggesting that the contribution of alternative pathways branching off or feeding into to the glycolytic pathway is relatively low. Interestingly, also in the absence of inhibitors (*i.e.* when V_5 was not zero) the predicted V_7 was close to the measured lactate release. This strongly suggests that the magnitude of steady-state mitochondrial pyruvate uptake (V_5) is much smaller than the rate of pyruvate-to-lactate conversion (V_4) and subsequent lactate release (V_7) in vehicle-treated cells. Since the lactate release predicted using $V_{\text{steady-state}}$ matched with the experimental lactate release rate it appears that $V_{\text{steady-state}}$ is a good measure of glucose flux. The fact that the measured lactate release was higher than the predicted lactate release for all three conditions might be due to hydrolysis of glycogen to G6P, thereby increasing V_3 and V_7 . In addition, we cannot exclude that glucogenic amino acids contribute to pyruvate and lactate production in our experiments. For analysis of the glycolytic flux, our strategy provides an alternative to measurement of the extracellular acidification rate (ECAR), which might not always provide a reliable estimate of glycolytic flux (Mookerjee et al., 2015).

Balancing glycolytic and mitochondrial ATP production

Analysis of ATP-linked mitochondrial O₂ consumption and P/O ratio in vehicle-treated cells suggested that ATP was generated by the OXPHOS system at a rate of 1.20 mM/min. Since $V_{\text{steady-state}}$ also equaled 1.20, this means that under vehicle conditions 50% of the total ATP is generated by glycolysis and 50% by OXPHOS. As a consequence, a 2-fold increase in $V_{\text{steady-state}}$ under conditions of OXPHOS inhibition fully compensates for the loss in OXPHOS-mediated ATP production. Indeed, model predictions suggested that the total cellular ATP production rate under steady-state conditions equaled 100% (vehicle), 95% (PA) and 126% (AA). Following 24 hours treatment, total cellular ATP content and total cell number were similar for vehicle- and inhibitor-treated cells. This is compatible with a mechanism in which glycolytic ATP production fully compensates for the loss in mitochondrial ATP production. A similar lack of effect on total ATP content was demonstrated in MEFs from *NDUFS4*^{-/-} mice with isolated CI deficiency (Valsecchi et al., 2012) and in fully glycolytic skin fibroblasts treated for 72 hours with the CI-inhibitor rotenone (Distelmaier et al., 2015). C2C12 myoblasts displayed a relatively high glycolytic and low mitochondrial pyruvate influx. This allowed a 2-fold increase in glycolytic flux to fully compensate for the lack of mitochondrial ATP production in PA- and AA-treated cells. This suggests that cells displaying a more oxidative metabolism would require a larger increase in glycolytic flux to maintain overall ATP production.

Conclusions

By combining experiments and mathematical modeling we here demonstrate that mitoenergetic dysfunction triggers a rapid compensatory increase in steady-state glucose uptake and consumption in C2C12 myoblasts. This mechanism maintains the balance between cellular ATP supply and demand, thereby preventing energy crisis in cells which mitochondrial ATP generation is compromised.

Acknowledgements

This work was supported by equipment grants of ZonMW (Netherlands Organization for Health Research and Development, No: 903-46-176), NWO (Netherlands Organization for Scientific Research, No: 911-02-008) and by the CSBR (Centres for Systems Biology Research) initiative from ZonMW (Grant: #CSBR09/013V). We thank Dr. Lionel Blanchet (Dept. of Biochemistry 286) for assistance with data analysis and Jan Verhagen (Dept. of Clinical Chemistry, Radboud University Medical Center) for performing lactate measurements.

Supplementary figures

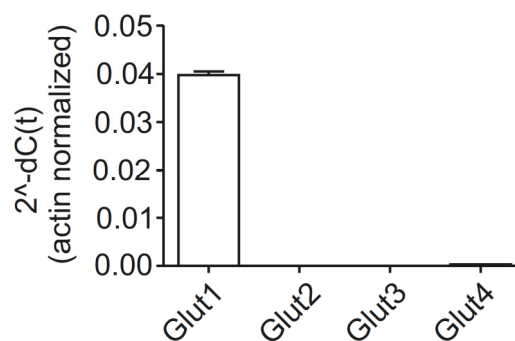


Figure S1. mRNA levels of Glut family members in C2C12 myoblasts and respirometry analysis. A qPCR with primers against mouse Glut1, Glut2, Glut3, and Glut4 was performed on cDNA generated from C2C12 myoblasts. Only mRNA of Glut1 was detected.

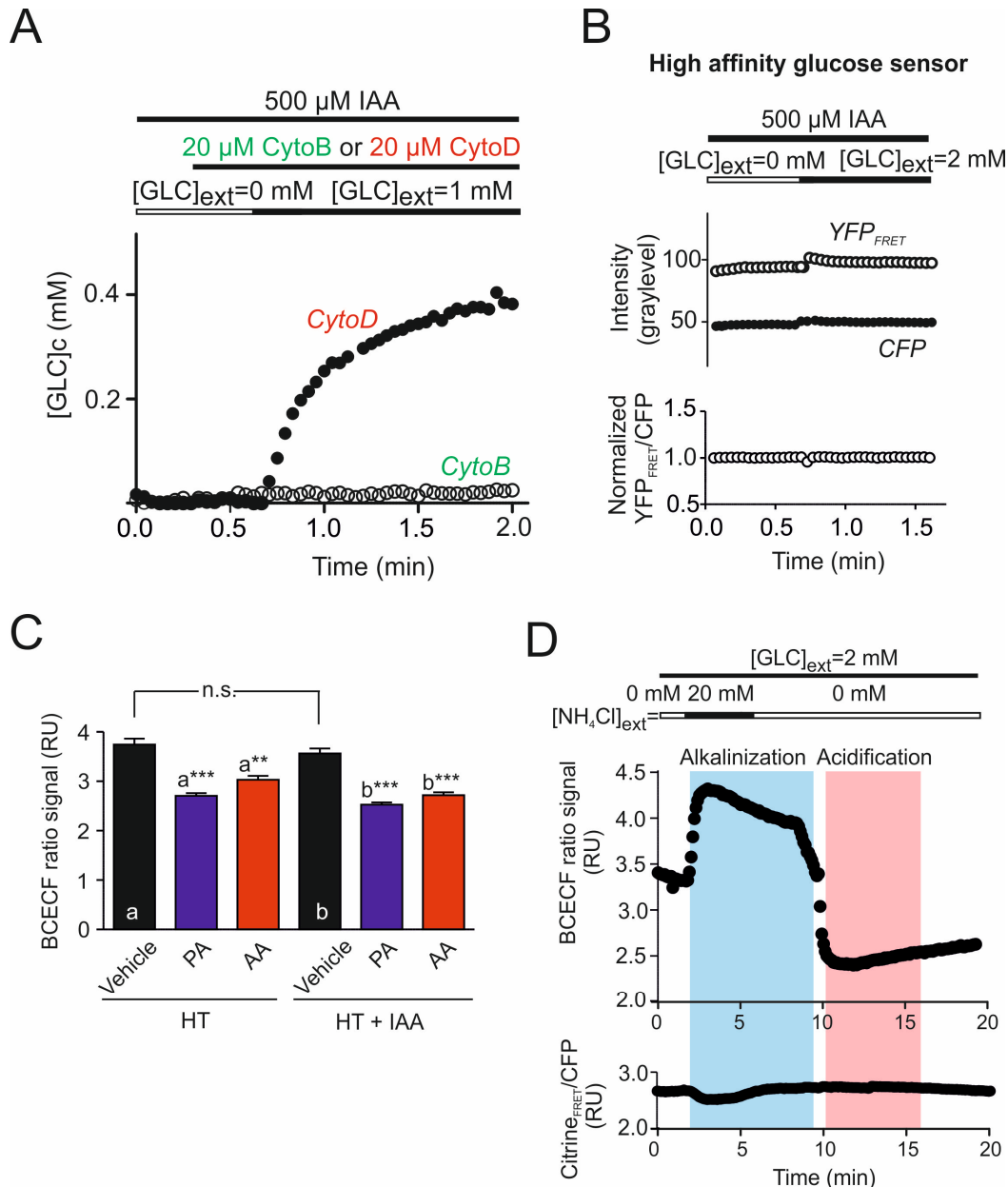


Figure S2. Validation of the experimental strategy for analysis of glucose uptake and consumption. (A) Typical glucose uptake in cells pretreated with CytoB (open symbols) or CytoD (filled symbols). Because CytoB might induce F-actin depolymerization, the structural analogue Cytochalasin D (CytoD), which has no effect on Gluts was used. In contrast to CytoB, glucose entry was not blocked by CytoD in IAA-treated cells. (B) Typical glucose uptake in cells expressing a high-affinity glucose sensor (FLIPglu-170n Δ 13V). (C) Effect of the various treatments on cytosolic pH. Cells were pretreated for 30 min with vehicle, PA or AA. Subsequently, cells were loaded with the pH sensor BCECF using a [GLC]_{ext} of 0 mM in the absence or presence of IAA. Statistical significance was determined using the Kruskal-Wallis test: N.s. not significant. (D) Effect of cytosolic pH changes on FLII fluorescence. Cytosolic pH was manipulated by transient extracellular addition ammonium chloride and monitored using the pH sensor BCECF (upper panel). In parallel experiments the response of FLII to these changes was determined (lower panel).

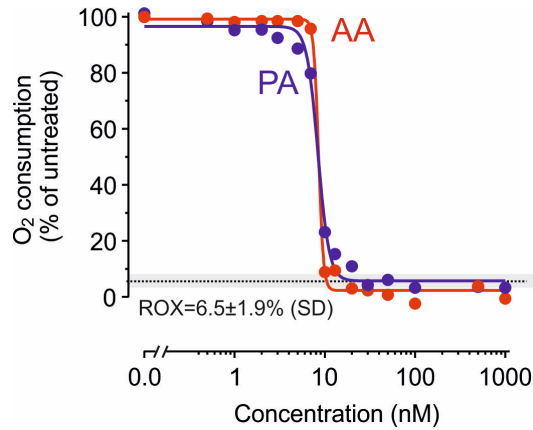


Figure S3. Dose-dependent inhibition of O₂ consumption by piericidin A and antimycin A in intact C2C12 cells. O₂ consumption rates of C2C12 cells in culture medium upon titration with piericidin A (PA) and antimycin A (AA). Respiration rates were normalized to basal respiration in the absence of inhibitor. The IC₅₀ value was determined by fitting a logistic equation ($y = [(A_1 - A_2) / (1 + (x / IC_{50})^p)] - A_2$) to the data ($R^2 > 0.95$), with A_1 being the initial respiration (*i.e.* 100%) and A_2 being the lowest respiration. Residual respiration (ROX) after rotenone (ROT) and antimycin A (AA) was displayed as percentage of basal respiration.

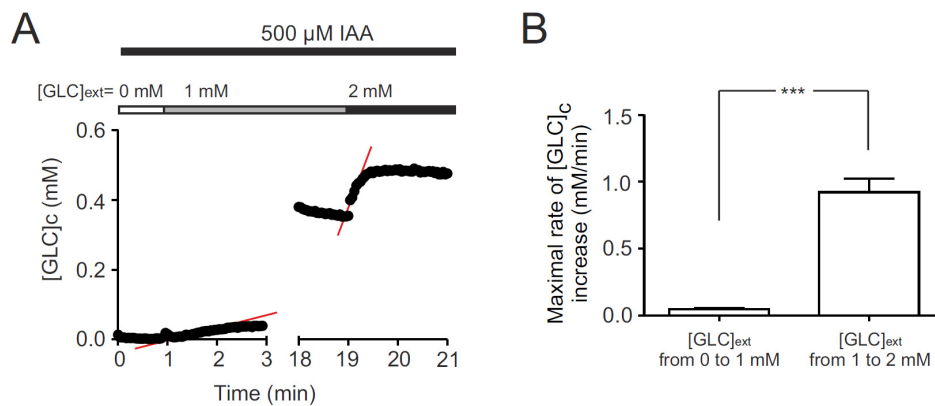


Figure S4. Effect of [GLC]_c on the maximal rate of [GLC]_c increase. (A) Typical kinetics of [GLC]_c upon acutely increasing [GLC]_{ext} from 0 to 1 mM (left part) and from 1 mM to 2 mM (after a 15 min waiting period; break). The experiment was carried out in the presence of IAA to block glucose consumption. The maximal rate of [GLC]_c increase was quantified using a linear fit (red lines). **(B)** Average maximal rate of [GLC]_c increase for the experiment depicted in panel A (N=2 experiments, n=18 cells).

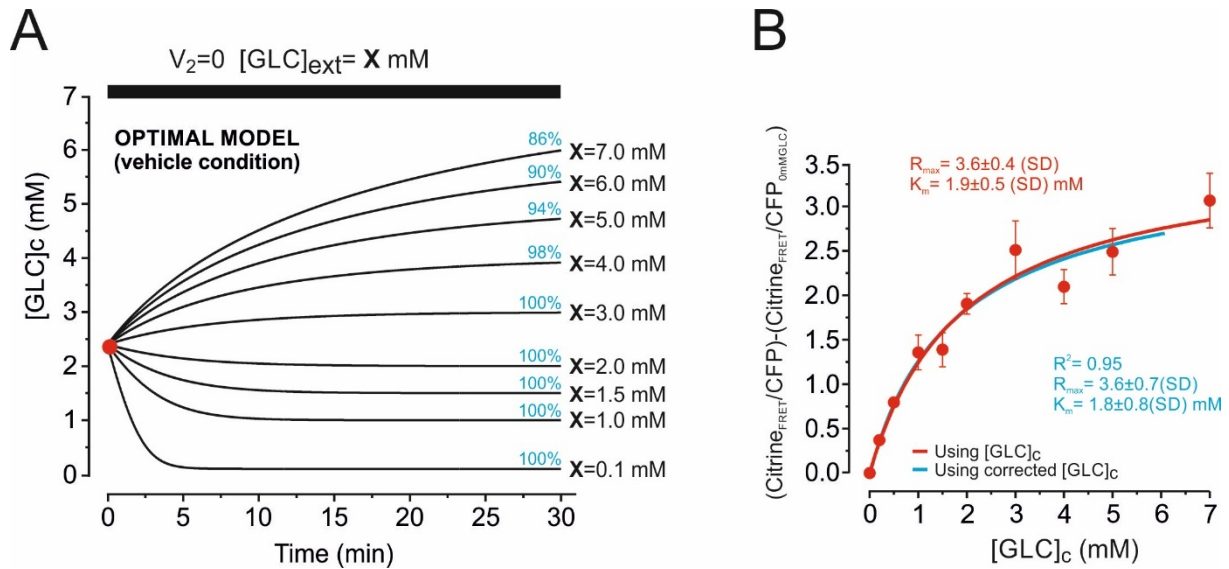


Figure S5. Effect of the magnitude of $[GLC]_{ext}$ on $[GLC]_c$ equilibration kinetics as predicted by the optimal model. (A) Simulations with the vehicle model were carried out to reflect the conditions during the FLII calibration protocol: At $t=t_0$ $[GLC]_{ext}$ increases to values (X) used during calibration (see Fig. 1C); the simulation time is 30 min to reflect the incubation time. Initial conditions: $[GLC]_{ext}=25$ mM, $[GLC]_c=2.4$ mM, $V_2=0$ to reflect the presence of IAA. After 30 min, full equilibration is predicted (*i.e.* $[GLC]_{ext}=[GLC]_c$) for $X=0.1$ mM, 1.0 mM, 1.5 mM, 2.0 mM, 3.0 mM and 4.0 mM. Partial equilibration was predicted for $X=5.0$ mM ($[GLC]_c$ equals 94% of $[GLC]_{ext}$), $X=6.0$ mM ($[GLC]_c$ equals 90% of $[GLC]_{ext}$) and $X=7.0$ mM ($[GLC]_c$ equals 86% of $[GLC]_{ext}$). The predicted partial equilibration at higher $[GLC]_{ext}$ did not affect the FLII calibration curve, since identical values for R^2 , R_{max} and K_m were obtained (panel B).

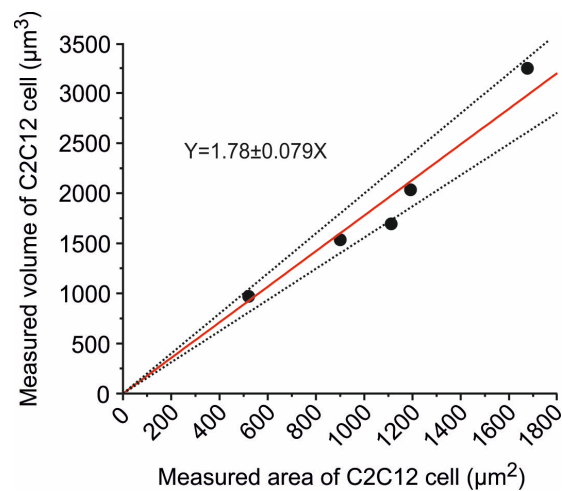


Figure S6. Area-volume relationship of C2C12 cells. To calculate the relationship between C2C12 cell area and volume we used data from 3D morphometric measurements of C2C12 cell (Slomka and Gefen, 2011). The relationship between area and volume was fitted using a linear equation (slope= 1.78 ± 0.08 , $p=0.001$, $R^2=0.98$). Dotted lines indicate 95% confidence limits.

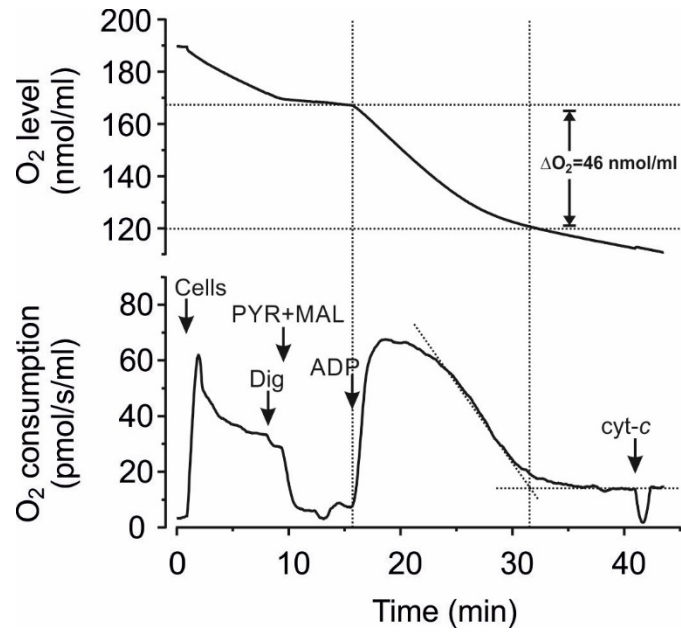


Figure S7. Quantification of P/O ratio in permeabilized C2C12 cells. C2C12 cells were added to the respirometry chamber and permeabilized using the detergent digitonin (Dig). Subsequently, pyruvate/malate (PYR+MAL) and ADP (220 nM) were added. The total amount of O₂ consumed (ΔO_2) following ADP addition allowed calculation of the P/O ratio. Mitochondrial integrity was assessed by adding cytochrome-c (cyt-c). This figure depicts a representative example of 4 independent experiments.

CHAPTER 4

Increased cellular glucose uptake in differentiating *Ndufs4* KO myoblasts



Adapted from:

Sander Grefte[#], Dania C. Liemburg-Apers[#], Ganesh R. Manjeri, Megan E. Breuer, Jori A. L. Wagenaars, Leanne H. J. de Ronde, Jan A. M. Smeitink, Peter H. G. M. Willems, Werner J. H. Koopman

[#]These authors contributed equally

(Submitted)

Abstract

Isolated complex I (CI) deficiency is among the most common mitochondrial oxidative phosphorylation (OXPHOS) disorders in humans. In Chapter 3 we demonstrated that chemical CI inhibition acutely stimulates the rate of glucose uptake in C2C12 mouse myoblasts. Here we quantified glucose uptake in primary myoblasts isolated from skeletal muscle of *Ndufs4* knockout (KO) mice with inherited CI deficiency. At high serum levels (41% of culture medium volume) and hyperglycemic external glucose concentration (25 mM), the rate of glucose uptake and mitochondrial O₂ consumption was similar for wild-type (WT) and KO myoblasts. At low serum levels (2% of culture medium volume), ATP-linked O₂ consumption increased in media containing 5 mM glucose or galactose compared to 25 mM glucose, albeit to the same extent in WT as in KO myoblasts. Interestingly, single cell glucose measurements revealed that the rate of glucose uptake increased to a greater extent in KO than in WT myoblasts in media containing 5 mM glucose or galactose compared to 25 mM glucose. This upregulation was not due to increased expression levels of glucose transporters (Glut1 or Glut4) and paralleled by increased levels of hydroethium-oxidizing reactive oxygen species. Our results suggest that mouse myoblasts become more dependent on OXPHOS-derived ATP when cultured under conditions of low serum and low glucose or galactose. In KO but not in WT myoblasts, this increased OXPHOS dependency is paralleled by a higher glucose uptake rate, suggesting that CI deficiency triggers a compensatory mechanism.

Introduction

Cellular energy metabolism is initiated by the uptake of metabolic substrates such as glucose. In most cells, glucose transporters (GLUTs) facilitate the passive transport of glucose across the plasma membrane. GLUTs are integral membrane proteins predicted to have 12 membrane spanning helices (Mueckler et al., 1985). Although 14 different Gluts have been described only some of them are localized to the plasma membrane and actually transport glucose (Joost et al., 2002, Carruthers et al., 2009). In skeletal muscle cells, GLUT1 is responsible for basal glucose uptake whereas insulin-stimulated glucose uptake is mediated by GLUT4 translocation to the plasma membrane (Thorens et al., 1990, Marette et al., 1992). After glucose is taken up by the cell, it is phosphorylated by hexokinases to form glucose-6-phosphate (G6P). The glycolytic conversion of G6P into pyruvate has a net yield of 2 ATP molecules per glucose molecule. Subsequent mitochondrial uptake and oxidation of pyruvate by the tricarboxylic acid (TCA) cycle yields another 2 ATP molecules per glucose molecule and reduces the electron carriers NAD^+ and FAD. Oxidation of NADH and FADH_2 by respectively the first (CI) and second (CII) multi-subunit complex of the oxidative phosphorylation (OXPHOS) system, releases energy which is used by CI-CIV to generate an electrical ($\Delta\psi$) and chemical (ΔpH) proton gradient over the mitochondrial inner membrane (MIM). The energy stored in this proton gradient is used by the fifth OXPHOS complex (the F_0F_1 -ATPase) to form ATP from ADP and inorganic phosphate (P_i). Depending on the coupling efficiency between proton pumping and ATP production, the OXPHOS system can yield another 30-32 molecules of ATP per molecule of glucose. The first complex of the OXPHOS system (CI) consists of 44 subunits which are assembled into a 1 MDa holo-complex (Walker, 1992, Smeitink et al., 1998, Balsa et al., 2012, Dieteren et al., 2012). CI deficiency is the most common OXPHOS disorder in humans (Smeitink et al., 2001, Koopman et al., 2010). Patients with CI deficiency suffer from a progressive multi-systemic disorder with an often fatal outcome (Smeitink and van den Heuvel, 1999, Koene et al., 2012). One of the subunits frequently mutated in CI deficiency is the 18 kDa accessory subunit NADH:ubiquinone oxidoreductase iron-sulfur protein 4 (NDUFS4), which is located in the peripheral arm of CI (Budde et al., 2003, Iuso et al., 2006, Petruzzella et al., 2001, Scacco et al., 2003, Calvaruso et al., 2012, Dieteren et al., 2012, Leshinsky-

Silver et al., 2009). Mutations in the *NDUFS4* gene generally results in truncation of the protein and absence of the C-terminal phosphorylation site, which is important for proper mitochondrial import and maturation of the precursor protein (Anderson et al., 2008, Papa et al., 2010, De Rasmio et al., 2008). As a consequence, mutations in *NDUFS4* generally lead to the complete absence of NDUFS4 protein and the accumulation of a ~830 kDa late stage CI assembly intermediate instead of fully assembled complex (Ugalde et al., 2004, Leshinsky-Silver et al., 2009, Assouline et al., 2012). In fibroblasts from patients bearing different mutations in this subunit, the residual CI activity ranges from 15-75% of the lowest control value (Koene et al., 2012, Verkaart et al., 2007b, Voets et al., 2012). *NDUFS4* mutations cause a Leigh-like syndrome, which presents as encephalopathy, optic atrophy, hypotonia, ataxia, neuropathy, and myopathy (Leigh, 1951). Generally, these symptoms appear a few months after birth and patients usually die a few years after the onset of symptoms (van den Heuvel et al., 1998, Petruzzella et al., 2001, Budde et al., 2000, Budde et al., 2003, Scacco et al., 2003, Petruzzella and Papa, 2002). Currently, there is no cure for CI deficiency and a better understanding of the metabolic consequences of *NDUFS4* mutations is required for the development of treatment strategies. To study this in more detail, a whole body knockout (KO) mouse model was created by deletion of the second exon of the *Ndufs4* gene (Kruse et al., 2008). This exon deletion causes complete absence of the Ndufs4 protein, resulting in a reduced stability of CI (Kruse et al., 2008, Valsecchi et al., 2012, Calvaruso et al., 2012). Although supercomplex formation with CIII provides partial CI stability and activity, the absence of Ndufs4 leads to a reduced expression level CI, suggesting unstable CI is degraded faster (Calvaruso et al., 2012). At birth, KO mice have a lower body weight compared to wild-type (WT) mice but appear healthy (Kruse et al., 2008). From about 5 weeks of age onward, the KO mice start to develop ataxic signs, dysfunctions in motor coordination, and failure to thrive, after which they die around 7 weeks of age (Kruse et al., 2008). The brain of 30-day-old KO mice displays an abnormal metabolic profile that includes accumulation of pyruvate, lactate, and glycolytic intermediates, which is consistent with clinical symptoms of Leigh syndrome (Johnson et al., 2013). To study intracellular pathophysiology, immortalized mouse embryonic fibroblasts (iMEFs) and primary mouse muscle and skin fibroblasts were obtained from wild-type (WT) and KO mice. Similar to patient fibroblasts, primary KO mouse muscle

and skin fibroblasts display increased reactive oxygen species (ROS) levels (based upon hydroethidium (HET) oxidation) (Valsecchi et al., 2013). In contrast, HET-oxidizable ROS levels were not increased in iMEFs, which might be due to a different cellular status (cell type, immortalization) (Valsecchi et al., 2012). However, it is to be expected that mitochondrial dysfunction mostly affects tissues with a high energy demand, such as muscle, which for the greater part depend on mitochondrial ATP production (Koopman et al., 2012). One of the compensatory mechanisms could be a switch to a more glycolytic mode of ATP production, which requires an increase in glucose uptake rate. For instance, in primary fibroblasts, CI dysfunction induces a complete reliance on glucose for cell survival (Distelmaier et al., 2015).

Here, primary myoblasts derived from *M. Soleus* from WT and KO mice were used to study the effect of inherited CI deficiency on glucose uptake. It was found that proliferating WT and KO myoblasts have similar rates of glucose uptake when cultured in proliferation medium containing high glucose and high serum levels. Switching to low serum and low glucose- or galactose-containing differentiation media increased ATP-linked oxygen consumption and revealed a significant increase in glucose uptake in KO myoblasts compared to WT. This increased glucose uptake rate in differentiating KO myoblasts is not due to upregulation of Glut1 or Glut4 expression and paralleled by increased levels of hydroethidium-oxidizing ROS.

Materials and Methods

Animals and housing conditions

Ndufs4 whole-body knockout (KO) and wild-type (WT) mice were generated by crossing heterozygote males and females with a mixed 129/sv x C57BL/6 background (Kruse et al., 2008). Animals were fed with a standard rodent diet *ad libitum* and housed at 21.0 °C, 60% humidity, and a standard light/dark (12 h/12 h) cycle. The Animal Experimentation Committee at the Radboud University Medical Centre approved, in accordance with Dutch laws and regulations regarding animal experimentation, breeding, and experiments.

Mouse behavioral studies

Only males were used for the behavioral studies, of which each animal was tested at 3, 5, and 6 weeks of life. Behavioral analysis was carried out by performing rotarod, rope grip, and grip strength analysis. On testing days, animal(s) were placed in the testing room for a 30 minute acclimation period. Animals were tested in one paradigm/day over the course of 3 days. The order of testing was consistent (for example, all animals were tested first on the rotarod on day 1, then the rope grip on day 2 and grip strength on day 3). After the day's testing was completed, all animals were returned to the colony room.

Rotarod

The rotarod paradigm was used to provide a quantitative readout of motor capabilities. The test consisted of a training period, during which the animals are exposed to the rotating rod, set at a constant 10 RPM, for 3 minutes. After the training period, the animals were tested a total of 3 times on the accelerating rotarod, with a 3 minute resting period in between each trial. The average time to fall from the rod (sec) is used as the readout parameter. The rotarod test is complete when the animal falls from the rod or if the animal remains on the rod until the maximum RPM is reached (300 sec).

Rope grip

The rope grip paradigm was used as a measure of muscular endurance. It consisted of a rope, suspended approximately 30 cm above the floor and approximately 100 cm long. Animals were placed on the middle of the rope, and allowed to grasp it with their fore paws only. The animal may then try to escape from the rope for an interval of 2 min. Normal rodent behavior dictates that the animal will try to escape by gripping the rope with all 4 limbs and crawling to either end of the rope, where they can then crawl to the floor, and safety. Animals with muscular dysfunctions will be unable to grip the rope properly, and will fall to the padded apparatus floor before the conclusion of the 2-minute test. The number of escapes during the 2 minutes was quantified, as well as how long (sec) the animals remained on the rope. The test was automatically concluded if the animal falls from the rope. The rope grip test was repeated 3 times (with a resting interval of 3 minutes), and the average number of escapes and average time on the rope were used as the readouts.

Grip strength

The grip strength paradigm was used as a measure for muscular forelimb strength. The device consisted of a single bar (TSE Systems, Germany). Animals will grasp the bar by instinct, which were gently retracted by the researcher until they were forced to release the bar. This was repeated 5 times for every animal and the average force exerted was used as the readout. Since body weight may play a role in the amount of force that was exerted, the measurements were corrected for body weight.

Myofiber and primary myoblast isolation

Female WT and KO mice (age: 38-42 days) were sacrificed by decapitation and *M. soleus* muscles were dissected. Individual myofibers were isolated as described in detail elsewhere (Collins and Zammit, 2009, Blanchet et al., 2014, Grefte et al., 2015). Isolated myofibers were cultured in proliferation medium consisting of DMEM (Invitrogen HQ, San Diego, CA, USA) supplemented with 30% (v/v) fetal bovine serum (FBS, PAA Laboratories, Cölbe, Germany), 10% (v/v) horse serum (HS, PAA Laboratories), 1% (v/v) chick embryo extract (CEE, MP Biomedicals Europe, Illkirch Cedex, France), 10 ng/ml basic fibroblast growth factor (bFGF, Invitrogen), and 1% (v/v) p/s (PAA Laboratories) for 3 days at 37 °C (95% air, 5% CO₂). In this period satellite cells grew out of the myofibers, which were then removed. Proliferating satellite cells (a.k.a. myoblasts) were trypsinized, pre-plated for 10 min in uncoated 6 wells-plate after which the non-adherent cells were transferred to a 6 wells-plate coated with Matrigel (1 mg/ml; Matrigel™ Basement Membrane Matrix, BD Bioscience, Bedford, MA, USA). WT and KO myoblasts were cultured for maximally one week and then used for experiments.

Transfection with glucose sensor

Myoblasts were electroporated with the glucose sensor FLII¹²Pglu-700μδ6 (Addgene Plasmid #17866) (Takanaga et al., 2008) using the Neon® Transfection System (Life Technologies). Coverslips (Ø24 mm) were first coated with 20 μg/ml fibronectin (Roche Diagnostics GmbH, Mannheim, Germany) for one hour and subsequently with 10 μl Matrigel to create a 'Matrigel-spot' for the cells. Cells were harvested, counted and washed with PBS. Per 10 μl Neon® Pipette Tip a suspension of 50,000-100,000 myoblasts in Resuspension Buffer R (Life Technologies) and 1 μg DNA was taken up. Cells were microporated in Electrolytic

Buffer E (Life Technologies) with a single pulse of 1350 V and a pulse width of 30 ms. Cells were recovered in pre-warmed proliferation medium without p/s at a density of 5,000 cells per 10 μ l (proliferation experiment) or 10,000 cells per 10 μ l (differentiation experiment). Matrigel was removed from spots and 10 μ l of microporated cells were seeded per spot. These spots were created to reduce the amount of cells necessary for microscopic analysis. After cell attachment (10 min), 3 ml proliferation medium without p/s was gently added and cells were further maintained at 37 °C (95% air, 5% CO₂).

Glucose uptake measurements

One day after transfection, the primary myoblasts were washed and incubated for 3 min in HEPES-Tris (HT) buffer (adjusted to pH 7.4 with Tris) containing 4.2 mM KCl, 132 mM NaCl, 10 mM HEPES, 1.2 mM MgCl₂ and 1 mM CaCl₂. Next, the original HT buffer was replaced with HT buffer containing 500 μ M iodoacetic acid (IAA, Sigma) and incubated for another 15 min. Subsequently, coverslips were mounted in an incubation chamber and placed on the stage of an inverted microscope (Axiovert 200 M, Carl Zeiss BV, Sliedrecht, The Netherlands) (Nooteboom et al., 2012), equipped with a x40/1.3 NA Plan NeoFluar objective (Carl Zeiss) and a CoolSNAP HQ monochrome CCD-camera (Roper Scientific, Vianen, The Netherlands). Microscopy hardware was controlled using Metafluor 6.0 software (Universal Imaging Corporation, Downingtown, PA, USA). FLII¹²Pglu-700 μ δ 6 was excited at 430 nm (CFP) for 300 ms using a Polychrome IV monochromator system (TILL Photonics, Gräfelfing, Germany). CFP fluorescence was detected using a 455DRLP dichroic mirror (XF2034, Omega Optical Inc, Brattleboro, VT, USA) and a 480AF30 (XF3075; Omega) emission filter. Citrine emission (Citrine_{FRET}) was measured using 430 nm excitation light (during 200 ms) and emission was detected using the 455DRLP dichroic mirror and a 535AF26 emission filter (XF3079; Omega). Time-lapse recordings were performed using an acquisition interval of 2.5 s. After a short baseline, HT buffer containing 4 mM glucose was added to the cells (1:1). Microscopy images were stored in native Metafluor format (12-bit; Universal Imaging Corporation) and analyzed off-line using Image Pro Plus 6.1 software (Media Cybernetics, Rockville, USA). Individual images were background corrected for each wavelength by subtracting the average intensity of an extracellular region of interest (ROI). Next, cell-derived fluorescence signals were quantified using cytosolic circular regions of interest (ROIs).

High-resolution respirometry

For every experiment, 2 ml of culture medium was collected. Myoblasts were trypsinized, washed and resuspended in the collected medium to 250,000 - 500,000 cells per 2 ml to measure cellular oxygen consumption using a two-chamber Oxygraph (Oroboros Instruments, Innsbruck, Austria) at 37 °C. First a basal oxygen consumption rate (basal) was obtained after which the complex V (CV)-inhibitor oligomycin A (OLI; 2.5 μM) was added to measure O₂ consumption related to mitochondrial proton leak (leak). Next 0.5 μM Carbonyl cyanide-4-(trifluoromethoxy)phenylhydrazone (FCCP) was added stepwise until the maximal O₂ consumption (maximal) was reached. Finally, rotenone (0.5 μM) and antimycin A (2.5 μM) were added together to determine non-mitochondrial O₂ consumption (ROX). This ROX value was subtracted from the basal, leak, and maximal oxygen consumption values. Finally, various derived parameters were calculated as follows (Dranka et al., 2011): non ATP-linked O₂ consumption ((leak/maximal)*100), ATP-linked O₂ consumption (((basal-leak)/maximal)*100) and reserve capacity (((maximal-basal)/maximal)*100).

Myoblasts differentiation

Approximately 4 hours after cell seeding or electroporation, cells were washed with PBS and placed in differentiation medium consisting of either DMEM containing 25 mM glucose (DM-HG; Invitrogen) or glucose-free DMEM (Invitrogen) supplemented with 5 mM glucose (DM-LG) or 5 mM galactose (DM-GAL). All media contained 2% (v/v) dialyzed fetal bovine serum (diFBS, Invitrogen) and 1% (v/v) p/s.

Quantitative PCR analysis

Myoblasts were seeded at 200,000 cells/well on matrigel-coated 6 wells plates and placed in differentiation medium as described above. After 24 hours cells were washed with cold PBS. Next, cells were lysed on ice using 300 μl lysis buffer (PureLink® RNA Mini Kit, Life technologies) containing 1% (v/v) β-mercaptoethanol per well. Homogenization was carried out using a 21 Gauge needle (BD Bioscience). Subsequently, RNA was extracted according to the manufacturer's protocol (PureLink® RNA Mini Kit, Life technologies). cDNA was generated from 1 μg RNA using the IScript cDNA synthesis kit (Biorad, Hercules, CA, USA) using the manufacturer's protocol. Quantitative real-time PCR was performed in a final

volume of 25 μ l containing 12.5 μ l SYBR[®]Green Supermix (Bio-Rad), 5 μ l (10x diluted) cDNA, 4.5 μ l RNase-free water, 1.5 μ l forward primer (2.5 μ M) and 1.5 μ l reverse primer (2.5 μ M). Primers for GAPDH and Glut1-4 (see below) were obtained from Biolegio (Nijmegen, The Netherlands). Amplification of cDNA was performed using a C1000 Thermal Cycler (Bio-Rad) and fluorescence was analyzed using the CFX96[™] Real-Time System (Bio-Rad). The PCR conditions were 95 °C for 3 minutes (1 cycle), 95 °C for 15 s and 60 °C for 30 seconds (39 cycles), and finally a temperature increase starting at 65 °C to 95 °C with 0.5 °C intervals. RNA expression was normalized against the mRNA level of GAPDH (DcT).

Glut1 TGCAGTTCGGCTATAACTG and GGTGGTTCATGTTTGATTG

Glut2 TGTGATCAATGCACCTCAAG and TCATAGTTAATGGCAGCTTTCC

Glut3 ACTCTTTGTCAACCGCTTTG and ATCTTGGCGAATCCCATAAG

Glut4 CTTGGCTCCCTTCAGTTTG and CACGTTGCATTGTAGCTCTG

GAPDH TGATGGGTGTGAACACGAG and GGGCCATCCACAGTCTTCTG

Western blot analysis

Cells were scraped and centrifuged at 600g for 5 min at 4 °C. Cell pellets were lysed in RIPA buffer consisting of 50 mM Tris-HCl (pH 7.4), 50 mM NaCl, 5 mM EDTA, 1% (w/v) deoxycholate, 1% (w/v) Triton X-100, 10 mM Na₄P₂O₇, 50 mM NaF, 0.1 mg/ml DNase, and 1x protease inhibitor cocktail. After 30 min rotation at 4 °C, cell suspensions were centrifuged at 15,000g for 10 min at 4 °C and supernatants were used for protein concentration determination by measuring the absorption at 280 nm using a Nanodrop 2000c spectrophotometer (Thermo Scientific). Proteins were denatured in sample buffer (250 mM Tris-HCl (pH 6.8), 160 mM dithiothreitol, 2% (w/v) SDS, 12% (v/v) glycerol, and 0.03% (w/v) bromophenol blue) at 70 °C for 10 min. Proteins (30 μ g/lane) were separated on 10% SDS-PAGE gels and transferred to polyvinylidene difluoride (PVDF) membranes (Novex, Life Technologies). Membranes were blocked with Odyssey blocking buffer (Li-Cor, Lincoln, NE, USA) in PBS (1:1) and incubated with polyclonal anti-GLUT1 (07-1401), polyclonal anti-GLUT4 (07-1404) (Millipore, Billerica, USA), and monoclonal anti- β -Actin (A5441) (Zwijndrecht, The Netherlands). For detection, IRDye 680RD-Conjugated Goat Anti-Mouse IgG (Li-Cor) and IRDye 800CW-Conjugated Goat Anti-Rabbit IgG (Li-Cor) secondary antibodies were used. Membranes were scanned and bands were quantified with Image Studio Lite version 4.0 software (Li-Cor).

Fluorescence microscopy of hydroethidium-oxidation, NAD(P)H autofluorescence, TMRM ($\Delta\Psi$)

The levels of H₂Et-oxidizing ROS were determined as described in detail previously (Grefte et al., 2015). Briefly myoblasts were loaded with 10 μ M H₂Et (Invitrogen) in culture medium for exactly 4.5 min, washed and transferred to a HT buffer. For NAD(P)H autofluorescence, cells were washed and transferred to a HT buffer. For TMRM fluorescence, cells were stained with 30 nM TMRM (Invitrogen) in the corresponding medium for exactly 25 min, washed and then transferred back to the original medium without TMRM. Coverslips were mounted in an incubation chamber and placed on the stage of an inverted microscope (Axiovert 200 M, Carl Zeiss). For H₂Et fluorescence, cells were excited at 490 nm for 100 ms using a monochromator (Polychrome IV, TILL Photonics). Fluorescence emission was directed to a CCD-camera using a 525DRLP dichroic mirror (Omega Optical Inc.) and a 565ALP emission filter (Omega Optical Inc.). For NAD(P)H autofluorescence, cells were excited at 360 nm for 1000 milliseconds using the Polychrome IV monochromator system and fluorescence emission was directed by a 430DCLP dichroic mirror (Omega Optical Inc, Brattleboro, VT, USA) and through a 480AF30 emission filter (Omega Optical Inc.). For TMRM fluorescence, cells were excited at 540 nm for 100 milliseconds and fluorescence emission was directed by a 560DRLP dichroic mirror (Omega Optical Inc.) and through a 565ALP emission filter (Omega Optical Inc.). Quantitative analyses were performed with the Metamorph 6.0 software (Universal Imaging Corporation). The mean fluorescence intensity in a mitochondrial-dense intracellular region (at least 10 different microscopic fields) was determined and corrected for background using an extracellular region of the same size.

Statistical analysis

Average values are presented as mean \pm standard error of the mean (SEM). Curve fitting was performed using Origin Pro 6.1 (OriginLab Corp., Northampton, USA) and statistical analysis was performed using GraphPad Prism 5 (Graphpad Software Inc., La Jolla, USA). Statistical significance relative to the indicated condition was determined using a One-way or Two-way ANOVA (followed by Bonferroni posttests) and marked by: *** (p<0.001), ** (p<0.01), and * (p<0.05).

Results

KO mice display decreased muscle endurance and strength

All KO mice displayed a severe progressive phenotype including loss of hair, motor dysfunction, ataxia, and died before the age of 45 days after birth as described previously (Kruse et al., 2008). At 3, 5, and 6 weeks after birth, WT and KO animals were subjected to rotarod, rope grip, and grip strength paradigms to determine their motor capabilities, muscle endurance, and muscle strength, respectively (Fig. 1). Three-weeks old KO mice displayed decreased motor capabilities and muscle endurance as indicated by the significant decreased time to fall during the rotarod and rope grip paradigms. At 5 and 6 weeks after birth these parameters in KO mice worsened confirming the progressive phenotype. Muscle (grip) strength of the KO mice was significantly decreased at 6 weeks of life. These data suggest that 5-6 weeks old KO mice display muscle dysfunction and therefore we isolated primary myoblasts from these animals to study whether glucose uptake was affected.

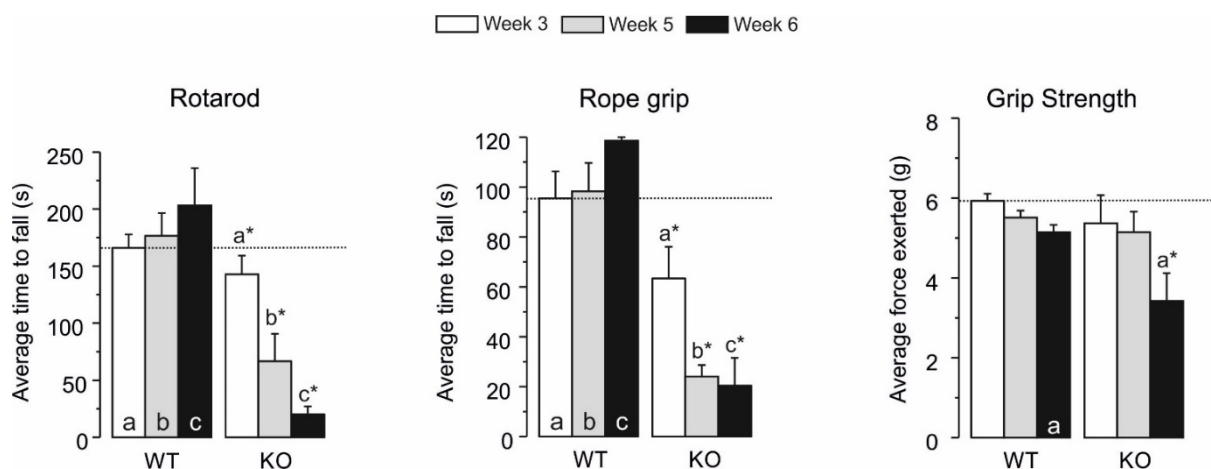


Figure 1. Rotarod, rope grip, and grip strength of WT and KO mice. WT and KO mice were tested at 3, 5, and 6 weeks of life for their motor capabilities, muscle endurance, and muscle strength using the rotarod, rope grip, and grip strength paradigms, respectively. Bar graphs represent mean values (WT, N=15 and KO, N=12 at 3 weeks; WT, N=14 and KO, N=9 at 5 and 6 weeks) and statistical significance between WT and KO is indicated by * ($p < 0.05$).

KO myoblasts show normal glucose uptake and oxygen consumption when cultured in high-glucose proliferation medium

For glucose uptake experiments primary myoblasts, derived from *M. Soleus*, were transfected with the glucose sensor FLII¹²Pglu-700 μ 86 (FLII), which consists of a glucose binding domain attached to cyan fluorescent protein (CFP) and the yellow fluorescent protein mutant Citrine (Takanaga et al., 2008). Glucose binding to the sensor increases the emission of Citrine upon CFP excitation (Citrine_{FRET}) and decreases the CFP emission upon CFP excitation (CFP). Glucose unbinding will induce the reverse effect and hence the emission ratio (Citrine_{FRET}/CFP) can be used as a measure of the intracellular glucose concentration (Takanaga et al., 2008). Glucose uptake was measured under zero-*trans* conditions in myoblasts pretreated with iodoacetic acid (IAA). The later was used to inhibit glucose consumption and allows for measurement of glucose uptake without underestimation due to glucose consumption (Chapter 3) (Liemburg-Apers et al., 2015a). Upon extracellular addition of 2 mM glucose the initial rate of increase in Citrine_{FRET}/CFP was quantified by fitting a linear equation to the steepest part of the Citrine_{FRET}/CFP increase (Fig. 2A). The slope of Citrine_{FRET}/CFP increase is a measure of the rate of glucose uptake (Chapter 3) (Liemburg-Apers et al., 2015a). The rate of glucose uptake was identical between WT and KO myoblasts cultured in proliferation medium containing 25 mM glucose (Fig. 2B). In addition, the average protein levels of Glut1, the primary Glut isoform in undifferentiated myoblasts (Al-Khalili et al., 2003), was not increased in lysates from KO myoblast compared to WT (Fig. 2C). Next, cellular O₂ consumption rates were examined in WT and KO primary myoblasts. KO myoblasts showed normal 'basal', 'leak' (CV-inhibitor OLI) and 'maximal' (CV-inhibitor OLI + mitochondrial uncoupler FCCP) O₂ consumption as compared to WT (Fig. 4A). Taken together, the above results suggest that KO myoblasts cultured in proliferation medium containing 25 mM glucose are not affected by the absence of *Ndufs4*.

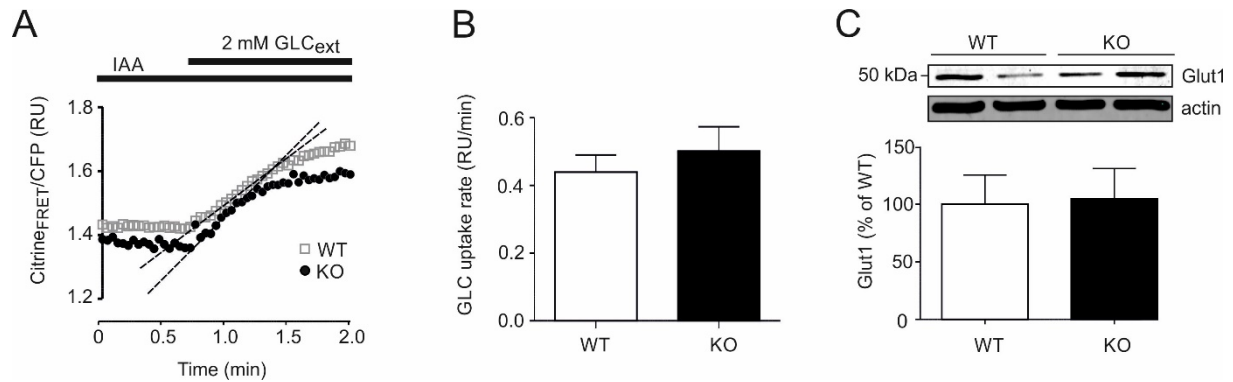


Figure 2. Glucose uptake in primary myoblasts cultured in proliferation medium. (A) Typical example of a glucose uptake experiment. Myoblasts expressing FLII were incubated in HT buffer containing 0 mM glucose for 18 min and 500 μ M IAA was added during the last 15 min. Next, 2 mM glucose was added to the cells. The Citrine_{FRET}/CFP was plotted in time. (B) The glucose uptake rate was quantified by fitting a linear equation to the part of steepest increase upon glucose addition as indicated by the dotted lines in panel B. Bar graphs represent the mean glucose uptake rate for WT (n=6 experiments) and KO (n=6 experiments). N=1 day. (C) Representative Western blot analysis of whole cell Glut1 expression in lysates from WT (2 mice) and KO (2 mice). Graph shows the average Glut1 optical densities normalized on actin optical densities for WT (6 mice) and KO (4 mice) myoblasts.

KO myoblasts show increased glucose uptake in low glucose and galactose differentiation medium

Empirical evidence suggests that proliferating cells rely less on OXPHOS-based ATP production than differentiated cells (Agathocleous et al., 2012). Therefore, we hypothesized that differentiation could make myoblasts more oxidative and reveal a higher glucose uptake rate in KO myoblasts. Myoblasts were cultured in differentiation medium (DM) containing 2% (low) FBS for 24 hours. The various differentiation media contained: 25 mM glucose (high glucose, DM-HG), 5 mM glucose (low glucose, DM-LG) or 5 mM galactose (DM-GAL). It is expected that cells become more dependent on OXPHOS-based ATP generation in DM-LG and DM-GAL (Elkalaf et al., 2013, Voets et al., 2012, Moran et al., 2010, van der Westhuizen et al., 2003). Reducing serum levels is known to induce myoblasts differentiation (Lawson and Purslow, 2000, Lattanzi et al., 2000, Columbaro et al., 2001, Faenza et al., 2003). However, visual inspection revealed that after 24 hours in differentiation medium, the majority of the myoblasts were not yet fully differentiated into multinuclear myotubes (Fig. 3A,B).

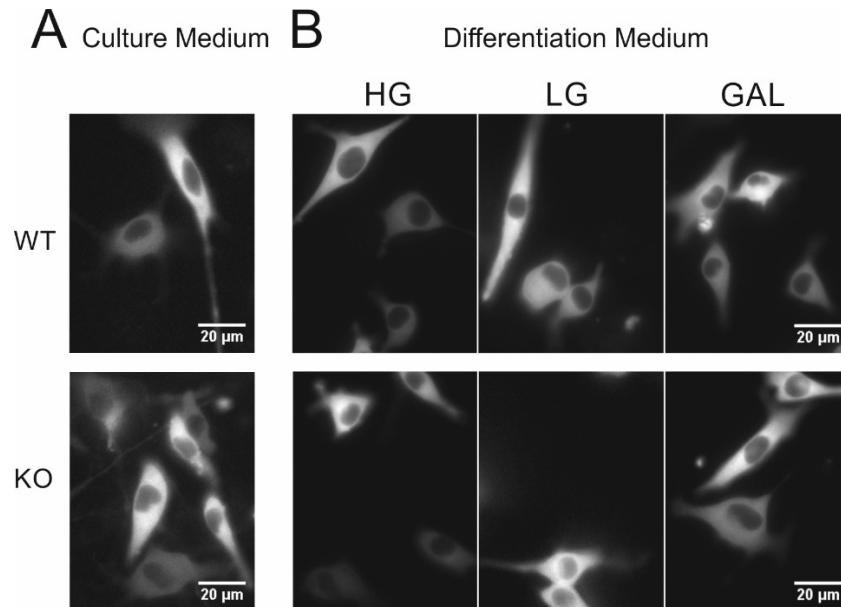


Figure 3. Typical images of FLII expressing WT and KO myoblasts cultured for 24 hours in (A) proliferation medium or in (B) DM-HG, DM-LG, or DM-GAL. Images show Citrine fluorescence intensities.

Basal, leak and maximal O₂ consumption did not differ between WT and KO myoblasts in DM-HG, DM-LG, and DM-GAL (Fig. 4B). However, both WT and KO myoblasts tended to display a higher basal O₂ consumption in DM-LG and DM-GAL. In the latter condition, leak O₂ consumption appeared slightly reduced. From these data the non-ATP linked (*i.e.* oligomycin-insensitive) and ATP-linked (*i.e.* oligomycin-sensitive) O₂ consumption and reserve capacity (*i.e.* FCCP-stimulated minus basal consumption) relative to the maximal O₂ consumption were calculated (Dranka et al., 2011) (Fig. 4C). The reserve capacity is considered an estimate of the amount of O₂ consumption available during conditions of increased ATP demand (Dranka et al., 2011). Switching to DM-GAL significantly increased ATP-linked O₂ consumption and decreased reserve capacity in both WT and KO myoblasts.

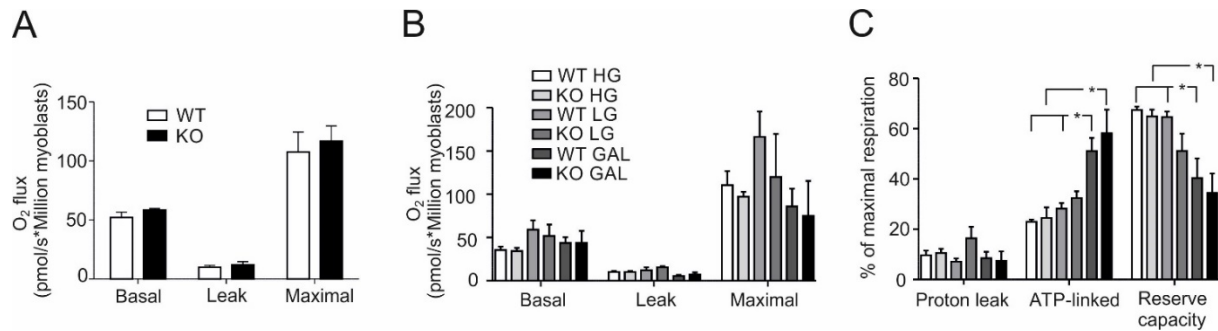


Figure 4. Oxygen consumption in primary myoblasts cultured in proliferation and differentiation medium. (A) Basal, leak and maximal oxygen consumption rates corrected for non-mitochondrial oxygen consumption rate of WT and KO myoblasts cultured in proliferation medium. Bar graphs represents mean values of 3 independent experiments. **(B)** Basal, leak and maximal oxygen consumption rates corrected for non-mitochondrial oxygen consumption rate of WT and KO myoblasts cultured for one day in DM-HG, DM-LG, DM-GAL. Bar graphs represents mean values of 3-4 independent experiments. **(C)** Proton leak, ATP linked oxygen consumption and reserve capacity were calculated from the values and conditions described in B. Bar graphs represent mean values of 3-4 independent experiments. One-way ANOVA Bonferroni posttests. * ($p < 0.005$).

Next, the rate of glucose uptake was measured in WT and KO myoblasts differentiated for 24 hours in DM-HG, DM-LG, or DM-GAL (Fig. 5A). Glucose uptake was significantly increased in DM-LG and DM-GAL conditions in both WT and KO myoblasts ($p < 0.01$ for WT; $p < 0.001$ for KO) (Fig. 5B). Under these conditions, glucose uptake was significantly faster in KO than in WT myoblasts ($p < 0.05$ for LG; $p < 0.001$ for galactose) (Fig. 5B). As shown in figure 2 of the general introduction, Glut4 expression is induced during C2C12 myoblasts differentiation. Therefore, it was determined which Gluts were expressed after 24 hours of differentiation and how DM-LG, and DM-GAL affected Glut expression in WT and KO myoblasts. QPCR analysis was unable to detect Glut2 and Glut3 but revealed that Glut1 and Glut4 were expressed in differentiating myoblasts (Fig. 5C). Although the protein levels of Glut1 were significantly increased in DM-GAL medium ($p < 0.05$), expression of this protein was not differentially affected (Fig. 5D). Glut4 expression was similar for DM-HG, DM-LG and DM-GAL condition and not significantly different between WT and KO myoblasts (Fig. 5E). These results suggest that KO myoblasts cultured in DM-LG or DM-GAL undergo a compensatory switch to a more glycolytic mode of ATP production.

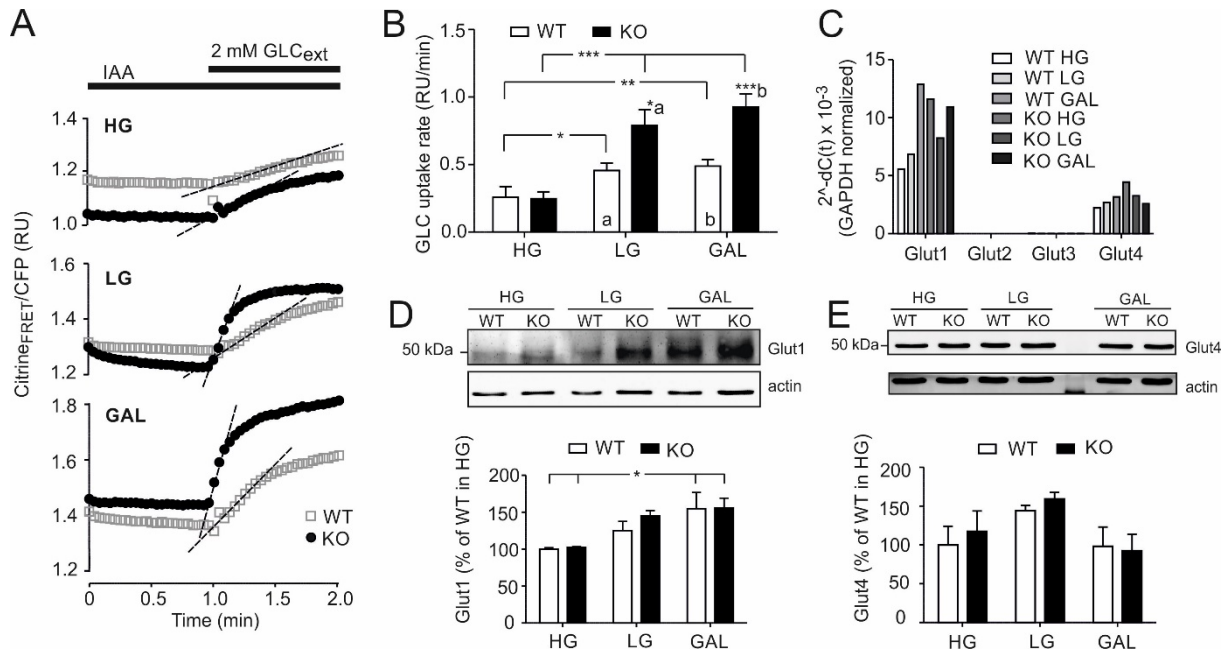


Figure 5. Glucose uptake in primary myoblasts cultured in differentiation medium. (A) Typical example of a glucose uptake experiment. Myoblasts expressing FLII were incubated in HT buffer containing 0 mM glucose for 18 min and 500 μ M IAA was added during the last 15 min. Next, 2 mM glucose was added to the cells. The Citrine_{FRET}/CFP was plotted in time. (B) The glucose uptake rate was quantified by fitting a linear equation to the part of steepest increase upon glucose addition as indicated by the dotted lines in panel A. Bar graphs represent the mean glucose uptake rate for WT HG (n=6 experiments), LG (n=6 experiments), GAL (n=6 experiments), and KO HG (n=6 experiments), LG (n=6 experiments), GAL (n=7 experiments). N=3 days. Two-way ANOVA Bonferroni posttest. (C) A qPCR with primers against mouse Glut1, Glut2, Glut3, and Glut4 was performed on cDNA generated from myoblasts cultured in DM-HG, DM-LG, and DM-GAL for 24 hours. Only mRNA of Glut1 and Glut4 were detected. N=1 (D) Representative Western blot analysis of whole cell Glut1 expression in lysates from WT and KO myoblasts cultured in DM-HG, DM-LG, or DM-GAL. Graph shows Glut1 optical densities normalized on actin optical densities for WT HG (4 mice), LG (3 mice), GAL (4 mice), and KO HG (4 mice), LG (3 mice), GAL (4 mice). (E) Representative Western blot analysis of whole cell Glut4 expression in lysates from WT and KO myoblasts cultured in DM-HG, DM-LG, or DM-GAL. Graph shows Glut4 optical densities normalized on actin optical densities for WT HG (4 mice), LG (3 mice), GAL (4 mice), and KO HG (4 mice), LG (3 mice), GAL (4 mice). Two-way ANOVA Bonferroni posttest *** = $p < 0.001$, ** = $p < 0.01$, * = $p < 0.05$.

KO myoblasts show increased hydroethidium oxidation in low glucose and galactose differentiation medium

In order to see how the different culturing conditions affected cellular pathology, NAD(P)H, H₂O₂-oxidizable ROS levels and $\Delta\Psi$ were measured in differentiating myoblasts. KO myoblasts were shown to have significantly increased NAD(P)H levels (Fig. 6A) and decreased $\Delta\Psi$ (Fig. 6B) in DM-HG, DM-LG, and DM-GAL. H₂O₂-oxidizable ROS levels (Fig. 6C) were similar between WT and KO myoblasts when differentiated in DM-HG. However, it is significantly increased ($p < 0.001$) in KO myoblasts when differentiated in DM-LG and DM-GAL.

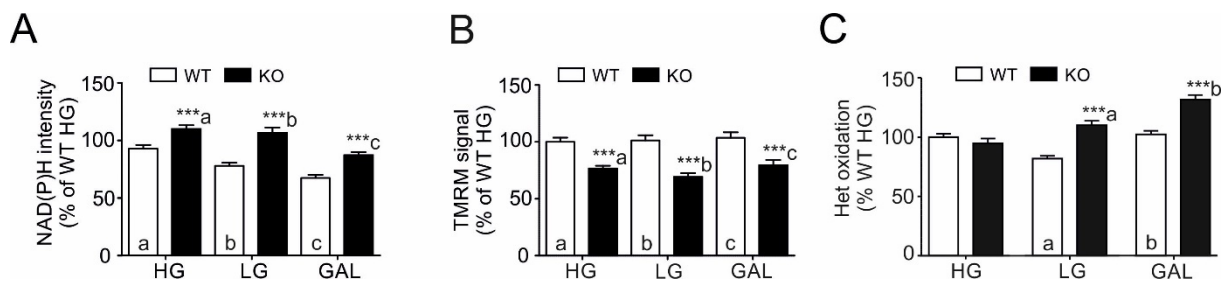


Figure 6. Cellular pathology in primary myoblasts cultured in differentiation medium. WT and KO myoblasts were differentiated for one day in DM-HG, DM-LG, DM-GAL after which (A) NAD(P)H autofluorescence, (B) TMRM fluorescence ($\Delta\Psi$) (C) the fluorescence of HET-oxidation products were measured in myoblasts using live-cell microscopy. Bar graphs represent mean values (WT HG: n=127, 212, and 170 cells; WT LG: n= 141, 218, and 144 cells; WT GAL: n= 100, 230, and 125 cells; KO HG; n= 137, 204, and 163 cells; KO LG: n= 104, 176, and 140 cells; KO GAL: n= 140, 190, and 123 cells for NAD(P)H, HET-oxidation, and TMRM respectively; all of 3 independent experiments) and statistical significance between the culturing conditions is indicated by *** ($p < 0.001$).

Discussion

To gain a better understanding of the cellular consequences and adaptation to CI dysfunction, glucose uptake was studied in proliferating and differentiating primary myoblasts from *Ndufs4* KO mice. In contrast to immortalized cells, primary cells still display some of their *in vivo* characteristics (Berggren et al., 2007). Because the absence of *Ndufs4* reduces CI stability and activity (Kruse et al., 2008, Calvaruso et al., 2012, Valsecchi et al., 2012), it was expected that KO myoblasts would display a more glycolytic mode of ATP production. However, in proliferation medium, no difference in the rate of glucose uptake and oxygen consumption was observed between WT and KO myoblasts. This could at least in part be due to the fact that proliferating cells are more glycolytic and rely less on OXPHOS for their ATP production than differentiated cells (Agathocleous et al., 2012). In addition, in order to keep primary myoblasts in an undifferentiated state, high serum levels (41%) and the growth factor basic fibroblasts growth factor (bFGF) were required. The latter induces HIF-1 α stabilization, leading to Glut1 upregulation and a glycolytic phenotype (Kihira et al., 2011). This glycolytic phenotype could mask the effects of CI deficiency on bioenergetics. To overcome the above potential drawbacks, myoblasts were cultured for 24 hours in differentiation medium in the absence of bFGF and in the presence of low serum levels (2%). Although the latter is known to induce myoblasts differentiation (Lattanzi et al., 2000, Lawson and Purslow, 2000, Columbaro et al., 2001, Faenza et al., 2003), we did not observe that

the majority of the WT and KO myoblasts fused into multinuclear myotubes within 24 hours. In differentiating KO myoblasts, intracellular pathophysiology was observed as a reduced $\Delta\Psi$ and an increased NAD(P)H autofluorescence. To further stimulate OXPHOS activity, next to a high external glucose concentration (25 mM; DM-HG), myoblasts were cultured in differentiation medium with a lower external glucose (5 mM; DM-LG), or glucose was displaced by galactose (DM-GAL). Culturing C2C12 myoblasts/myotubes at a normal external glucose concentration (5 mM) stimulates mitochondrial oxidative metabolism (Elkalaf et al., 2013). In addition, culturing in galactose medium stimulates OXPHOS-mediated ATP production (Moran et al., 2010, van der Westhuizen et al., 2003, Voets et al., 2012). The latter probably results from the fact that conversion of galactose into glucose-1-phosphate is very slow, thereby forcing cells to generate ATP from mitochondrial pyruvate oxidation (Reitzer et al., 1979). Our experimental results demonstrate that primary WT and KO mouse myoblasts display increased ATP-linked oxygen consumption and a decreased reserve capacity in DM-GAL compared to DM-HG, suggesting a shift from glycolytic towards mitochondrial ATP production. Furthermore, HET-oxidation was higher in KO myoblasts compared to WT in both DM-LG and DM-GAL. Moreover, culturing in DM-LG and DM-GAL medium revealed a significant higher rate of glucose uptake in KO compared to WT myoblasts. We propose a mechanism in which KO myoblasts cultured in DM-HG mainly use glycolysis for their ATP production (Fig. 7A). Switching to DM-LG and especially DM-GAL forces KO myoblasts to use their mitochondria for ATP production, which increases HET-oxidizing ROS (Fig. 7B). This ROS might be involved in the stimulation of glucose/galactose uptake to meet a higher pyruvate demand. However, basal O_2 consumption was not higher in KO myoblasts compared to WT, suggesting that mitochondrial pyruvate consumption is not increased. Alternatively, the increased glucose/galactose uptake could serve to produce more NADPH via the pentose phosphate pathway (PPP) for ROS scavenging (Le Goffe et al., 2002, Andrisse et al., 2014). However, the latter would suggest normal HET-oxidation in KO myoblasts, which was not observed, suggesting that the increased glucose uptake was not able to fully reduce the ROS levels. However, it is not known whether HET-oxidation would be even higher in KO myoblasts if glucose uptake was not stimulated.

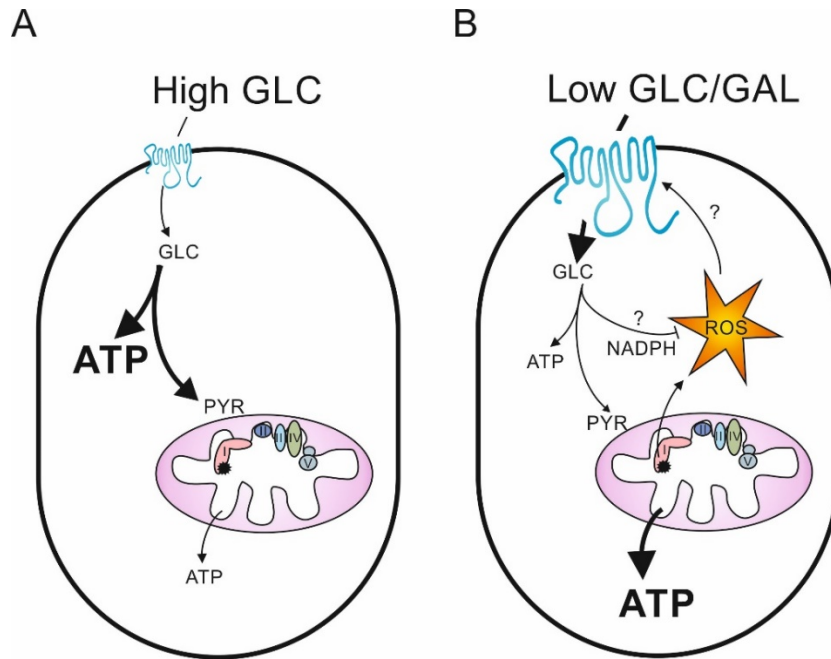


Figure 7. Proposed mechanism of cellular adaptation in KO myoblasts. (A) In high glucose differentiation medium (DM-HG) myoblasts mainly use glycolysis for their ATP production. (B) In low glucose (DM-LG) or galactose (DM-GAL) differentiation medium ATP-linked O₂ consumption and ROS levels are increased. This ROS might be involved in the stimulation of glucose uptake. Increased glucose uptake can increase NADPH production for ROS scavenging. GAL, galactose; GLC, glucose; PYR, pyruvate; ROS, reactive oxygen species.

ROS can stimulate glucose uptake via various different mechanisms (see General introduction). The increased H₂O₂-oxidation in KO myoblasts cultured in DM-LG and DM-GAL compared to DM-HG, suggests that ROS might be involved in the regulation of glucose uptake under these conditions. Using anti-oxidants the role of ROS in the regulation of glucose uptake in KO myoblasts cultured in DM-LG and DM-GAL could be further investigated. Interestingly, the increased rate of glucose uptake in KO myoblasts cultured in DM-LG and DM-GAL is not due to upregulation of Glut1 or Glut4. This is compatible with the fact that the magnitude of the rate of glucose uptake not always correlates with Glut1 expression levels (Abbud et al., 2000, Barnes et al., 2002, Hamrahian et al., 1999, Shetty et al., 1993, Shi et al., 1995). One explanation is that ROS induces a translocation of Glut1 and/or Glut4 to the plasma membrane in KO myoblasts as a response to an increased energy demand (see General introduction) (Chambers et al., 2009, Liemburg-Apers et al., 2015b). On the other hand, it could also be that ROS increases the intrinsic activity of Glut1 and/or Glut4 in KO myoblasts. Changes in the intrinsic activity of Glut1 upon OXPHOS inhibition have been reported previously and metabolic regulation by AMPK has been suggested to play a role in this (Abbud et al., 2000, Barnes et

al., 2002). Remarkably, both WT and KO myoblasts died after culturing for 24 hours in DM-GAL containing the AMPK inhibitor compound C (data not shown), suggesting that AMPK activity is essential for the survival of myoblasts. Nevertheless, the role of AMPK in the regulation of glucose uptake in KO myoblasts is not clear.

In conclusion, the glycolytic phenotype of primary myoblasts cultured in high serum- and bFGF-containing medium can be reversed by switching to DM-LG and especially DM-GAL. Under these conditions KO myoblasts display an increased level of H₂O₂-oxidizing ROS and an increased rate of glucose uptake compared to WT myoblasts. The latter is not due to upregulation of Glut1 or Glut4 expression.

Acknowledgements

This work was supported by equipment grants of ZonMW (Netherlands Organization for Health Research and Development, No: 903-46-176) and NWO (Netherlands Research) initiative from ZonMW (Grant: #CSBR09/013V) and the Dutch Energy4All foundation.

CHAPTER 5

Stimulation of glucose influx by acute mitoenergetic dysfunction requires LKB1, AMPK and Sirt2



Dania C. Liemburg-Apers, Jori A. L. Wagenaars, Jan A. M. Smeitink, Peter H. G. M. Willems, Werner J. H. Koopman

Abstract

Mitochondrial oxidative phosphorylation (OXPHOS) plays a central role in cellular energy production. We recently demonstrated using C2C12 myoblasts that acute mitoenergetic dysfunction triggers a compensatory increase in steady-state glucose flux to maintain ATP homeostasis. Here we aimed to highlight the mechanism by which acute OXPHOS inhibition stimulates glucose uptake in these cells. Treatment (30 min) with the OXPHOS inhibitors piericidin A or antimycin A greatly increased the maximal rate of glucose uptake. This uptake was mediated by Glut1, the mRNA level and plasma membrane abundance of which was not increased by inhibitor treatment. Piericidin A and antimycin A stimulated phosphorylation of AMP-activated protein kinase (AMPK) and, to a lesser extent, phosphorylation of serine-threonine liver kinase B1 (LKB1). Knockdown (KD) or chemical inhibition of AMPK greatly reduced the inhibitor-induced stimulation of glucose uptake. KD of LKB1 reduced the piericidin A- and antimycin A-induced increase in pAMPK levels and glucose uptake. Activated AMPK mediated *the novo* synthesis of NAD(H), maintaining a constant level of this nucleotide under conditions of mitochondrial inhibition. Inhibition of the NAD⁺-dependent deacetylating enzyme Sirt2 diminished the increased rate of glucose uptake, suggesting its activity - which is preserved by NAD⁺-synthesis - is necessary for the stimulation of glucose uptake. However, Sirt2 activity does not appear to be the driving force as the NAD⁺ precursor NMN only moderately stimulated glucose uptake. In addition, although Glut1 was found to be acetylated, mitochondrial inhibition did not appear to modulate the acetylation status. Our findings support a model in which acute mitoenergetic dysfunction stimulates Glut1-mediated via a LKB1-, AMPK-, and Sirt2-dependant mechanism.

Introduction

Glucose is one of the major substrates for ATP production and is passively taken up by cells via a family of facilitative glucose transporters (Gluts). Glut-mediated glucose transport depends on the gradient between the concentration of extracellular glucose ($[GLC]_{ext}$) and cytosolic glucose ($[GLC]_c$). In the cytosol glucose is phosphorylated by hexokinase (HK) to form glucose-6-phosphate (G6P). This means that the magnitude of the glucose gradient across the plasma membrane, and thereby the rate of Glut-mediated glucose influx, is largely determined by HK activity (Barros, Glia, 2007). Glucose is converted by the glycolysis pathway into pyruvate, a process yielding two ATP per glucose molecule. Pyruvate can be converted into lactate and released from the cell or taken up by mitochondria. In the latter case, pyruvate oxidation by the tricarboxylic acid (TCA) cycle yields another ATP and reduces four NAD^+ (into $NADH$) and one FAD molecule (into $FADH_2$). $NADH$ and $FADH_2$ are oxidized by complex I (CI) and complex II (CII) of the mitochondrial electron transport chain (ETC), respectively. The electrons released by these oxidations are subsequently transported to complex III (CIII; by coenzyme Q_{10}) and complex IV (CIV; by cytochrome-c). At CIV, the electrons are donated to molecular oxygen (O_2). Within the ETC, the energy released by the electron transport is used to drive proton transport out of the mitochondrial matrix (by CI, CIII and CIV). The resulting matrix-directed proton-motive force (PMF) is then used by the mitochondrial F_0F_1 -ATPase (CV) to drive ATP production via chemiosmotic coupling (Mitchell, 1961). Together, CI-CV constitute the mitochondrial oxidative phosphorylation (OXPHOS) system, which has a maximal yield of 32 ATP per molecule glucose.

Each OXPHOS complex consists of multiple subunits and requires the assistance of proteinaceous assembly factors to catalyze its biogenesis (Nouws et al., 2012, Acin-Perez and Enriquez, 2014). Mutations in structural subunits or assembly chaperones induce mitochondrial disease in humans (van den Heuvel and Smeitink, 2001, Koene et al., 2012, Loeffen et al., 2000). Interestingly, inherited CI deficiencies are the most common OXPHOS disorders (Skladal et al., 2003), whereas statin-induced myopathy was linked to its off-target effect on CIII (Schirris et al., 2015). Moreover, empirical evidence suggests that CI inhibition mediates the action of the antidiabetic drug metformin and is relevant in cancer treatment

(Schockel et al., 2015, Zhang et al., 2014, Chen et al., 2007, Vatrinet et al., 2015). In addition to inborn errors of energy metabolism, mitoenergetic dysfunction has also been linked to diabetes, obesity and neurodegenerative disorders (Koopman et al., 2013, Chandra and Singh, 2011, Correia et al., 2012, Costa and Scorrano, 2012, Martin, 2011, Patti and Corvera, 2010, Ritov et al., 2010, Swerdlow, 2012, Finsterer and Mahjoub, 2013).

To cope with mitoenergetic dysfunction and prevent energy crisis, cells can increase their glycolytic ATP production (Elstrom et al., 2004, Epstein et al., 2014, Liemburg-Apers et al., 2015a). In this respect, an increased glycolytic rate was observed in fibroblasts from patients with myoclonic epilepsy and ragged-red fibers (MERRF) syndrome (Wu and Wei, 2012) and cells chronically treated with the CI inhibitor rotenone (Distelmaier et al., 2015). Also silencing of the CI gene *NDUFS3* triggered a glycolytic switch (Suhane et al., 2013). Increasing the glycolytic rate in some cases requires an increase in Glut-mediated glucose uptake capacity (Barros et al., 2007). The Glut family consists of 14 members of which Glut1 is the best studied and most abundant isoform in proliferating cells (Mann et al., 2003). Glut1 is an integral membrane glycoprotein consisting of 12 membrane spanning α -helices (Mueckler et al., 1985). Although monomeric Glut1 is a functional transporter, dimeric and tetrameric structures greatly accelerate its catalytic activity (Hebert and Carruthers, 1992, Zottola et al., 1995). Long-term upregulation of glucose uptake usually involves an increased level of Glut1 protein at the plasma membrane (Wang et al., 2013, Wu and Wei, 2012). However, the Glut1 transport activity can also be increased within 2 hours in response to oxidative stress (Prasad and Ismail-Beigi, 1999), metabolic stress (Barnes et al., 2002, Jing and Ismail-Beigi, 2007, Mercado et al., 1989, Shetty et al., 1993, Shi et al., 1995, Hamrahian et al., 1999, Koseoglu and Beigi, 1999, Cura and Carruthers, 2012, Abbud et al., 2000) and anoxia (Wheeler, 1988). Mechanistically, Glut1 transport capacity can be stimulated by: (i) increasing the translocation of Glut1-containing vesicles from the cytosol to the plasma membrane (Cura and Carruthers, 2012, Jing et al., 2008, Wheeler, 1988) or (ii) 'unmasking' of Glut1 transporters already present at the plasma membrane (*i.e.* enhancing the accessibility of Glut1 to glucose) (Abbud et al., 2000, Barnes et al., 2002, Hamrahian et al., 1999, Shetty et al., 1993, Shi et al., 1995, Mercado et al., 1989).

In chapter 3 we demonstrated that acute (30 min) inhibition of CI by piericidin A (PA) or CIII by antimycin A (AA) increased glucose uptake and consumption in C2C12 myoblasts (Liemburg-Apers et al., 2015a). The latter fully compensated for the loss in mitochondrial ATP production and thereby maintained ATP homeostasis, as supported by the fact that the amount of total cellular ATP was not significantly altered in cells treated for 24 hours with PA- and AA (Liemburg-Apers et al., 2015a). Combining the above experimental strategy with mathematical modeling led us to propose that mitoenergetic dysfunction evokes a rapid compensatory increase in steady-state glucose uptake and consumption to prevent energy crisis in cells with a compromised mitochondrial ATP generation. In this study we investigate the mechanism by which acute CI and CIII inhibition stimulate glucose uptake in C2C12 cells.

Our results show that the amount of Glut1 at the plasma membrane remains constant upon inhibition of CI/CIII, suggesting activation of Glut1 transporters already present at this site. This activation of Glut1 requires the activity of LKB1, AMPK, and Sirt2.

Materials and methods

Chemicals

Sodium iodoacetic acid (IAA), Antimycin A (AA), 5-Aminoimidazole-4-carboxamide ribonucleotide (AICAR), 2-cyano-3-[5-(2,5-dichlorophenyl)-2-furanyl]-N-5-quinoliny-2-propenamide (AGK2), β -nicotinamide mononucleotide (NMN), trichostatin A (TSA), 4-hydroxy-2,2,6,6-tetramethylpiperidin-1-oxyl (4-Hydroxy-TEMPO or Tempol), and 4-amino-5-(4-chlorophenyl)-7-(dimethylethyl)pyrazolo[3,4-d]pyrimidine (PP2) were obtained from Sigma-Aldrich (Zwijndrecht, The Netherlands). Piericidin A (PA) was obtained from Enzo Life Sciences (Raamsdonksveer, The Netherlands). 6-[4-[2-(1-Piperidinyloxy)phenyl]-3-(4-pyridinyl)pyrazolo[1,5-a]pyrimidine (Compound C) was obtained from Calbiochem (Billerica, MA). 6-hydroxy-2,5,7,8-tetramethylchroman-2-carboxylic acid (Trolox) was obtained from Fluka (Buchs, Switzerland). 2-morpholino-6-(thianthren-1-yl)-4H-pyran-4-one (KU55933) was obtained from Abcam (Cambridge, UK).

Cell culture

C2C12 myoblasts were cultured at 37 °C (95% air, 5% CO₂) in Dulbecco's modified eagle's medium (DMEM-32430; Life Technologies Invitrogen, Bleiswijk, The Netherlands), supplemented with 10% (v/v) fetal bovine serum (FBS) (10270-106; Life Technologies Invitrogen). For glucose measurements myoblasts were seeded in Fluorodishes® (#FD35-100; World Precision Instruments, Sarasota, USA) at a density of 40,000 cells/dish.

Transfection

One day after seeding, 1 µg DNA was mixed with 6 µl lipofectamine (Life Technologies Invitrogen) in 0.5 ml FBS-free DMEM. Following 20 min incubation at room temperature the transfection mix was added to the cells in FBS-free DMEM. After 6 hours this medium was replaced by DMEM containing 10% FBS. The glucose sensor FLII¹²Pglu-700µδ6 (FLII) (Addgene Plasmid #17866) (Takanaga et al., 2008) was a gift from Dr. Wolf Frommer (Department of Plant Biology, Carnegie Institution for Science, CA, USA).

Single cell glucose uptake measurements

These experiments were carried out using a protocol described in detail previously (Liemburg-Apers et al., 2015a). Cells were washed and incubated for 3 min in HEPES-Tris (HT) buffer (adjusted to pH 7.4 with Tris) containing 4.2 mM KCl, 132 mM NaCl, 10 mM HEPES, 1.2 mM MgCl₂ and 1 mM CaCl₂. Next, cells were placed on an inverted microscope (Axiovert 200 M, Carl Zeiss BV, Sliedrecht, The Netherlands). FLII was excited at 430 nm (CFP) for 300 ms, CFP fluorescence was detected using a 455DRLP dichroic mirror and a 480AF30 emission filter. Citrine emission (Citrine_{FRET}) was measured using 430 nm excitation light (during 200 ms) and emission was detected using the 455DRLP dichroic mirror and a 535AF26 emission filter. Time-lapse recordings were performed using an acquisition interval of 2.5 s. Individual images were background corrected for the individual wavelengths by subtracting the average intensity in an extracellular region of interest (ROI). Next, cell-derived fluorescence signals were quantified using cytosolic circular regions of interest (ROIs). Citrine_{FRET}/CFP emission ratios were converted to [GLC]_c using a previously generated *in situ* calibration curve (Liemburg-Apers et al., 2015a). Per experiment a minimum of 15 cells was analyzed.

Quantitative PCR analysis

This was carried out as described previously (Liemburg-Apers et al., 2015a). The primer sequences were:

Glut1: TGCAGTTCGGCTATAACACTG and GGTGGTCCATGTTTGATTG,

Glut2: TGTGATCAATGCACCTCAAG and TCATAGTT-AATGGCAGCTTTCC,

Glut3: ACTCTTTGTCAACCGCTTTG and ATCTTGGCGAATCC-CATAAG,

Glut4: CTTGGCTCCCTTCAGTTTG and CACGTTGCATTGTAGCTCTG,

Actin: CTAAGGCCAACCGTGAAAAG and TACGACCAGAGGCATACAGG.

Preparation of whole cell lysates

After treatment cells were scraped and centrifuged at 600 g for 5 min at 4 °C. Cell pellets were lysed in RIPA buffer containing 50 mM Tris-HCl (pH 7.4), 50 mM NaCl, 5 mM EDTA, 1% (w/v) deoxycholate, 1% (w/v) Triton X-100, 10 mM Na₄P₂O₇, 50 mM NaF, 0.1 mg/ml DNase, and 1x protease inhibitor cocktail. For pSrc analysis vanadate (1 mM) was added to the RIPA buffer. After 30 min incubation under gentle rotation at 4 °C, cell suspensions were centrifuged at 15,000g for 10 min at 4 °C and supernatants were used for protein concentration determination by measuring the absorption at 280 nm using a Nanodrop 2000c spectrophotometer (Thermo Fisher Scientific, Waltham, MA, USA).

Western blot analysis

Proteins were denatured in sample buffer containing 250 mM Tris-HCl (pH 6.8), 160 mM dithiothreitol, 2% (w/v) SDS, 12% (v/v) glycerol, and 0.03% (w/v) bromophenol blue at 70 °C for 10 min. Proteins (30 µg/lane) were separated on 10% SDS-PAGE gels and transferred to polyvinylidene difluoride (PVDF) or nitrocellulose membranes (Novex, Thermo Fisher Scientific). Membranes were blocked with Odyssey blocking buffer (Li-Cor, Lincoln, NE, USA) diluted 1:1 in PBS (v/v) and incubated with primary antibodies. Polyclonal anti-Glut1 (07-1401), monoclonal anti-LKB1 (05-832), and polyclonal anti-phosphoLKB1(Ser431) (09-495) were obtained from Millipore (Billerica, USA). Polyclonal anti-AMPK (2532L), monoclonal anti-phosphoAMPK (Thr172) (2535L), and anti-phospho-Acetyl-CoA Carboxylase (Ser79) (3661S) were obtained from Cell Signaling (Bioke, Leiden, the Netherlands). Monoclonal anti-β-Actin (A5441) was obtained from Sigma. Polyclonal anti-phosphoSrc (Tyr418) (44-660G) was obtained from Invitrogen. For detection, IRDye 680RD-Conjugated Goat Anti-Mouse IgG and IRDye 800CW-

Conjugated Goat Anti-Rabbit IgG (Li-Cor, Lincoln, NE, USA) secondary antibodies were used. Membranes were scanned and band intensities were quantified with Image Studio Lite version 4.0 software (Li-Cor). Recombinant Src (14-117; Upstate, Millipore) was phosphorylated *in vitro* (Weigand et al., 2012).

Cell surface protein biotinylation

Biotinylation was performed using the Pierce Cell Surface protein isolation kit (89881; Thermo Fisher Scientific) according to the manufacturer's protocol. For each condition two confluent T175 culture flasks were used. After treatment cells were incubated with Sulfo-NHS-SS-Biotin and biotinylated proteins were purified using NeutrAvidin Agarose Resin. Purified biotinylated proteins were loaded on a Western blot and visualized using an anti-Glut1 antibody (see above).

Gene knock-down

AMPK knock-down was performed by transfecting 75,000 cells with 60 ng siRNA directed against AMPK α 1 and AMPK α 2 subunits (sc-45313) or scramble siRNA (sc-37007) (Santa Cruz Bioconnect Life Sciences, Huissen, The Netherlands). LKB1 knock-down was performed by transfecting 75,000 cells with 100 nM siRNA directed against LKB1 (s74499) or scramble (Silencer select negative control No. 1) (Life Technologies Invitrogen). Transfection with siRNA was performed using the Neon[®] Transfection System (Life Technologies Invitrogen) according to manufacturer's protocol for C2C12 myoblasts. One day after siRNA addition cells were transfected with FLII using lipofectamine (see the above section on transfection). Two day after siRNA addition cells were used for experiments.

NAD(H) measurements

Per sample 50,000 cells were seeded in a 6 well plate and used the next day for measurements. For AMPK knock-down experiments cells were transfected with siRNA, seeded in 6 wells plates and used for measurement 2 days later. After treatment cells were scraped and NAD⁺ and NADH were quantified using the EnzyFluo[™] NAD⁺/NADH Assay Kit (EFND-100, BioAssay Systems, Hayward, CA, USA) according to the manufacturer's protocol. Upon the addition of reagent the optical density (OD) at 560 nm was measured using a 2 min interval on the Synergy 2 multi-mode reader (Biotek, Abcoude, The Netherlands). The Δ OD (10 min) values were normalized to vehicle per experiment.

Hydroethidium oxidation

The levels of hydroethidium (HEt)-oxidizing ROS were determined as described in detail previously (Grefte et al., 2015, Forkink et al., 2015). Cells were pretreated for 30 min with mitochondrial inhibitors followed by an 18 min incubation in the absence of glucose of which the last 15 min were in the presence of IAA and the last 5 min in the presence of 10 μ M HEt (Life Technologies Invitrogen). Next, the cells were washed with HT buffer and Fluorodishes® were mounted in an incubation chamber and placed on the stage of an inverted microscope (Axiovert 200 M, Carl Zeiss). Cells were excited at 490 nm for 100 ms using a monochromator (Polychrome IV, TILL Photonics). Fluorescence emission was detected by a 565ALP emission filter. Quantitative analyses were performed using Metamorph 6.0 software (Universal Imaging Corporation). The mean fluorescence intensity in a mitochondria-dense and nuclear region was determined for at least 10 different microscopic fields and corrected for background intensity using an extracellular region of identical size.

Immunoprecipitation

For protein acetylation analysis, lysate preparation and immuno-precipitation (IP) were performed in the presence of nicotinamide (NAM; 10 mM) and trichostatin A (TSA; 1 μ M). IP of acetylated proteins was performed by incubating 1 g of protein cell lysate with 5 μ g mouse anti-acetyl-lysine (clone 4G12, Millipore) overnight under gentle rotation at 4 °C. On the following day 100 μ l Dynabeads® Protein G (Novex, Thermo Fisher Scientific) were added and incubated for 2 hours under gentle rotation at 4 °C. The beads were washed 3x with PBS and proteins were eluted in 30 μ l 4x sample buffer at 70 °C for 10 min and loaded on Western blot. Acetylated-Glut1 was quantified by correcting the Glut1 signal for the loading control anti-acetyl-lysine heavy chain (HC). IP of Glut1 was performed by covalently cross-linking rabbit anti-Glut1 (ab32551, Abcam, Cambridge, UK) to Dynabeads® Protein G. After a 10 min incubation under gentle rotation of 50 μ l Dynabeads® Protein G with 5 μ g anti-Glut, beads were washed 3x in conjugation buffer containing 20 mM sodium phosphate, 0.15 M NaCl (pH 7-9) and incubated for 30 min under gentle rotation at RT in conjugation buffer containing 5 mM of the amine-to-amine crosslinker bis(sulfosuccinimidyl)suberate (BS³; Thermo Fisher Scientific). Cross-linking was quenched by adding 16 mM Tris (pH 7.5) and

incubated for 15 min under gentle rotation at RT. Next, beads were washed 3x in PBS-T (PBS + 0.01% Tween) and incubated with 2 g protein cell lysate for 15 min under gentle rotation at RT. Beads were washed 3x with PBS and proteins were eluted in 30 μ l 4x sample buffer at 70 °C for 10 min and loaded on Western blot. The amount of acetylated-Glut1 was quantified by normalizing the acetylation signal to the Glut1 signal.

Statistical analysis

Average values are presented as mean \pm standard error of the mean (SEM). Curve fitting and statistical analysis were performed using Origin Pro 6.1 (OriginLab Corp., Northampton, USA) and GraphPad Prism 5 (Graphpad Software Inc., La Jolla, USA). Unless stated otherwise, statistical significance relative to the indicated condition was determined using a Kruskal-Wallis (followed by a Dunn's post hoc test) or a Two-way ANOVA (followed by Bonferroni post hoc test) and marked by: *** ($p < 0.001$), ** ($p < 0.01$) or * ($p < 0.05$).

Results

Acute OXPHOS inhibition stimulates glucose uptake

To quantify glucose uptake, C2C12 myoblasts were transfected with the glucose sensor FLII¹²Pglu-700 μ δ 6 (FLII) (Takanaga et al., 2008) and imaged using epifluorescence microscopy. FLII consists of a glucose binding domain attached to CFP and the YFP-variant Citrine. The binding and unbinding of glucose triggers conformational changes within the sensor that affects the efficiency of fluorescence resonance energy transfer (FRET) from CFP to Citrine. The Citrine_{FRET}/YFP emission ratio is a measure of the free cytosolic intracellular glucose concentration ([GLC]_c) and was previously calibrated *in situ* in C2C12 cells (Liemburg-Apers et al., 2015a). To study the effects of acute OXPHOS inhibition on glucose uptake, cells were first pretreated (30 min) with vehicle (0.01% ethanol), the CI inhibitor PA (100 nM), or the CIII inhibitor AA (20 nM). Importantly, we demonstrated previously that these inhibitor regimes fully blocked mitochondrial O₂ consumption and mitochondrial ATP production in C2C12 cells (Liemburg-Apers et al., 2015a). Next, the cells were depleted of glucose by placing them in a glucose-free medium for 18 min. During the last 15 min of incubation, this medium

contained the Glyceraldehyde 3-phosphate dehydrogenase (GAPDH) inhibitor iodoacetic acid (IAA) to inhibit glucose consumption. IAA (500 μ M) was required to prevent underestimation of glucose uptake due to glucose consumption (Liemburg-Apers et al., 2015a). Then, glucose uptake was measured by adding 2 mM of glucose to the cells. Quantification of the maximal rate of linear increase (Fig. 1A; lines), which is a measure of the rate of glucose uptake (Liemburg-Apers et al., 2015a), demonstrated that PA- and AA-treatment increased glucose uptake from 0.4 mM/min (vehicle) to 3 mM/min (Fig. 1B).

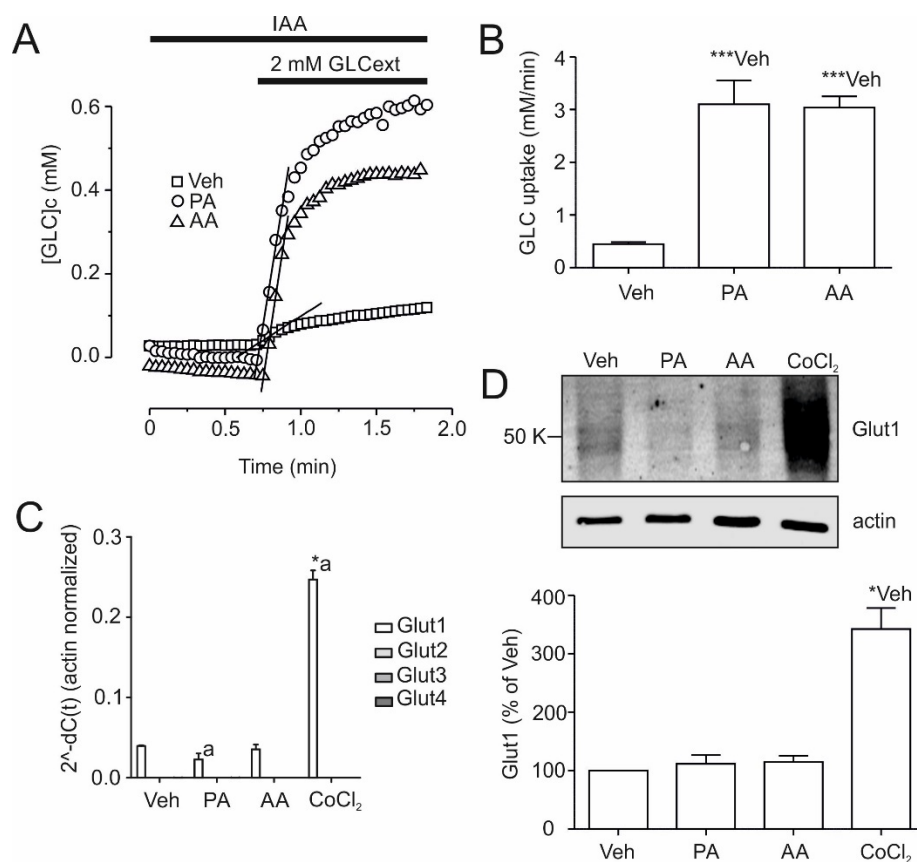


Figure 1. Acute OXPHOS inhibition stimulates Glut1-mediated glucose uptake in C2C12 myoblasts. (A) Myoblasts were incubated for 30 min with vehicle (Veh), PA or AA. Glucose uptake was analyzed using fluorescence microscopy of cells expressing the glucose sensor FLII. Prior to imaging, myoblasts were incubated for 18 min in the absence of glucose, the last 15 min of which was in the presence of the glucose consumption inhibitor IAA. Next, the FLII fluorescence emission ratio (Citrine_{FRET}/YFP) was measured during addition of 2 mM extracellular glucose. Citrine_{FRET}/YFP was calibrated, allowing calculation of [GLC]_c in mM. The maximal rate of [GLC]_c increase (lines), was quantified and taken as a measure of glucose uptake rate. **(B)** The maximal rate of glucose uptake in vehicle, PA- and AA-treated cells. **(C)** QPCR analysis of Glut1-Glut4 expression in cells pretreated with vehicle (Veh), PA, AA or the positive control CoCl₂. Expression levels were normalized on actin expression. **(D)** Western blot analysis of Glut1 protein levels for the conditions depicted in panel C. Protein levels were normalized on actin protein and the vehicle condition levels. Statistics: Mean values (+SEM) represent 7 independent experiments (Panel B) or 3 independent experiments (Panel C, D). Significant differences with the indicated columns/conditions are marked by *p<0.05 and ***(p<0.001).

Stimulation of glucose uptake by acute OXPHOS inhibition is mediated by Glut1 in C2C12 myoblasts

QPCR analysis revealed the presence of Glut1 mRNA, whereas Glut2, Glut3 and Glut4 were not detected (Fig. 1C). The faster rate of glucose uptake in PA- and AA-treated cells was neither paralleled by elevated levels of Glut1 mRNA, nor by appearance of the other Glut isoforms. As a positive control cells were exposed to CoCl₂ (250 μM, 4.5 h), a treatment previously demonstrated to increase GLUT1 expression (Barnes et al., 2002, Behrooz and Ismail-Beigi, 1997). CoCl₂ greatly increased the levels of Glut1 mRNA without inducing expression of the other Glut isoforms (Fig. 1C). In case of Glut1, a Western blot analysis of whole cell homogenates was performed under conditions mimicking the microscopy assay (*i.e.* myoblasts were pretreated for 30 min with mitochondrial inhibitors followed by an 18 min incubation in the absence of glucose of which the last 15 min were in the presence of IAA). Glut1 protein was detected as smeared bands (Fig. 1D), probably due to glycosylation (Asano et al., 1991). Quantification of Glut1 protein levels yielded no significant differences between the vehicle, PA and AA conditions whereas CoCl₂ clearly increased these levels (Fig. 1D). Taken together, these results are compatible with our previous findings (Liemburg-Apers et al., 2015a) in suggesting that PA and AA stimulate Glut1-mediated cellular glucose uptake and that this stimulation is not due to Glut1 upregulation.

Acute OXPHOS inhibition does not increase plasma membrane Glut1 levels

Since the Western blot analysis in Figure 1D was carried out using whole cell homogenates, it cannot be ruled out that PA- and AA-treatment increase Glut1 levels at the plasma membrane. To analyze these levels we performed biotinylation of cell surface Glut1 using non cell-permeable biotin (Barnes et al., 2002). We also assessed the effect of IAA, since GAPDH is known to play a role in vesicular transport (Zala et al., 2013). To this end, myoblasts were pretreated for 30 min with vehicle, PA, or AA. Next cells were incubated in HT buffer without glucose for 18 min, the last 15 min of which were in the absence or presence of IAA. The levels of biotinylated Glut1 were not affected by PA, AA, or IAA treatment (Fig. 2). This suggests that the inhibitor-induced stimulation of glucose uptake is not due to increased levels of Glut1 at the plasma membrane.

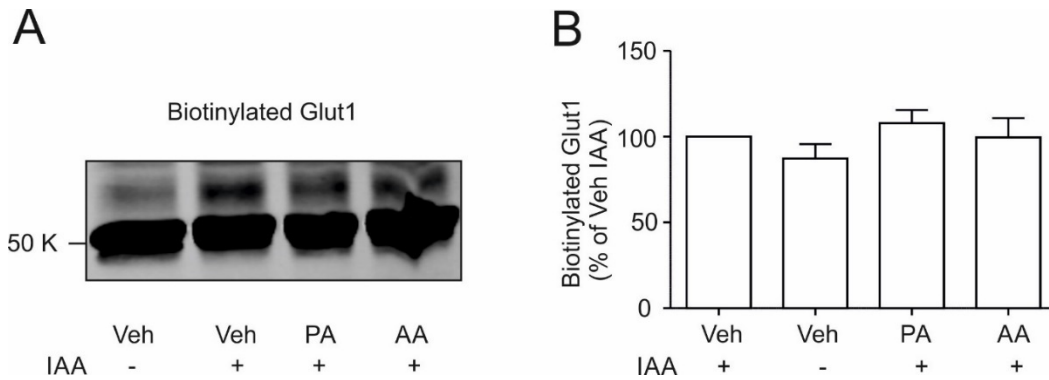


Figure 2. Acute inhibition of OXPHOS or glucose consumption does not affect Glut1 levels at the plasma membrane. (A) Levels of biotinylated Glut1 in vehicle- (in the absence and presence of IAA), PA- and AA-treated cells. (B) Mean levels (+SEM) of biotinylated Glut1 representing 3 independent experiments. No significant differences were observed.

Stimulation of Glut1-mediated glucose uptake by acute OXPHOS inhibition is paralleled by Thr172-phosphorylation of AMPK

Increased Glut1-mediated glucose uptake during metabolic dysfunction has been linked to increased Thr172-phosphorylation (activation) of the energy stress sensor AMP-activated protein kinase (AMPK) (Abbud et al., 2000, Barnes et al., 2002, Cura and Carruthers, 2012, John et al., 2008, Wu et al., 2013). To determine whether AMPK activation plays a role in our model system, myoblasts were first pretreated for 30 min with vehicle, PA, or AA. Next, cells were incubated in HT buffer without glucose for 18 min, the last 15 min of which were in the presence of IAA. Relative to vehicle, PA- and AA-treatment induced a 3-fold increase in the levels of Thr172-phosphorylated AMPK (pAMPK) without affecting the level of AMPK (Fig. 3A). Also phosphorylation of acetyl-CoA carboxylase 1 at Ser79 (from ACC1 to pACC1), which is stimulated by pAMPK, was slightly increased in PA- and AA-treated cells ($p=0.06$; Fig. S1A). This suggests that the increase in pAMPK level represents active pAMPK. Exogenous AMPK activation using 5-aminoimidazole-4-carboxamide ribonucleotide (AICAR; 500 μ M, 30 min) increased both pAMPK levels (Fig. S1B) and glucose uptake (Fig. 3B). However, AICAR stimulated glucose uptake to a lesser extent than PA. Co-incubation of AICAR and PA revealed no additive effect on glucose uptake (Fig. 3B), suggesting AICAR and PA stimulate glucose uptake via the same mechanism.

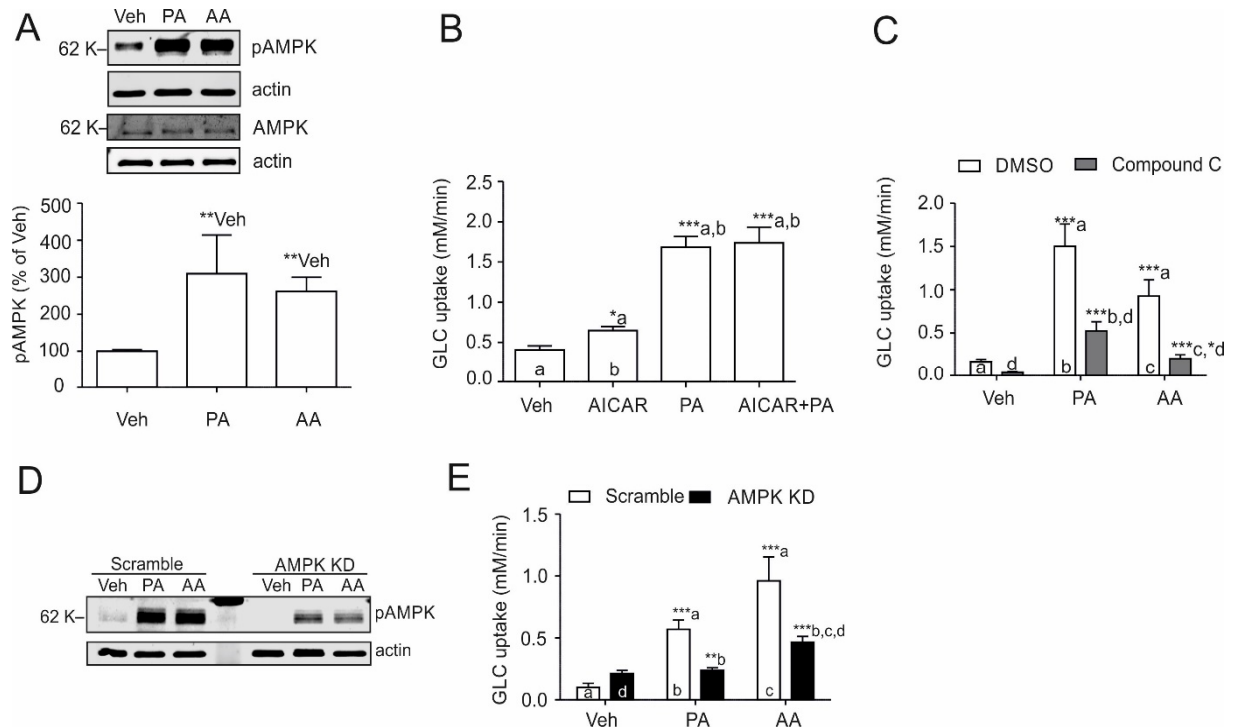


Figure 3. Stimulation of Glut1-mediated glucose uptake by acute OXPHOS inhibition requires AMPK. (A) Western blot analysis of the levels of AMPK and pAMPK in vehicle-, PA- and AA-treated cells. Protein levels were normalized on actin protein and the vehicle condition levels. (B) Effect of AICAR alone and in combination with PA on the rate of glucose uptake. (C) Effect of the AMPK-inhibitor Compound C on the rate of glucose uptake for the conditions depicted in panel A. (D) Typical Western blot showing the effects after 2 days of transfection with scramble or AMPK- α 1/ α 2 siRNA (AMPK KD) for vehicle-, PA- and AA-treated cells. Actin was used as a loading control. (E) Effect of scramble and AMPK- α 1/ α 2 siRNA transfection on the rate of glucose uptake in vehicle-, PA- and AA-treated cells. Statistics: Mean values (+SEM) represent 3 independent experiments (Panel F), 4 independent experiments (Panel B, D) or 7 independent experiments (Panel A). Significant differences with the indicated columns/conditions are marked by * $p < 0.05$, ** $p < 0.01$ and *** $p < 0.001$.

Stimulation of Glut1-mediated glucose uptake by acute OXPHOS inhibition is prevented by chemical AMPK inhibition and AMPK knockdown

To determine whether AMPK activity was required for PA- and AA-induced stimulation of glucose uptake, cells were pretreated with the cell permeable AMPK inhibitor Compound C (20 μ M, 2 hours). This compound binds to the AMPK α 2 catalytic subunit in a pocket that partially overlaps with the putative ATP-binding pocket (Handa et al., 2011). Pretreatment with Compound C did not significantly affect glucose uptake in the vehicle condition (Fig. 3C). However, compound C greatly reduced the PA- and AA-stimulated increase in glucose uptake (Fig. 3C) and lowered AA-stimulated ACC phosphorylation (Fig. S1C). These findings suggest that AMPK activity is required for inhibitor-induced stimulation of Glut1-mediated glucose uptake. However, evidence was provided that Compound C also displays

off-target effects (Bain et al., 2007, Vogt et al., 2011, Liu et al., 2014). Therefore, we next used a knockdown (KD) strategy using siRNAs co-targeting the $\alpha 1$ and $\alpha 2$ catalytic subunits of AMPK. KD of AMPK reduced the levels of pAMPK in vehicle-, PA- and AA-treated cells (Fig. 3D). AMPK KD did not affect glucose uptake in the vehicle condition (Fig. 3E). Similar to Compound C, AMPK KD greatly reduced the stimulated glucose uptake in PA- and AA-treated cells (Fig. 3E). This reduction was not due to AMPK KD lowering Glut1 protein levels (Fig. S1D). The above findings suggest that acute OXHOS inhibition activates glucose uptake by a mechanism involving Thr172-phosphorylation and ensuing activation of AMPK.

Stimulation of Glut1-mediated glucose uptake by acute OXPHOS inhibition involves LKB1

In mammals, Thr172-phosphorylation of AMPK is primarily mediated by two upstream kinases (Hardie et al., 2012): (i) the LKB1-STRAD-MO25 complex, which was originally identified as a tumor suppressor, and (ii) Ca^{2+} /calmodulin-activated protein kinase kinase β (CaMKK or CaMKK2). Mechanistically, LKB1-STRAD-MO25 induces a high basal-level of Thr172-phosphorylation that is modulated by the binding of AMP to the AMPK γ -subunit. The latter stimulates AMPK phosphorylation and inhibits its dephosphorylation (Hawley et al., 1995, Davies et al., 1995). LKB1 is activated by Ser431-phosphorylation (yielding pLKB1) during a variety of conditions (Gan and Li, 2014). This activation results in binding of pLKB1 to AMPK and its subsequent Thr172-phosphorylation and activation (Xie et al., 2006). To investigate the potential role of LKB1 in our model system, cells were pretreated for 30 min with vehicle, PA, or AA. Next, they were incubated in HT buffer without glucose for 18 min, the last 15 min of which were in the presence of IAA. PA- and AA-treatment slightly increased the levels of pLKB1 (Fig. 4A). Knockdown of LKB1 reduced the inhibitor-induced stimulation of AMPK Thr172-phosphorylation (Fig. 4B). LKB1 knockdown did not affect glucose uptake in vehicle- or PA-treated cells but reduced this parameter in AA-treated cells (Fig. 4C). These results suggest that LKB1 is involved in mediating the stimulation of glucose uptake in AA-inhibited cells.

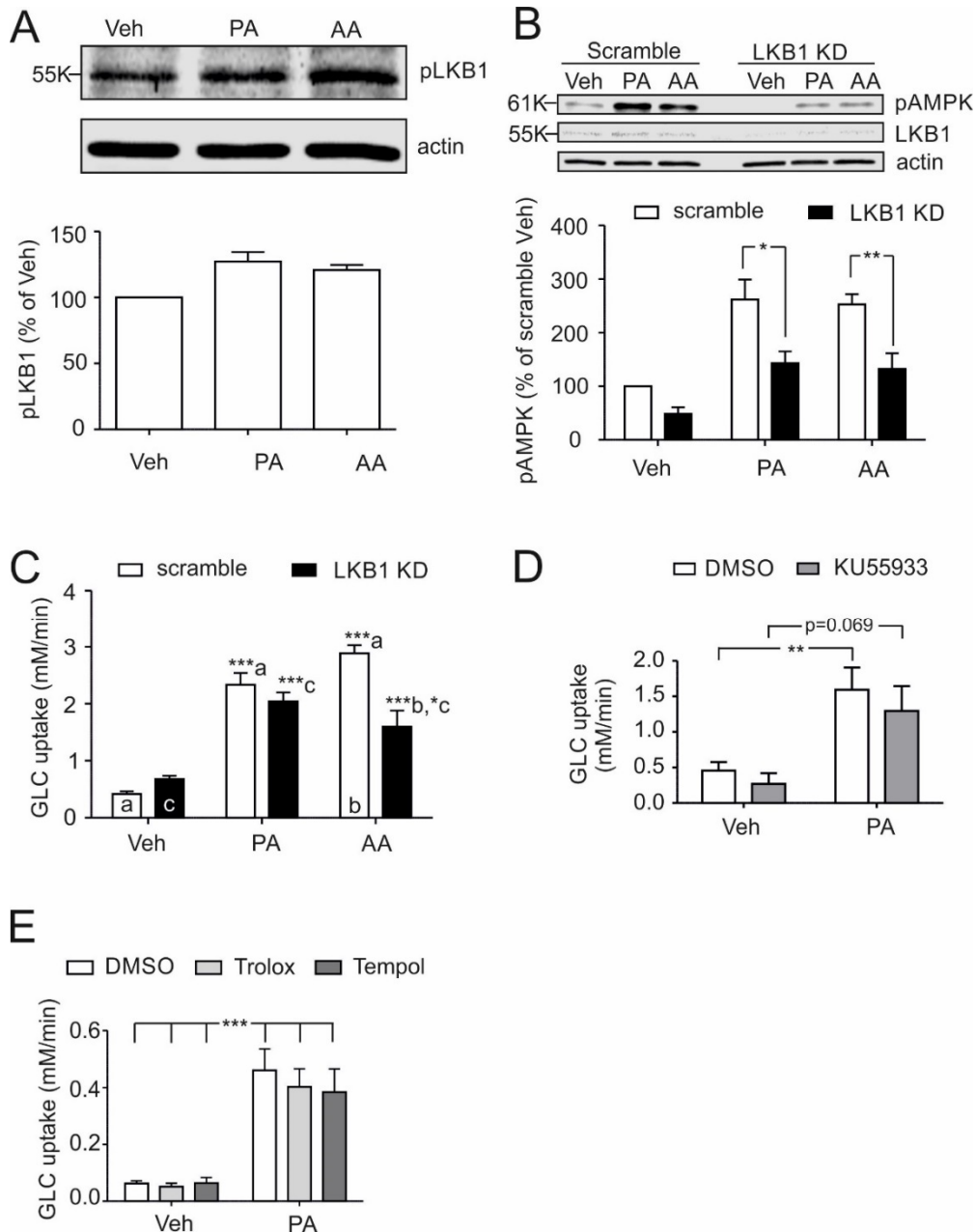


Figure 4. Stimulation of Glut1-mediated glucose uptake by acute OXPHOS inhibition involves LKB1. (A) Western blot analysis of the levels of pLKB1 in vehicle-, PA- and AA-treated cells. Protein levels were normalized on actin protein and the vehicle condition levels. (B) Typical Western blot showing the effects after 2 days of transfection with scramble or LKB1 siRNA (LKB1 KD) on LKB1 and pAMPK levels for vehicle-, PA- and AA-treated cells. Protein levels were normalized on actin protein and the vehicle condition levels. (C) Effect of scramble and LKB1 siRNA transfection on the rate of glucose uptake in vehicle-, PA- and AA-treated cells. (D) Effect of the ATM-inhibitor KU55933 on the rate of glucose uptake for vehicle- and PA-treated cells. (E) The effect of the antioxidants Trolox and Tempol on the rate of glucose uptake for vehicle- and PA-treated cells. Statistics: Mean values (+SEM) represent 2 independent experiments (Panel E), 3 independent experiments (Panel A, B, C), or 4 independent experiments (Panel D). Significant differences with the indicated columns/conditions are marked by * $p < 0.05$, ** $p < 0.01$ and *** $(p < 0.001)$.

Stimulation of Glut1-mediated glucose uptake by acute OXPHOS inhibition does not involve ATM, Src or ROS

The above suggests that additional modes of regulation are involved in PA-induced stimulation of glucose uptake. The kinase ataxia-telangiectasia mutated (ATM) was demonstrated to activate AMPK by an LKB1-independent mechanism in AICAR treated cells (Sun et al., 2007). However, pre-treatment with the ATM inhibitor KU55933 (1 μ M, 1 hour (Hickson et al., 2004)) did not prevent the PA-induced increase in glucose uptake (Fig. 4D) arguing against involvement of ATM.

Inhibitor-induced and inherited mitochondrial dysfunction are generally associated with an increase in ROS levels (Koopman et al., 2013, Koopman et al., 2012, Willems et al., 2015, Zorov et al., 2014) and hydrogen peroxide has been suggested to play a role in LKB1-independent AMPK activation by inducing oxidative modification of the AMPK α subunit (Mungai et al., 2011, Zmijewski et al., 2010). Previous studies provided evidence that antioxidants diminished hydrogen peroxide-associated activation of AMPK (Colombo and Moncada, 2009) and that Trolox and Tempol reduce hydrogen peroxide levels in living cells (Chen et al., 2013b, Peus et al., 2001). Although PA treatment increased the levels of hydroethidium (HET)-oxidizing ROS (Fig. S1E), co-incubation with the antioxidants Trolox (30 μ M, 30 min) or Tempol (400 μ M; 30 min), were unable to prevent the PA-induced increase in pAMPK (Fig. S1F) and glucose uptake (Fig. 4E). This suggest that HET-oxidizing and/or Trolox/Tempol-sensitive ROS are not mediating the stimulation of AMPK phosphorylation and glucose uptake. In leukemic cells, glucose uptake was increased by ROS-stimulated Glut1 phosphorylation mediated by the tyrosine kinase Src (Prata et al., 2008). ROS-induced activation of Src was suggested to be mediated by oxidation of the Cys245 and Cys487 residues, followed by an increase in Src autophosphorylation (Giannoni et al., 2005). Myoblasts were pretreated for 30 min with vehicle, PA, or AA. Next, cells were incubated in HT buffer without glucose for 18 min, the last 15 min of which were in the presence of IAA. Inhibitor treatment did not stimulate Tyr418 phosphorylation of Src (Fig. S1G). Compatible with this result, the Src inhibitor PP2 (20 μ M, 30 min) did not affect the PA-induced increase in glucose uptake (Fig. S1H). These results argue against involvement of Src in mediating the stimulation of glucose uptake in OXPHOS-inhibited cells.

Total cellular NADH and NAD⁺ amount is increased and NAD⁺/NADH ratio is decreased in PA- and AA-treated cells

Finally, it was assessed how AMPK activation leads to stimulation of Glut1-mediated glucose uptake. Because AMPK activity is involved in NAD⁺ synthesis (Canto et al., 2009, Fulco et al., 2008) and CI oxidizes NADH, the effect of PA and AA treatment on NAD⁺ and NADH levels was assessed. Myoblasts were pretreated for 30 min with vehicle, PA, or AA and then incubated in HT buffer without glucose for 18 min, the last 15 min of which were in the presence of IAA. PA- and AA-treatment increased total cellular NADH content (Fig. 5A), whereas NAD⁺ content also appeared elevated (Fig. 5B). As a consequence, inhibitor-treated cells displayed a reduced NAD⁺/NADH ratio (Fig. 5C), compatible with the previously reported increased lactate release by these cells (Liemburg-Apers et al., 2015a). The increase in NADH without a decrease in NAD⁺ suggests *the novo* synthesis of NAD⁺ upon PA or AA treatment. Knockdown of AMPK prevented the PA- and AA-induced increase in total cellular NADH (Fig. 5D) and lowered total cellular NAD⁺ (Fig. 5E). However, the inhibitor-induced drop in NAD⁺/NADH ratio was not affected by AMPK knockdown (Fig. 5F). These results suggest that AMPK is involved in *the novo* synthesis of NAD⁺ upon PA or AA treatment.

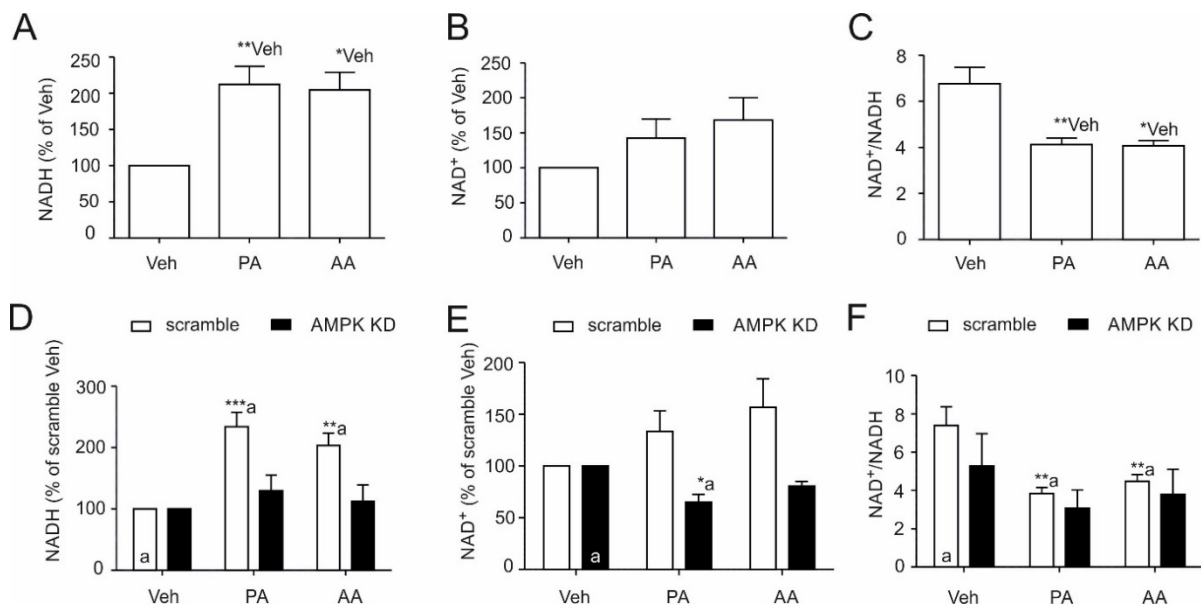


Figure 5. NAD⁺/NADH is decreased by acute OXPHOS inhibition. (A) NADH levels **(B)** NAD⁺ and **(C)** NAD⁺/NADH in vehicle-, PA- and AA-treated cells. **(D)** NADH, **(E)** NAD⁺ and **(F)** NAD⁺/NADH after 2 days of transfection with scramble or AMPK- α 1/ α 2 siRNA (AMPK KD) in vehicle-, PA- and AA-treated cells. Statistics: Mean values (+SEM) represent 4 independent experiments (Panel D, E, F), or 5 independent experiments (Panel A, B, C). Significant differences with the indicated columns/conditions are marked by * p <0.05, ** p <0.01 and *** p <0.001).

Sirt2 activity is necessary for the PA- and AA-induced stimulation of glucose uptake

The NAD⁺-dependent deacetylating enzymes Sirtuins are involved in metabolic regulation. In order to assess a possible role of NAD⁺ and NADH in glucose uptake, myoblasts were treated with the NAD⁺ precursor nicotinamide mononucleotide (NMN; 1 mM, 24 hours (Yoshino et al., 2011)). This treatment increased total cellular NAD⁺ levels (Fig. S2A), but did not affect NADH levels (Fig. S2B). Under vehicle conditions, NMN slightly increased glucose uptake by itself (p=0.09; Fig. 6A), whereas in PA-treated cells, stimulation of glucose uptake was not affected. In order to assess the possible role of Sirtuins in our model system, we specifically inhibited the cytosolic Sirtuin 2 (*i.e.* Sirt2) (Poulose and Raju, 2015). In vehicle-treated cells, the Sirt2 inhibitor AGK2 (5 μM, 2 hours; (Outeiro et al., 2007)) stimulated glucose uptake (Fig. 6B). This suggests that active Sirt2 prevents glucose uptake. Enigmatically, AGK2 inhibited the increased glucose uptake in PA- and AA-treated cells, suggesting that Sirt2 activity is required for stimulation of glucose uptake in inhibitor-treated cells. AGK2-treatment did not prevent PA- and AA-induced AMPK phosphorylation (Fig. S2C). This suggests that the AGK2 effects occur downstream of AMPK activation.

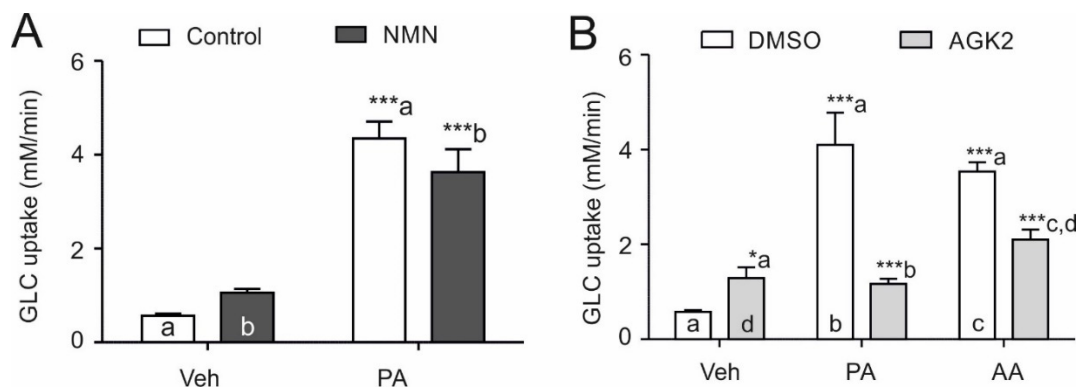


Figure 6. Stimulation of Glut1-mediated glucose uptake by acute OXPHOS inhibition involves Sirt2. (A) Effect of the NAD⁺ precursor NMN on the rate of glucose uptake for vehicle- and PA-treated cells. (B) Effect of the Sirt2-inhibitor AGK2 on the rate of glucose uptake for vehicle-, PA-, and AA-treated cells. Statistics: Mean values (+SEM) represent 3 independent experiments (Panel A) or 5 independent experiments (Panel B). Significant differences with the indicated columns/conditions are marked by *p<0.05 and ***(p<0.001).

Glut1 acetylation is not affected by PA or AA treatment

The acetylation status of Glut1 was reported to be increased by sodium butyrate inhibition of HDACs (Chen et al., 2015). In order to assess whether Sirt2 regulates Glut1-acetylation, acetylated-lysine residues were immunoprecipitated and the level of Glut1 was detected on Western blot. The acetylation status of Glut1 was not affected by PA or AA treatment (Fig. 7A). To confirm Glut1 acetylation, Glut1 was immunoprecipitated and acetyl-lysine was analyzed on Western blot. A band specific for anti-acetyl-lysine was found to colocalize with Glut1 (Fig. 7B). Again, the acetylation status of Glut1 was not affected by PA or AA treatment (Fig. 7B). These results agree against regulation of Glut1-mediated glucose uptake by Glut1 deacetylation.

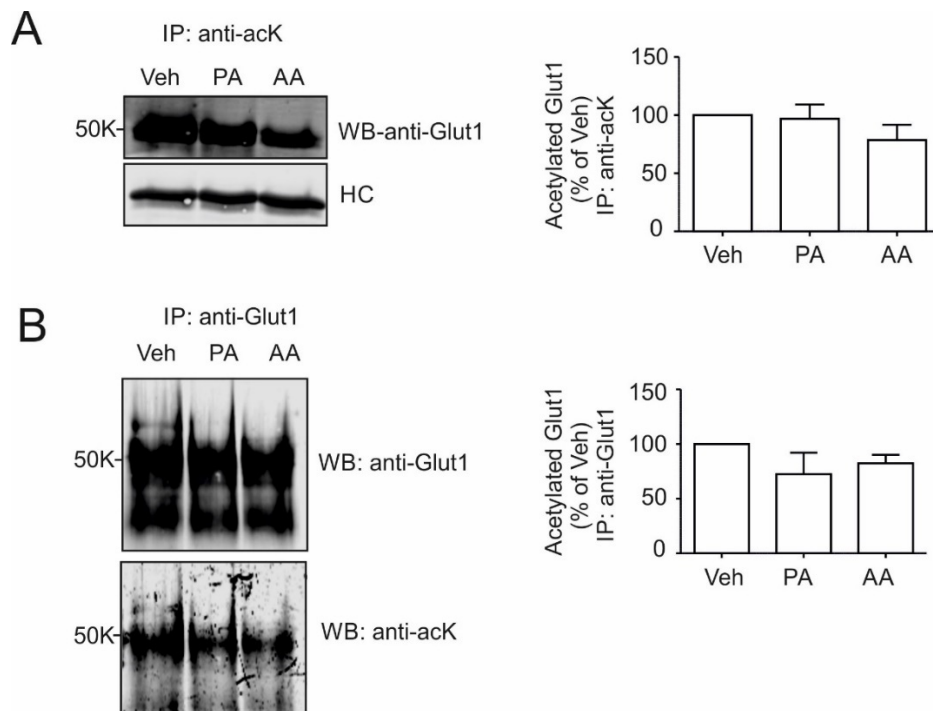


Figure 7. Acetylation status of Glut1. (A) Western blot analysis of the level of Glut1 in anti-acetyl-lysine (anti-acK)-immunoprecipitated samples from vehicle-, PA- and AA-treated cells. Protein levels were normalized on the heavy chain (HC) levels and the vehicle condition levels. (B) Western blot analysis of Glut1 (upper panel) and anti-acK (lower panel) in Glut1-immunoprecipitated samples from vehicle-, PA-, and AA-treated cells. Acetylated-Glut1 levels were normalized on total Glut1 levels and on vehicle condition levels. Statistics: Mean values (+SEM) represent 4 independent experiments (Panel B) or 6 independent experiments (Panel A). No significant differences were observed.

Discussion

Regulation of Glut1-mediated glucose uptake upon metabolic stress is an important cellular adaptation and a more detailed understanding of its molecular mechanism is relevant in a broad spectrum of metabolic disorders including mitochondrial dysfunction, cancer, and diabetes. Here we show that a 30 min incubation of mitochondrial CI or CIII increases the rate of glucose uptake without an increase in Glut1 membrane abundance, suggesting activation of Glut1 preexisting at the plasma membrane. This activation requires the activity of LKB1, AMPK, and Sirt2.

Stimulation of glucose uptake by short-term inhibition of OXPHOS complexes has been described before (Hamrahian et al., 1999, Jing et al., 2008, Koseoglu and Beigi, 1999, Mercado et al., 1989, Shetty et al., 1993, Shi et al., 1995). As already expected from the short time frame in which this increased glucose uptake rate occurred, this was not due to upregulation of Glut1 expression. Furthermore, the fact that Glut1 plasma membrane abundance was not affected by CI- or CIII-inhibition suggests that the rate of Glut1 internalization was not decreased and/or the rate of Glut1-vesicle translocation to the plasma membrane was not increased. In line with this, inhibition of ATM, which promotes plasma membrane localization of Glut1 in myoblasts (Andrisse et al., 2013), did not diminish the increased rate of glucose uptake induced by PA. Activation of Glut1 preexisting at the plasma membrane upon metabolic stress has been described before in other cell types (Abbud et al., 2000, Barnes et al., 2002, Koseoglu and Beigi, 1999, Shetty et al., 1993, Shi et al., 1995). In Chapter 3 we showed that the increased rate of glucose uptake induced by PA and AA was mediated by an increase in the V_{max} of glucose transport, whereas the K_m was not affected (Liemburg-Apers et al., 2015a). This suggests activation or unmasking of inactive Glut1 at the plasma membrane. Glut1 is allosterically inhibited by ATP and under conditions of reduced ATP levels, the V_{max} of Glut1 increases (Carruthers, 1986). This may suggest that the increased rate of glucose uptake induced by mitochondrial inhibition is mediated by the release of ATP-mediated inhibition. However, Glut1 activity continued to be increased after the ATP levels return to normal in CI-inhibited clone 9 cells

(Mercado et al., 1989). This suggests that although reduced ATP levels could initially play a role in Glut1 regulation, other modes of regulation are involved.

Acute metabolic stress was reported to stimulate Glut1-mediated glucose uptake in an AMPK-dependent manner (Abbud et al., 2000, Barnes et al., 2002, Jing et al., 2008). We found that both PA and AA induced AMPK activation. In addition, AMPK activation by AICAR stimulated the rate of glucose uptake under vehicle conditions. Importantly, inhibition of AMPK activity or knockdown (AMPK KD) of the α 1- and α 2-subunits of AMPK (partially) diminished the increased rate of glucose uptake induced by PA and AA. The incomplete inhibition of glucose uptake by AMPK KD could be because pAMPK was not fully reduced. Since glucose uptake was measured by single cell microscopy it is likely that part of the cells that were measured were not transfected with siRNA. Nevertheless, a significant decrease in the rate of glucose uptake under PA and AA conditions was observed by AMPK KD.

Next it was assessed how AMPK is activated in response to mitochondrial inhibition. Acute mitochondrial inhibition is known to increase the AMP/ATP ratio (Jing and Ismail-Beigi, 2007, Mercado et al., 1989, Shetty et al., 1993). Increased binding of AMP to the γ -subunit of AMPK was shown to enhance phosphorylation of the α -subunit by the upstream AMPK kinase LKB1 (Woods et al., 2003, Shaw et al., 2004, Hardie, 2014, Hardie and Ashford, 2014). We found a moderate increase in the level of phosphorylated LKB1 upon PA and AA treatment. This is in agreement with a model proposed by Hardie, which suggests a high basal LKB1 activity leading to a continuous phosphorylation of AMPK α at Thr172, which in the absence of AMP, is rapidly dephosphorylated (Hardie, 2011). However, the binding of AMP causes a conformational change that inhibits the dephosphorylation of AMPK (Sanders et al., 2007, Davies et al., 1995). Knockdown of LKB1 (LKB1 KD), significantly reduced PA- and AA-induced phosphorylation of AMPK and AA-induced stimulation of glucose uptake. Interestingly, LKB1 KD did not reduce PA-induced stimulation of the glucose uptake. It is possible that in the absence of LKB1, PA activates AMPK via an alternative route. Although PA increased ROS levels, which can activate AMPK directly or via ATM (Guo et al., 2010, Kurz et al., 2004, Zmijewski et al., 2010), two anti-oxidants and ATM inhibition did not diminish

the increased rate of glucose uptake. Of note, the anti-oxidants Trolox and Tempol only partially diminished the PA-induced H₂O₂-oxidation (data not shown). Hence it is possible that the remaining ROS is sufficient to activate AMPK and/or Glut1. Alternatively, AMPK-independent signaling could be involved although this is not expected because AMPK KD completely diminished PA-induced stimulation of glucose uptake.

The mechanism by which AMPK stimulates Glut1-mediated glucose uptake under conditions of metabolic stress has been the topic of research for over a decade (Abbud et al., 2000, Barnes et al., 2002, Jing and Ismail-Beigi, 2007). Co-immunoprecipitation studies showed that Glut1 is not associated with pAMPK under conditions of metabolic stress, suggesting Glut1 is not a direct phosphorylation target of AMPK. More likely, AMPK indirectly modulates Glut1 activity. AMPK stimulates Sirt1 activity via *the novo* synthesis of its co-substrate NAD⁺ (Canto et al., 2009, Fulco et al., 2008, Brandauer et al., 2013). Sirtuins sense the energy status of the cell and deacetylate proteins involved in many cellular processes such as cell cycle regulation, genomic stability, and energy metabolism (Choudhary et al., 2009, Choudhary et al., 2014). PA and AA increased NADH levels, which is expected to be due to glycolysis-mediated reduction of NAD⁺ and the absence of OXPHOS-mediated oxidation of NADH. This was expected to reduce NAD⁺ levels. However, NAD⁺ levels were not decreased, suggesting *the novo* synthesis of NAD⁺. A similar observation was made in CI-deficient myoblasts of the heart, where upregulation of nicotinamide phosphoribosyl transferase (Nampt) was found to be responsible for the increased NAD⁺ levels (Karamanlidis et al., 2013). Nampt is the rate-limiting enzyme in NAD⁺ synthesis and its expression is regulated by AMPK (Fulco et al., 2008). Hence it was assessed whether NAD⁺ synthesis was decreased by AMPK KD. Indeed, AMPK KD reduced NAD⁺ levels upon PA/AA treatment, suggesting that AMPK is involved in maintaining equal NAD⁺ levels and perhaps preserving Sirtuins activity under conditions of mitochondrial dysfunction. However, although AMPK mediated regulation of Nampt expression takes place at the level of translation, it takes at least 8 hours before Nampt protein levels are increased in muscle cells upon AICAR treatment (Brandauer et al., 2013). This is much longer compared to the 30 min treatment with PA or AA. In addition, AMPK can increase the NAD⁺ level by stimulation of mitochondrial fatty

acid oxidation, but this takes at least 4 hours (Canto et al., 2009). Although it is possible that these mechanisms occur faster in PA and AA treated myoblasts, it is expected that other modes of regulation are involved in the AMPK-mediated NAD^+ synthesis. In order to assess the effect of NAD^+ on glucose uptake, the Nampt product NMN was used. As expected, under vehicle conditions NMN treatment increased NAD^+ levels. This increase in NAD^+ slightly although not significantly increased the rate of glucose uptake. Based on the above described effects we speculated that AMPK-mediated preservation of Sirtuin activity is necessary for the stimulation of glucose uptake under PA and AA conditions. To test this hypothesis, Sirt2 was specifically inhibited. In contrast to other Sirtuins, Sirt2 localizes predominantly in the cytosol, where it has specific targets such as tubulin (North et al., 2003, Rauh et al., 2013). Inhibition of Sirt2 activity diminished both PA- and AA-induced glucose uptake, suggesting its function is necessary for the stimulation of glucose uptake. Interestingly, Sirt2 inhibition stimulated glucose uptake under vehicle conditions suggesting Sirt2 has a dual effect of glucose uptake. Under basal conditions it may prevent excessive glucose uptake whereas under metabolic stress it mediates the stimulation of glucose uptake. In the nucleus Sirt1 deacetylates LKB1, leading to AMPK activation (Lan et al., 2008). However, we found that Sirt2 inhibition did not diminish PA and AA induced AMPK phosphorylation, indicating that Sirt2 operates downstream of AMPK. A great number of glycolytic enzymes are found to be heavily acetylated and reversible acetylation is believed to fine tune metabolic adaptation and insulin signaling in muscle (Philp et al., 2014, LaBarge et al., 2015). Moreover, Sirt2 is critical for Akt activation by insulin (Ramakrishnan et al., 2014). Although Glut1 was found to be acetylated, the degree of acetylation was not altered by PA- or AA-treatment. Although Sirt2 activity is necessary for the stimulation of glucose uptake, it is not the driving force because: (i) PA and AA induced activation of AMPK preserves but does not increase NAD^+ levels and (ii) increasing the level of NAD^+ with NMN only moderately stimulated glucose uptake. We propose a mechanism as depicted in figure 8 in which acute OXPHOS inhibition increases the AMP/ATP ratio, leading to inhibition of AMPK dephosphorylation and stimulation of LKB1-mediated AMPK phosphorylation. While glycolysis reduces NAD^+ , phosphorylated AMPK stimulates NAD^+ synthesis, maintaining equal levels of this nucleotide. NAD^+ is necessary for basal Sirt2 activity, which function is to deacetylate an unknown target 'X'. The fact

that AMPK activity is sufficient to stimulate Glut1 activity whereas Sirt2 activity is not, suggests an additional AMPK-mediated phosphorylation of 'X'. Sequential phosphorylation and deacetylation has also been described for the activation of peroxisome proliferator-activated receptor-gamma coactivator (PGC)-1 α (Canto et al., 2009). Phosphorylated and deacetylated 'X' would activate Glut1 via a yet unknown mechanism.

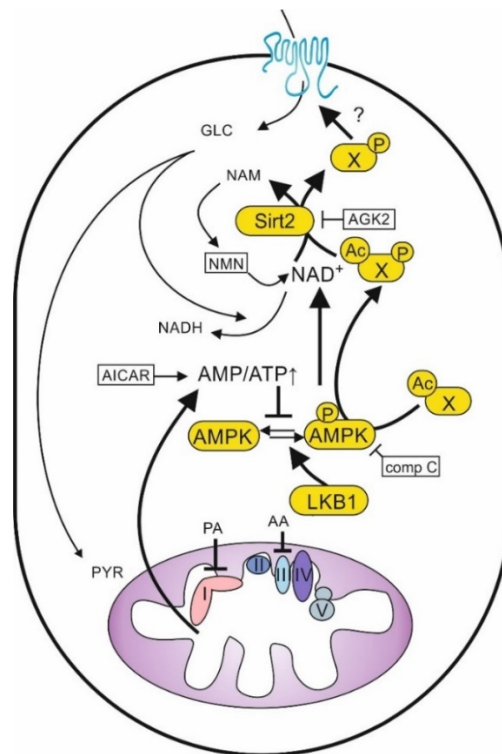


Figure 8. Proposed mechanism for Glut1 activation by acute OXPHOS inhibition. See discussion for more details. AA, antimycin A; Ac; acetylated; comp C, compound C; GLC, glucose; NAM; nicotinamide; NMN, nicotinamide mononucleotide; P, phosphorylated; PA, piericidin A.

A possible candidate for 'X' is Akt, which promotes a glycolytic phenotype in various cell types (Elstrom et al., 2004, Higaki et al., 2008). Acetylation of Akt at the Lys20 residue prevents plasma membrane localization and activation of Akt by PI3K (Sundaresan et al., 2011), whereas Akt deacetylation by Sirt2 was reported to promote its activity (Dan et al., 2012, Chen et al., 2013a). Importantly, phosphorylation of Sirt2 by AMPK at residue Thr101 was found necessary for Akt-Sirt2 interaction and subsequent activation by PI3K (Ramakrishnan et al., 2014). However, AMPK-mediated phosphorylation of Akt has not been described. Interestingly, one of the down-stream targets of Akt is mTOR/RAPTOR, which stimulates glucose uptake without increasing Glut1 plasma membrane abundance

(Wieman et al., 2007). Interestingly, inhibition of mTOR/RAPTOR by rapamycin reduced HK expression and the glycolytic flux in mice lacking the CI-subunit Ndufs4 (Johnson et al., 2013), suggesting mTOR/RAPTOR activity promotes glycolysis.

In summary, LKB1, AMPK, and Sirt2 activity appears to be necessary for the stimulation of glucose uptake by acute OXPHOS inhibition but the exact mode of regulation remains unclear. Further research should focus on which protein(s) activate Glut1 and how they are affected by reversible acetylation and phosphorylation.

Acknowledgements

This work was supported by equipment grants of ZonMW (Netherlands Organization for Health Research and Development, No: 903-46-176), NWO (Netherlands Organization for Scientific Research, No: 911-02-008) and by the CSBR (Centres for Systems Biology Research) initiative from ZonMW (Grant: #CSBR09/013V).

Supplementary figures

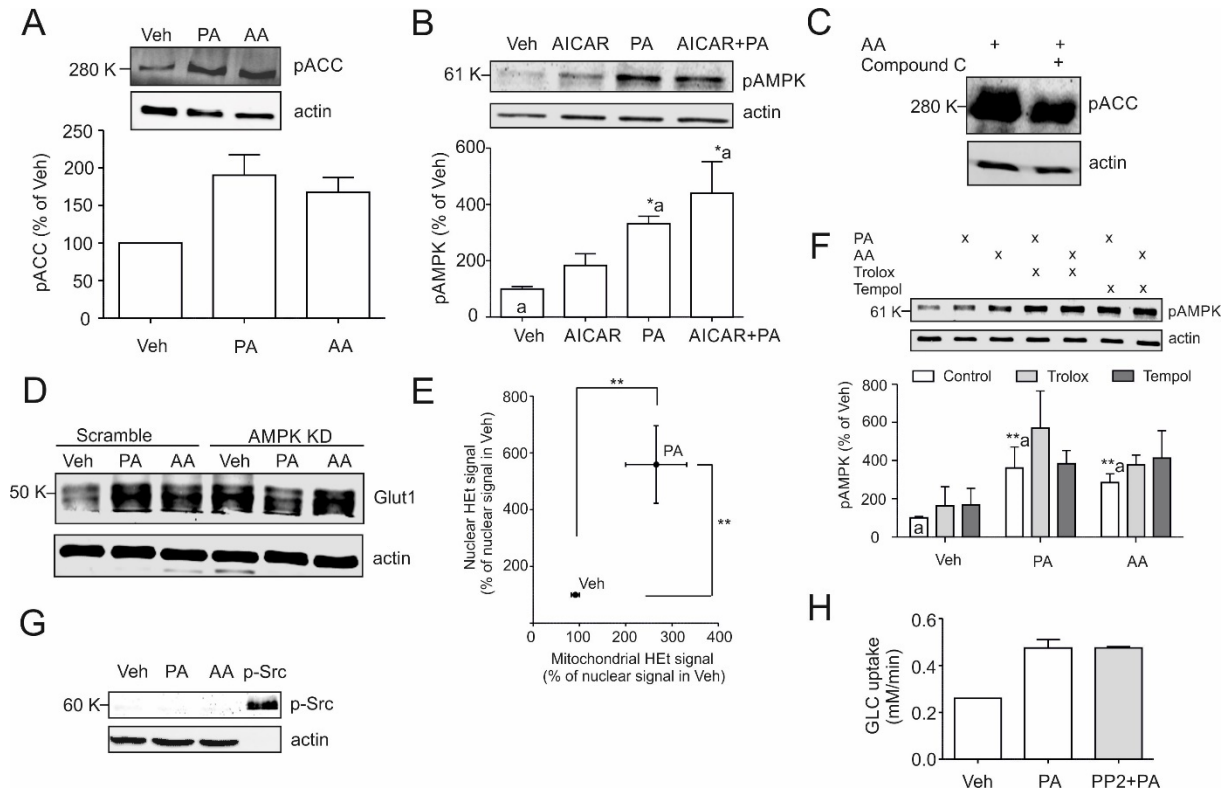


Figure S1. (A) Western blot analysis of the levels of pACC in vehicle-, PA- and AA-treated cells. Protein levels were normalized on actin protein and the vehicle condition levels. (B) Western blot analysis of the levels of pAMPK in vehicle-, AICAR-, PA- and PA+AICAR-treated cells. Protein levels were normalized on actin protein and the vehicle condition levels. (C) Typical Western blot showing the effects of compound C on pACC levels for AA-treated cells. Actin was used as a loading control. (D) Typical Western blot showing the effects after 2 days of transfection with scramble or AMPK- $\alpha 1/\alpha 2$ siRNA (AMPK KD) on Glut1 levels for vehicle-, PA- and AA-treated cells. Actin was used as a loading control. (E) Nuclear and mitochondrial HET-oxidation levels in vehicle- and PA-treated cells. HET-oxidation levels were normalized on nuclear signal in vehicle. (F) Western blot analysis of the effect of Trolox and Tempol on the levels of pAMPK in vehicle-, PA- and AA-treated cells. Protein levels were normalized on actin protein and the vehicle condition levels. (G) Typical Western blot of pSrc in vehicle-, PA-, and AA-treated cells. Phosphorylated recombinant Src was used as a positive control. Actin was used as a loading control. (H) Effect of the Src-inhibitor PP2 on the rate of glucose uptake for vehicle- and PA-treated cells. Mean values (+SEM) represent 3 independent experiments (Panel A, B, F) or 5 independent experiments (Panel E). Significant differences with the indicated columns/conditions are marked by * $p < 0.05$ and ** $p < 0.01$.

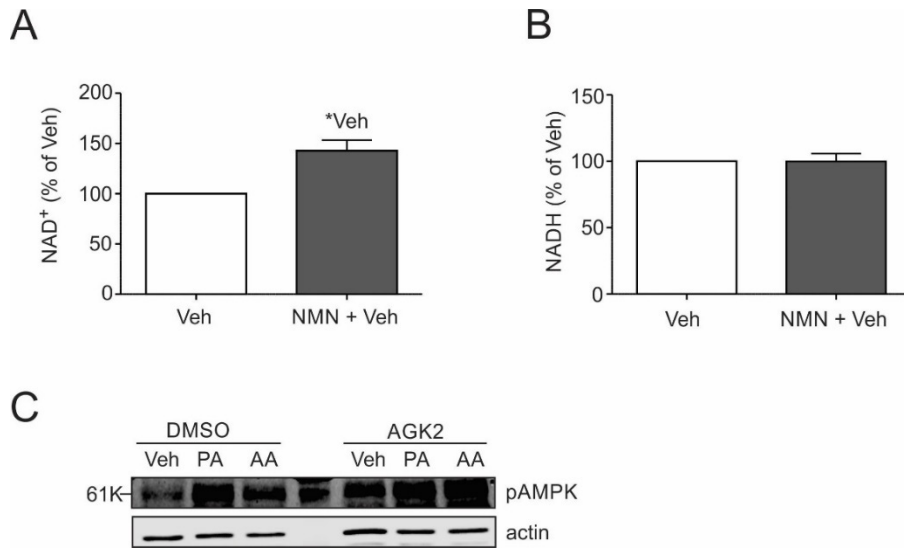


Figure S2. (A, B) Effect of NMN on (panel A) NAD⁺ and (panel B) NADH levels in vehicle-treated cells. (C) Typical Western blot showing the effects of AGK2 on pAMPK levels for vehicle-, PA- and AA-treated cells. Actin was used as a loading control. Statistics: Mean values (+SEM) represent 2 independent experiments (Panel A, B). Significant differences with the indicated columns/conditions are marked by * $p < 0.05$.

CHAPTER 6

General discussion



Partially published in:

Liemburg-Apers DC, Willems PH, Koopman, WJ, Grefte S.

Arch Toxicol. (2015) 89(8):1209-26

Sander Grefte[#], Dania C. Liemburg-Apers[#], Ganesh R. Manjeri, Megan E. Breuer, Jori A.L. Wagenaars, Leanne H.J. de Ronde, Jan A.M. Smeitink, Peter H.G.M. Willems, Werner J.H. Koopman

[[#]These authors contributed equally]

(Submitted)

Introduction

Glucose is an important source of energy for ATP production by glycolysis in the cytosol and the oxidative phosphorylation (OXPHOS) system in the mitochondria. OXPHOS dysfunction often triggers an increase in the rate of glucose uptake and glycolysis (Jing et al., 2008, Shetty et al., 1993, Shi et al., 1995, Wu and Wei, 2012). The aim of this thesis was to assess the role of glucose in OXPHOS dysfunction. In order to do so the FRET-based glucose sensor FLII¹²Pglu-700 μ δ 6 (FLII) described in **Chapter 2** was used to develop a microscopic assay for live-cell quantitative glucose uptake measurements (**Chapter 3**). This assay was used to study the regulation (**Chapter 4 and 5**) and biochemical consequences (**Chapter 3**) of enhanced glucose uptake in CI- and CIII-dysfunctional myoblasts. In this chapter the findings from the studies in chapter 3, 4, and 5 will be integrated and discussed in a broader perspective.

Metabolic consequences of glucose uptake stimulation by OXPHOS dysfunction

Both pharmacologic inhibition of CI or CIII in C2C12 myoblasts (**Chapter 3**) and genetic deletion of the CI subunit Ndufs4 in primary mouse myoblasts (**Chapter 4**) triggered an increase in the rate of glucose uptake. This enhanced glucose uptake has several cellular biochemical consequences. In this section the effect of glucose uptake stimulation on the production of ATP, lactate, and reactive oxygen species (ROS) will be discussed.

Glucose uptake stimulation and ATP production

Dysfunction of one of the components of the OXPHOS system can lower the mitochondrial ATP production rate (Porteous et al., 1998, Janssen et al., 2006, Jonckheere et al., 2010, Gajewski et al., 2003). Since OXPHOS generates the majority of total ATP produced from glucose catabolism, an increase in the glycolytic ATP production is required to compensate for a reduced mitochondrial ATP production. In **Chapter 3** the glycolytic flux and ATP production were predicted using a mathematical model, which was parameterized using glucose uptake and glucose consumption kinetic data. The model predicted a 2-fold

increase in the steady-state glucose flux and ATP production rate under the condition of OXPHOS inhibition, which was confirmed empirically. Comparing this increased ATP production rate to the mitochondrial ATP production rate under normal conditions revealed that this 2-fold increase was sufficient to compensate for the lack of mitochondrial ATP production. This full compensation by glycolytic ATP was confirmed by the absence of a reduction in total ATP levels after 24 hours of OXPHOS inhibition. Importantly, malignant cells such as the C2C12 myoblast cell line generally have a high glycolytic flux compared to the mitochondrial flux, allowing only a 2-fold increase in glycolytic ATP production to be compensatory. However, in (primary) cells with a higher basal mitochondrial flux, the increase in glycolytic flux required to compensate for mitochondrial ATP production is expected to be higher. On the other hand, although OXPHOS activity is usually reduced in patient cells, it is not zero as is the case for full OXPHOS inhibition (Jonckheere et al., 2010). This suggests less compensation by glycolytic ATP is required in patient cells. Thus, ATP might not be a problem as the glycolytic ATP production can compensate and the ATP consumption is minimal under resting condition. However, under conditions of increased ATP demand, such as hormone or electrical stimulation (Visch et al., 2006b, Koopman et al., 2003), even a small reduction in the total ATP production capacity may induce problems such as disturbed calcium homeostasis (Willems et al., 2008). In addition, the compensatory increase in glycolytic ATP production is important to maintain the mitochondrial membrane potential ($\Delta\Psi$) (Nicholls, 1977). Glycolytic ATP can be used by CV operating in reverse-mode in order to pump protons out of the mitochondrial matrix. In this manner $\Delta\Psi$, which is necessary for osmotic homeostasis, is preserved and necrotic cell death is prevented (Elstrom et al., 2004, Huber et al., 2011, Nicholls, 1977). Interestingly, in skeletal muscle from *Ndufs4* KO mice which has 20-30% residual CI activity (Calvaruso et al., 2012, Alam et al., 2015), mitochondrial ATP production after ischemic reperfusion was not significantly reduced (Kruse et al., 2008). This might be due to overcapacity of CI as will be discussed in more detail in another section.

Glucose uptake stimulation and lactate production

Another biochemical consequence of the increased glycolytic flux is an elevation of pyruvate and lactate production (**Chapter 3**). In addition, OXPHOS dysfunction increases the NADH/NAD⁺ ratio (**Chapter 5**), which inhibits pyruvate

dehydrogenase (PDH) and shifts the reaction of the NADH-oxidizing lactate dehydrogenase (LDH) towards lactate production. This results in an increased lactate secretion and decreased pyruvate secretion upon OXPHOS inhibition (Fig. 1). Hence one of the hallmarks of mitochondrial dysfunction is an elevated lactate/pyruvate ratio in blood, which is termed hyperlactatemia (Robinson, 2006). Lactate secretion appears to be crucial for reducing ETC electron input as inhibition of LDH enhanced oxidative stress and cell death in tumor cells (Le et al., 2010), whereas stimulating pyruvate-to-lactate conversion reduced oxidative stress (Brand, 1997). However, when the liver is unable to process the elevated lactate levels, fatal lactic acidosis can follow (Loeffen et al., 2000).

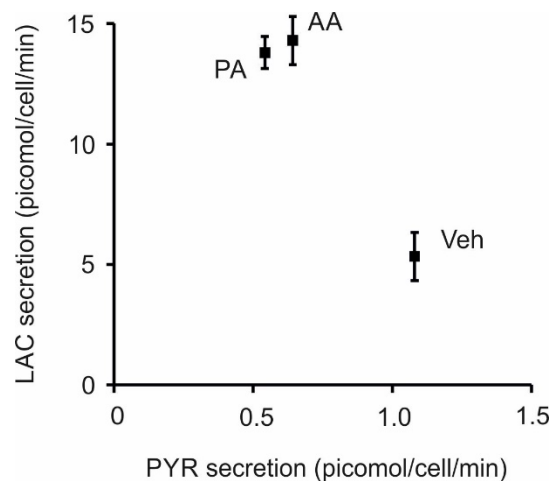


Figure 1. C2C12 myoblasts were incubated in culture medium (25 mM glucose) containing the CI inhibitor piericidin A (100 nM), the CIII inhibitor antimycin A (20 nM), or vehicle (0.01% ethanol). After 30 min the lactate (LAC) and pyruvate (PYR) levels in the medium were measured as described in Chapter 3.

Glucose uptake stimulation and ROS production

As described in the general introduction, mitochondrial dysfunction can cause excessive ROS production and even oxidative stress. In CI inhibited C2C12 myoblasts (**Chapter 5**) and *Ndufs4* KO primary myoblasts cultured in low glucose or galactose (**Chapter 4**), both the rate of glucose uptake and the level of H₂O₂-oxidizable ROS were increased, whereas these parameters were both normal in *Ndufs4* KO myoblasts cultured in high glucose. This suggests a causal relation between ROS and glucose uptake. ROS-induced signaling can stimulate glucose uptake via various different mechanisms (Fig. 2; arrow 1) (Liemburg-Apers et al., 2015b). However, pretreatment with different antioxidants or inhibition of the ROS-activated GLUT1 activators ATM and Src, did not diminish the stimulation of

glucose uptake in CI-inhibited C2C12 myoblasts (**Chapter 5**). This suggests ROS is not involved in the stimulation of glucose uptake under CI-inhibited condition. Vice versa, a high glycolytic flux was associated with increased ROS levels (Talior et al., 2003, Zhou et al., 2005), whereas inhibition of mitochondrial pyruvate uptake lowered ROS levels (Nishikawa et al., 2000, Yu et al., 2006). Increased glycolytic flux is generally associated with and increased TCA cycle flux (Ishihara et al., 1996). The latter results in accumulation of OXPHOS substrates and elevated NADH/NAD⁺ and FADH₂/FAD ratios (Ido, 2007, Ying, 2008). A high level of mitochondrial NADH leads to a fully reduced FMN site in CI, potentially stimulating superoxide production (Kussmaul and Hirst, 2006). Similarly, a more reduced ETC might stimulate superoxide formation by CIII (Turrens et al., 1985). Reduced ubiquinone, in combination with a highly negative (hyperpolarized) $\Delta\psi$, favors reverse electron transfer from CII to CI, which also stimulates superoxide production (Batandier et al., 2006, Murphy, 2009). Hyperglycemic conditions induced mitochondrial fragmentation in clone 9 liver cells, H9c2 cardiomyoblasts, and smooth muscle cells, which was strictly required to allow increased ROS production (Yu et al., 2011). However, induction of mitochondrial fragmentation by over-expression of the fission-promoting protein Drp1 (Dynamin-related protein 1), did not stimulate ROS levels in HeLa cells, suggesting that increased ROS levels are not a *de facto* consequence of mitochondrial fragmentation (Distelmaier et al., 2012). It was proposed that fragmented mitochondria might produce more ROS due to a bigger relative membrane surface (allowing better uptake of metabolic substrates) and ensuing $\Delta\psi$ hyperpolarization (Yu et al., 2006). High extracellular glucose levels stimulate TXNIP expression (Stoltzman et al., 2008), which can aggravate oxidative stress by binding Trx via disulfide bridges and thereby inhibiting its reducing potential (Hwang et al., 2014, Kaimul et al., 2007, Li et al., 2015, Nishiyama et al., 1999, Schulze et al., 2004). Taken together, the current experimental evidence suggests that increased glucose uptake and glycolytic conversion to pyruvate can increase ROS levels (Fig. 2; arrow 2). The above raises the question whether the increased ROS levels in CI dysfunction cells are a consequence of the increased rate of glucose uptake and glycolytic flux. Based on the fact that the majority of pyruvate produced by glycolysis is converted to lactate and the mitochondrial flux is relatively low in CI-/CIII-inhibited cells (**Chapter 5**), a high ETC electron input is not expected. However, for the primary KO myoblasts this might be different. In

order to answer this question, H₂O₂-oxidation levels should be measured in CI-inhibited cells with a diminished stimulation of glucose uptake. If diminishing the increased rate of glucose would lower or even normalize the ROS levels, it is likely that the increased rate of glucose uptake contributes to mitochondrial ROS production in CI-dysfunctional myoblasts. Alternatively, because glucose can be used by the pentose phosphate pathway (PPP) to produce the antioxidant recycling cofactor NADPH (Fig. 2; arrow 3), ROS levels might even be higher in the absence of increased glucose uptake.

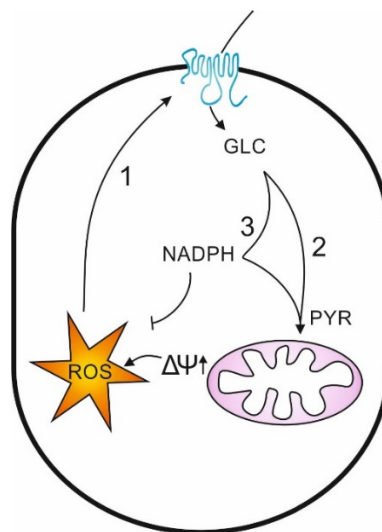


Figure 2. ROS stimulates glucose uptake (1). Glycolytic conversion of glucose into pyruvate and subsequent pyruvate entry into the mitochondria (2) stimulates ROS production by hyperpolarizing the mitochondrial membrane potential ($\Delta\psi\uparrow$). Glucose flux through the pentose phosphate pathway generates NADPH (3), which is an important cofactor in ROS scavenging. GLC, glucose; PYR, pyruvate; ROS, reactive oxygen species.

Interestingly, in *Ndufs4* KO mice, rapamycin treatment induced a metabolic shift away from glycolysis towards amino acid catabolism, whereas oxidative stress markers were not reduced (Johnson et al., 2013). Moreover, rapamycin enhanced survival and attenuated disease progression (Johnson et al., 2013). Although it is not clear whether reduced glycolysis is a cause or consequence of the attenuated disease progression upon rapamycin treatment, this suggests that oxidative stress is not affected by the glucose metabolism. Furthermore, it suggests that oxidative stress plays a minor role in the pathological symptoms of the *Ndufs4* KO mice. On the other hand, in *Drosophila*, overexpression of either GLUT3, the glycolytic enzyme PFK or the PPP enzyme G6PDH, rescued the reduced lifespan induced by down-regulation of the CI subunit ND3 (Besson et al., 2015). In addition, in a

Drosophila model of Huntington's disease, overexpression of G6PDH but not PFK increased the fly survival (Besson et al., 2015), suggesting NADPH-mediated ROS scavenging is involved in survival. In conclusion, it appears that an increased glycolytic flux has both favorable and unfavorable consequences and the balance between these consequences are organism- and/or cell type-specific.

Regulation of glucose uptake by mitochondrial dysfunction

The increased rate of glucose uptake observed in primary differentiating *Ndufs4* KO myoblasts cultured in low glucose or galactose was not due to upregulation of Glut1 or Glut4 (**Chapter 4**). Because of the limited availability of these primary *Ndufs4* KO myoblasts, the mechanism of this regulation was studied in C2C12 myoblasts. In order to induce CI dysfunction, this complex was pharmacologically inhibited with piericidin A (PA). Of note, the CI-inhibitor rotenone kills dopaminergic neurons and inhibits myoblasts differentiation in a CI- and OXPHOS-independent manner (Choi et al., 2015, Grefte et al., 2015). The fact that the CIII inhibitor antimycin A (AA) induced similar effects on cell signaling compared to PA (**Chapter 5**), suggests that the PA-/AA-induced glucose uptake stimulation is at least OXPHOS-dependent. For optimal comparison of the mode of Glut1-regulation in PA-treated myoblasts with the primary KO myoblasts, upregulation of Glut1 expression was prevented by performing a short-term (30 min) CI-inhibition. Indeed, this short-term inhibition of CI did not trigger an upregulation of Glut1 (**Chapter 5**). As further shown in **Chapter 5**, Glut1 stimulation by mitochondrial dysfunction is regulated by LKB1, AMPK and Sirt2 activity. The role of protein acetylation in the regulation of energy metabolism is emerging. However, the exact role reversible acetylation on protein function remains to be elucidated (LaBarge et al., 2015). We found that although Glut1 is acetylated, it is not a direct deacetylation target of Sirt2 (**Chapter 5**). Interestingly, hexokinase (HK) was also found to be heavily acetylated (Lundby et al., 2012, Choudhary et al., 2009), suggesting a common regulatory mechanism for both HK and Glut1 activity.

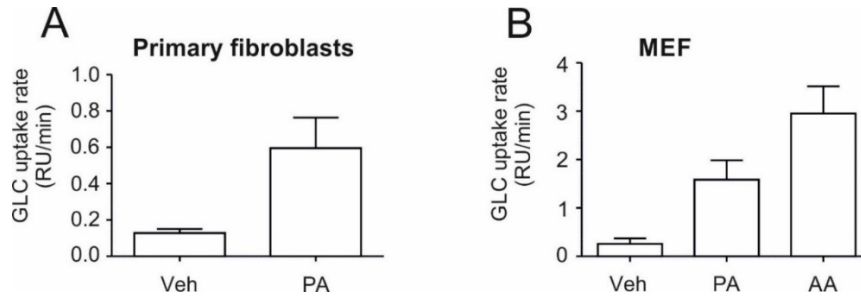


Figure 3. The rate of glucose (GLC) uptake in primary skin fibroblasts (C5120) and mouse embryonic fibroblasts (MEF) treated for 30 min with vehicle (Veh; 0.01% ethanol), pipecolinic acid (PA; 100 nM), or antimycin A (AA, 20 nM). The rate of glucose uptake was measured as described in Chapter 3. N=1 independent experiment.

Remarkably, in **Chapter 3**, calculation of the flux control coefficient of glucose uptake on the glucose flux was close to zero under both control and OXPHOS inhibited conditions. Of note, stimulation of glucose uptake by OXPHOS inhibitors is not cell type specific as it was also observed in control primary human skin fibroblasts (Fig. 3A) and mouse embryonic fibroblasts (MEFs) (Fig. 3B). Therefore, it seems counter intuitive that while stimulation of glucose uptake is so well regulated and occurs in various cell types, it has no effect on the glucose flux. In order to assess whether the increased glucose uptake capacity indeed has no effect on the glucose flux, lactate secretion was measured under AMPK knockdown (KD) conditions (*i.e.* diminished glucose uptake stimulation). Preliminary data suggests that lactate secretion is lower under AMPK KD conditions compared to scramble in PA- and AA-treated cells (Fig. 4). This argues against the low flux control coefficient for glucose uptake. However, the fact that lactate secretion is also reduced in the vehicle-treated cells, suggests that this AMPK KD-mediated reduction in lactate secretion is independent of glucose uptake. Of note, AMPK-mediated stimulation of HK activity cannot be excluded.

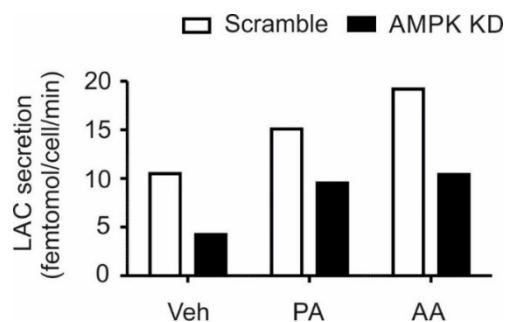


Figure 4. C2C12 myoblasts were transfected with scramble or AMPK $\alpha 1/\alpha 2$ siRNA. After 2 days myoblasts were incubated in HT buffer (2 mM glucose) containing the CI-inhibitor PA (100 nM), the CIII-inhibitor AA (20 nM), or vehicle (0.01% ethanol). After 60 min the lactate (LAC) levels in HT buffer were measured as described in Chapter 3. N=1 independent experiment.

Knowing the exact residues of Glut1 that are modified by mitochondrial inhibition, allows for more specific targeting of Glut1 and a better understanding of the role of glucose uptake stimulation on the glycolytic flux. In addition, it would be interesting to investigate whether the same signaling events also regulate the increased rate of glucose uptake in primary *Ndufs4* KO myoblasts. Moreover, it is of great interest whether mitochondrial dysfunction also triggers an increase in glucose uptake in CI patient cells and whether the same signaling events as in C2C12 myoblasts are involved. Murine Glut1 is highly similar to human GLUT1 (97% sequence identity), suggesting they are regulated in the same manner. However, since the CI-/CIII-inhibitors were used at concentrations that fully inhibit mitochondrial respiration, it is possible that they triggers a different mode of regulation compared to a genetic model with residual CI activity. In addition, is possible that in mitochondrial patient cells, long term adaptation triggers both upregulation of GLUT expression and activation of GLUTs at the plasma membrane.

Model systems for studying mitochondrial dysfunction

Fibroblasts derived from CI-deficient patients are extensively studied and show several cellular pathophysiological consequences such as decreased $\Delta\Psi$, increased levels of ROS and NAD(P)H, and aberrant calcium and ATP handling and mitochondrial morphology (Distelmaier et al., 2009b, Koopman et al., 2005, Verkaar et al., 2007b, Visch et al., 2006a). In addition, several mouse models have been created to study the pathophysiology of CI dysfunction (Breuer et al., 2013b). The *Ndufs4* whole-body KO mouse shows similar clinical phenotypes as compared to human patients and ultimately dies before the age of 50 days (Kruse et al., 2008). To study intracellular pathophysiology, immortalized mouse embryonic fibroblasts (iMEFs) and primary mouse muscle and skin fibroblasts were previously obtained from WT and KO mice. Similar to patient fibroblasts, primary KO mouse muscle and skin fibroblasts display increased H₂O₂-oxidizable ROS level (Valsecchi et al., 2013). In contrast, H₂O₂-oxidizable ROS levels were not increased in iMEFs, which might be due to a different cellular status (cell type, immortalization) (Valsecchi et al., 2012). However, CI deficiency generally affects high-energy demanding tissues that rely on mitochondrial ATP production

(skeletal muscle, heart, brain) (Koopman et al., 2012). Therefore, in **Chapter 4** primary myoblasts derived from skeletal muscles of WT and KO mice were used as a cellular model. Because a glycolytic phenotype could potentially mask CI-dysfunction and (intra)cellular pathophysiology in KO myoblasts, the effect of different culturing conditions on the rate of glucose uptake and O₂ consumption was assessed (**Chapter 4**). In order to prevent differentiation of primary myoblast, proliferation medium contained the growth factor bFGF. In this medium, no differences in the rate of glucose uptake and O₂ consumption between WT and KO myoblast were observed. Because bFGF stabilizes HIF-1 α , it promotes a glycolytic phenotype (Kihira et al., 2011). Switching to differentiation medium containing high glucose (25 mM), low glucose (5 mM), or galactose (5 mM) and no bFGF, revealed that low glucose and especially galactose instead of glucose increased the ATP-linked O₂ consumption rates in KO myoblasts (**Chapter 4**). The rate of glucose uptake was also significantly higher in KO myoblasts cultured in differentiation medium containing low glucose or galactose, suggesting CI dysfunction triggers a compensatory mechanism. This improves the study of the (intra)cellular pathophysiology as a consequence of CI dysfunction. Interestingly, in C2C12 myoblasts cultured in 25 mM glucose, the rate of glucose uptake was significantly increased by CI inhibition (**Chapter 3**). This difference might be due to residual CI activity (KO myoblasts) versus no residual CI activity (PA treatment). In differentiating KO myoblasts intracellular pathophysiology was observed as a reduced $\Delta\Psi$, an increased NAD(P)H and H₂O₂-oxidizable ROS levels (**Chapter 4**). Most of these changes are in accordance to previous results using primary skin fibroblasts from CI-deficient patients (Distelmaier et al., 2009a, Koopman et al., 2007, Verkaart et al., 2007b) and primary fibroblasts derived from these KO mice (Valsecchi et al., 2013). This suggests a uniform cellular CI-dysfunctional pathophysiology between fibroblasts and skeletal muscle cells derived from mice and between human and murine fibroblasts. To our surprise, however, basal O₂ consumption rate of KO myoblasts were normal (**Chapter 4**). In order to analyze whether this basal O₂ consumption was CI-driven, two CI inhibitors (PA and rotenone) were used. Surprisingly, these CI inhibitors acutely reduced basal O₂ consumption rates in KO myoblasts derived from extensor digitorum longus (EDL) muscle (Fig. 5). This suggests that sufficient amount residual CI activity is still present in KO myoblasts.

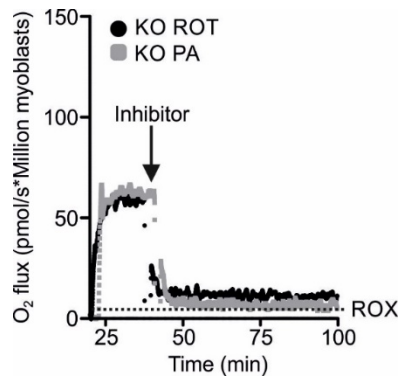


Figure 5. O₂ consumption rates of EDL-derived KO myoblasts. After reaching a steady basal O₂ consumption rate, 100 nM rotenone (ROT) or 100 nM piericidin A (PA) was added to inhibit CI. Dotted line indicates non-mitochondrial O₂ consumption rate (ROX).

However, previous studies showed absence of the Ndufs4 subunit and thereby less stable complex I (Calvaruso et al., 2012, Valsecchi et al., 2013). This altogether suggests that these KO myoblasts are not CI deficient but rather have a dysfunctional CI. This might also explain the intracellular pathophysiology regarding H₂O₂-oxidizable ROS and mitochondrial membrane potential in KO myoblasts in the absence of decreased basal O₂ consumption rates (**Chapter 4**). But how could a normal CI-sensitive basal O₂ consumption rate be observed in these KO myoblasts? Most likely, an over-capacity of CI exists and therefore a critical level of CI inhibition needs to be reached before any effects on mitochondrial ATP production and/or O₂ consumption rate can be observed. Recently, it was shown that skeletal muscle mitochondria derived from these KO mice had 20% residual CI activity while having normal ATP production capacity (Alam et al., 2015). Using an *in silico* model it became clear that this (and other) parameter is severely affected when CI activity is decreased by more than 90% (Alam et al., 2015). In accordance to these results, O₂ consumption rate and ATP production in skeletal muscle-derived mitochondria was only affected when CI activity was decreased by more than 80% (using rotenone) (Rossignol et al., 1999). Moreover, the O₂ consumption rate and ATP production were only affected in brain mitochondria derived from a non-synaptic region when CI activity was reduced by 60-72% (Davey et al., 1997, Davey and Clark, 1996). However, this value was 25% in brain mitochondria derived from a synaptic region (Davey et al., 1997, Davey et al., 1998) indicating tissue- and regional-specific differences. These

findings all support a biochemical (mitochondrial) threshold effect (Rossignol et al., 2003). The above (*i.e.* absence of aberrant O₂ consumption rate and ATP) suggests that a metabolic problem (based on O₂ consumption rate and ATP production) does not occur in skeletal muscle tissue of the KO mice, which might also not be the primary tissue being affected by CI dysfunction (*i.e.* normal functioning of myoblasts) (Quintana et al., 2010). However, *in vivo* limited substrate (nutrient) availability and/or increased cellular activity could still result in restricted ATP levels and muscle pathology.

Outlook

OXPPOS dysfunction leads to a wide variety of both multi-systemic and tissue-specific disorders and has been linked to many age-related diseases such as Parkinson's disease, Alzheimer's disease, Huntington's disease, amyotrophic lateral sclerosis (ALS), diabetes type II, and cancer (Breuer et al., 2013a, Chandra and Singh, 2011, Martin, 2011, Ritov et al., 2010, Swerdlow, 2012, Thorburn, 2004). Besides inherited disorders, OXPPOS dysfunction can be a consequence of drug off-target effects (Wallace, 2008). Currently there is no cure for patients suffering from an OXPPOS disorder. More in depth knowledge of the adaptive responses triggered by OXPPOS dysfunction can aid a rational design of intervention strategies. Although mitochondrial disorders comprise a phenotypically and genetically heterogeneous group of disorders, based on studies performed in this thesis and current literature (Abbud et al., 2000, Barnes et al., 2002, Besson et al., 2015, Distelmaier et al., 2015, Hamrahian et al., 1999, Haran and Gross, 2014, Jing and Ismail-Beigi, 2007, Koseoglu and Beigi, 1999, Shetty et al., 1993, Shi et al., 1995, Suhane et al., 2013, Wu and Wei, 2012), stimulation of glucose uptake seems to be a general adaptive response. Moreover, the key role that both glucose uptake and mitochondria play in energy metabolism makes this knowledge applicable to a large group of metabolic-related diseases. For instance, in the case of type II diabetes, induction of enhanced glucose uptake could aid in lowering blood glucose levels. However, additional strategies might be necessary to prevent excessive lactate or ROS formation. In the case of cancer, inhibition of enhanced glucose uptake by tumor cells might reduce tumor growth. This thesis provides new insights in the regulation of glucose uptake by CI dysfunction and the cellular

consequences of enhanced glucose metabolism on which future research can build. For instance, a more detailed understanding of the role of AMPK and Sirt2 in Glut1 stimulation could lead to more selective targeting.

References

Summary

Samenvatting

Dankwoord

Curriculum Vitae

List of publications



References

- Abbud, W., Habinowski, S., Zhang, J. Z., Kendrew, J., Elkairi, F. S., Kemp, B. E., Witters, L. A. & Ismail-Beigi, F. (2000) Stimulation of AMP-activated protein kinase (AMPK) is associated with enhancement of Glut1-mediated glucose transport. *Arch Biochem Biophys*, 380, 347-52.
- Acin-Perez, R. & Enriquez, J. A. (2014) The function of the respiratory supercomplexes: the plasticity model. *Biochim Biophys Acta*, 1837, 444-50.
- Afanas'ev, I. (2011) Reactive oxygen species signaling in cancer: comparison with aging. *Aging Dis*, 2, 219-30.
- Agathocleous, M., Love, N. K., Randlett, O., Harris, J. J., Liu, J., Murray, A. J. & Harris, W. A. (2012) Metabolic differentiation in the embryonic retina. *Nat Cell Biol*, 14, 859-64.
- Al-Khalili, L., Chibalin, A. V., Kannisto, K., Zhang, B. B., Permert, J., Holman, G. D., Ehrenborg, E., Ding, V. D., Zierath, J. R. & Krook, A. (2003) Insulin action in cultured human skeletal muscle cells during differentiation: assessment of cell surface GLUT4 and GLUT1 content. *Cell Mol Life Sci*, 60, 991-8.
- Alam, M. T., Manjeri, G. R., Rodenburg, R. J., Smeitink, J. A., Notebaart, R. A., Huynen, M., Willems, P. H. & Koopman, W. J. (2015) Skeletal muscle mitochondria of NDUFS4(-/-) mice display normal maximal pyruvate oxidation and ATP production. *Biochim Biophys Acta*, 1847, 526-33.
- Alexander, A. & Walker, C. L. (2010) Differential localization of ATM is correlated with activation of distinct downstream signaling pathways. *Cell Cycle*, 9, 3685-6.
- Anderson, S. L., Chung, W. K., Frezzo, J., Papp, J. C., Ekstein, J., Dimauro, S. & Rubin, B. Y. (2008) A novel mutation in NDUFS4 causes Leigh syndrome in an Ashkenazi Jewish family. *J Inherit Metab Dis*, 31 Suppl 2, S461-7.
- Andrisse, S., Koehler, R. M., Chen, J. E., Patel, G. D., Vallurupalli, V. R., Ratliff, B. A., Warren, D. E. & Fisher, J. S. (2014) Role of GLUT1 in regulation of reactive oxygen species. *Redox Biol*, 2, 764-71.
- Andrisse, S., Patel, G. D., Chen, J. E., Webber, A. M., Spears, L. D., Koehler, R. M., Robinson-Hill, R. M., Ching, J. K., Jeong, I. & Fisher, J. S. (2013) ATM and GLUT1-S490 phosphorylation regulate GLUT1 mediated transport in skeletal muscle. *PLoS One*, 8, e66027.
- Arner, E. S. (2009) Focus on mammalian thioredoxin reductases--important selenoproteins with versatile functions. *Biochim Biophys Acta*, 1790, 495-526.
- Asano, T., Katagiri, H., Takata, K., Lin, J. L., Ishihara, H., Inukai, K., Tsukuda, K., Kikuchi, M., Hirano, H., Yazaki, Y. & Et Al. (1991) The role of N-glycosylation of GLUT1 for glucose transport activity. *J Biol Chem*, 266, 24632-6.
- Assouline, Z., Jambou, M., Rio, M., Bole-Feysot, C., De Lonlay, P., Barnerias, C., Desguerre, I., Bonnemains, C., Guillermet, C., Steffann, J., Munnich, A., Bonnefont, J. P., Rotig, A. & Lebre, A. S. (2012) A constant and similar assembly defect of mitochondrial respiratory chain complex I allows rapid identification of NDUFS4 mutations in patients with Leigh syndrome. *Biochim Biophys Acta*, 1822, 1062-9.
- Augustin, R. (2010) The protein family of glucose transport facilitators: It's not only about glucose after all. *IUBMB Life*, 62, 315-33.
- Baer, S. C., Casaubon, L. & Younes, M. (1997) Expression of the human erythrocyte glucose transporter Glut1 in cutaneous neoplasia. *J Am Acad Dermatol*, 37, 575-7.
- Bain, J., Plater, L., Elliott, M., Shpiro, N., Hastie, C. J., Mclauchlan, H., Klevernic, I., Arthur, J. S., Alessi, D. R. & Cohen, P. (2007) The selectivity of protein kinase inhibitors: a further update. *Biochem J*, 408, 297-315.

- Baker, G. F. & Widdas, W. F. (1988) Parameters for 3-O-methyl glucose transport in human erythrocytes and fit of asymmetric carrier kinetics. *J Physiol*, 395, 57-76.
- Bakker, B. M., Walsh, M. C., Ter Kuile, B. H., Mensonides, F. I., Michels, P. A., Opperdoes, F. R. & Westerhoff, H. V. (1999) Contribution of glucose transport to the control of the glycolytic flux in *Trypanosoma brucei*. *Proc Natl Acad Sci U S A*, 96, 10098-103.
- Balsa, E., Marco, R., Perales-Clemente, E., Szklarczyk, R., Calvo, E., Landazuri, M. O. & Enriquez, J. A. (2012) NDUFA4 is a subunit of complex IV of the mammalian electron transport chain. *Cell Metab*, 16, 378-86.
- Barnes, K., Ingram, J. C., Porras, O. H., Barros, L. F., Hudson, E. R., Fryer, L. G., Fougelle, F., Carling, D., Hardie, D. G. & Baldwin, S. A. (2002) Activation of GLUT1 by metabolic and osmotic stress: potential involvement of AMP-activated protein kinase (AMPK). *J Cell Sci*, 115, 2433-42.
- Barros, L. F., Bittner, C. X., Loaiza, A. & Porras, O. H. (2007) A quantitative overview of glucose dynamics in the gliovascular unit. *Glia*, 55, 1222-37.
- Barros, L. F., Bittner, C. X., Loaiza, A., Ruminot, I., Larenas, V., Moldenhauer, H., Oyarzun, C. & Alvarez, M. (2009) Kinetic validation of 6-NBDG as a probe for the glucose transporter GLUT1 in astrocytes. *J Neurochem*, 109 Suppl 1, 94-100.
- Batandier, C., Guigas, B., Detaille, D., El-Mir, M. Y., Fontaine, E., Rigoulet, M. & Leverve, X. M. (2006) The ROS production induced by a reverse-electron flux at respiratory-chain complex 1 is hampered by metformin. *J Bioenerg Biomembr*, 38, 33-42.
- Batt, E. R. & Schachter, D. (1973) Transport of monosaccharides. I. Asymmetry in the human erythrocyte mechanism. *J Clin Invest*, 52, 1686-97.
- Behrooz, A. & Ismail-Beigi, F. (1997) Dual control of glut1 glucose transporter gene expression by hypoxia and by inhibition of oxidative phosphorylation. *J Biol Chem*, 272, 5555-62.
- Bell, G. I., Kayano, T., Buse, J. B., Burant, C. F., Takeda, J., Lin, D., Fukumoto, H. & Seino, S. (1990) Molecular biology of mammalian glucose transporters. *Diabetes Care*, 13, 198-208.
- Berg, J., Hung, Y. P. & Yellen, G. (2009) A genetically encoded fluorescent reporter of ATP:ADP ratio. *Nat Methods*, 6, 161-6.
- Berggren, J. R., Tanner, C. J. & Houmard, J. A. (2007) Primary cell cultures in the study of human muscle metabolism. *Exerc Sport Sci Rev*, 35, 56-61.
- Bermejo, C., Haerizadeh, F., Takanaga, H., Chermak, D. & Frommer, W. B. (2010) Dynamic analysis of cytosolic glucose and ATP levels in yeast using optical sensors. *Biochem J*, 432, 399-406.
- Bertram, R. & Pernarowski, M. (1998) Glucose diffusion in pancreatic islets of Langerhans. *Biophys J*, 74, 1722-31.
- Besson, M. T., Alegria, K., Garrido-Gerter, P., Barros, L. F. & Lievens, J. C. (2015) Enhanced neuronal glucose transporter expression reveals metabolic choice in a HD *Drosophila* model. *PLoS One*, 10, e0118765.
- Bittner, C. X., Loaiza, A., Ruminot, I., Larenas, V., Sotelo-Hitschfeld, T., Gutierrez, R., Cordova, A., Valdebenito, R., Frommer, W. B. & Barros, L. F. (2010) High resolution measurement of the glycolytic rate. *Front Neuroenergetics*, 2.
- Blanchet, L., Buydens, M. C., Smeitink, J. A., Willems, P. H. & Koopman, W. J. (2011) Isolated mitochondrial complex I deficiency: explorative data analysis of patient cell parameters. *Curr Pharm Des*, 17, 4023-33.
- Blanchet, L., Grefte, S., Smeitink, J. A., Willems, P. H. & Koopman, W. J. (2014) Photo-induction and automated quantification of reversible mitochondrial permeability transition pore opening in primary mouse myotubes. *PLoS One*, 9, e114090.
- Blodgett, D. M., De Zutter, J. K., Levine, K. B., Karim, P. & Carruthers, A. (2007) Structural basis of GLUT1 inhibition by cytoplasmic ATP. *J Gen Physiol*, 130, 157-68.

- Bonder, E. M. & Mooseker, M. S. (1986) Cytochalasin B slows but does not prevent monomer addition at the barbed end of the actin filament. *J Cell Biol*, 102, 282-8.
- Borst, J. W., Hink, M. A., Van Hoek, A. & Visser, A. J. (2005) Effects of refractive index and viscosity on fluorescence and anisotropy decays of enhanced cyan and yellow fluorescent proteins. *J Fluoresc*, 15, 153-60.
- Brand, K. (1997) Aerobic glycolysis by proliferating cells: protection against oxidative stress at the expense of energy yield. *J Bioenerg Biomembr*, 29, 355-64.
- Brandauer, J., Vienberg, S. G., Andersen, M. A., Ringholm, S., Risis, S., Larsen, P. S., Kristensen, J. M., Frosig, C., Leick, L., Fentz, J., Jorgensen, S., Kiens, B., Wojtaszewski, J. F., Richter, E. A., Zierath, J. R., Goodyear, L. J., Pilegaard, H. & Trebak, J. T. (2013) AMP-activated protein kinase regulates nicotinamide phosphoribosyl transferase expression in skeletal muscle. *J Physiol*, 591, 5207-20.
- Breuer, M. E., Koopman, W. J., Koene, S., Nootboom, M., Rodenburg, R. J., Willems, P. H. & Smeitink, J. A. (2013a) The role of mitochondrial OXPHOS dysfunction in the development of neurologic diseases. *Neurobiol Dis*, 51, 27-34.
- Breuer, M. E., Willems, P. H., Smeitink, J. A., Koopman, W. J. & Nootboom, M. (2013b) Cellular and animal models for mitochondrial complex I deficiency: a focus on the NDUF54 subunit. *IUBMB Life*, 65, 202-8.
- Brown, R. S. & Wahl, R. L. (1993) Overexpression of Glut-1 glucose transporter in human breast cancer. An immunohistochemical study. *Cancer*, 72, 2979-85.
- Brunelle, J. K., Bell, E. L., Quesada, N. M., Vercauteren, K., Tiranti, V., Zeviani, M., Scarpulla, R. C. & Chandel, N. S. (2005) Oxygen sensing requires mitochondrial ROS but not oxidative phosphorylation. *Cell Metab*, 1, 409-14.
- Budde, S. M., Van Den Heuvel, L. P., Janssen, A. J., Smeets, R. J., Buskens, C. A., Demeirleir, L., Van Coster, R., Baethmann, M., Voit, T., Trijbels, J. M. & Smeitink, J. A. (2000) Combined enzymatic complex I and III deficiency associated with mutations in the nuclear encoded NDUF54 gene. *Biochem Biophys Res Commun*, 275, 63-8.
- Budde, S. M., Van Den Heuvel, L. P., Smeets, R. J., Skladal, D., Mayr, J. A., Boelen, C., Petruzzella, V., Papa, S. & Smeitink, J. A. (2003) Clinical heterogeneity in patients with mutations in the NDUF54 gene of mitochondrial complex I. *J Inherit Metab Dis*, 26, 813-5.
- Calvaruso, M. A., Willems, P., Van Den Brand, M., Valsecchi, F., Kruse, S., Palminter, R., Smeitink, J. & Nijtmans, L. (2012) Mitochondrial complex III stabilizes complex I in the absence of NDUF54 to provide partial activity. *Hum Mol Genet*, 21, 115-20.
- Canto, C., Gerhart-Hines, Z., Feige, J. N., Lagouge, M., Noriega, L., Milne, J. C., Elliott, P. J., Puigserver, P. & Auwerx, J. (2009) AMPK regulates energy expenditure by modulating NAD⁺ metabolism and SIRT1 activity. *Nature*, 458, 1056-60.
- Carlberg, I. & Mannervik, B. (1985) Glutathione reductase. *Methods Enzymol*, 113, 484-90.
- Carruthers, A. (1986) ATP regulation of the human red cell sugar transporter. *J Biol Chem*, 261, 11028-37.
- Carruthers, A. (1990) Facilitated diffusion of glucose. *Physiol Rev*, 70, 1135-76.
- Carruthers, A., Dezutter, J., Ganguly, A. & Devaskar, S. U. (2009) Will the original glucose transporter isoform please stand up! *Am J Physiol Endocrinol Metab*, 297, E836-48.
- Chae, H. Z., Kim, H. J., Kang, S. W. & Rhee, S. G. (1999) Characterization of three isoforms of mammalian peroxiredoxin that reduce peroxides in the presence of thioredoxin. *Diabetes Res Clin Pract*, 45, 101-12.
- Chambers, M. A., Moylan, J. S., Smith, J. D., Goodyear, L. J. & Reid, M. B. (2009) Stretch-stimulated glucose uptake in skeletal muscle is mediated by reactive oxygen species and p38 MAP-kinase. *J Physiol*, 587, 3363-73.

- Chandel, N. S., Maltepe, E., Goldwasser, E., Mathieu, C. E., Simon, M. C. & Schumacker, P. T. (1998) Mitochondrial reactive oxygen species trigger hypoxia-induced transcription. *Proc Natl Acad Sci U S A*, 95, 11715-20.
- Chandel, N. S., McClintock, D. S., Feliciano, C. E., Wood, T. M., Melendez, J. A., Rodriguez, A. M. & Schumacker, P. T. (2000) Reactive oxygen species generated at mitochondrial complex III stabilize hypoxia-inducible factor-1 α during hypoxia: a mechanism of O₂ sensing. *J Biol Chem*, 275, 25130-8.
- Chandra, D. & Singh, K. K. (2011) Genetic insights into OXPHOS defect and its role in cancer. *Biochim Biophys Acta*, 1807, 620-5.
- Chang, T. S., Cho, C. S., Park, S., Yu, S., Kang, S. W. & Rhee, S. G. (2004) Peroxiredoxin III, a mitochondrion-specific peroxidase, regulates apoptotic signaling by mitochondria. *J Biol Chem*, 279, 41975-84.
- Chen, C., Pore, N., Behrooz, A., Ismail-Beigi, F. & Maity, A. (2001) Regulation of glut1 mRNA by hypoxia-inducible factor-1. Interaction between H-ras and hypoxia. *J Biol Chem*, 276, 9519-25.
- Chen, J., Chan, A. W., To, K. F., Chen, W., Zhang, Z., Ren, J., Song, C., Cheung, Y. S., Lai, P. B., Cheng, S. H., Ng, M. H., Huang, A. & Ko, B. C. (2013a) SIRT2 overexpression in hepatocellular carcinoma mediates epithelial to mesenchymal transition by protein kinase B/glycogen synthase kinase-3 β /beta-catenin signaling. *Hepatology*, 57, 2287-98.
- Chen, S. K., Hsu, C. H., Tsai, M. L., Chen, R. H. & Drummen, G. P. (2013b) Inhibition of oxidative stress by low-molecular-weight polysaccharides with various functional groups in skin fibroblasts. *Int J Mol Sci*, 14, 19399-415.
- Chen, Y., Du, J., Zhao, Y. T., Zhang, L., Lv, G., Zhuang, S., Qin, G. & Zhao, T. C. (2015) Histone deacetylase (HDAC) inhibition improves myocardial function and prevents cardiac remodeling in diabetic mice. *Cardiovasc Diabetol*, 14, 99.
- Chen, Y., Mcmillan-Ward, E., Kong, J., Israels, S. J. & Gibson, S. B. (2007) Mitochondrial electron-transport-chain inhibitors of complexes I and II induce autophagic cell death mediated by reactive oxygen species. *J Cell Sci*, 120, 4155-66.
- Choi, W. S., Kim, H. W. & Xia, Z. (2015) JNK inhibition of VMAT2 contributes to rotenone-induced oxidative stress and dopamine neuron death. *Toxicology*, 328, 75-81.
- Choudhary, C., Kumar, C., Gnad, F., Nielsen, M. L., Rehman, M., Walther, T. C., Olsen, J. V. & Mann, M. (2009) Lysine acetylation targets protein complexes and co-regulates major cellular functions. *Science*, 325, 834-40.
- Choudhary, C., Weinert, B. T., Nishida, Y., Verdin, E. & Mann, M. (2014) The growing landscape of lysine acetylation links metabolism and cell signalling. *Nat Rev Mol Cell Biol*, 15, 536-50.
- Chowdhury, H. H., Kreft, M., Jensen, J. & Zorec, R. (2014) Insulin induces an increase in cytosolic glucose levels in 3T3-L1 cells with inhibited glycogen synthase activation. *Int J Mol Sci*, 15, 17827-37.
- Cloherty, E. K., Diamond, D. L., Heard, K. S. & Carruthers, A. (1996) Regulation of GLUT1-mediated sugar transport by an antiport/uniport switch mechanism. *Biochemistry*, 35, 13231-9.
- Cloherty, E. K., Levine, K. B. & Carruthers, A. (2001) The red blood cell glucose transporter presents multiple, nucleotide-sensitive sugar exit sites. *Biochemistry*, 40, 15549-61.
- Collins, C. A. & Zammit, P. S. (2009) Isolation and grafting of single muscle fibres. *Methods Mol Biol*, 482, 319-30.
- Colombo, S. L. & Moncada, S. (2009) AMPK α 1 regulates the antioxidant status of vascular endothelial cells. *Biochem J*, 421, 163-9.
- Columbaro, M., Mattioli, E., Lattanzi, G., Rutigliano, C., Ognibene, A., Maraldi, N. M. & Squarzone, S. (2001) Staurosporine treatment and serum starvation promote the cleavage of emerin in

- cultured mouse myoblasts: involvement of a caspase-dependent mechanism. *FEBS Lett*, 509, 423-9.
- Cooper, D. R., Watson, J. E., Patel, N., Illingworth, P., Acevedo-Duncan, M., Goodnight, J., Chalfant, C. E. & Mischak, H. (1999) Ectopic expression of protein kinase C β 1, - δ , and - ϵ , but not - β 2 or - ζ , provide for insulin stimulation of glucose uptake in NIH-3T3 cells. *Arch Biochem Biophys*, 372, 69-79.
- Cornford, E. M., Hyman, S. & Swartz, B. E. (1994) The human brain GLUT1 glucose transporter: ultrastructural localization to the blood-brain barrier endothelia. *J Cereb Blood Flow Metab*, 14, 106-12.
- Correia, S. C., Santos, R. X., Cardoso, S., Carvalho, C., Candeias, E., Duarte, A. I., Placido, A. I., Santos, M. S. & Moreira, P. I. (2012) Alzheimer disease as a vascular disorder: where do mitochondria fit? *Exp Gerontol*, 47, 878-86.
- Cosentino, C., Grieco, D. & Costanzo, V. (2011) ATM activates the pentose phosphate pathway promoting anti-oxidant defence and DNA repair. *EMBO J*, 30, 546-55.
- Costa, V. & Scorrano, L. (2012) Shaping the role of mitochondria in the pathogenesis of Huntington's disease. *EMBO J*, 31, 1853-64.
- Cox, A. G., Winterbourn, C. C. & Hampton, M. B. (2010) Mitochondrial peroxiredoxin involvement in antioxidant defence and redox signalling. *Biochem J*, 425, 313-25.
- Cura, A. J. & Carruthers, A. (2012) AMP kinase regulation of sugar transport in brain capillary endothelial cells during acute metabolic stress. *Am J Physiol Cell Physiol*, 303, C806-14.
- Dan, L., Klimenkova, O., Klimiankou, M., Klusman, J. H., Van Den Heuvel-Eibrink, M. M., Reinhardt, D., Welte, K. & Skokowa, J. (2012) The role of sirtuin 2 activation by nicotinamide phosphoribosyltransferase in the aberrant proliferation and survival of myeloid leukemia cells. *Haematologica*, 97, 551-9.
- Davey, G. P., Canevari, L. & Clark, J. B. (1997) Threshold effects in synaptosomal and nonsynaptic mitochondria from hippocampal CA1 and paramedian neocortex brain regions. *J Neurochem*, 69, 2564-70.
- Davey, G. P. & Clark, J. B. (1996) Threshold effects and control of oxidative phosphorylation in nonsynaptic rat brain mitochondria. *J Neurochem*, 66, 1617-24.
- Davey, G. P., Peuchen, S. & Clark, J. B. (1998) Energy thresholds in brain mitochondria. Potential involvement in neurodegeneration. *J Biol Chem*, 273, 12753-7.
- Davies, S. P., Helps, N. R., Cohen, P. T. & Hardie, D. G. (1995) 5'-AMP inhibits dephosphorylation, as well as promoting phosphorylation, of the AMP-activated protein kinase. Studies using bacterially expressed human protein phosphatase-2C alpha and native bovine protein phosphatase-2AC. *FEBS Lett*, 377, 421-5.
- De Rasmio, D., Gattoni, G., Papa, F., Santeramo, A., Pacelli, C., Cocco, T., Micelli, L., Sardaro, N., Larizza, M., Scivetti, M., Milano, S. & Signorile, A. (2011) The beta-adrenoceptor agonist isoproterenol promotes the activity of respiratory chain complex I and lowers cellular reactive oxygen species in fibroblasts and heart myoblasts. *Eur J Pharmacol*, 652, 15-22.
- De Rasmio, D., Panelli, D., Sardanelli, A. M. & Papa, S. (2008) cAMP-dependent protein kinase regulates the mitochondrial import of the nuclear encoded NDUFS4 subunit of complex I. *Cell Signal*, 20, 989-97.
- De Zutter, J. K., Levine, K. B., Deng, D. & Carruthers, A. (2013) Sequence determinants of GLUT1 oligomerization: analysis by homology-scanning mutagenesis. *J Biol Chem*, 288, 20734-44.
- Deichmann, U., Schuster, S., Mazat, J. P. & Cornish-Bowden, A. (2014) Commemorating the 1913 Michaelis-Menten paper Die Kinetik der Invertinwirkung: three perspectives. *FEBS J*, 281, 435-63.

- Deng, D., Xu, C., Sun, P., Wu, J., Yan, C., Hu, M. & Yan, N. (2014) Crystal structure of the human glucose transporter GLUT1. *Nature*, 510, 121-5.
- Deuschle, K., Chaudhuri, B., Okumoto, S., Lager, I., Lalonde, S. & Frommer, W. B. (2006) Rapid metabolism of glucose detected with FRET glucose nanosensors in epidermal cells and intact roots of Arabidopsis RNA-silencing mutants. *Plant Cell*, 18, 2314-25.
- Deuschle, K., Fehr, M., Hilpert, M., Lager, I., Lalonde, S., Looger, L. L., Okumoto, S., Persson, J., Schmidt, A. & Frommer, W. B. (2005a) Genetically encoded sensors for metabolites. *Cytometry A*, 64, 3-9.
- Deuschle, K., Okumoto, S., Fehr, M., Looger, L. L., Kozhukh, L. & Frommer, W. B. (2005b) Construction and optimization of a family of genetically encoded metabolite sensors by semirational protein engineering. *Protein Sci*, 14, 2304-14.
- Deves, R. & Krupka, R. M. (1978) Cytochalasin B and the kinetics of inhibition of biological transport: a case of asymmetric binding to the glucose carrier. *Biochim Biophys Acta*, 510, 339-48.
- Dieteren, C. E., Koopman, W. J., Swarts, H. G., Peters, J. G., Maczuga, P., Van Gemst, J. J., Masereeuw, R., Smeitink, J. A., Nijtmans, L. G. & Willems, P. H. (2012) Subunit-specific incorporation efficiency and kinetics in mitochondrial complex I homeostasis. *J Biol Chem*, 287, 41851-60.
- Dieteren, C. E., Willems, P. H., Vogel, R. O., Swarts, H. G., Fransen, J., Roepman, R., Crienen, G., Smeitink, J. A., Nijtmans, L. G. & Koopman, W. J. (2008) Subunits of mitochondrial complex I exist as part of matrix- and membrane-associated subcomplexes in living cells. *J Biol Chem*, 283, 34753-61.
- Distelmaier, F., Koopman, W. J., Van Den Heuvel, L. P., Rodenburg, R. J., Mayatepek, E., Willems, P. H. & Smeitink, J. A. (2009a) Mitochondrial complex I deficiency: from organelle dysfunction to clinical disease. *Brain*, 132, 833-42.
- Distelmaier, F., Valsecchi, F., Forkink, M., Van Emst-De Vries, S., Swarts, H. G., Rodenburg, R. J., Verwiel, E. T., Smeitink, J. A., Willems, P. H. & Koopman, W. J. (2012) Trolox-sensitive reactive oxygen species regulate mitochondrial morphology, oxidative phosphorylation and cytosolic calcium handling in healthy cells. *Antioxid Redox Signal*, 17, 1657-69.
- Distelmaier, F., Valsecchi, F., Liemburg-Apers, D. C., Lebiecinska, M., Rodenburg, R. J., Heil, S., Keijer, J., Fransen, J., Imamura, H., Danhauser, K., Seibt, A., Violet, B., Gellerich, F. N., Smeitink, J. A., Wieckowski, M. R., Willems, P. H. & Koopman, W. J. (2015) Mitochondrial dysfunction in primary human fibroblasts triggers an adaptive cell survival program that requires AMPK- α . *Biochim Biophys Acta*, 1852, 529-40.
- Distelmaier, F., Visch, H. J., Smeitink, J. A., Mayatepek, E., Koopman, W. J. & Willems, P. H. (2009b) The antioxidant Trolox restores mitochondrial membrane potential and Ca²⁺-stimulated ATP production in human complex I deficiency. *J Mol Med (Berl)*, 87, 515-22.
- Dott, W., Mistry, P., Wright, J., Cain, K. & Herbert, K. E. (2014) Modulation of mitochondrial bioenergetics in a skeletal muscle cell line model of mitochondrial toxicity. *Redox Biol*, 2, 224-33.
- Dranka, B. P., Benavides, G. A., Diers, A. R., Giordano, S., Zelickson, B. R., Reily, C., Zou, L., Chatham, J. C., Hill, B. G., Zhang, J., Landar, A. & Darley-Usmar, V. M. (2011) Assessing bioenergetic function in response to oxidative stress by metabolic profiling. *Free Radic Biol Med*, 51, 1621-35.
- Drozdowicz-Tomsia, K., Anwer, A. G., Cahill, M. A., Madlum, K. N., Maki, A. M., Baker, M. S. & Goldys, E. M. (2014) Multiphoton fluorescence lifetime imaging microscopy reveals free-to-bound NADH ratio changes associated with metabolic inhibition. *J Biomed Opt*, 19, 086016.
- Ebert, B. L., Firth, J. D. & Ratcliffe, P. J. (1995) Hypoxia and mitochondrial inhibitors regulate expression of glucose transporter-1 via distinct Cis-acting sequences. *J Biol Chem*, 270, 29083-9.

- Eguez, L., Lee, A., Chavez, J. A., Miinea, C. P., Kane, S., Lienhard, G. E. & McGraw, T. E. (2005) Full intracellular retention of GLUT4 requires AS160 Rab GTPase activating protein. *Cell Metab*, 2, 263-72.
- Elkalaf, M., Andel, M. & Trnka, J. (2013) Low glucose but not galactose enhances oxidative mitochondrial metabolism in C2C12 myoblasts and myotubes. *PLoS One*, 8, e70772.
- Elstrom, R. L., Bauer, D. E., Buzzai, M., Karnauskas, R., Harris, M. H., Plas, D. R., Zhuang, H., Cinalli, R. M., Alavi, A., Rudin, C. M. & Thompson, C. B. (2004) Akt stimulates aerobic glycolysis in cancer cells. *Cancer Res*, 64, 3892-9.
- Emerling, B. M., Plataniias, L. C., Black, E., Nebreda, A. R., Davis, R. J. & Chandel, N. S. (2005) Mitochondrial reactive oxygen species activation of p38 mitogen-activated protein kinase is required for hypoxia signaling. *Mol Cell Biol*, 25, 4853-62.
- Emerling, B. M., Weinberg, F., Snyder, C., Burgess, Z., Mutlu, G. M., Viollet, B., Budinger, G. R. & Chandel, N. S. (2009) Hypoxic activation of AMPK is dependent on mitochondrial ROS but independent of an increase in AMP/ATP ratio. *Free Radic Biol Med*, 46, 1386-91.
- Epstein, T., Xu, L., Gillies, R. J. & Gatenby, R. A. (2014) Separation of metabolic supply and demand: aerobic glycolysis as a normal physiological response to fluctuating energetic demands in the membrane. *Cancer Metab*, 2, 7.
- Esposito, L. A., Kokoszka, J. E., Waymire, K. G., Cottrell, B., Macgregor, G. R. & Wallace, D. C. (2000) Mitochondrial oxidative stress in mice lacking the glutathione peroxidase-1 gene. *Free Radic Biol Med*, 28, 754-66.
- Esworthy, R. S., Ho, Y. S. & Chu, F. F. (1997) The Gpx1 gene encodes mitochondrial glutathione peroxidase in the mouse liver. *Arch Biochem Biophys*, 340, 59-63.
- Ewald, J. C., Reich, S., Baumann, S., Frommer, W. B. & Zamboni, N. (2011) Engineering genetically encoded nanosensors for real-time in vivo measurements of citrate concentrations. *PLoS One*, 6, e28245.
- Faenza, I., Bavelloni, A., Fiume, R., Lattanzi, G., Maraldi, N. M., Gilmour, R. S., Martelli, A. M., Suh, P. G., Billi, A. M. & Cocco, L. (2003) Up-regulation of nuclear PLCbeta1 in myogenic differentiation. *J Cell Physiol*, 195, 446-52.
- Farrell, C. L. & Pardridge, W. M. (1991) Blood-brain barrier glucose transporter is asymmetrically distributed on brain capillary endothelial luminal and abluminal membranes: an electron microscopic immunogold study. *Proc Natl Acad Sci U S A*, 88, 5779-83.
- Fehr, M., Lalonde, S., Lager, I., Wolff, M. W. & Frommer, W. B. (2003) In vivo imaging of the dynamics of glucose uptake in the cytosol of COS-7 cells by fluorescent nanosensors. *J Biol Chem*, 278, 19127-33.
- Fehr, M., Takanaga, H., Ehrhardt, D. W. & Frommer, W. B. (2005) Evidence for high-capacity bidirectional glucose transport across the endoplasmic reticulum membrane by genetically encoded fluorescence resonance energy transfer nanosensors. *Mol Cell Biol*, 25, 11102-12.
- Fernandes, R., Hosoya, K. & Pereira, P. (2011) Reactive oxygen species downregulate glucose transport system in retinal endothelial cells. *Am J Physiol Cell Physiol*, 300, C927-36.
- Filippin, L., Magalhaes, P. J., Di Benedetto, G., Colella, M. & Pozzan, T. (2003) Stable interactions between mitochondria and endoplasmic reticulum allow rapid accumulation of calcium in a subpopulation of mitochondria. *J Biol Chem*, 278, 39224-34.
- Finsterer, J. & Mahjoub, S. Z. (2013) Presentation of adult mitochondrial epilepsy. *Seizure*, 22, 119-23.
- Forkink, M., Willems, P. H., Koopman, W. J. & Grefte, S. (2015) Live-cell assessment of mitochondrial reactive oxygen species using dihydroethidine. *Methods Mol Biol*, 1264, 161-9.

- Freeman, H., Shimomura, K., Cox, R. D. & Ashcroft, F. M. (2006) Nicotinamide nucleotide transhydrogenase: a link between insulin secretion, glucose metabolism and oxidative stress. *Biochem Soc Trans*, 34, 806-10.
- Fryer, L. G., Fougere, F., Barnes, K., Baldwin, S. A., Woods, A. & Carling, D. (2002) Characterization of the role of the AMP-activated protein kinase in the stimulation of glucose transport in skeletal muscle cells. *Biochem J*, 363, 167-74.
- Fulco, M., Cen, Y., Zhao, P., Hoffman, E. P., Mcburney, M. W., Sauve, A. A. & Sartorelli, V. (2008) Glucose restriction inhibits skeletal myoblast differentiation by activating SIRT1 through AMPK-mediated regulation of Nampt. *Dev Cell*, 14, 661-73.
- Funaki, M., Randhawa, P. & Janmey, P. A. (2004) Separation of insulin signaling into distinct GLUT4 translocation and activation steps. *Mol Cell Biol*, 24, 7567-77.
- Gajewski, C. D., Yang, L., Schon, E. A. & Manfredi, G. (2003) New insights into the bioenergetics of mitochondrial disorders using intracellular ATP reporters. *Mol Biol Cell*, 14, 3628-35.
- Galloway, C. A. & Yoon, Y. (2012) Perspectives on: SGP symposium on mitochondrial physiology and medicine: what comes first, misshape or dysfunction? The view from metabolic excess. *J Gen Physiol*, 139, 455-63.
- Gambhir, S. S. (2002) Molecular imaging of cancer with positron emission tomography. *Nat Rev Cancer*, 2, 683-93.
- Gan, R. Y. & Li, H. B. (2014) Recent progress on liver kinase B1 (LKB1): expression, regulation, downstream signaling and cancer suppressive function. *Int J Mol Sci*, 15, 16698-718.
- Geraghty, K. M., Chen, S., Harthill, J. E., Ibrahim, A. F., Toth, R., Morrice, N. A., Vandermoere, F., Moorhead, G. B., Hardie, D. G. & Mackintosh, C. (2007) Regulation of multisite phosphorylation and 14-3-3 binding of AS160 in response to IGF-1, EGF, PMA and AICAR. *Biochem J*, 407, 231-41.
- Giannoni, E., Buricchi, F., Raugei, G., Ramponi, G. & Chiarugi, P. (2005) Intracellular reactive oxygen species activate Src tyrosine kinase during cell adhesion and anchorage-dependent cell growth. *Mol Cell Biol*, 25, 6391-403.
- Gnaiger, E. (2001) Bioenergetics at low oxygen: dependence of respiration and phosphorylation on oxygen and adenosine diphosphate supply. *Respir Physiol*, 128, 277-97.
- Gorga, F. R. & Lienhard, G. E. (1981) Equilibria and kinetics of ligand binding to the human erythrocyte glucose transporter. Evidence for an alternating conformation model for transport. *Biochemistry*, 20, 5108-13.
- Gould, G. W. & Holman, G. D. (1993) The glucose transporter family: structure, function and tissue-specific expression. *Biochem J*, 295 (Pt 2), 329-41.
- Graybill, C., Van Hoek, A. N., Desai, D., Carruthers, A. M. & Carruthers, A. (2006) Ultrastructure of human erythrocyte GLUT1. *Biochemistry*, 45, 8096-107.
- Grefte, S., Wagenaars, J. A., Jansen, R., Willems, P. H. & Koopman, W. J. (2015) Rotenone inhibits primary murine myotube formation via Raf-1 and ROCK2. *Biochim Biophys Acta*.
- Griesbeck, O., Baird, G. S., Campbell, R. E., Zacharias, D. A. & Tsien, R. Y. (2001) Reducing the environmental sensitivity of yellow fluorescent protein. Mechanism and applications. *J Biol Chem*, 276, 29188-94.
- Guaiquil, V. H., Vera, J. C. & Golde, D. W. (2001) Mechanism of vitamin C inhibition of cell death induced by oxidative stress in glutathione-depleted HL-60 cells. *J Biol Chem*, 276, 40955-61.
- Guillet-Deniau, I., Leturque, A. & Girard, J. (1994) Expression and cellular localization of glucose transporters (GLUT1, GLUT3, GLUT4) during differentiation of myogenic cells isolated from rat fetuses. *J Cell Sci*, 107 (Pt 3), 487-96.

- Gunnink, S. M., Kerk, S. A., Kuiper, B. D., Alabi, O. D., Kuipers, D. P., Praamsma, R. C., Wrobel, K. E. & Louters, L. L. (2014) Alkaline pH activates the transport activity of GLUT1 in L929 fibroblast cells. *Biochimie*, 99, 189-94.
- Guo, Z., Kozlov, S., Lavin, M. F., Person, M. D. & Paull, T. T. (2010) ATM activation by oxidative stress. *Science*, 330, 517-21.
- Guzy, R. D., Hoyos, B., Robin, E., Chen, H., Liu, L., Mansfield, K. D., Simon, M. C., Hammerling, U. & Schumacker, P. T. (2005) Mitochondrial complex III is required for hypoxia-induced ROS production and cellular oxygen sensing. *Cell Metab*, 1, 401-8.
- Guzy, R. D. & Schumacker, P. T. (2006) Oxygen sensing by mitochondria at complex III: the paradox of increased reactive oxygen species during hypoxia. *Exp Physiol*, 91, 807-19.
- Hamill, S., Cloherty, E. K. & Carruthers, A. (1999) The human erythrocyte sugar transporter presents two sugar import sites. *Biochemistry*, 38, 16974-83.
- Hamrahian, A. H., Zhang, J. Z., Elkhairi, F. S., Prasad, R. & Ismail-Beigi, F. (1999) Activation of Glut1 glucose transporter in response to inhibition of oxidative phosphorylation. *Arch Biochem Biophys*, 368, 375-9.
- Handa, N., Takagi, T., Saijo, S., Kishishita, S., Takaya, D., Toyama, M., Terada, T., Shirouzu, M., Suzuki, A., Lee, S., Yamauchi, T., Okada-Iwabuchi, M., Iwabuchi, M., Kadowaki, T., Minokoshi, Y. & Yokoyama, S. (2011) Structural basis for compound C inhibition of the human AMP-activated protein kinase alpha2 subunit kinase domain. *Acta Crystallogr D Biol Crystallogr*, 67, 480-7.
- Haran, M. & Gross, A. (2014) Balancing glycolysis and mitochondrial OXPHOS: lessons from the hematopoietic system and exercising muscles. *Mitochondrion*, 19 Pt A, 3-7.
- Hardie, D. G. (2011) Energy sensing by the AMP-activated protein kinase and its effects on muscle metabolism. *Proc Nutr Soc*, 70, 92-9.
- Hardie, D. G. (2014) AMP-activated protein kinase: maintaining energy homeostasis at the cellular and whole-body levels. *Annu Rev Nutr*, 34, 31-55.
- Hardie, D. G. & Ashford, M. L. (2014) AMPK: regulating energy balance at the cellular and whole body levels. *Physiology (Bethesda)*, 29, 99-107.
- Hardie, D. G., Ross, F. A. & Hawley, S. A. (2012) AMPK: a nutrient and energy sensor that maintains energy homeostasis. *Nat Rev Mol Cell Biol*, 13, 251-62.
- Hatefi, Y. & Yamaguchi, M. (1996) Nicotinamide nucleotide transhydrogenase: a model for utilization of substrate binding energy for proton translocation. *FASEB J*, 10, 444-52.
- Hawley, S. A., Ross, F. A., Chevtzoff, C., Green, K. A., Evans, A., Fogarty, S., Towler, M. C., Brown, L. J., Ogunbayo, O. A., Evans, A. M. & Hardie, D. G. (2010) Use of cells expressing gamma subunit variants to identify diverse mechanisms of AMPK activation. *Cell Metab*, 11, 554-65.
- Hawley, S. A., Selbert, M. A., Goldstein, E. G., Edelman, A. M., Carling, D. & Hardie, D. G. (1995) 5'-AMP activates the AMP-activated protein kinase cascade, and Ca²⁺/calmodulin activates the calmodulin-dependent protein kinase I cascade, via three independent mechanisms. *J Biol Chem*, 270, 27186-91.
- Hayashi, M., Sakata, M., Takeda, T., Yamamoto, T., Okamoto, Y., Sawada, K., Kimura, A., Minekawa, R., Tahara, M., Tasaka, K. & Murata, Y. (2004) Induction of glucose transporter 1 expression through hypoxia-inducible factor 1alpha under hypoxic conditions in trophoblast-derived cells. *J Endocrinol*, 183, 145-54.
- Hebert, D. N. & Carruthers, A. (1992) Glucose transporter oligomeric structure determines transporter function. Reversible redox-dependent interconversions of tetrameric and dimeric GLUT1. *J Biol Chem*, 267, 23829-38.

- Hickson, I., Zhao, Y., Richardson, C. J., Green, S. J., Martin, N. M., Orr, A. I., Reaper, P. M., Jackson, S. P., Curtin, N. J. & Smith, G. C. (2004) Identification and characterization of a novel and specific inhibitor of the ataxia-telangiectasia mutated kinase ATM. *Cancer Res*, 64, 9152-9.
- Higaki, Y., Mikami, T., Fujii, N., Hirshman, M. F., Koyama, K., Seino, T., Tanaka, K. & Goodyear, L. J. (2008) Oxidative stress stimulates skeletal muscle glucose uptake through a phosphatidylinositol 3-kinase-dependent pathway. *Am J Physiol Endocrinol Metab*, 294, E889-97.
- Hogan, A., Heyner, S., Charron, M. J., Copeland, N. G., Gilbert, D. J., Jenkins, N. A., Thorens, B. & Schultz, G. A. (1991) Glucose transporter gene expression in early mouse embryos. *Development*, 113, 363-72.
- Holman, G. D., Kozka, I. J., Clark, A. E., Flower, C. J., Saltis, J., Habberfield, A. D., Simpson, I. A. & Cushman, S. W. (1990) Cell surface labeling of glucose transporter isoform GLUT4 by bis-mannose photolabel. Correlation with stimulation of glucose transport in rat adipose cells by insulin and phorbol ester. *J Biol Chem*, 265, 18172-9.
- Hou, B. H., Takanaga, H., Grossmann, G., Chen, L. Q., Qu, X. Q., Jones, A. M., Lalonde, S., Schweissgut, O., Wiechert, W. & Frommer, W. B. (2011) Optical sensors for monitoring dynamic changes of intracellular metabolite levels in mammalian cells. *Nat Protoc*, 6, 1818-33.
- Huber, H. J., Dussmann, H., Kilbride, S. M., Rehm, M. & Prehn, J. H. (2011) Glucose metabolism determines resistance of cancer cells to bioenergetic crisis after cytochrome-c release. *Mol Syst Biol*, 7, 470.
- Hunte, C., Zickermann, V. & Brandt, U. (2010) Functional modules and structural basis of conformational coupling in mitochondrial complex I. *Science*, 329, 448-51.
- Huppertz, C., Fischer, B. M., Kim, Y. B., Kotani, K., Vidal-Puig, A., Sliker, L. J., Sloop, K. W., Lowell, B. B. & Kahn, B. B. (2001) Uncoupling protein 3 (UCP3) stimulates glucose uptake in muscle cells through a phosphoinositide 3-kinase-dependent mechanism. *J Biol Chem*, 276, 12520-9.
- Hurd, T. R., Requejo, R., Filipovska, A., Brown, S., Prime, T. A., Robinson, A. J., Fearnley, I. M. & Murphy, M. P. (2008) Complex I within oxidatively stressed bovine heart mitochondria is glutathionylated on Cys-531 and Cys-704 of the 75-kDa subunit: potential role of CYS residues in decreasing oxidative damage. *J Biol Chem*, 283, 24801-15.
- Hutter, E., Renner, K., Pfister, G., Stockl, P., Jansen-Durr, P. & Gnaiger, E. (2004) Senescence-associated changes in respiration and oxidative phosphorylation in primary human fibroblasts. *Biochem J*, 380, 919-28.
- Hwang, J., Suh, H. W., Jeon, Y. H., Hwang, E., Nguyen, L. T., Yeom, J., Lee, S. G., Lee, C., Kim, K. J., Kang, B. S., Jeong, J. O., Oh, T. K., Choi, I., Lee, J. O. & Kim, M. H. (2014) The structural basis for the negative regulation of thioredoxin by thioredoxin-interacting protein. *Nat Commun*, 5, 2958.
- Ido, Y. (2007) Pyridine nucleotide redox abnormalities in diabetes. *Antioxid Redox Signal*, 9, 931-42.
- Imamura, H., Nhat, K. P., Togawa, H., Saito, K., Iino, R., Kato-Yamada, Y., Nagai, T. & Noji, H. (2009) Visualization of ATP levels inside single living cells with fluorescence resonance energy transfer-based genetically encoded indicators. *Proc Natl Acad Sci U S A*, 106, 15651-6.
- Ishihara, H., Nakazaki, M., Kanegae, Y., Inukai, K., Asano, T., Katagiri, H., Yazaki, Y., Kikuchi, M., Miyazaki, J., Saito, I. & Oka, Y. (1996) Effect of mitochondrial and/or cytosolic glycerol 3-phosphate dehydrogenase overexpression on glucose-stimulated insulin secretion from MIN6 and HIT cells. *Diabetes*, 45, 1238-44.
- Iuso, A., Scacco, S., Piccoli, C., Bellomo, F., Petruzzella, V., Trentadue, R., Minuto, M., Ripoli, M., Capitanio, N., Zeviani, M. & Papa, S. (2006) Dysfunctions of cellular oxidative metabolism in

- patients with mutations in the NDUFS1 and NDUFS4 genes of complex I. *J Biol Chem*, 281, 10374-80.
- Ivan, M., Kondo, K., Yang, H., Kim, W., Valiando, J., Ohh, M., Salic, A., Asara, J. M., Lane, W. S. & Kaelin, W. G., Jr. (2001) HIF α targeted for VHL-mediated destruction by proline hydroxylation: implications for O₂ sensing. *Science*, 292, 464-8.
- Iyer, N. V., Kotch, L. E., Agani, F., Leung, S. W., Laughner, E., Wenger, R. H., Gassmann, M., Gearhart, J. D., Lawler, A. M., Yu, A. Y. & Semenza, G. L. (1998) Cellular and developmental control of O₂ homeostasis by hypoxia-inducible factor 1 α . *Genes Dev*, 12, 149-62.
- Janssen, A. J., Trijbels, F. J., Sengers, R. C., Wintjes, L. T., Ruitenbeek, W., Smeitink, J. A., Morava, E., Van Engelen, B. G., Van Den Heuvel, L. P. & Rodenburg, R. J. (2006) Measurement of the energy-generating capacity of human muscle mitochondria: diagnostic procedure and application to human pathology. *Clin Chem*, 52, 860-71.
- Jardetzky, O. (1966) Simple allosteric model for membrane pumps. *Nature*, 211, 969-70.
- Jensen, T. E., Schjerling, P., Viollet, B., Wojtaszewski, J. F. & Richter, E. A. (2008) AMPK α 1 activation is required for stimulation of glucose uptake by twitch contraction, but not by H₂O₂, in mouse skeletal muscle. *PLoS One*, 3, e2102.
- Jing, M., Cheruvu, V. K. & Ismail-Beigi, F. (2008) Stimulation of glucose transport in response to activation of distinct AMPK signaling pathways. *Am J Physiol Cell Physiol*, 295, C1071-82.
- Jing, M. & Ismail-Beigi, F. (2007) Critical role of 5'-AMP-activated protein kinase in the stimulation of glucose transport in response to inhibition of oxidative phosphorylation. *Am J Physiol Cell Physiol*, 292, C477-87.
- John, S. A., Ottolia, M., Weiss, J. N. & Ribalet, B. (2008) Dynamic modulation of intracellular glucose imaged in single cells using a FRET-based glucose nanosensor. *Pflugers Arch*, 456, 307-22.
- Johnson, S. C., Yanos, M. E., Kayser, E. B., Quintana, A., Sangesland, M., Castanza, A., Uhde, L., Hui, J., Wall, V. Z., Gagnidze, A., Oh, K., Wasko, B. M., Ramos, F. J., Palmiter, R. D., Rabinovitch, P. S., Morgan, P. G., Sedensky, M. M. & Kaeberlein, M. (2013) mTOR inhibition alleviates mitochondrial disease in a mouse model of Leigh syndrome. *Science*, 342, 1524-8.
- Jonckheere, A. I., Huigsloot, M., Janssen, A. J., Kappen, A. J., Smeitink, J. A. & Rodenburg, R. J. (2010) High-throughput assay to measure oxygen consumption in digitonin-permeabilized cells of patients with mitochondrial disorders. *Clin Chem*, 56, 424-31.
- Joost, H. G., Bell, G. I., Best, J. D., Birnbaum, M. J., Charron, M. J., Chen, Y. T., Doege, H., James, D. E., Lodish, H. F., Moley, K. H., Moley, J. F., Mueckler, M., Rogers, S., Schurmann, A., Seino, S. & Thorens, B. (2002) Nomenclature of the GLUT/SLC2A family of sugar/polyol transport facilitators. *Am J Physiol Endocrinol Metab*, 282, E974-6.
- Jose, C., Bellance, N. & Rossignol, R. (2011) Choosing between glycolysis and oxidative phosphorylation: a tumor's dilemma? *Biochim Biophys Acta*, 1807, 552-61.
- Jung, D. W., Ha, H. H., Zheng, X., Chang, Y. T. & Williams, D. R. (2011) Novel use of fluorescent glucose analogues to identify a new class of triazine-based insulin mimetics possessing useful secondary effects. *Mol Biosyst*, 7, 346-58.
- Jung, K. H., Lee, J. H., Thien Quach, C. H., Paik, J. Y., Oh, H., Park, J. W., Lee, E. J., Moon, S. H. & Lee, K. H. (2013) Resveratrol suppresses cancer cell glucose uptake by targeting reactive oxygen species-mediated hypoxia-inducible factor-1 α activation. *J Nucl Med*, 54, 2161-7.
- Jung, S. N., Yang, W. K., Kim, J., Kim, H. S., Kim, E. J., Yun, H., Park, H., Kim, S. S., Choe, W., Kang, I. & Ha, J. (2008) Reactive oxygen species stabilize hypoxia-inducible factor-1 α protein and stimulate transcriptional activity via AMP-activated protein kinase in DU145 human prostate cancer cells. *Carcinogenesis*, 29, 713-21.
- Kaimul, A. M., Nakamura, H., Masutani, H. & Yodoi, J. (2007) Thioredoxin and thioredoxin-binding protein-2 in cancer and metabolic syndrome. *Free Radic Biol Med*, 43, 861-8.

- Kakhlon, O. & Cabantchik, Z. I. (2002) The labile iron pool: characterization, measurement, and participation in cellular processes(1). *Free Radic Biol Med*, 33, 1037-46.
- Karamanlidis, G., Lee, C. F., Garcia-Menendez, L., Kolwicz, S. C., Jr., Suthammarak, W., Gong, G., Sedensky, M. M., Morgan, P. G., Wang, W. & Tian, R. (2013) Mitochondrial complex I deficiency increases protein acetylation and accelerates heart failure. *Cell Metab*, 18, 239-50.
- Kc, S., Carcamo, J. M. & Golde, D. W. (2005) Vitamin C enters mitochondria via facilitative glucose transporter 1 (Glut1) and confers mitochondrial protection against oxidative injury. *FASEB J*, 19, 1657-67.
- Kihira, Y., Yamano, N., Izawa-Ishizawa, Y., Ishizawa, K., Ikeda, Y., Tsuchiya, K., Tamaki, T. & Tomita, S. (2011) Basic fibroblast growth factor regulates glucose metabolism through glucose transporter 1 induced by hypoxia-inducible factor-1alpha in adipocytes. *Int J Biochem Cell Biol*, 43, 1602-11.
- Kim, J. S., Saengsirisuwan, V., Sloniger, J. A., Teachey, M. K. & Henriksen, E. J. (2006) Oxidant stress and skeletal muscle glucose transport: roles of insulin signaling and p38 MAPK. *Free Radic Biol Med*, 41, 818-24.
- Kletzien, R. F. & Perdue, J. F. (1973) The inhibition of sugar transport in chick embryo fibroblasts by cytochalasin B. Evidence for a membrane-specific effect. *J Biol Chem*, 248, 711-9.
- Koene, S., Rodenburg, R. J., Van Der Knaap, M. S., Willemsen, M. A., Sperl, W., Laugel, V., Ostergaard, E., Tarnopolsky, M., Martin, M. A., Nesbitt, V., Fletcher, J., Edvardson, S., Procaccio, V., Slama, A., Van Den Heuvel, L. P. & Smeitink, J. A. (2012) Natural disease course and genotype-phenotype correlations in Complex I deficiency caused by nuclear gene defects: what we learned from 130 cases. *J Inherit Metab Dis*, 35, 737-47.
- Kohn, A. D., Barthel, A., Kovacina, K. S., Boge, A., Wallach, B., Summers, S. A., Birnbaum, M. J., Scott, P. H., Lawrence, J. C., Jr. & Roth, R. A. (1998) Construction and characterization of a conditionally active version of the serine/threonine kinase Akt. *J Biol Chem*, 273, 11937-43.
- Koopman, W. J., Distelmaier, F., Smeitink, J. A. & Willems, P. H. (2013) OXPHOS mutations and neurodegeneration. *EMBO J*, 32, 9-29.
- Koopman, W. J., Nijtmans, L. G., Dieteren, C. E., Roestenberg, P., Valsecchi, F., Smeitink, J. A. & Willems, P. H. (2010) Mammalian mitochondrial complex I: biogenesis, regulation, and reactive oxygen species generation. *Antioxid Redox Signal*, 12, 1431-70.
- Koopman, W. J., Renders, M., Oosterhof, A., Van Kuppevelt, T. H., Van Engelen, B. G. & Willems, P. H. (2003) Upregulation of Ca²⁺ removal in human skeletal muscle: a possible role for Ca²⁺-dependent priming of mitochondrial ATP synthesis. *Am J Physiol Cell Physiol*, 285, C1263-9.
- Koopman, W. J., Verkaart, S., Visch, H. J., Van Emst-De Vries, S., Nijtmans, L. G., Smeitink, J. A. & Willems, P. H. (2007) Human NADH:ubiquinone oxidoreductase deficiency: radical changes in mitochondrial morphology? *Am J Physiol Cell Physiol*, 293, C22-9.
- Koopman, W. J., Visch, H. J., Verkaart, S., Van Den Heuvel, L. W., Smeitink, J. A. & Willems, P. H. (2005) Mitochondrial network complexity and pathological decrease in complex I activity are tightly correlated in isolated human complex I deficiency. *Am J Physiol Cell Physiol*, 289, C881-90.
- Koopman, W. J., Willems, P. H. & Smeitink, J. A. (2012) Monogenic mitochondrial disorders. *N Engl J Med*, 366, 1132-41.
- Koseoglu, M. H. & Beigi, F. I. (1999) Mechanism of stimulation of glucose transport in response to inhibition of oxidative phosphorylation: analysis with myc-tagged Glut1. *Mol Cell Biochem*, 194, 109-16.

- Kozlovsky, N., Rudich, A., Potashnik, R., Ebina, Y., Murakami, T. & Bashan, N. (1997) Transcriptional activation of the Glut1 gene in response to oxidative stress in L6 myotubes. *J Biol Chem*, 272, 33367-72.
- Kramer, H. F., Witczak, C. A., Fujii, N., Jessen, N., Taylor, E. B., Arnolds, D. E., Sakamoto, K., Hirshman, M. F. & Goodyear, L. J. (2006) Distinct signals regulate AS160 phosphorylation in response to insulin, AICAR, and contraction in mouse skeletal muscle. *Diabetes*, 55, 2067-76.
- Krumschnabel, G., Fontana-Ayoub, M., Sumbalova, Z., Heidler, J., Gauper, K., Fasching, M. & Gnaiger, E. (2015) Simultaneous high-resolution measurement of mitochondrial respiration and hydrogen peroxide production. *Methods Mol Biol*, 1264, 245-61.
- Krupka, R. M. & Deves, R. (1981) An experimental test for cyclic versus linear transport models. The mechanisms of glucose and choline transport in erythrocytes. *J Biol Chem*, 256, 5410-6.
- Kruse, S. E., Watt, W. C., Marcinek, D. J., Kapur, R. P., Schenkman, K. A. & Palmiter, R. D. (2008) Mice with mitochondrial complex I deficiency develop a fatal encephalomyopathy. *Cell Metab*, 7, 312-20.
- Kuipers, D. P., Scripture, J. P., Gunnink, S. M., Salie, M. J., Schotanus, M. P., Ubels, J. L. & Louters, L. L. (2013) Differential regulation of GLUT1 activity in human corneal limbal epithelial cells and fibroblasts. *Biochimie*, 95, 258-63.
- Kumar, B., Koul, S., Khandrika, L., Meacham, R. B. & Koul, H. K. (2008) Oxidative stress is inherent in prostate cancer cells and is required for aggressive phenotype. *Cancer Res*, 68, 1777-85.
- Kurz, E. U., Douglas, P. & Lees-Miller, S. P. (2004) Doxorubicin activates ATM-dependent phosphorylation of multiple downstream targets in part through the generation of reactive oxygen species. *J Biol Chem*, 279, 53272-81.
- Kussmaul, L. & Hirst, J. (2006) The mechanism of superoxide production by NADH:ubiquinone oxidoreductase (complex I) from bovine heart mitochondria. *Proc Natl Acad Sci U S A*, 103, 7607-12.
- Kuznetsov, A. V., Veksler, V., Gellerich, F. N., Saks, V., Margreiter, R. & Kunz, W. S. (2008) Analysis of mitochondrial function in situ in permeabilized muscle fibers, tissues and cells. *Nat Protoc*, 3, 965-76.
- Labarge, S., Migdal, C. & Schenk, S. (2015) Is acetylation a metabolic rheostat that regulates skeletal muscle insulin action? *Mol Cells*, 38, 297-303.
- Lakowicz, J. R. 2006. Principles of fluorescence spectroscopy. 3rd ed. New York: Springer.
- Lan, F., Cacicedo, J. M., Ruderman, N. & Ido, Y. (2008) SIRT1 modulation of the acetylation status, cytosolic localization, and activity of LKB1. Possible role in AMP-activated protein kinase activation. *J Biol Chem*, 283, 27628-35.
- Larance, M., Ramm, G., Stockli, J., Van Dam, E. M., Winata, S., Wasinger, V., Simpson, F., Graham, M., Junutula, J. R., Guilhaus, M. & James, D. E. (2005) Characterization of the role of the Rab GTPase-activating protein AS160 in insulin-regulated GLUT4 trafficking. *J Biol Chem*, 280, 37803-13.
- Lattanzi, G., Ognibene, A., Sabatelli, P., Capanni, C., Toniolo, D., Columbaro, M., Santi, S., Riccio, M., Merlini, L., Maraldi, N. M. & Squarzoni, S. (2000) Emerin expression at the early stages of myogenic differentiation. *Differentiation*, 66, 208-17.
- Lawson, M. A. & Purslow, P. P. (2000) Differentiation of myoblasts in serum-free media: effects of modified media are cell line-specific. *Cells Tissues Organs*, 167, 130-7.
- Le, A., Cooper, C. R., Gouw, A. M., Dinavahi, R., Maitra, A., Deck, L. M., Royer, R. E., Vander Jagt, D. L., Semenza, G. L. & Dang, C. V. (2010) Inhibition of lactate dehydrogenase A induces oxidative stress and inhibits tumor progression. *Proc Natl Acad Sci U S A*, 107, 2037-42.

- Le Goffe, C., Vallette, G., Charrier, L., Candelon, T., Bou-Hanna, C., Bouhours, J. F. & Laboissee, C. L. (2002) Metabolic control of resistance of human epithelial cells to H₂O₂ and NO stresses. *Biochem J*, 364, 349-59.
- Lee, E. E., Ma, J., Sacharidou, A., Mi, W., Salato, V. K., Nguyen, N., Jiang, Y., Pascual, J. M., North, P. E., Shaul, P. W., Mettlen, M. & Wang, R. C. (2015) A Protein Kinase C Phosphorylation Motif in GLUT1 Affects Glucose Transport and is Mutated in GLUT1 Deficiency Syndrome. *Mol Cell*, 58, 845-53.
- Leigh, D. (1951) Subacute necrotizing encephalomyelopathy in an infant. *J Neurol Neurosurg Psychiatry*, 14, 216-21.
- Leshinsky-Silver, E., Lebre, A. S., Minai, L., Saada, A., Steffann, J., Cohen, S., Rotig, A., Munnich, A., Lev, D. & Lerman-Sagie, T. (2009) NDUFS4 mutations cause Leigh syndrome with predominant brainstem involvement. *Mol Genet Metab*, 97, 185-9.
- Levine, K. B., Cloherty, E. K., Hamill, S. & Carruthers, A. (2002) Molecular determinants of sugar transport regulation by ATP. *Biochemistry*, 41, 12629-38.
- Li, L., Zhu, K., Liu, Y., Wu, X., Wu, J., Zhao, Y. & Zhao, J. (2015) Targeting thioredoxin-1 with siRNA exacerbates oxidative stress injury after cerebral ischemia/reperfusion in rats. *Neuroscience*, 284, 815-23.
- Lieb, W. R. & Stein, W. D. (1974) Testing and characterizing the simple carrier. *Biochim Biophys Acta*, 373, 178-96.
- Liemburg-Apers, D. C., Schirris, T. J. J., Russel, F. G. M., Willems, P. H. G. M. & Koopman, W. J. H. (2015a) Mitochondrial dysfunction triggers a rapid compensatory increase in steady-state glucose flux. *Biophysical Journal*.
- Liemburg-Apers, D. C., Willems, P. H., Koopman, W. J. & Grefte, S. (2015b) Interactions between mitochondrial reactive oxygen species and cellular glucose metabolism. *Arch Toxicol*, 89, 1209-26.
- Liochev, S. I. & Fridovich, I. (1994) The role of O₂⁻ in the production of HO₂·: in vitro and in vivo. *Free Radic Biol Med*, 16, 29-33.
- Liu, Q., Vera, J. C., Peng, H. & Golde, D. W. (2001) The predicted ATP-binding domains in the hexose transporter GLUT1 critically affect transporter activity. *Biochemistry*, 40, 7874-81.
- Liu, X., Chhipa, R. R., Nakano, I. & Dasgupta, B. (2014) The AMPK inhibitor compound C is a potent AMPK-independent antiangiogenic agent. *Mol Cancer Ther*, 13, 596-605.
- Loeffen, J. L., Smeitink, J. A., Trijbels, J. M., Janssen, A. J., Triepels, R. H., Sengers, R. C. & Van Den Heuvel, L. P. (2000) Isolated complex I deficiency in children: clinical, biochemical and genetic aspects. *Hum Mutat*, 15, 123-34.
- Lowe, A. G. & Walmsley, A. R. (1986) The kinetics of glucose transport in human red blood cells. *Biochim Biophys Acta*, 857, 146-54.
- Luiken, J. J., Coort, S. L., Koonen, D. P., Van Der Horst, D. J., Bonen, A., Zorzano, A. & Glatz, J. F. (2004) Regulation of cardiac long-chain fatty acid and glucose uptake by translocation of substrate transporters. *Pflugers Arch*, 448, 1-15.
- Lundby, A., Lage, K., Weinert, B. T., Bekker-Jensen, D. B., Secher, A., Skovgaard, T., Kelstrup, C. D., Dmytriiev, A., Choudhary, C., Lundby, C. & Olsen, J. V. (2012) Proteomic analysis of lysine acetylation sites in rat tissues reveals organ specificity and subcellular patterns. *Cell Rep*, 2, 419-31.
- Mailloux, R. J., Jin, X. & Willmore, W. G. (2014) Redox regulation of mitochondrial function with emphasis on cysteine oxidation reactions. *Redox Biol*, 2, 123-39.
- Mann, G. E., Yudilevich, D. L. & Sobrevia, L. (2003) Regulation of amino acid and glucose transporters in endothelial and smooth muscle cells. *Physiol Rev*, 83, 183-252.

- Mansfield, K. D., Guzy, R. D., Pan, Y., Young, R. M., Cash, T. P., Schumacker, P. T. & Simon, M. C. (2005) Mitochondrial dysfunction resulting from loss of cytochrome c impairs cellular oxygen sensing and hypoxic HIF- α activation. *Cell Metab*, 1, 393-9.
- Marette, A., Richardson, J. M., Ramlal, T., Balon, T. W., Vranic, M., Pessin, J. E. & Klip, A. (1992) Abundance, localization, and insulin-induced translocation of glucose transporters in red and white muscle. *Am J Physiol*, 263, C443-52.
- Marin-Hernandez, A., Gallardo-Perez, J. C., Rodriguez-Enriquez, S., Encalada, R., Moreno-Sanchez, R. & Saavedra, E. (2011) Modeling cancer glycolysis. *Biochim Biophys Acta*, 1807, 755-67.
- Martin, L. J. (2011) Mitochondrial pathobiology in ALS. *J Bioenerg Biomembr*, 43, 569-79.
- Martinez-Reyes, I. & Cuezva, J. M. (2014) The H(+)-ATP synthase: a gate to ROS-mediated cell death or cell survival. *Biochim Biophys Acta*, 1837, 1099-112.
- Mcmahon, R. J. & Frost, S. C. (1995) Nutrient control of GLUT1 processing and turnover in 3T3-L1 adipocytes. *J Biol Chem*, 270, 12094-9.
- Meglasson, M. D. & Matschinsky, F. M. (1983) Discrimination of glucose anomers by glucokinase from liver and transplantable insulinoma. *J Biol Chem*, 258, 6705-8.
- Mercado, C. L., Loeb, J. N. & Ismail-Beigi, F. (1989) Enhanced glucose transport in response to inhibition of respiration in Clone 9 cells. *Am J Physiol*, 257, C19-28.
- Merry, T. L., Steinberg, G. R., Lynch, G. S. & Mcconell, G. K. (2010) Skeletal muscle glucose uptake during contraction is regulated by nitric oxide and ROS independently of AMPK. *Am J Physiol Endocrinol Metab*, 298, E577-85.
- Mitchell, P. (1961) Coupling of phosphorylation to electron and hydrogen transfer by a chemi-osmotic type of mechanism. *Nature*, 191, 144-8.
- Mitsumoto, Y. & Klip, A. (1992) Development regulation of the subcellular distribution and glycosylation of GLUT1 and GLUT4 glucose transporters during myogenesis of L6 muscle cells. *J Biol Chem*, 267, 4957-62.
- Mookerjee, S. A., Goncalves, R. L., Gerencser, A. A., Nicholls, D. G. & Brand, M. D. (2015) The contributions of respiration and glycolysis to extracellular acid production. *Biochim Biophys Acta*, 1847, 171-81.
- Moran, M., Rivera, H., Sanchez-Arago, M., Blazquez, A., Merinero, B., Ugalde, C., Arenas, J., Cuezva, J. M. & Martin, M. A. (2010) Mitochondrial bioenergetics and dynamics interplay in complex I-deficient fibroblasts. *Biochim Biophys Acta*, 1802, 443-53.
- Morita, A., Tanimoto, K., Murakami, T., Morinaga, T. & Hosoi, Y. (2014) Mitochondria are required for ATM activation by extranuclear oxidative stress in cultured human hepatoblastoma cell line Hep G2 cells. *Biochem Biophys Res Commun*, 443, 1286-90.
- Moussa, R., Baierl, A., Steffen, V., Kubitzki, T., Wiechert, W. & Pohl, M. (2014) An evaluation of genetically encoded FRET-based biosensors for quantitative metabolite analyses in vivo. *J Biotechnol*, 191, 250-9.
- Mueckler, M., Caruso, C., Baldwin, S. A., Panico, M., Blench, I., Morris, H. R., Allard, W. J., Lienhard, G. E. & Lodish, H. F. (1985) Sequence and structure of a human glucose transporter. *Science*, 229, 941-5.
- Mungai, P. T., Waypa, G. B., Jairaman, A., Prakriya, M., Dokic, D., Ball, M. K. & Schumacker, P. T. (2011) Hypoxia triggers AMPK activation through reactive oxygen species-mediated activation of calcium release-activated calcium channels. *Mol Cell Biol*, 31, 3531-45.
- Murphy, M. P. (2009) How mitochondria produce reactive oxygen species. *Biochem J*, 417, 1-13.
- Murrant, C. L., Andrade, F. H. & Reid, M. B. (1999) Exogenous reactive oxygen and nitric oxide alter intracellular oxidant status of skeletal muscle fibres. *Acta Physiol Scand*, 166, 111-21.
- Naftalin, R. J. (2008) Alternating carrier models of asymmetric glucose transport violate the energy conservation laws. *Biophys J*, 95, 4300-14.

- Nagai, H., Noguchi, T., Takeda, K. & Ichijo, H. (2007) Pathophysiological roles of ASK1-MAP kinase signaling pathways. *J Biochem Mol Biol*, 40, 1-6.
- Nagai, T., Sawano, A., Park, E. S. & Miyawaki, A. (2001) Circularly permuted green fluorescent proteins engineered to sense Ca²⁺. *Proc Natl Acad Sci U S A*, 98, 3197-202.
- Ng, Y., Ramm, G., Lopez, J. A. & James, D. E. (2008) Rapid activation of Akt2 is sufficient to stimulate GLUT4 translocation in 3T3-L1 adipocytes. *Cell Metab*, 7, 348-56.
- Nicholls, D. G. (1977) The effective proton conductance of the inner membrane of mitochondria from brown adipose tissue. Dependency on proton electrochemical potential gradient. *Eur J Biochem*, 77, 349-56.
- Nishikawa, T., Edelstein, D., Du, X. L., Yamagishi, S., Matsumura, T., Kaneda, Y., Yorek, M. A., Beebe, D., Oates, P. J., Hammes, H. P., Giardino, I. & Brownlee, M. (2000) Normalizing mitochondrial superoxide production blocks three pathways of hyperglycaemic damage. *Nature*, 404, 787-90.
- Nishioka, T., Oda, Y., Seino, Y., Yamamoto, T., Inagaki, N., Yano, H., Imura, H., Shigemoto, R. & Kikuchi, H. (1992) Distribution of the glucose transporters in human brain tumors. *Cancer Res*, 52, 3972-9.
- Nishiyama, A., Matsui, M., Iwata, S., Hirota, K., Masutani, H., Nakamura, H., Takagi, Y., Sono, H., Gon, Y. & Yodoi, J. (1999) Identification of thioredoxin-binding protein-2/vitamin D(3) up-regulated protein 1 as a negative regulator of thioredoxin function and expression. *J Biol Chem*, 274, 21645-50.
- Niwa, K., Inanami, O., Yamamori, T., Ohta, T., Hamasu, T. & Kuwabara, M. (2003) Redox regulation of PI3K/Akt and p53 in bovine aortic endothelial cells exposed to hydrogen peroxide. *Antioxid Redox Signal*, 5, 713-22.
- Nooteboom, M., Forkink, M., Willems, P. H. G. M. & Koopman, W. J. H. (2012) Live-cell quantification of mitochondrial functional parameters. Humana Press Inc, USA.
- North, B. J., Marshall, B. L., Borra, M. T., Denu, J. M. & Verdin, E. (2003) The human Sir2 ortholog, SIRT2, is an NAD⁺-dependent tubulin deacetylase. *Mol Cell*, 11, 437-44.
- Nouws, J., Nijtmans, L. G., Smeitink, J. A. & Vogel, R. O. (2012) Assembly factors as a new class of disease genes for mitochondrial complex I deficiency: cause, pathology and treatment options. *Brain*, 135, 12-22.
- Okoh, V., Deoraj, A. & Roy, D. (2011) Estrogen-induced reactive oxygen species-mediated signalings contribute to breast cancer. *Biochim Biophys Acta*, 1815, 115-33.
- Okumoto, S., Takanaga, H. & Frommer, W. B. (2008) Quantitative imaging for discovery and assembly of the metabo-regulome. *New Phytol*, 180, 271-95.
- Otaegui, P. J., Ontiveros, M., Ferre, T., Riu, E., Jimenez, R. & Bosch, F. (2002) Glucose-regulated glucose uptake by transplanted muscle cells expressing glucokinase counteracts diabetic hyperglycemia. *Hum Gene Ther*, 13, 2125-33.
- Ouiddir, A., Planes, C., Fernandes, I., Vanhese, A. & Clerici, C. (1999) Hypoxia upregulates activity and expression of the glucose transporter GLUT1 in alveolar epithelial cells. *Am J Respir Cell Mol Biol*, 21, 710-8.
- Outeiro, T. F., Kontopoulos, E., Altmann, S. M., Kufareva, I., Strathearn, K. E., Amore, A. M., Volk, C. B., Maxwell, M. M., Rochet, J. C., Mclean, P. J., Young, A. B., Abagyan, R., Feany, M. B., Hyman, B. T. & Kazantsev, A. G. (2007) Sirtuin 2 inhibitors rescue alpha-synuclein-mediated toxicity in models of Parkinson's disease. *Science*, 317, 516-9.
- Ozkan, P. & Mutharasan, R. (2002) A rapid method for measuring intracellular pH using BCECF-AM. *Biochim Biophys Acta*, 1572, 143-8.
- Pacher, P., Schulz, R., Liaudet, L. & Szabo, C. (2005) Nitrosative stress and pharmacological modulation of heart failure. *Trends Pharmacol Sci*, 26, 302-10.

- Palmada, M., Boehmer, C., Akel, A., Rajamanickam, J., Jeyaraj, S., Keller, K. & Lang, F. (2006) SGK1 kinase upregulates GLUT1 activity and plasma membrane expression. *Diabetes*, 55, 421-7.
- Papa, S., Scacco, S., De Rasmio, D., Signorile, A., Papa, F., Panelli, D., Nicastro, A., Scaringi, R., Santeramo, A., Roca, E., Trentadue, R. & Larizza, M. (2010) cAMP-dependent protein kinase regulates post-translational processing and expression of complex I subunits in mammalian cells. *Biochim Biophys Acta*, 1797, 649-58.
- Patergnani, S., Baldassari, F., De Marchi, E., Karkucinska-Wieckowska, A., Wieckowski, M. R. & Pinton, P. (2014) Methods to monitor and compare mitochondrial and glycolytic ATP production. *Methods Enzymol*, 542, 313-32.
- Patti, M. E. & Corvera, S. (2010) The role of mitochondria in the pathogenesis of type 2 diabetes. *Endocr Rev*, 31, 364-95.
- Peeters, E. A., Bouten, C. V., Oomens, C. W., Bader, D. L., Snoeckx, L. H. & Baaijens, F. P. (2004) Anisotropic, three-dimensional deformation of single attached cells under compression. *Ann Biomed Eng*, 32, 1443-52.
- Petruzzella, V. & Papa, S. (2002) Mutations in human nuclear genes encoding for subunits of mitochondrial respiratory complex I: the NDUFS4 gene. *Gene*, 286, 149-54.
- Petruzzella, V., Vergari, R., Puziferri, I., Boffoli, D., Lamantea, E., Zeviani, M. & Papa, S. (2001) A nonsense mutation in the NDUFS4 gene encoding the 18 kDa (AQDQ) subunit of complex I abolishes assembly and activity of the complex in a patient with Leigh-like syndrome. *Hum Mol Genet*, 10, 529-35.
- Peus, D., Meves, A., Pott, M., Beyerle, A. & Pittelkow, M. R. (2001) Vitamin E analog modulates UVB-induced signaling pathway activation and enhances cell survival. *Free Radic Biol Med*, 30, 425-32.
- Philp, A., Rowland, T., Perez-Schindler, J. & Schenk, S. (2014) Understanding the acetylome: translating targeted proteomics into meaningful physiology. *Am J Physiol Cell Physiol*, 307, C763-73.
- Pi, J. & Collins, S. (2010) Reactive oxygen species and uncoupling protein 2 in pancreatic beta-cell function. *Diabetes Obes Metab*, 12 Suppl 2, 141-8.
- Pinheiro, C. H., Silveira, L. R., Nachbar, R. T., Vitzel, K. F. & Curi, R. (2010) Regulation of glycolysis and expression of glucose metabolism-related genes by reactive oxygen species in contracting skeletal muscle cells. *Free Radic Biol Med*, 48, 953-60.
- Pitkanen, S. & Robinson, B. H. (1996) Mitochondrial complex I deficiency leads to increased production of superoxide radicals and induction of superoxide dismutase. *J Clin Invest*, 98, 345-51.
- Porteous, W. K., James, A. M., Sheard, P. W., Porteous, C. M., Packer, M. A., Hyslop, S. J., Melton, J. V., Pang, C. Y., Wei, Y. H. & Murphy, M. P. (1998) Bioenergetic consequences of accumulating the common 4977-bp mitochondrial DNA deletion. *Eur J Biochem*, 257, 192-201.
- Poulose, N. & Raju, R. (2015) Sirtuin regulation in aging and injury. *Biochim Biophys Acta*, 1852, 2442-55.
- Prasad, R. K. & Ismail-Beigi, F. (1999) Mechanism of stimulation of glucose transport by H₂O₂: role of phospholipase C. *Arch Biochem Biophys*, 362, 113-22.
- Prata, C., Maraldi, T., Fiorentini, D., Zambonin, L., Hakim, G. & Landi, L. (2008) Nox-generated ROS modulate glucose uptake in a leukaemic cell line. *Free Radic Res*, 42, 405-14.
- Purich, D. L. & Fromm, H. J. (1971) The kinetics and regulation of rat brain hexokinase. *J Biol Chem*, 246, 3456-63.
- Quintana, A., Kruse, S. E., Kapur, R. P., Sanz, E. & Palmiter, R. D. (2010) Complex I deficiency due to loss of Ndufs4 in the brain results in progressive encephalopathy resembling Leigh syndrome. *Proc Natl Acad Sci U S A*, 107, 10996-1001.

- Rahman, S., Blok, R. B., Dahl, H. H., Danks, D. M., Kirby, D. M., Chow, C. W., Christodoulou, J. & Thorburn, D. R. (1996) Leigh syndrome: clinical features and biochemical and DNA abnormalities. *Ann Neurol*, 39, 343-51.
- Ramakrishnan, G., Davaakhuu, G., Kaplun, L., Chung, W. C., Rana, A., Atfi, A., Miele, L. & Tzivion, G. (2014) Sirt2 deacetylase is a novel AKT binding partner critical for AKT activation by insulin. *J Biol Chem*, 289, 6054-66.
- Rauh, D., Fischer, F., Gertz, M., Lakshminarasimhan, M., Bergbrede, T., Aladini, F., Kambach, C., Becker, C. F., Zerweck, J., Schutkowski, M. & Steegborn, C. (2013) An acetylome peptide microarray reveals specificities and deacetylation substrates for all human sirtuin isoforms. *Nat Commun*, 4, 2327.
- Reitzer, L. J., Wice, B. M. & Kennell, D. (1979) Evidence that glutamine, not sugar, is the major energy source for cultured HeLa cells. *J Biol Chem*, 254, 2669-76.
- Rich, P. R. (2003) The molecular machinery of Keilin's respiratory chain. *Biochem Soc Trans*, 31, 1095-105.
- Ritov, V. B., Menshikova, E. V., Azuma, K., Wood, R., Toledo, F. G., Goodpaster, B. H., Ruderman, N. B. & Kelley, D. E. (2010) Deficiency of electron transport chain in human skeletal muscle mitochondria in type 2 diabetes mellitus and obesity. *Am J Physiol Endocrinol Metab*, 298, E49-58.
- Robinson, B. H. (2006) Lactic acidemia and mitochondrial disease. *Mol Genet Metab*, 89, 3-13.
- Rossignol, R., Faustin, B., Rocher, C., Malgat, M., Mazat, J. P. & Letellier, T. (2003) Mitochondrial threshold effects. *Biochem J*, 370, 751-62.
- Rossignol, R., Letellier, T., Malgat, M., Rocher, C. & Mazat, J. P. (2000) Tissue variation in the control of oxidative phosphorylation: implication for mitochondrial diseases. *Biochem J*, 347 Pt 1, 45-53.
- Rossignol, R., Malgat, M., Mazat, J. P. & Letellier, T. (1999) Threshold effect and tissue specificity. Implication for mitochondrial cytopathies. *J Biol Chem*, 274, 33426-32.
- Rumsey, S. C., Kwon, O., Xu, G. W., Burant, C. F., Simpson, I. & Levine, M. (1997) Glucose transporter isoforms GLUT1 and GLUT3 transport dehydroascorbic acid. *J Biol Chem*, 272, 18982-9.
- Rungaldier, S., Oberwagner, W., Salzer, U., Csaszar, E. & Prohaska, R. (2013) Stomatin interacts with GLUT1/SLC2A1, band 3/SLC4A1, and aquaporin-1 in human erythrocyte membrane domains. *Biochim Biophys Acta*, 1828, 956-66.
- Rydstrom, J. (2006) Mitochondrial NADPH, transhydrogenase and disease. *Biochim Biophys Acta*, 1757, 721-6.
- Sabens Liedhegner, E. A., Gao, X. H. & Mieyal, J. J. (2012) Mechanisms of altered redox regulation in neurodegenerative diseases--focus on S--glutathionylation. *Antioxid Redox Signal*, 16, 543-66.
- Saleem, A., Safdar, A., Kitaoka, Y., Ma, X., Marquez, O. S., Akhtar, M., Nazli, A., Suri, R., Turnbull, J. & Tarnopolsky, M. A. (2015) Polymerase gamma mutator mice rely on increased glycolytic flux for energy production. *Mitochondrion*, 21C, 19-26.
- Salvi, M., Battaglia, V., Brunati, A. M., La Rocca, N., Tibaldi, E., Pietrangeli, P., Marocci, L., Mondovi, B., Rossi, C. A. & Toninello, A. (2007) Catalase takes part in rat liver mitochondria oxidative stress defense. *J Biol Chem*, 282, 24407-15.
- San Martin, A., Ceballo, S., Baeza-Lehnert, F., Lerchundi, R., Valdebenito, R., Contreras-Baeza, Y., Alegria, K. & Barros, L. F. (2014) Imaging mitochondrial flux in single cells with a FRET sensor for pyruvate. *PLoS One*, 9, e85780.
- San Martin, A., Ceballo, S., Ruminot, I., Lerchundi, R., Frommer, W. B. & Barros, L. F. (2013) A genetically encoded FRET lactate sensor and its use to detect the Warburg effect in single cancer cells. *PLoS One*, 8, e57712.

- Sanchez-Gomez, F. J., Espinosa-Diez, C., Dubey, M., Dikshit, M. & Lamas, S. (2013) S-glutathionylation: relevance in diabetes and potential role as a biomarker. *Biol Chem*, 394, 1263-80.
- Sanders, M. J., Grondin, P. O., Hegarty, B. D., Snowden, M. A. & Carling, D. (2007) Investigating the mechanism for AMP activation of the AMP-activated protein kinase cascade. *Biochem J*, 403, 139-48.
- Sandstrom, M. E., Zhang, S. J., Bruton, J., Silva, J. P., Reid, M. B., Westerblad, H. & Katz, A. (2006) Role of reactive oxygen species in contraction-mediated glucose transport in mouse skeletal muscle. *J Physiol*, 575, 251-62.
- Sanjuan-Pla, A., Cervera, A. M., Apostolova, N., Garcia-Bou, R., Victor, V. M., Murphy, M. P. & Mccreath, K. J. (2005) A targeted antioxidant reveals the importance of mitochondrial reactive oxygen species in the hypoxic signaling of HIF-1alpha. *FEBS Lett*, 579, 2669-74.
- Sano, H., Kane, S., Sano, E., Miinea, C. P., Asara, J. M., Lane, W. S., Garner, C. W. & Lienhard, G. E. (2003) Insulin-stimulated phosphorylation of a Rab GTPase-activating protein regulates GLUT4 translocation. *J Biol Chem*, 278, 14599-602.
- Scacco, S., Petruzzella, V., Budde, S., Vergari, R., Tamborra, R., Panelli, D., Van Den Heuvel, L. P., Smeitink, J. A. & Papa, S. (2003) Pathological mutations of the human NDUFS4 gene of the 18-kDa (AQDQ) subunit of complex I affect the expression of the protein and the assembly and function of the complex. *J Biol Chem*, 278, 44161-7.
- Schirris, T. J., Renkema, G. H., Ritschel, T., Voermans, N. C., Bilos, A., Van Engelen, B. G., Brandt, U., Koopman, W. J., Beyrath, J. D., Rodenburg, R. J., Willems, P. H., Smeitink, J. A. & Russel, F. G. (2015) Statin-Induced Myopathy Is Associated with Mitochondrial Complex III Inhibition. *Cell Metab*, 22, 399-407.
- Schockel, L., Glasauer, A., Basit, F., Bitschar, K., Truong, H., Erdmann, G., Algire, C., Hagebarth, A., Willems, P. H., Kopitz, C., Koopman, W. J. & Heroult, M. (2015) Targeting mitochondrial complex I using BAY 87-2243 reduces melanoma tumor growth. *Cancer Metab*, 3, 11.
- Schroedl, C., McClintock, D. S., Budinger, G. R. & Chandel, N. S. (2002) Hypoxic but not anoxic stabilization of HIF-1alpha requires mitochondrial reactive oxygen species. *Am J Physiol Lung Cell Mol Physiol*, 283, L922-31.
- Schulze, P. C., Yoshioka, J., Takahashi, T., He, Z., King, G. L. & Lee, R. T. (2004) Hyperglycemia promotes oxidative stress through inhibition of thioredoxin function by thioredoxin-interacting protein. *J Biol Chem*, 279, 30369-74.
- Shaw, R. J., Kosmatka, M., Bardeesy, N., Hurley, R. L., Witters, L. A., Depinho, R. A. & Cantley, L. C. (2004) The tumor suppressor LKB1 kinase directly activates AMP-activated kinase and regulates apoptosis in response to energy stress. *Proc Natl Acad Sci U S A*, 101, 3329-35.
- Shetty, M., Loeb, J. N., Vikstrom, K. & Ismail-Beigi, F. (1993) Rapid activation of GLUT-1 glucose transporter following inhibition of oxidative phosphorylation in clone 9 cells. *J Biol Chem*, 268, 17225-32.
- Shi, Y., Liu, H., Vanderburg, G., Samuel, S. J., Ismail-Beigi, F. & Jung, C. Y. (1995) Modulation of GLUT1 intrinsic activity in clone 9 cells by inhibition of oxidative phosphorylation. *J Biol Chem*, 270, 21772-8.
- Skladal, D., Halliday, J. & Thorburn, D. R. (2003) Minimum birth prevalence of mitochondrial respiratory chain disorders in children. *Brain*, 126, 1905-12.
- Slomka, N. & Gefen, A. (2011) Cell-to-cell variability in deformations across compressed myoblasts. *J Biomech Eng*, 133, 081007.
- Smeitink, J. & Van Den Heuvel, L. (1999) Human mitochondrial complex I in health and disease. *Am J Hum Genet*, 64, 1505-10.

- Smeitink, J., Van Den Heuvel, L. & Dimauro, S. (2001) The genetics and pathology of oxidative phosphorylation. *Nat Rev Genet*, 2, 342-52.
- Smeitink, J. A., Loeffen, J. L., Triepels, R. H., Smeets, R. J., Trijbels, J. M. & Van Den Heuvel, L. P. (1998) Nuclear genes of human complex I of the mitochondrial electron transport chain: state of the art. *Hum Mol Genet*, 7, 1573-9.
- Sogin, D. C. & Hinkle, P. C. (1978) Characterization of the glucose transporter from human erythrocytes. *J Supramol Struct*, 8, 447-53.
- Stoltzman, C. A., Peterson, C. W., Breen, K. T., Muoio, D. M., Billin, A. N. & Ayer, D. E. (2008) Glucose sensing by MondoA:MLX complexes: a role for hexokinases and direct regulation of thioredoxin-interacting protein expression. *Proc Natl Acad Sci U S A*, 105, 6912-7.
- Suhane, S., Kanzaki, H., Arumugaswami, V., Murali, R. & Ramanujan, V. K. (2013) Mitochondrial NDUFS3 regulates the ROS-mediated onset of metabolic switch in transformed cells. *Biol Open*, 2, 295-305.
- Sun, Y., Connors, K. E. & Yang, D. Q. (2007) AICAR induces phosphorylation of AMPK in an ATM-dependent, LKB1-independent manner. *Mol Cell Biochem*, 306, 239-45.
- Sundaresan, N. R., Pillai, V. B., Wolfgeher, D., Samant, S., Vasudevan, P., Parekh, V., Raghuraman, H., Cunningham, J. M., Gupta, M. & Gupta, M. P. (2011) The deacetylase SIRT1 promotes membrane localization and activation of Akt and PDK1 during tumorigenesis and cardiac hypertrophy. *Sci Signal*, 4, ra46.
- Swerdlow, R. H. (2012) Mitochondria and cell bioenergetics: increasingly recognized components and a possible etiologic cause of Alzheimer's disease. *Antioxid Redox Signal*, 16, 1434-55.
- Szablewski, L. (2013) Expression of glucose transporters in cancers. *Biochim Biophys Acta*, 1835, 164-9.
- Takanaga, H., Chaudhuri, B. & Frommer, W. B. (2008) GLUT1 and GLUT9 as major contributors to glucose influx in HepG2 cells identified by a high sensitivity intramolecular FRET glucose sensor. *Biochim Biophys Acta*, 1778, 1091-9.
- Takanaga, H. & Frommer, W. B. (2010) Facilitative plasma membrane transporters function during ER transit. *FASEB J*, 24, 2849-58.
- Talior, I., Yarkoni, M., Bashan, N. & Eldar-Finkelman, H. (2003) Increased glucose uptake promotes oxidative stress and PKC-delta activation in adipocytes of obese, insulin-resistant mice. *Am J Physiol Endocrinol Metab*, 285, E295-302.
- Taylor, E. B., An, D., Kramer, H. F., Yu, H., Fujii, N. L., Roeckl, K. S., Bowles, N., Hirshman, M. F., Xie, J., Feener, E. P. & Goodyear, L. J. (2008) Discovery of TBC1D1 as an insulin-, AICAR-, and contraction-stimulated signaling nexus in mouse skeletal muscle. *J Biol Chem*, 283, 9787-96.
- Thong, F. S., Bilan, P. J. & Klip, A. (2007) The Rab GTPase-activating protein AS160 integrates Akt, protein kinase C, and AMP-activated protein kinase signals regulating GLUT4 traffic. *Diabetes*, 56, 414-23.
- Thorburn, D. R. (2004) Mitochondrial disorders: prevalence, myths and advances. *J Inherit Metab Dis*, 27, 349-62.
- Thorens, B., Flier, J. S., Lodish, H. F. & Kahn, B. B. (1990) Differential regulation of two glucose transporters in rat liver by fasting and refeeding and by diabetes and insulin treatment. *Diabetes*, 39, 712-9.
- Toyoda, T., Hayashi, T., Miyamoto, L., Yonemitsu, S., Nakano, M., Tanaka, S., Ebihara, K., Masuzaki, H., Hosoda, K., Inoue, G., Otaka, A., Sato, K., Fushiki, T. & Nakao, K. (2004) Possible involvement of the alpha1 isoform of 5'AMP-activated protein kinase in oxidative stress-stimulated glucose transport in skeletal muscle. *Am J Physiol Endocrinol Metab*, 287, E166-73.

- Tsuboi, T., Lippiat, J. D., Ashcroft, F. M. & Rutter, G. A. (2004) ATP-dependent interaction of the cytosolic domains of the inwardly rectifying K⁺ channel Kir6.2 revealed by fluorescence resonance energy transfer. *Proc Natl Acad Sci U S A*, 101, 76-81.
- Turrens, J. F., Alexandre, A. & Lehninger, A. L. (1985) Ubisemiquinone is the electron donor for superoxide formation by complex III of heart mitochondria. *Arch Biochem Biophys*, 237, 408-14.
- Tyler, D. D. (1975) A protective function of superoxide dismutase during respiratory chain activity. *Biochim Biophys Acta*, 396, 335-46.
- Ugalde, C., Janssen, R. J., Van Den Heuvel, L. P., Smeitink, J. A. & Nijtmans, L. G. (2004) Differences in assembly or stability of complex I and other mitochondrial OXPHOS complexes in inherited complex I deficiency. *Hum Mol Genet*, 13, 659-67.
- Ulanovskaya, O. A., Cui, J., Kron, S. J. & Kozmin, S. A. (2011) A pairwise chemical genetic screen identifies new inhibitors of glucose transport. *Chem Biol*, 18, 222-30.
- Valko, M., Rhodes, C. J., Moncol, J., Izakovic, M. & Mazur, M. (2006) Free radicals, metals and antioxidants in oxidative stress-induced cancer. *Chem Biol Interact*, 160, 1-40.
- Valsecchi, F., Grefte, S., Roestenberg, P., Joosten-Wagenaars, J., Smeitink, J. A., Willems, P. H. & Koopman, W. J. (2013) Primary fibroblasts of NDUFS4(-/-) mice display increased ROS levels and aberrant mitochondrial morphology. *Mitochondrion*, 13, 436-43.
- Valsecchi, F., Monge, C., Forkink, M., De Groof, A. J., Benard, G., Rossignol, R., Swarts, H. G., Van Emst-De Vries, S. E., Rodenburg, R. J., Calvaruso, M. A., Nijtmans, L. G., Heeman, B., Roestenberg, P., Wieringa, B., Smeitink, J. A., Koopman, W. J. & Willems, P. H. (2012) Metabolic consequences of NDUFS4 gene deletion in immortalized mouse embryonic fibroblasts. *Biochim Biophys Acta*, 1817, 1925-36.
- Van Den Heuvel, L., Ruitenbeek, W., Smeets, R., Gelman-Kohan, Z., Elpeleg, O., Loeffen, J., Trijbels, F., Mariman, E., De Bruijn, D. & Smeitink, J. (1998) Demonstration of a new pathogenic mutation in human complex I deficiency: a 5-bp duplication in the nuclear gene encoding the 18-kD (AQDQ) subunit. *Am J Hum Genet*, 62, 262-8.
- Van Den Heuvel, L. & Smeitink, J. (2001) The oxidative phosphorylation (OXPHOS) system: nuclear genes and human genetic diseases. *Bioessays*, 23, 518-25.
- Van Der Westhuizen, F. H., Van Den Heuvel, L. P., Smeets, R., Veltman, J. A., Pfundt, R., Van Kessel, A. G., Ursing, B. M. & Smeitink, J. A. (2003) Human mitochondrial complex I deficiency: investigating transcriptional responses by microarray. *Neuropediatrics*, 34, 14-22.
- Van Eunen, K., Rossell, S., Bouwman, J., Westerhoff, H. V. & Bakker, B. M. (2011) Quantitative analysis of flux regulation through hierarchical regulation analysis. *Methods Enzymol*, 500, 571-95.
- Vatrinet, R., Iommarini, L., Kurelac, I., De Luise, M., Gasparre, G. & Porcelli, A. M. (2015) Targeting respiratory complex I to prevent the Warburg effect. *Int J Biochem Cell Biol*, 63, 41-5.
- Verkaart, S., Koopman, W. J., Cheek, J., Van Emst-De Vries, S. E., Van Den Heuvel, L. W., Smeitink, J. A. & Willems, P. H. (2007a) Mitochondrial and cytosolic thiol redox state are not detectably altered in isolated human NADH:ubiquinone oxidoreductase deficiency. *Biochim Biophys Acta*, 1772, 1041-51.
- Verkaart, S., Koopman, W. J., Van Emst-De Vries, S. E., Nijtmans, L. G., Van Den Heuvel, L. W., Smeitink, J. A. & Willems, P. H. (2007b) Superoxide production is inversely related to complex I activity in inherited complex I deficiency. *Biochim Biophys Acta*, 1772, 373-81.
- Vinals, F., Fandos, C., Santalucia, T., Ferre, J., Testar, X., Palacin, M. & Zorzano, A. (1997) Myogenesis and MyoD down-regulate Sp1. A mechanism for the repression of GLUT1 during muscle cell differentiation. *J Biol Chem*, 272, 12913-21.

- Visch, H. J., Koopman, W. J., Leusink, A., Van Emst-De Vries, S. E., Van Den Heuvel, L. W., Willems, P. H. & Smeitink, J. A. (2006a) Decreased agonist-stimulated mitochondrial ATP production caused by a pathological reduction in endoplasmic reticulum calcium content in human complex I deficiency. *Biochim Biophys Acta*, 1762, 115-23.
- Visch, H. J., Koopman, W. J., Zeegers, D., Van Emst-De Vries, S. E., Van Kuppeveld, F. J., Van Den Heuvel, L. W., Smeitink, J. A. & Willems, P. H. (2006b) Ca²⁺-mobilizing agonists increase mitochondrial ATP production to accelerate cytosolic Ca²⁺ removal: aberrations in human complex I deficiency. *Am J Physiol Cell Physiol*, 291, C308-16.
- Voets, A. M., Huigsloot, M., Lindsey, P. J., Leenders, A. M., Koopman, W. J., Willems, P. H., Rodenburg, R. J., Smeitink, J. A. & Smeets, H. J. (2012) Transcriptional changes in OXPHOS complex I deficiency are related to anti-oxidant pathways and could explain the disturbed calcium homeostasis. *Biochim Biophys Acta*, 1822, 1161-8.
- Vogt, J., Traynor, R. & Sapkota, G. P. (2011) The specificities of small molecule inhibitors of the TGF β s and BMP pathways. *Cell Signal*, 23, 1831-42.
- Vollers, S. S. & Carruthers, A. (2012) Sequence determinants of GLUT1-mediated accelerated-exchange transport: analysis by homology-scanning mutagenesis. *J Biol Chem*, 287, 42533-44.
- Walker, J. E. (1992) The NADH:ubiquinone oxidoreductase (complex I) of respiratory chains. *Q Rev Biophys*, 25, 253-324.
- Wallace, D. C. (1999) Mitochondrial diseases in man and mouse. *Science*, 283, 1482-8.
- Wallace, K. B. (2008) Mitochondrial off targets of drug therapy. *Trends Pharmacol Sci*, 29, 361-6.
- Wang, C. H., Wang, C. C., Huang, H. C. & Wei, Y. H. (2013) Mitochondrial dysfunction leads to impairment of insulin sensitivity and adiponectin secretion in adipocytes. *FEBS J*, 280, 1039-50.
- Weigand, K. M., Swarts, H. G., Fedosova, N. U., Russel, F. G. & Koenderink, J. B. (2012) Na,K-ATPase activity modulates Src activation: a role for ATP/ADP ratio. *Biochim Biophys Acta*, 1818, 1269-73.
- Weisiger, R. A. & Fridovich, I. (1973) Mitochondrial superoxide simutase. Site of synthesis and intramitochondrial localization. *J Biol Chem*, 248, 4793-6.
- Wheeler, T. J. (1988) Translocation of glucose transporters in response to anoxia in heart. *J Biol Chem*, 263, 19447-54.
- Wieman, H. L., Horn, S. R., Jacobs, S. R., Altman, B. J., Kornbluth, S. & Rathmell, J. C. (2009) An essential role for the Glut1 PDZ-binding motif in growth factor regulation of Glut1 degradation and trafficking. *Biochem J*, 418, 345-67.
- Wieman, H. L., Wofford, J. A. & Rathmell, J. C. (2007) Cytokine stimulation promotes glucose uptake via phosphatidylinositol-3 kinase/Akt regulation of Glut1 activity and trafficking. *Mol Biol Cell*, 18, 1437-46.
- Willems, P. H., Rossignol, R., Dieteren, C. E., Murphy, M. P. & Koopman, W. J. (2015) Redox Homeostasis and Mitochondrial Dynamics. *Cell Metab*, 22, 207-18.
- Willems, P. H., Valsecchi, F., Distelmaier, F., Verkaart, S., Visch, H. J., Smeitink, J. A. & Koopman, W. J. (2008) Mitochondrial Ca²⁺ homeostasis in human NADH:ubiquinone oxidoreductase deficiency. *Cell Calcium*, 44, 123-33.
- Willemse, M., Janssen, E., De Lange, F., Wieringa, B. & Fransen, J. (2007) ATP and FRET--a cautionary note. *Nat Biotechnol*, 25, 170-2.
- Wilson, J. E. (1995) Hexokinases. *Rev Physiol Biochem Pharmacol*, 126, 65-198.
- Wilson, J. E. (2003) Isozymes of mammalian hexokinase: structure, subcellular localization and metabolic function. *J Exp Biol*, 206, 2049-57.

- Wood, S. M., Wiesener, M. S., Yeates, K. M., Okada, N., Pugh, C. W., Maxwell, P. H. & Ratcliffe, P. J. (1998) Selection and analysis of a mutant cell line defective in the hypoxia-inducible factor-1 alpha-subunit (HIF-1alpha). Characterization of hif-1alpha-dependent and -independent hypoxia-inducible gene expression. *J Biol Chem*, 273, 8360-8.
- Woods, A., Johnstone, S. R., Dickerson, K., Leiper, F. C., Fryer, L. G., Neumann, D., Schlattner, U., Wallimann, T., Carlson, M. & Carling, D. (2003) LKB1 is the upstream kinase in the AMP-activated protein kinase cascade. *Curr Biol*, 13, 2004-8.
- Wretman, C., Lionikas, A., Widegren, U., Lannergren, J., Westerblad, H. & Henriksson, J. (2001) Effects of concentric and eccentric contractions on phosphorylation of MAPK(erk1/2) and MAPK(p38) in isolated rat skeletal muscle. *J Physiol*, 535, 155-64.
- Wu, F., Yang, F., Vinnakota, K. C. & Beard, D. A. (2007) Computer modeling of mitochondrial tricarboxylic acid cycle, oxidative phosphorylation, metabolite transport, and electrophysiology. *J Biol Chem*, 282, 24525-37.
- Wu, N., Zheng, B., Shaywitz, A., Dagon, Y., Tower, C., Bellinger, G., Shen, C. H., Wen, J., Asara, J., McGraw, T. E., Kahn, B. B. & Cantley, L. C. (2013) AMPK-dependent degradation of TXNIP upon energy stress leads to enhanced glucose uptake via GLUT1. *Mol Cell*, 49, 1167-75.
- Wu, S. B. & Wei, Y. H. (2012) AMPK-mediated increase of glycolysis as an adaptive response to oxidative stress in human cells: implication of the cell survival in mitochondrial diseases. *Biochim Biophys Acta*, 1822, 233-47.
- Wu, S. B., Wu, Y. T., Wu, T. P. & Wei, Y. H. (2014) Role of AMPK-mediated adaptive responses in human cells with mitochondrial dysfunction to oxidative stress. *Biochim Biophys Acta*, 1840, 1331-1344.
- Xie, Z., Dong, Y., Zhang, M., Cui, M. Z., Cohen, R. A., Riek, U., Neumann, D., Schlattner, U. & Zou, M. H. (2006) Activation of protein kinase C zeta by peroxynitrite regulates LKB1-dependent AMP-activated protein kinase in cultured endothelial cells. *J Biol Chem*, 281, 6366-75.
- Yin, F., Sancheti, H. & Cadenas, E. (2012) Silencing of nicotinamide nucleotide transhydrogenase impairs cellular redox homeostasis and energy metabolism in PC12 cells. *Biochim Biophys Acta*, 1817, 401-9.
- Ying, W. (2008) NAD⁺/NADH and NADP⁺/NADPH in cellular functions and cell death: regulation and biological consequences. *Antioxid Redox Signal*, 10, 179-206.
- Yoshino, J., Mills, K. F., Yoon, M. J. & Imai, S. (2011) Nicotinamide mononucleotide, a key NAD(+) intermediate, treats the pathophysiology of diet- and age-induced diabetes in mice. *Cell Metab*, 14, 528-36.
- Young, C. D., Lewis, A. S., Rudolph, M. C., Ruehle, M. D., Jackman, M. R., Yun, U. J., Ilkun, O., Pereira, R., Abel, E. D. & Anderson, S. M. (2011) Modulation of glucose transporter 1 (GLUT1) expression levels alters mouse mammary tumor cell growth in vitro and in vivo. *PLoS One*, 6, e23205.
- Yu, T., Jhun, B. S. & Yoon, Y. (2011) High-glucose stimulation increases reactive oxygen species production through the calcium and mitogen-activated protein kinase-mediated activation of mitochondrial fission. *Antioxid Redox Signal*, 14, 425-37.
- Yu, T., Robotham, J. L. & Yoon, Y. (2006) Increased production of reactive oxygen species in hyperglycemic conditions requires dynamic change of mitochondrial morphology. *Proc Natl Acad Sci U S A*, 103, 2653-8.
- Zala, D., Hinckelmann, M. V., Yu, H., Lyra Da Cunha, M. M., Liot, G., Cordelieres, F. P., Marco, S. & Saudou, F. (2013) Vesicular glycolysis provides on-board energy for fast axonal transport. *Cell*, 152, 479-91.
- Zhang, J. Z., Abbud, W., Prohaska, R. & Ismail-Beigi, F. (2001) Overexpression of stomatin depresses GLUT-1 glucose transporter activity. *Am J Physiol Cell Physiol*, 280, C1277-83.

- Zhang, X., Fryknas, M., Hernlund, E., Fayad, W., De Milito, A., Olofsson, M. H., Gogvadze, V., Dang, L., Pahlman, S., Schughart, L. A., Rickardson, L., D'arcy, P., Gullbo, J., Nygren, P., Larsson, R. & Linder, S. (2014) Induction of mitochondrial dysfunction as a strategy for targeting tumour cells in metabolically compromised microenvironments. *Nat Commun*, 5, 3295.
- Zhou, J., Deo, B. K., Hosoya, K., Terasaki, T., Obrosova, I. G., Brosius, F. C., 3rd & Kumagai, A. K. (2005) Increased JNK phosphorylation and oxidative stress in response to increased glucose flux through increased GLUT1 expression in rat retinal endothelial cells. *Invest Ophthalmol Vis Sci*, 46, 3403-10.
- Zmijewski, J. W., Banerjee, S., Bae, H., Friggeri, A., Lazarowski, E. R. & Abraham, E. (2010) Exposure to hydrogen peroxide induces oxidation and activation of AMP-activated protein kinase. *J Biol Chem*, 285, 33154-64.
- Zorov, D. B., Juhaszova, M. & Sollott, S. J. (2014) Mitochondrial reactive oxygen species (ROS) and ROS-induced ROS release. *Physiol Rev*, 94, 909-50.
- Zottola, R. J., Cloherty, E. K., Coderre, P. E., Hansen, A., Hebert, D. N. & Carruthers, A. (1995) Glucose transporter function is controlled by transporter oligomeric structure. A single, intramolecular disulfide promotes GLUT1 tetramerization. *Biochemistry*, 34, 9734-47.
- Zou, C., Wang, Y. & Shen, Z. (2005) 2-NBDG as a fluorescent indicator for direct glucose uptake measurement. *J Biochem Biophys Methods*, 64, 207-15.

Summary

Glucose is one of the major energy sources for our body. In the majority of cells glucose is taken up by glucose transporter (GLUT)-mediated facilitated diffusion. Inside the cell, glucose is used to produce ATP and pyruvate by the enzymes of the glycolytic pathway in the cytosol. Pyruvate is taken up by mitochondria where it is converted by pyruvate dehydrogenase (PDH) to acetyl-coenzyme A. The latter is oxidized by the tricarboxylic acid (TCA) cycle, yielding reduced electron carriers that serve as substrates for the oxidative phosphorylation (OXPHOS) system in the mitochondria to produce ATP. The OXPHOS system consists of five multi-subunit complexes (CI-CV) and produces the majority of total ATP. Mutations in one of the subunits of the OXPHOS system can cause mitochondrial dysfunction leading to a wide variety of pathological conditions. Currently there is no cure for patients suffering from a mitochondrial disorder and a better understanding of the metabolic consequences is required for the development of treatment strategies. One of the frequently observed adaptive responses to OXPHOS dysfunction is a switch to a more glycolytic mode of ATP production. This often requires an increase in the rate of glucose uptake and glycolysis. In this thesis, the role of glucose in OXPHOS-dysfunctional myoblasts was assessed.

Chapter 1 gives an introduction about GLUT-mediated glucose uptake and the modes of GLUT regulation. Furthermore, OXPHOS disorders and their effect on the production of reactive oxygen species (ROS) are presented. Finally, the interplay between ROS and glucose uptake is discussed.

Because the current methods for glucose uptake measurements are limited in their spatial and temporal resolution, we developed a new microscopy assay for live, single-cell, quantitative glucose uptake measurements. In this assay, a protein-based sensor was used to visualize the intracellular glucose concentration. In **Chapter 2**, different fluorescence resonance energy-transfer (FRET)-based glucose sensors are compared and their applications are discussed. In **Chapter 3**, the glucose sensor with the highest dynamic range was used to develop the glucose uptake assay and to determine the kinetic parameters of glucose uptake and consumption in C2C12 myoblasts. Using this assay we found that a short-term

inhibition of CI or CIII induced a significant increase in the V_{\max} of glucose uptake and consumption. The kinetic parameters of glucose uptake and consumption were used to construct a mathematical model, which predicted a 2-fold increase in the steady-state glucose flux under CI-/CIII-inhibited conditions. Combining model predictions and empirical evidence, we found that this compensatory increase in glycolytic flux was sufficient to compensate for the lack of mitochondrial ATP production in CI-/CIII-inhibited C2C12 myoblasts. However, the fold increase necessary to compensate for reduced mitochondrial ATP production might vary depending on the cell type, the basal glycolytic and mitochondrial flux values, the residual ATP production rate after OXPHOS inhibition, and the ATP demand. Importantly, the combined approach of kinetic modeling and experimental analysis presented in this chapter, provides a tool to determine the glycolytic flux rate, which can help to answer various research questions.

Opposed to the full chemical OXPHOS inhibition, patient cells usually display residual OXPHOS activity. Therefore, in **Chapter 4** the effect of OXPHOS-dysfunction on glucose uptake was studied in a primary myoblasts isolated from *Ndufs4* knockout (KO) mice, a genetic model of isolated CI-deficiency. It was found that the glycolytic phenotype of myoblasts cultured in proliferation medium could be reversed by switching to differentiating medium containing 5 mM glucose or galactose. Under these conditions, KO myoblasts displayed a higher rate of glucose uptake compared to wild-type. Interestingly, this increased rate of glucose uptake was not due to upregulation of Glut1 or Glut4.

Because of the limited availability of the primary KO myoblasts, the mode of regulation of Glut1-mediated glucose uptake was studied in CI-/CIII-inhibited C2C12 myoblasts in **Chapter 5**. For optimal comparison with the primary KO myoblasts, Glut1 upregulation was prevented by performing a short-term (30 min) inhibition of CI/CIII. It was found that while the amount of Glut1 at the plasma membrane remained the same, Glut1 activity was increased by a signaling cascade involving LKB1, AMPK, and Sirt2. Glut1 did not appear to be a direct target of Sirt2-mediated deacetylation, although Glut1 was found to be acetylated. The role of Sirt2 in the stimulation of Glut1 activity has not been described before and may provide a target for future research and possible treatment strategies.

Finally, **Chapter 6** integrates the findings from the studies in chapter 3, 4, and 5 and discusses these in a broader perspective. The biochemical consequences of enhanced glucose uptake, such as the production of ATP, lactate, and ROS are discussed. In addition, the physiological relevance of the regulation of Glut1 activity is assessed. In addition, the suitability of primary myoblasts derived from *Ndufs4* KO mice as a model for CI-dysfunction is discussed. In conclusion, in this thesis I gained insight into the interplay between OXPHOS-dysfunction and glucose uptake. These insights can be used in future research for the treatment of a wide variety of metabolic disorders.

Samenvatting

De enkelvoudige suiker glucose is een van de voornaamste energiebronnen voor ons lichaam. In de meeste lichaamscellen wordt glucose passief opgenomen met behulp van glucose transporters (GLUTs). Deze GLUTs faciliteren de glucose diffusie van buiten de cel (hogere glucose concentratie) naar binnen in de cel (lagere glucose concentratie). In de cel wordt de energie die is opgeslagen in de chemische verbindingen van glucose vrijgemaakt met behulp van de enzymen van 1) de glycolyse, 2) het pyruvaat dehydrogenase complex, 3) de citroenzuurcyclus en 4) het oxidatieve fosforylering systeem. De vrijgekomen energie wordt gebruikt om adenosine trifosfaat (ATP) te maken. ATP is de energie valuta van de cel. Het merendeel van de ATP wordt gemaakt door het oxidatieve fosforylering systeem. Dit systeem bestaat uit vijf grote eiwitcomplexen (complex I-V) die zich bevinden in het binnenste membraan van de mitochondriën, de energiefabrieken van de cel. Mutaties in een van deze eiwitcomplexen leidt tot mitochondriële dysfunctie en een breed scala aan klachten en symptomen. Tot op heden is er geen genezing mogelijk voor patiënten met een mitochondriële aandoening. Betere kennis over de cellulaire consequenties van mitochondriële aandoeningen kan bijdragen aan de ontwikkeling van medicijnen. Een van de veel voorkomende aanpassingsmechanismes van de cel, is de overgang naar een meer glycolytische manier van ATP productie. Dit vereist vaak een verhoging van de glucose opname en glycolyse snelheid. Dit proefschrift gaat over de rol die glucose speelt in spiercellen met een verminderde activiteit van het oxidatieve fosforylering systeem.

Hoofdstuk 1 geeft een introductie over GLUT gemedieerde glucose opname en de regulatie van GLUTs. Hierbij is vooral gefocust op GLUT1 omdat dit de enige glucose transporter is die voorkomt in de in dit onderzoek gebruikte spiercellen. Ook wordt mitochondriële dysfunctie en het effect hiervan op de productie van reactieve zuurstof moleculen besproken. Verder wordt de relatie tussen deze reactieve zuurstof moleculen en glucose opname bediscussieerd.

Omdat de huidige methoden voor glucose opname metingen gelimiteerd zijn in hun ruimtelijke- en tijdsresolutie, hebben we een nieuwe microscopie methode

ontwikkelt om glucose opname in levende cellen te kwantificeren. In dit protocol wordt gebruik gemaakt van een sensor om de glucose concentratie in de cel te kunnen visualiseren. In **hoofdstuk 2** worden verschillende glucosesensoren met elkaar vergeleken en de toepassingen worden besproken. Deze sensoren zijn eiwitten die glucose-binding rapporteren door middel van veranderingen in 'fluorescentie resonantie energie overdracht'. In **hoofdstuk 3** is de glucosesensor met het grootste dynamische bereik gebruikt voor de ontwikkeling van de glucose opname methode. Met behulp van deze methode zijn de kinetische parameters van glucose opname en consumptie bepaald in de spiercellijn C2C12. Hierbij is gevonden dat de maximale snelheid van glucose opname en consumptie significant toenam door remming van complex I of III. De gemeten kinetische parameters zijn gebruikt om een wiskundig model te bouwen. Dit model voorspelde een verdubbeling van de glucose snelheid (flux) in complex I of III geremde C2C12 spiercellen. Door voorspellingen en experimenten te combineren vonden we dat deze verdubbeling van de glucose flux voldoende was om te compenseren voor het gebrek aan mitochondriële ATP productie in complex I of III geremde C2C12 cellen. Hoeveel de glucose flux moet toenemen om te compenseren hangt echter af van het celtype, de basale glycolyse en mitochondriële snelheid, de ATP productie na mitochondriële remming en het ATP verbruik. Van belang is dat de glucose flux goed bepaald kan worden door de gecombineerde aanpak van modeleren en experimentele data. Deze aanpak kan helpen bij het beantwoorden van een breed scala aan biologische vraagstukken.

In tegenstelling tot (volledige) chemische remming van de oxidatieve fosforylering, hebben patiënten cellen meestal een restactiviteit. Daarom hebben we in **hoofdstuk 4** gebruikt gemaakt van een genetisch muismodel met complex I-deficiëntie. Deze muis mist het complex I-eiwit Ndufs4 en vertoont veel van de symptomen die patiënten ook vertonen. We hebben spiercellen uit deze muis geïsoleerd en gebruikt om het effect van complex I-deficiëntie op glucose opname te bestuderen. Het bleek dat de conditie waaronder deze spiercellen gekweekt werden van cruciaal belang was voor de balans tussen glycolyse en oxidatieve fosforylering. Om een zo groot mogelijk effect van complex I-deficiëntie te zien kozen we voor de conditie waarbij cellen voornamelijk afhankelijk zijn van oxidatieve fosforylering voor hun ATP productie. Onder deze conditie vonden we

dat de glucose opname snelheid significant hoger was in complex I-deficiënte spiercellen vergeleken met spiercellen van gezonde muizen. Opmerkelijk was dat deze verhoogde glucose opname snelheid niet kwam door een toename van het aantal glucose transporters dat tot expressie kwam.

Omdat de spiercellen uit de muis schaars waren, hebben we gekozen om de regulatie van glucose opname in de complex I geremde C2C12 cellijn te bestuderen in **hoofdstuk 5**. Om de glucose opname regulatie in de geremde cellijn zo goed mogelijk te kunnen vergelijken met de spiercellen uit de complex I-deficiënte muis was het van belang om te voorkomen dat de Glut expressie toenam. Dit hebben we voorkomen door te kiezen voor een korte (30 min) remming van complex I. We vonden dat de hoeveelheid beschikbare Glut1 op het celmembraan niet toenam door complex I-remming. De activiteit van Glut1 bleek echter wel toe te nemen en dit werd geïnduceerd door een signaleringscascade waar de eiwitten LKB1, AMPK en Sirt2 bij betrokken waren. Glut1 bleek geacetyleerd te zijn en omdat Sirt2 acetylgroepen van eiwitten kan verwijderen was de hypothese dat Sirt2 Glut1 deacetyleert door complex I-remming. Dit bleek echter niet het geval. Het lijkt erop dat er nog meer signaleringseiwitten betrokken zijn bij Glut1 activatie. Echter, de betrokkenheid van Sirt2 is een bevinding die nieuwe aanknopingspunten verschaft voor toekomstig onderzoek. Bovendien kan Sirt2 een nieuw doelwit zijn voor de ontwikkeling van medicijnen tegen een breed scala van metabole ziektes.

Uiteindelijk wordt in **hoofdstuk 6** de bevonden resultaten samengebracht en in een breder perspectief geplaatst. De biochemische consequenties van verhoogde glucose opname voor de cel worden besproken. Voorbeelden hiervan zijn de productie van ATP, lactaat en reactieve zuurstof moleculen. Ook wordt de fysiologische relevantie van de regulatie van Glut1 besproken. Verder wordt de geschiktheid van de spiercellen uit het complex I-deficiënte muismodel als een nieuw celmodel voor complex I-deficiëntie besproken. In dit proefschrift heb ik inzicht gekregen in de wisselwerking tussen een mitochondriële dysfunctie en glucose opname. Deze informatie kan gebruikt worden voor toekomstig onderzoek.

Dankwoord

Hier wil ik graag ALLE mensen bedanken die betrokken zijn geweest bij het tot stand komen van dit proefschrift en die mij hebben gesteund tijdens de weg ernaar toe. Zonder iemand tekort te doen wil ik graag een aantal mensen in het bijzonder bedanken.

Werner, als co-promotor en mijn directe begeleider maakte je altijd tijd voor mij vrij om data te bespreken en manuscripten door te lezen. We waren het niet altijd meteen met elkaar eens maar na lange en uitvoerige discussies bleek vaak dat onze ideeën niet zo ver van elkaar af lagen. Ik heb ontzettend veel van je geleerd en ben erg blij met alle hulp bij het tot stand komen van dit proefschrift. Bedankt voor alle inzet, tijd en moeite.

Peter, als co-promotor hielp je mij om prioriteiten te stellen en waakte je ervoor dat de gemaakte tijdsplanning behaald werd. Jij wist helderheid te brengen in bergen aan data en ideeën. Aan de andere kant hecht je ook veel aan een goede balans tussen werk en privé en was je altijd geïnteresseerd in mijn thuissituatie. Bedankt voor alle toewijding.

Jan Smeitink, als promotor en hoofd van het CSBB project, waar het onderzoek in dit proefschrift deel van uit maakt, hielp je mij het uiteindelijke doel voor ogen te houden. Tijdens mijn stage bij LKN liet je mij het belang van onderzoek voor mitochondriële patiënten zien, waardoor ik mijn keuze maakte voor dit promotieonderzoek. Ik wil je bedanken voor het vertrouwen in mij en het in goede banen leiden van het gehele CSBB project.

Roland Brock, als tweede promotor gaf je mij de mogelijkheid om gebruik te maken van het Biochemie lab en alle expertise en faciliteiten die daarbij horen. Tijdens mijn stage bij Biochemie van de Integratieve Systemen viel het me al op hoe goed georganiseerd dit lab is en dat zorgde er mede voor dat ik hier ook mijn promotieonderzoek wou doen. Bedankt voor de mogelijkheid om bij Biochemie mijn promotieonderzoek te kunnen uitvoeren.

Jori, ontzettend bedankt voor alle hulp met de vele experimenten, isolaties en transfecties. Zeker tegen het eind heb je me veel werk uit handen genomen ondanks dat het niet altijd meezat. Jouw inzet en talent om alles draaiend te houden is duidelijk merkbaar op het lab. Verder wil ik je ook bedanken voor alle gezelligheid op het lab en daarbuiten. Ik ben heel blij dat jij mijn paranimf wilt zijn.

Marleen, na samen gestudeerd te hebben in Enschede en Nijmegen hebben we op hetzelfde lab onze promotieonderzoeken gedaan. Jij was wat eerder begonnen waardoor je voor mij een voorbeeld was en ik geregeld bij je kwam aankloppen voor advies. Ook buiten het lab ben je een goede vriendin waar ik mee kan lachen maar ook veel steun aan heb. Bedankt voor alle goede adviezen, steun en gezelligheid. Ik ben heel blij dat jij mijn paranimf wil zijn.

Sander, jij was een luisterend oor wanneer alles tegen zat en ik het even niet meer zag zitten. Dankzij jouw nuchtere houding wist je alles te relativeren. Bedankt voor alle steun maar ook alle gezelligheid op het lab en daarbuiten. Ook wil ik je bedanken voor de samenwerking aan het Archives of Toxicology review en Ndufs4 KO myoblasten paper.

Marco, toen ik mijn promotieonderzoek begon was jij degene die mij wegwijs maakte op het lab en introduceerde op de Roper. Bovendien kon ik altijd bij je terecht met vragen en was je mijn klankbord voor het bespreken van ideeën. Bedankt voor alle hulp.

Tom, bedankt voor je hulp en advies bij van alles en nog wat en natuurlijk de samenwerking aan het Biophysical Journal paper. Jouw inzet en gedrevenheid in het onderzoek zijn een ware inspiratie.

Herman, bedankt voor je hulp met kloneren en het maken van baculovirussen.

My former colleagues at the CSBB project, Julien, Megan, Lauriane, Ria, Lionel, and Herma, thanks for many inspiring meetings and discussions. I would also like to thank all the other colleagues at Biochemistry and PharmaTox for all the fun and unforgettable moments we shared.

Mijn studenten Ralph Slijkerman, Nelleke Kisteman en Martijn van der Made. Jullie waren gemotiveerde studenten en erg plezierig om mee samen te werken. Ik heb veel geleerd van het begeleiden van jullie stages en vond het leuk om jullie te zien ontwikkelen tot zelfstandige onderzoekers. Bedankt dat jullie kozen voor mij als stagebegeleidster.

Mijn lieve vrienden Janneke, Mark, Jorieke, Jeroen en Stefan. Bedankt voor alle gezellige momenten samen en jullie interesse in mijn promotieonderzoek.

Siny en Tjeerd, ik voel me altijd erg thuis bij jullie en waardeer jullie interesse in mijn promotieonderzoek enorm.

Mam en pap, dankzij het vertrouwen dat jullie mij geven ga ik zelfverzekerd nieuwe uitdagingen aan. Jullie moedigen mij aan om mijn hart te volgen en te doen wat ik leuk vind. Bedankt voor jullie onvoorwaardelijke liefde en steun bij alles wat ik doe.

Luciano, mama's liefste, jij maakt mij altijd vrolijk. Ik vond het gezellig om samen in het weekend even naar het lab te gaan. Je begrijpt al best goed wat voor onderzoek mama gedaan heeft op het lab. Ik ben super trots op jou!

Lieve Mello, zonder jouw eindeloze steun, liefde en positieve houding waren de afgelopen 4 jaar wel erg zwaar geweest. Je hebt me veel ontzorgd waardoor ik mijn promotieonderzoek kon combineren met ons gezin. Bedankt lieve schat, voor ALLES!



Thank you

Curriculum Vitae

Dania Liemburg-Apers werd geboren op 14 juli 1985 te Hoofddorp en groeide op in Hengelo. Hier behaalde zij haar havo-diploma aan de Grundel in 2002. Na een jaar Propedeuse Toegepaste Psychologie koos zij voor de bachelor Biologie & Medisch Laboratoriumonderzoek aan de Saxion Hogeschool in Enschede. Tijdens haar stage bij de afdeling Membraan Enzymologie van het UMC Utrecht deed zij onderzoek naar het transport van glycosphingolipides over celmembranen onder begeleiding van dr. David Halter. Tijdens haar afstudeerstage karakteriseerde zij spiercellen van patiënten met mitochondriële aandoeningen onder begeleiding van dr. Merel Huigsloot bij de onderzoeksgroep Mitochondrial Biochemistry binnen de afdeling Kindergeneeskunde van het Radboud UMC in Nijmegen. In 2007 behaalde zij haar bachelorsdiploma met als afstudeerrichting biochemie. Hierna volgde zij de master Moleculaire Levenswetenschappen aan de Universiteit van Nijmegen. Tijdens haar eerste stage deed zij onderzoek naar de rol van reactieve zuurstof moleculen in de ontwikkeling van auto-immuunziektes onder begeleiding van dr. Helma Pluk bij de afdeling Biomoleculaire Chemie van het Radboud Institute for Molecular Life Sciences (RIMLS). Tijdens haar afstudeerstage deed zij onder begeleiding van dr. Merel Hermans onderzoek naar de rol van phospholipase C in T-cel signalering bij de afdeling Biochemie van het RIMLS. In 2011 behaalde zij haar mastersdiploma (*Cum Laude*). Hierna begon zij aan het promotieonderzoek beschreven in dit proefschrift onder begeleiding van prof. dr. Jan Smeitink, prof dr. Roland Brock, dr. Peter Willems en dr. Werner Koopman bij de onderzoeksgroep Membraan Biochemie van de afdeling Biochemie binnen het RIMLS. Haar onderzoek maakte deel uit van het ZonMw gefinancierde Centre for Systems Biology and Bioenergetics (CSBB).

List of publications

Liemburg-Apers, D. C., Wagenaars, J. A. L., Smeitink, J. A. M., Willems, P. H. & Koopman, W. J. (2015) Stimulation of glucose influx by acute mitoenergetic dysfunction requires LKB1, AMPK and Sirt2 (Submitted)

Grefte, S.[#], **Liemburg-Apers, D. C.**[#], Manjeri, G. R., Breuer, M. E., Wagenaars, J. A. L., de Ronde, L. H. J. Smeitink, J. A. M., Willems, P. H. & Koopman, W. J. (2015) Myoblasts derived from NDUFS4 ^{-/-} mice show normal myotube formation but display increased intracellular ROS levels (Submitted) [#]equal contribution

Liemburg-Apers, D. C., Schirris, T. J., Russel, F. G., Willems, P. H. & Koopman, W. J. (2015) Mitoenergetic Dysfunction Triggers a Rapid Compensatory Increase in Steady-State Glucose Flux. *Biophys J*, 109, 1372-86.

Liemburg-Apers, D. C., Willems, P. H., Koopman, W. J. & Grefte, S. (2015) Interactions between mitochondrial reactive oxygen species and cellular glucose metabolism. *Arch Toxicol*, 89, 1209-26.

Distelmaier, F., Valsecchi, F., **Liemburg-Apers, D. C.**, Lebiedzinska, M., Rodenburg, R. J., Heil, S., Keijer, J., Fransen, J., Imamura, H., Danhauser, K., Seibt, A., Viollet, B., Gellerich, F. N., Smeitink, J. A., Wieckowski, M. R., Willems, P. H. & Koopman, W. J. (2015) Mitochondrial dysfunction in primary human fibroblasts triggers an adaptive cell survival program that requires AMPK-alpha. *Biochim Biophys Acta*, 1852, 529-40.

Forkink, M., Manjeri, G. R., **Liemburg-Apers, D. C.**, Nibbeling, E., Blanchard, M., Wojtala, A., Smeitink, J. A., Wieckowski, M. R., Willems, P. H. & Koopman, W. J. (2014) Mitochondrial hyperpolarization during chronic complex I inhibition is sustained by low activity of complex II, III, IV and V. *Biochim Biophys Acta*, 1837, 1247-56.

Liemburg-Apers, D. C., Imamura, H., Forkink, M., Nooteboom, M., Swarts, H. G., Brock, R., Smeitink, J. A., Willems, P. H. & Koopman, W. J. (2011) Quantitative glucose and ATP sensing in mammalian cells. *Pharm Res*, 28, 2745-57.

